

**Seismic Strain Rates  
and the State of Tectonic Stress  
in the Southern California Region**

Thesis by  
Weishi Huang

In Partial Fulfillment of the Requirements  
for the Degree of  
Doctor of Philosophy

California Institute of Technology

Pasadena, California

1995

(Defended April 26, 1995)

© 1995

Weishi Huang

All Rights Reserved

## Acknowledgments

I thank people in this Division, particularly in the Seismological Laboratory. The faculty, staff, and fellow students have been very helpful to me during my residence at Caltech. Without their help, this thesis would not be possible. Chronologically, I would like to thank Prof. Ding, Guoyu in China for his initial advice on doing scientific research. I thank Prof. Clarence R. Allen for his introduction and persuasion of me to come to Caltech, and for his kindness of being my academic advisor during my first two years at Caltech. I thank Dr. Hiroo Kanamori for his insightful advice on science and continuous support for research. I benefited very much from the perceptive guidance of Dr. Leon T. Silver, who together with Dr. Kanamori unhesitatingly served as my thesis advisors shortly after Clarence Allen became a professor emeritus. It has been a very unique experience in my life working with both a seismologist and a geologist. When I tell some of my friends I have two advisors in two different fields, they think I am doing two Ph.D. dissertations!

One of the unique advantages of this division is that students are assigned an academic advisor in addition to the regular thesis advisor. I thank Dr. Don L. Anderson, my academic advisor after Clarence Allen. He is always ready to sign my registration card and gives me feedback promptly if I have a manuscript for him to review. I would also like to thank Drs. Rob Clayton and Joann Stock for serving to be my thesis committee members and for their critical review of my thesis. Some other faculty members or research associates such as Egill Hauksson, Tom Heaton, and Kerry Sieh are also thanked for their comments on my thesis work.

I am grateful to the staff in the Seismological Laboratory and the librarians in the Division. Particularly worthy of mentioning are Patricia Kelly, a retired librarian in this division, who carefully did the editorial reading and checking of my thesis, and Ann Freeman for her help throughout the thesis study. I enjoyed very much my friendship

with my fellow students. I thank Shawn Larsen for his contribution by developing the computer code, MPLOT, with which computer graphing becomes so handy, Lianshe Zhao for his help on computer programming, and my officemates, Xiao-dong Song, Paul Tackley, Doug Dreger, and Cathy Smither for the time they shared with me. Some others have made life enjoyable at Caltech. Here are some of them with whom I interacted most: Eddie Garnero, Brad Wood, Yushe Zhang, Hua-Wei Zhou, Wenbo Yang, Hong-Kie Thio, Blair Zajac, Craig Scrivner, Helen Qian, Shingo Watada, and Guo-Fong Ma, and many others.

Finally, I feel indebted to my wife, Qinghong, for her love and support and to my parents for their encouragement of me in pursuing higher education. To them, I present this thesis.

## Abstract

I determine 505 fault plane solutions from the first motions of P-waves for the background seismicity ( $3.0 \leq M \leq 6.0$ , 1981-1991) and collect mechanisms of major earthquakes ( $M \geq 6.0$ , 1927-1994) from the literature in the southern California region. Then I study the seismic strain and tectonic stress fields in individual domains (ten in total) by analyzing these mechanism data. The seismic strain tensors are obtained by tensorial summation of individual seismic moment tensors. The tectonic stress tensors are determined by performing numerical inversions of the slip vector data, using Angelier's (1990) method. The findings are summarized as follows:

- (1) Of the 505 fault plane solutions for the 1981-1991 background seismicity, 54% are strike-slip (SF), 21% reverse (RF), 17% normal (NF), and 8% oblique-slip faulting (OS) events. The catalog of the major earthquakes for the period 1927-1994 also displays similar proportions of the faulting mechanisms;
- (2) The similarity of the focal mechanisms can be measured by a parameter, seismic consistency ( $Sc$ ) introduced by Apperson (1991). It is defined as the ratio of the scalar moment of the total moment tensor to the sum of the scalar moments of individual moment tensors. In southern California, the Brawley fault (BYF) domain shows the highest  $Sc$  (0.70), whereas the White Wolf fault (WWF) domain displays the lowest  $Sc$  (0.44).  $Sc$  values in other domains vary between the above two values;
- (3) The depths of possible low-angle faults inferred from the fault plane solutions vary from 20 km in the Transverse ranges where N-S convergence dominates, to only 1 km in the southern Sierra Nevada fault (SSNF) domain where E-W divergence dominates. Our current data do not show the existence of a single unified seismically-active master detachment in the seismogenic zone;

- (4) The axes of the maximum principal stress,  $\sigma_1$ , are oriented N6°E  $\pm 11^\circ$ , whereas those of the maximum principal strain,  $\epsilon_1$ , are oriented N5°E  $\pm 21^\circ$ ;
- (5) The strain and stress tensors are similar to each other in the Mojave (MVE), San Jacinto (SJF), Elsinore (ESF), BYF, western and eastern Transverse Ranges (WTR, ETR) domains, but dissimilar in the central Transverse Ranges (CTR), Newport-Inglewood fault (NIF), WWF, and SSNF domains. Areas with small values of  $\Phi = (\sigma_2 - \sigma_3)/(\sigma_1 - \sigma_3)$  ( $< 0.35$ ) such as the WTR, CTR, and NIF domains are associated with more than 40% of RF events. Areas with  $\Phi$  values around 0.5 such as the SJF, ETR, WWF, ESF, BYF, and MVE domains are associated with more than 47% of SF events. The SSNF domain has a large  $\Phi$  ( $> 0.65$ ) and shows 49% of NF events. Variation of the state of stress appears to be in the Transverse Ranges where hypocenters are generally deep. Other areas show a relatively stable state of stress throughout the seismogenic depth;
- (6) Seismic fraction of deformation,  $\eta$ , is a measure of the deformation mode. It is defined as the ratio of seismic strain rate to the total deformation rate. Because of the limited seismic data, we can usually estimate the apparent instead of the real seismic fraction of deformation. Therefore, caution must be exercised in applying the values of  $\eta$  to evaluations of seismic potential. In southern California, there are some indications that areas in which seismic deformation nearly accounts for the total deformation are typically associated with cold and rigid batholithic rocks or high seismic velocity anomalies such as in the SJF, south central MVE, WWF, and possibly the ETR domains. However, areas with low seismic velocity anomalies are not free of earthquakes as seen, for example, in the BYF domain, which shows  $\eta = 0.6-1.0$ . Other domains show  $\eta < 0.4$ . The problem of whether the missing deformation is being released aseismically or has accumulated elastically remains to be resolved.

## Table of Contents

<i>Acknowledgements</i> .....	iii
<i>Abstract</i> .....	v
<b>Chapter 1 Introduction</b> .....	1
<b>Chapter 2 Earthquake Data</b> .....	4
2.1 <i>Background Seismicity (1981-1991)</i> .....	6
2.2 <i>Major Earthquakes (1900-1994)</i> .....	11
<b>Chapter 3 Characteristics of Source Mechanisms</b> ...	16
3.1 <i>Classification of Focal Mechanisms</i> .....	16
3.2 <i>Detachment-type Mechanisms</i> .....	26
3.3 <i>Seismic Consistency (Sc)</i> .....	36
3.4 <i>P, T, and N Axes Orientations</i> .....	40
3.5 <i>Summary</i> .....	46
<b>Chapter 4 Seismic Strain and Tectonic Stress</b> .....	47
4.1 <i>Introduction</i> .....	47
4.2 <i>Seismic Strain Tensor</i> .....	49
4.3 <i>Tectonic Stress Tensor</i> .....	51
4.4 <i>Physical Implications</i> .....	52
4.5 <i>Results in Southern California</i> .....	54
4.6 <i>Geological Insights</i> .....	58
4.7 <i>Stress Ratio</i> .....	59
4.8 <i>Interpretations</i> .....	67
4.9 <i>Summary</i> .....	69

## **Chapter 5**

<b>Seismic Deformation and Geological Environment ...</b>	<b>70</b>
<i>5.1 Motivation</i> .....	70
<i>5.2 Seismic Deformation in Individual Domains</i> .....	75
<i>5.3 Geological Tour of Individual Domains</i> .....	81
<i>5.3.1 Southern Sierra Nevada Fault (SSNF) Domain</i> .....	81
<i>5.3.2 White Wolf Fault (WWF) Domain</i> .....	84
<i>5.3.3 Mojave (MVE) Domain</i> .....	87
<i>5.3.4 Western Transverse Ranges (WTR) Domain</i> .....	91
<i>5.3.5 Central Transverse Ranges (CTR) Domain</i> .....	95
<i>5.3.6 Eastern Transverse Ranges (ETR) Domain</i> .....	109
<i>5.3.7 Newport-Inglewood Fault (NIF) Domain</i> .....	112
<i>5.3.8 Elsinore Fault (ESF) Domain</i> .....	115
<i>5.3.9 San Jacinto Fault (SJF) Domain</i> .....	117
<i>5.3.10 Brawley Fault (BYF) Domain</i> .....	120
<i>5.4 Comparison of Seismic, Geodetic, and Geologic Data</i> .....	122
<i>5.4.1 Problems of the Comparisons</i> .....	122
<i>5.4.2 Assessment of Deformation Mode</i> .....	125
<i>5.5 Concluding Remarks</i> .....	138
<b>Appendix</b> .....	<b>139</b>
<b>Bibliography</b> .....	<b>176</b>

## List of Tables

2.1 Comparison of focal mechanisms by different investigators .....	9
2.2 Listed major earthquakes between 1900 and 1994 .....	13
3.1 Detachment-type mechanisms .....	27
4.1 Orientations of Principal axes of the strain and stress tensors .....	55
5.1 Calculated results of the strain tensors in each domain .....	76
5.2 Listed focal mechanisms in the SAF, CTR domain .....	102
5.3 Geodetic strain rates in each domain .....	128
5.4 Comparison between geodetic and seismic strain rates .....	129
A1 Listed earthquakes and mechanisms (1981-1991) .....	139

## List of Figures

2.1 Seismicity map of southern California, 1981-1991 .....	5
2.2 Comparison of focal mechanisms determined by different investigators .....	8
2.3 Major earthquakes (1900-1994) in southern California .....	10
2.4 Seismic energy in each deforming domain .....	12
3.1(a) Ternary diagram of focal mechanisms for the background seismicity (1981-1991) .....	17
3.1(b) Ternary diagram of focal mechanisms for the major earthquakes (1900-1994) .....	17
3.2 Spatial distributions of different focal mechanisms .....	20
3.3 Ternary diagrams of focal mechanisms in each domain .....	21
3.4 Preponderance comparison of focal mechanisms for each domain ....	24
3.5 Depth distributions of different focal mechanisms .....	25
3.6(a) Spatial distribution of detachment-type mechanism .....	30
3.6(b) Cross section view of the detachment structures .....	31
3.7 Sketchy diagrams illustrating occurrence of detachments .....	32
3.8 Block diagram illustrating imbricate or cross thrusts .....	34
3.9 Diagrams illustrating the relationship between $S_c$ and focal parameters .....	37
3.10 Relationship between stress ratio, $S_c$ , and faulting patterns .....	38
3.11 Horizontal projection of P and T axes of individual earthquakes ....	41
3.12 Equal-area projection of P, T, and N axes .....	42

3.13(a) Equal-area projection of P axes for each domain .....	43
3.13(b) Equal-area projection of T axes for each domain .....	44
3.13(c) Equal-area projection of N axes for each domain .....	45
4.1 Graphic illustration of seismic strain and tectonic stress .....	48
4.2 P-wave radiation pattern of a total moment tensor .....	50
4.3 Inconsistency of the principal axes resulting from the existence of weak zones .....	53
4.4 Comparision of seismic strain and stress tensors .....	56
4.5 Tensor difference measured by TD and Sc .....	57
4.6(a) Vertical variations of the stress tensors in each domain .....	60
4.6(b) Stress ratios obtained below and above 10 km .....	61
4.7 Relationship between the stress ratio and faulting patterns .....	63
4.8 3D Mohr diagrams explaining the faulting patterns .....	65
4.9 Relationship between fault orientation and direction of the maximum principal stress axis .....	68
5.1 Plot illustrating the setup of the coordinate system .....	71
5.2 Horizontal projection of the principal strain rates in each domain .....	80
5.3 Generalized seismotectonic map of the SSNF domain .....	82
5.4 Generalized seismotectonic map of the WWF domain .....	84
5.5 Generalized seismotectonic map of the MVE domain .....	89

5.6	Two explanations for the Landers earthquake .....	90
5.7	Generalized seismotectonic map of the WTR domain .....	92
5.8	Seismicity map (1971-1994), CTR .....	96
5.9	Major earthquakes and slip directions, CTR .....	99
5.10	Earthquakes on the SAF, CTR .....	101
5.11	Ternary diagram for earthquake on the SAF, CTR .....	105
5.12	Generalized geologic map, CTR .....	106
5.13	Cross section across the San Gabriel Mountains .....	108
5.14	Generalized seismotectonic map of the ETR domain .....	110
5.15	Generalized seismotectonic map of the NIF domain .....	114
5.16	Generalized seismotectonic map of the ESF and SJF domains .....	116
5.17	Generalized seismotectonic map of the BYF domain .....	119
5.18	Diagram illustrating the difference of deformation rates from seismology, geology, and geodesy .....	122
5.19	Diagram showing the relationship between average recurrence interval and seismic strain rates .....	124
5.20	Horizontal projection of the principal axes from seismology and geodesy .....	130
5.21	Apparent seismic fraction of deformation in each domain .....	131
5.22	Seismic energy vs. time in each domain .....	133
5.23	Simplified geologic map of southern California .....	135
A1	P-wave first motions and focal mechanisms for the background seismicity (1981-1990) .....	152
A2	First motions and focal mechanisms for the SAF, CTR .....	175

## Chapter 1

### Introduction

This thesis deals with an interdisciplinary subject involving both seismology and geology. Seismology provides us with a quantitative analysis of seismic sources and the associated deformation. For example, Brune (1968) used the scalar seismic moment introduced by Aki (1966) to estimate seismic slip on major continental faults. Kanamori (1971, 1977) applied the same method to subduction zones and compared the seismic deformation with plate motions. Anderson (1979) assessed the maximum potential earthquakes in various faults of southern California by integrating geologic slip rates on individual faults. Kostrov (1974) expanded Brune's method to three dimensions by correlating the seismic moment tensor with the strain tensor. This method was applied to Tibet and southwestern Asia (Molnar and Deng, 1984) and the Mediterranean region (Jackson and McKenzie, 1988; Jackson et al., 1994). Similar applications of seismic moment tensors to tectonics were also presented by Molnar (1979), Ekström and England (1989), Frohlich and Apperson (1992), and Anderson et al. (1993). In the aspect of regional kinematics, Holt et al. (1991) and Holt and Haines (1993) quantitatively estimated the rotation about a vertical axis in addition to the horizontal translation of the deforming blocks in southwestern Asia by inverting a continuous function of strain variation with space.

Another piece of important information provided by the earthquake data concerns the tectonic stress field. With the fault plane solution data, it is possible to study the state of stress in which earthquakes occur (see Raleigh and Healy, 1972), and analyze the directions of principal stresses and their relative values (see Angelier, 1979, 1984). Numerical inversion of tectonic stress fields was originally applied to structural geology in an attempt to reconstruct the paleostress field under which faults and/or

slickensides were formed (see Angelier, 1979). This method has now been expanded to use slip vectors obtained from focal mechanisms to obtain the current tectonic stress field (Gephart and Forsyth, 1984; Michael, 1984, 1987; Angelier, 1990).

From the geological point of view, Allen et al. (1965), after regional studies of seismicity in southern California, pointed out that earthquakes occur on active faults that can be prerecognized from studies of geomorphology and Quaternary geology. Since then, many efforts have been spent in the study of active faults in order to determine fault slip rates and earthquake recurrence intervals (e.g. Clark et al., 1972; Allen, 1975; Sieh, 1978a,b; Sieh and Jahns, 1984). Well constrained Holocene or Quaternary slip rates on many major faults are now available in southern California (see Wesnousky, 1986). They have been used for comparisons with the geodetic measurements, which quantitatively monitor the present-day deformation across many major faults and over the whole southern California region (see Savage, 1983; Ward, 1992; Johnson et al., 1994). Compared to 30 years ago, we now have a better kinematic picture of fault motion in southern California (see Bird and Rosenstock, 1984). More and more data show that the boundary between the North American and Pacific plates in southern California is not a simple one. This is exemplified by the diversity of fault geometry and fault plane solutions of recent major earthquakes. In addition to the general northwest-southeast movements, N-S shortening is evident and complicates the ongoing kinematics of deforming blocks. Possible decollement or detachment structures down to the seismogenic zone, which is typically 15 kilometers (see Sibson, 1982, 1984) have been inferred geologically (Ehlig, 1968; Yeats, 1981; Davis et al., 1989) and geophysically (Anderson, 1971; Hadley and Kanamori, 1978; Webb and Kanamori, 1985; Huang et al., 1993a). Strain partitioning is inevitable in oblique collision, and the associated deformation is expected to be complex (see Lettis and Hanson, 1991; Molnar, 1992). One of the common structures resulting from oblique

convergence is the fold and thrust belt. Fold and thrust belts have been geologically observed in the western and central Transverse Ranges (Namson and Davis, 1988; Davis et al, 1989), geodetically measured across the Santa Maria Basin (Feigl et al., 1990) and seismically interpreted in the Los Angeles Basin (Hauksson, 1990).

Since 1978 when the southern California seismic network was largely expanded, the accuracy of locating earthquakes has been greatly improved, both horizontally and vertically (see Hutton et al., 1991). It is now possible to determine reliable focal mechanisms of events as small as  $M=3.0$  from P-wave first motion data. With these data, quantitative analyses of faulting patterns and the associated deformation become feasible. Motivated by the large amount of data and the general concerns for seismic hazard in southern California, I investigate the relationship between seismic deformation and the geological environment in the hope of contributing to a better quantitatively understanding of seismic behavior and earthquake potential.

This thesis consists of five chapters. Chapter 1 is the introduction. Chapter 2 describes seismic data acquisition procedures. Chapter 3 summarizes the basic characteristics of focal mechanisms and explores their tectonic significance. Chapter 4 compares the seismic strain fields and the tectonic stress fields. Chapter 5 discusses the relationship among seismic, geodetic and geologic deformation and implications for seismic potential. The appendix tabulates the original data.

## Chapter 2

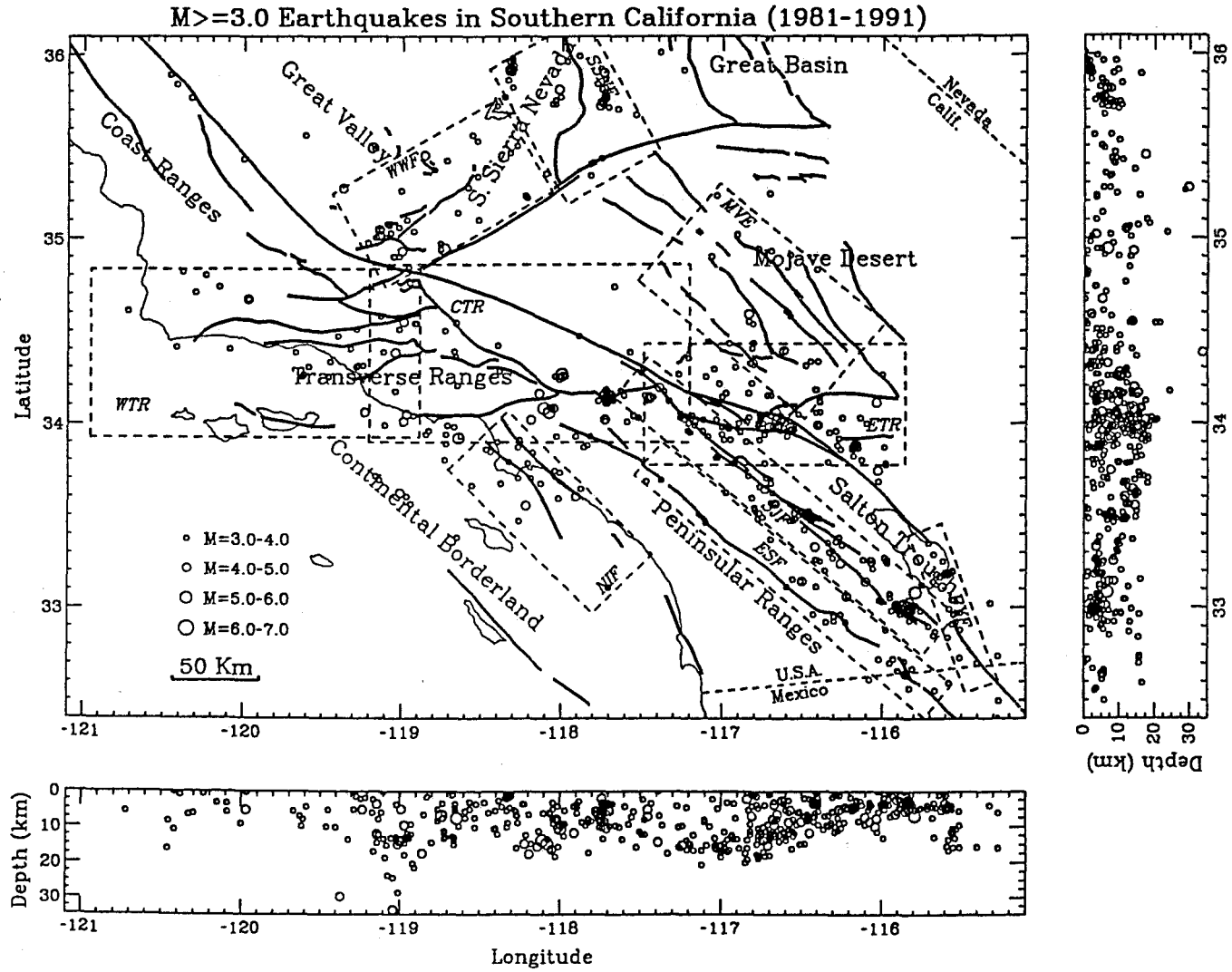
### Earthquake Data

Except in the central Transverse Ranges where a few events with magnitudes smaller than 3.0 are studied in detail, the majority of the seismic data used are  $M \geq 3.0$  events, of which focal mechanisms are determined from the P-wave first motions. They are all distributed within the region between latitudes  $32.4^\circ$  N and  $36.1^\circ$  N and between longitudes  $115.1^\circ$  W and  $121.1^\circ$  W. The studied region encompasses the extensional areas such as the southwestern end of the Great Basin, and the northern terminus of the Gulf of California, or the Salton Trough, strike-slip regimes such as the Peninsular Ranges, the Mojave Desert, as well as the convergent regime of the Transverse Ranges (Figure 2.1). The time interval is from 1981 to 1991 for  $3.0 \leq M < 6.0$  events, which are regarded as the background seismicity. Because of the diffuse distribution of seismicity, it is necessary to study the seismic characteristics domain by domain. Ten domains are divided based on the geographical distribution of seismicity and the tectonic setting, as indicated by the dashed lines in Figure 2.1. Overlapping between adjacent domains is allowed for some domains because of the ambiguity of the domain boundaries. Over 98% of the earthquakes are encompassed in the domains delineated by the dashed lines of Figure 2.1. For major events of  $M \geq 5.8$ , the time interval is extended to the beginning of this century (1900-1994).

---

Figure 2.1 Map showing the background seismicity ( $3.0 \leq M < 6.0$ , 1981-1991) and domain division. The abbreviations are: CTR, central Transverse Ranges; ESF, Elsinore fault; ETR, eastern Transverse Ranges; MVE, Mojave Desert domain; NIF, Newport-Inglewood fault domain; SJF, San Jacinto fault domain; SSNF, southern Sierra Nevada fault domain; WTR, western Transverse Ranges; WWF, White Wolf fault domain. Throughout this thesis, these abbreviations are used. The figure on the right is a latitudinal cross section. The one at the bottom is a longitudinal cross section of focus depths.

Figure 2.1



## 2.1 Background seismicity (1981 to 1991)

Earthquakes from the CIT/USGS catalog for the 10-year period from 1981 to 1990, with  $M_L \geq 3.0$  are selected. For the year 1991, only the largest event of that year - the Sierra Madre  $M_L = 5.8$  earthquake in the central Transverse Ranges, is used. In total, 505 events are chosen and focal mechanisms determined (Table A1, Appendix A). All of them, except those that have been relocated and published by other workers, are quality-A earthquakes, with epicenter error less than 1 km and hypocenter error less than 2 km.\* Most of the phase data of P-wave first motions are picked up by the USGS/CIT data analysts. We check and add P wave first motion polarities to the events that originally had less than 20 P-wave phase data so that the fault plane solutions can be better constrained. The takeoff angles of the P-waves are determined using the HYPOINVERSE program (Klein, 1985) with the southern California velocity structure model constructed by Hadley and Kanamori (1977). The focal mechanisms are determined using a grid-search algorithm, FPFIT, written by Reasenber and Oppenheimer (1985). In most cases, the fault planes can be constrained to within  $5^\circ$  in strike and dip, and  $10^\circ$  in rake. Jones (1988) noted that even significant changes in the velocity model would not change the solutions more than  $5^\circ$  for the events along the San Andreas fault. Comparing some of the events we determined using the southern California velocity structure model with those that are determined by other workers using different velocity structure models, we found that except for a few events with a small number of P-wave first arrivals, the solutions are in general very similar (Figure 2.2, Table 2.1). Therefore, we decided to use the southern California velocity model throughout this study. From Figure 2.1 it is noted that the San Andreas fault, except at the southeastern bend where it branches into the Banning fault and the Mission

---

\*see, for example, Hutton et al. (1980) for definition of location quality.

Creek fault, was seismically quiet. Seismicity in the past 10 years can be outlined in the following three areas: the southern Sierra Nevada, the Transverse Ranges (the eastern Transverse Ranges in particular), and the San Jacinto fault zone. At the bottom and to the right of Figure 2.1 are cross sections of focal depth versus longitudinal and latitudinal distances, respectively. Most earthquakes are located at depths above 15 kilometers. A few are below 20 km. Earthquakes with deeper hypocenters are concentrated in the Transverse Ranges, in particular the western Transverse Ranges. This has been noted by Bryant and Jones (1992).

---

Figure 2.2 Comparison of focal mechanisms determined by different investigators using various velocity models. The first column on the left is time in the order of year, month, day, hour, and minute.

Comparison of Focal Mechanisms determined by Different Investigators

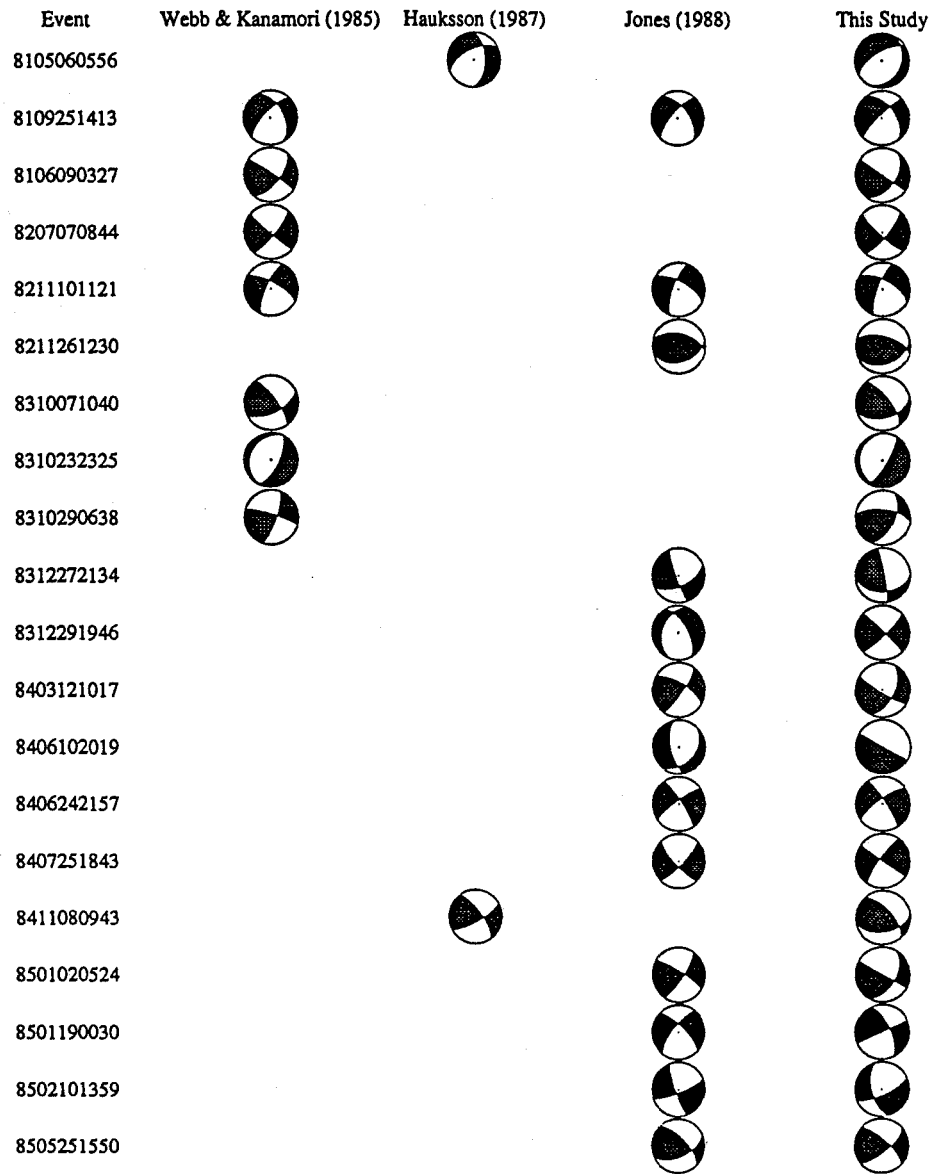


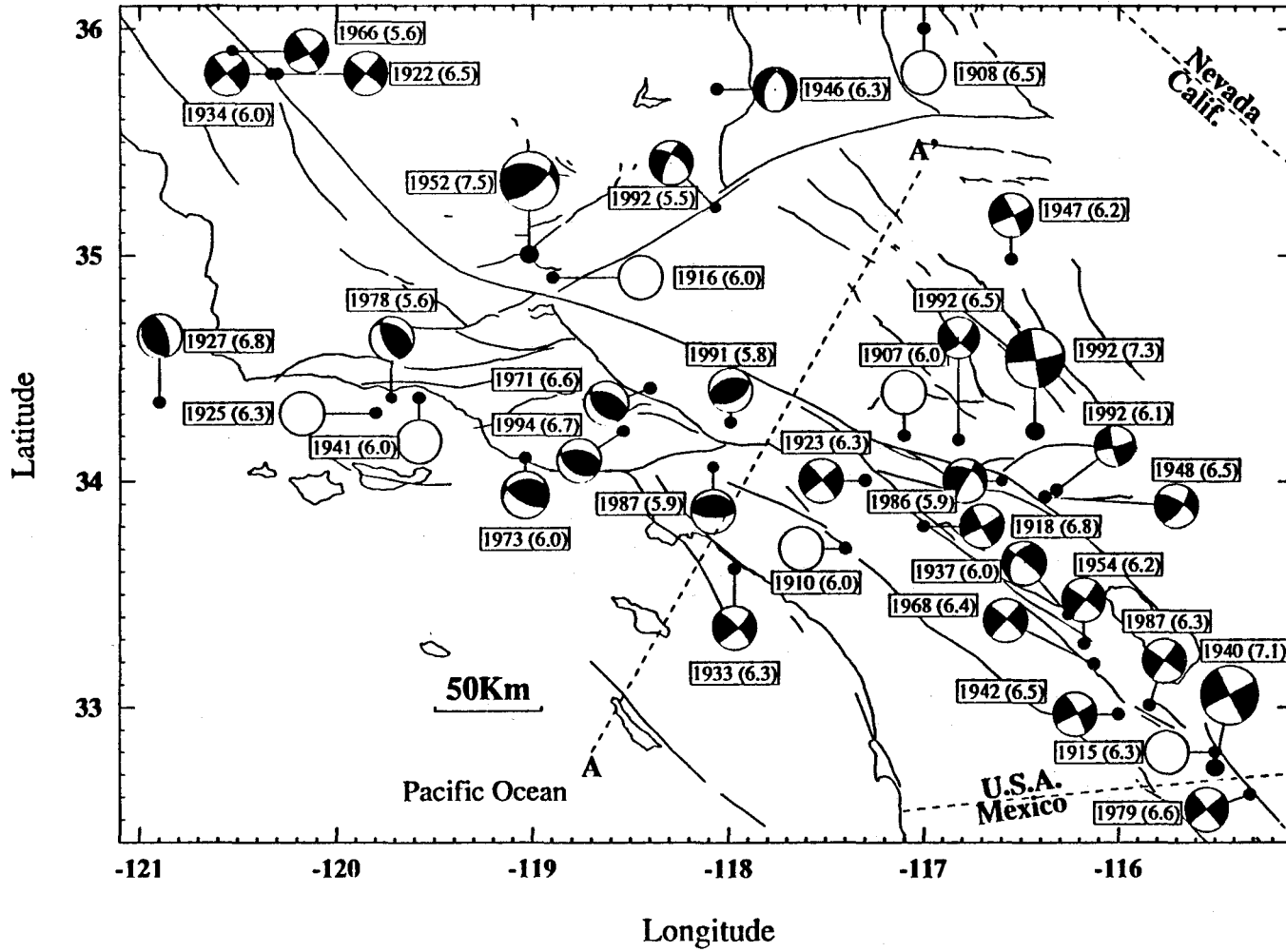
Figure 2.2

Table 2.1 Comparison of Focal Mechanisms from Different Researchers

Event		Webb & Kanamori (1985)					Hauksson (1987)					Jones (1988)					This Study				
Date	Time	M	D(Km)	Dip	Rake	Strike	M	D(Km)	Dip	Rake	Strike	M	D(Km)	Dip	Rake	Strike	M	D(Km)	Dip	Rake	Strike
810506	0556						3.1	5.0	55	-140	0						3.1	13.31	30	-120	25
810925	1413	3.3	20.0	70	-43	223						3.2	20.0	71	-36	221	3.1	21.43	80	-40	225
820609	0327	3.2	13.8	63	6.7	38											3.1	17.29	50	0	35
820707	0844	3.6	13.8	78	-4.1	40											3.5	14.02	75	-10	40
821110	1121	3.6	9.2	75	-21	203						4.2	9.4	72	-26	199	4.2	8.31	75	-30	200
821126	1230											3.1	12.9	42	69	75	3.1	11.57	35	60	70
831007	1040	3.1	13.6	60	19	64											3.1	18.89	45	30	75
831023	2335	3.1	12.9	66	-89	26											3.1	15.08	75	-80	30
831029	0638	3.4	12	75	10	20											3.4	11.83	55	30	25
831227	2134											3.1	2.7	58.3	-9	66	3.1	2.82	40	10	80
831229	1946											3.6	9.6	61	241	331	3.6	5.38	85	170	-45
840312	1017											3.5	13.5	78	22	34.5	3.5	12.74	55	-10	25
840610	2019											3.1	5.6	65.2	240.3	169.3	3.1	5.73	90	90	-60
840624	2157											3.5	7.3	80	350	235	3.5	6.96	75	-10	235
840725	1843											3.4	3.9	77	347	44	3.4	4.05	80	0	215
841108	0943						3.2	8.9	75	20	60						3.2	5.7	45	40	80
850102	0524											3.8	9.5	76	11	34	3.8	8.74	50	0	30
850119	0030											3.5	3.3	71	199	314	3.8	2.76	65	180	-25
850210	1359											3.6	1.1	80	190	160	3.6	1.59	60	-160	165
850525	1550											3.2	14.2	56	31	65	3.2	14.65	70	20	50

Figure 2.3

### M<sub>w</sub> ≥ 5.5 Earthquakes and Focal Mechanisms (1900-1994)



---

Figure 2.3 Major earthquakes,  $M \geq 5.8$ , 1900-1994. Open circles indicate events with no fault plane solutions due to lack of instrumental records. Southeast of line AA' strike-slip faulting mechanisms are dominant, whereas northwest of line AA' complex faulting mechanisms exist with reverse faulting mechanisms dominant.

## 2.2 Major Earthquakes (1900-1994)

For this period, we only collected events that are larger than  $M \geq 5.8$  (Table 2.2). Events since 1927 were well recorded instrumentally, and hence their locations, magnitudes, moments and/or focal mechanisms are constrained reasonably well. Most of them have been studied and published by many workers. As a magnitude comparison, we followed Kanamori's (1985) method to determine the surface wave magnitudes for the 1925, 1941 Santa Barbara Channel events, and the 1923 event on the northern San Jacinto fault. In general, the surface wave magnitude  $M_s$  is slightly larger than  $M_L$ , the Richter local magnitude scale. Figure 2.3 shows their spatial distributions and the associated focal mechanisms. The open circles indicate that no focal mechanisms are available because of the lack of instrumental records. Fault plane solutions are determinable for most of the events, and they correlate very well with the surface geology. For example, the San Jacinto fault zone is typically associated with strike-slip events, while the Transverse Ranges are associated with reverse or oblique-slip events. From Figure 2.3, we can divide the southern California region into two subregions using a NE-SW trending line AA'\*. Southeast of AA', the mechanisms are relatively uniform and characterized by the San Andreas type strike-slip fault pattern whereas northwest of AA' the mechanisms are complex, both in orientations and mechanisms. They are

---

\*This line was also recognized by Sykes and Seeber (1985) who pointed out the symmetric feature of the bends on the San Andreas fault in southern California.

dominated by reverse mechanisms with diverse orientations of fault planes. The SSNF domain shows dominant N-S trending normal faulting. The WWF and WTR, CTR show dominant reverse faulting events. This indicates that instantaneous block motions associated with major earthquakes in southern California are very complex. It is an oversimplification to only consider the strike-slip movements. It is worthwhile to point out that every domain outlined in Figure 2.1 has experienced at least one  $M \geq 6.0$  event, indicating relatively uniform distribution of major earthquakes in the region as a whole. However, the released seismic energy varies widely from domain to domain. The White Wolf fault (WWF) and Mojave (MVE) domains together take up more than 50% of the total released seismic energy (Figure 2.4).

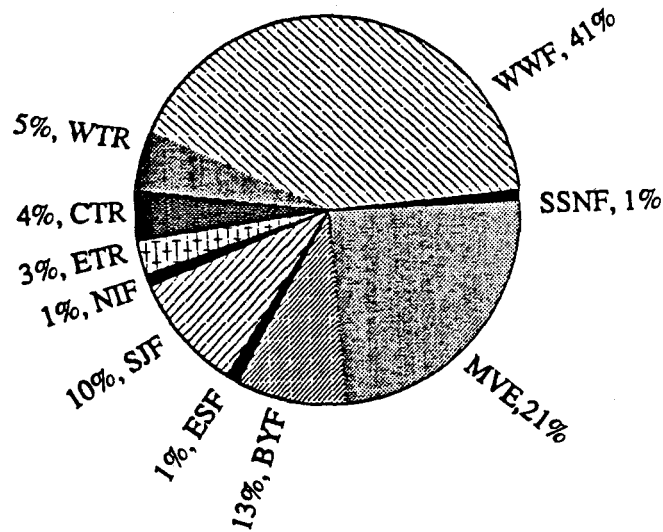


Figure 2.4 Proportions of released seismic energy in different domains. The WWF domain has the largest earthquake and hence the greatest amount of energy released, reaching 41% of the total energy since the beginning of this century.

Table 2.2 Earthquakes of  $M \geq 5.5$  in Southern California (1900-1994)

No.	Year	Mon	Day	Lat N°	Long W°	$M_L$	$M_w$	$M_s$	dip°	rake°	strike°	$M_0(10^{25})$ dyne.cm	Refs.
1	1907	9	20	34.20	117.10	6.0			?	?	?	≤0.1	1
2	1908	11	4	36.00	117.00	6.5			?	?	?	?	1
3	1910	5	15	33.70	117.40	6.0			?	?	?	≤0.1	1
4	1915	6	23	32.80	115.50	6.3			?	?	?	0.5	1
5	1916	10	23	34.90	118.90	6.0			?	?	?	≤0.1	1
6	1918	4	21	33.80	117.00	6.8			87	-176	150	15.0	1,1a
7	1922	3	10	35.80	120.30	6.5			?	?	?	1.0	*,1
8	1923	7	23	34.00	117.30	6.3		6.4	85	180	320	1.0	1,1a
9	1925	6	29	34.30	119.80	6.3		7.0	?	?	?	20.0	1
10	1927	11	4	34.35	120.90		6.8		66	95	340	20.0	2
11	1933	3	11	33.61	117.97	6.3	6.6		80	-170	315	10.0	3,1
12	1933	3	11	33.68	118.05	5.5			?	?	?	2.0	A
13	1934	6	8	35.80	120.33	6.0			88	167	325	?	*
14	1937	3	25	33.41	116.26	6.0			83	-136	309	0.75	4
15	1938	5	31	33.70	117.51	5.5			?	?	?	?	7
16	1940	5	19	32.73	115.50	6.7	7.1		90	180	332	48.0	5
17	1940	5	19	32.76	115.48	5.5			?	?	?	?	A
18	1940	5	19	32.76	115.48	5.5			?	?	?	?	A
19	1940	5	19	32.76	115.48	5.5			?	?	?	?	A
20	1941	7	1	34.37	119.58	6.0		6.0	?	?	?	0.9	6
21	1942	10	21	32.97	116.00	6.5			88	10	61	2.4	4
22	1942	10	22	33.23	115.72	5.5			?	?	?	?	A
23	1943	8	29	34.27	116.97	5.5			?	?	?	?	7
24	1943	12	22	34.33	115.80	5.5			?	?	?	?	7
25	1945	8	15	33.22	116.13	5.7			?	?	?	?	7
26	1946	3	15	35.73	118.06	6.3			45	243	346	1.0	8,1
27	1946	7	18	34.53	115.98	5.6			?	?	?	?	7
28	1947	4	10	34.98	116.55	6.2			85	8	65	3.0	9
29	1947	7	24	34.02	116.50	5.5			?	?	?	?	7
30	1948	12	4	33.93	116.38	6.5			70	160	300	1.0	10
31	1949	5	2	34.02	115.68	5.9			?	?	?	?	7
32	1950	7	29	33.12	115.57	5.5			?	?	?	?	7
33	1951	1	24	32.98	115.73	5.6			?	?	?	?	7
34	1951	12	26	32.82	118.35	5.9			?	?	?	?	7
35	1952	7	21	35.00	119.02	7.2	7.5	7.7	63	55	50	200.0	11,1
36	1952	7	21	35.00	119.03	5.6			?	?	?	?	A
37	1952	7	21	35.00	119.00	6.4			?	?	?	3.0	A,1
38	1952	7	21	35.13	118.77	5.5			?	?	?	?	A
39	1952	7	23	35.37	118.58	6.1			?	?	?	0.4	A,1
40	1952	7	23	35.22	118.82	5.7			?	?	?	?	A

No.	Year	Mon	Day	Lat N°	Long W°	M <sub>L</sub>	M <sub>w</sub>	M <sub>s</sub>	dip°	rake°	strike°	M <sub>0</sub> (10 <sup>25</sup> ) dyne.cm	Refs.
41	1952	7	25	35.32	118.49	5.7			?	?	?	?	A
42	1952	7	25	35.32	118.52	5.7			?	?	?	?	A
43	1952	7	29	35.38	118.85	6.1			?	?	?	3.0	A
44	1952	7	31	35.03	118.60	5.8			?	?	?	?	A
45	1952	8	22	35.03	118.92	5.8			?	?	?	?	A
46	1953	6	14	32.95	115.72	5.5			?	?	?	?	A
47	1954	1	12	35.00	119.02	5.9			?	?	?	?	A
48	1954	3	19	33.28	116.18	6.2			85	175	307	2.2	4
49	1954	3	19	33.28	116.18	5.5			?	?	?	?	A
50	1966	6	28	35.90	120.53	5.6			88	167	325	2.6	12
51	1968	4	9	33.19	116.13	6.4			83	180	312	6.0	13
52	1969	4	28	33.34	116.35	5.8			80	180	305	0.48	14
53	1971	2	9	34.41	118.40	6.4	6.6	6.6	52	72	293	10.0	15,1
54	1971	2	9	34.41	118.40	5.8			?	?	?	?	A
55	1971	2	9	34.41	118.40	5.8			?	?	?	?	A
56	1973	2	21	34.10	119.04	6.0			62	113	120	0.1	16,1
57	1978	8	13	34.37	119.72	5.1	6.0	5.6	40	60	300	1.1	17
58	1979	10	15	32.61	115.32	6.6			90	180	320	?	18
59	1979	10	16	33.01	115.56	5.5			?	?	?	?	16
60	1980	2	25	33.56	116.51	5.5			?	?	?	?	19
61	1981	4	26	33.10	115.63	5.7			?	?	?	?	16
62	1986	7	8	34.00	116.61	5.9			45	180	300	?	20
63	1987	10	1	34.06	118.08	5.9			25	90	270	?	21
64	1987	11	24	33.08	115.78	5.9			90	180	305	?	#
65	1987	11	24	33.01	115.84	6.3			90	180	305	?	22
66	1991	06	28	34.26	117.99	5.8	5.6		45	80	60	0.33	C
67	1992	04	23	33.96	116.32	6.1	6.1		85	-10	75	1.9	C
68	1992	06	28	34.22	116.43	7.4	7.3		90	175	350	100	C
69	1992	06	28	34.18	116.82	6.5	6.4		70	-10	45	4.5	C
70	1992	07	11	35.21	118.07	5.5	5.1		75	-30	25	0.07	C
71	1994	01	17	34.22	118.54	6.6	6.7		40	110	125	15	C

\*: Mechanism based on the same wave form as that of the 1966 event in Parkfield;

A: Aftershock;

1: Epicenter from Topozada et al. (1978), Moment from Hanks et al. (1975);

1a: Mechanisms from Doser (1992);

2: Helmberger et al. (1992);

3: Hauksson & Gross (1991);

4: Focal mechanism from Doser (1990b). Moment is average of Doser (1990b) and Bent & Helmberger (1991);

- 5: Doser & Kanamori (1987);
- 6: Coffman & Hake (1973), Real et al. (1978) (cited by Yerkes, 1985);
- 7: Hileman et al. (1973);
- 8: Mechanism is from Dollar & Helmberger's (1985) work. They determined the mechanism of the  $M_L=4.0$ , 1962 event, and suggested that this event may have the same mechanism as that of the 1946  $M_L=6.3$  event;
- 9: Doser (1990a);
- 10: This mechanism is obtained by comparing the two references. Richter et al. (1958) from the preliminary P wave first motions inferred that the mechanism was right-lateral with thrust slip. The fault plane strikes NW, approximately corresponding to the surface attitude of the Mission Creek fault, which is at a high angle ( $73^\circ$ ) dip to NE; Nicholson et al. (1987) by analysis and comparison of wave forms of the 1948 and 1986 events concluded that these two events have similar mechanisms. But the 1948 event has a higher dip angle to the NE, with 20%-30% thrust.
- 11: Mechanism from Gutenberg (1955). Stein & Thatcher's work (1981) suggests that the dip angle of the fault plane changes along the fault strike, from  $75^\circ$  at the southwestern end to  $20^\circ$  at the northeastern end;
- 12: Mechanism from McEvelly et al. (1967). Moment from Kanamori & Anderson (1975);
- 13: Allen & Nordquist (1972);
- 14: Bent & Helmberger (1991);
- 15: Whitcomb et al. (1973);
- 16: Mechanism from Stierman and Ellsworth (1976). Moment from Hanks et al. (1975);
- 17: Mechanism from Lee et al. (1978); Magnitude cited by Corbett and Johnson (1982); Moment from Wallace et al., (1981);
- 18: Johnson et al. (1982);
- 19: Sanders et al. (1981);
- 20: Jones et al. (1986);
- 21: Hauksson & Jones (1989);
- 22: Magistrale et al. (1989);
- #: This is the first main shock of the 1987 Superstition earthquakes. Because of the immediate foreshocks, the first motions of the P-Wave were obscured, and a high quality mechanism could not be determined (Magistrale, 1990). But based on aftershocks and surface geology, the two main shocks can be regarded as occurring on conjugate faults. Thus, they have the same mechanism.
- C: Mechanisms from personal communication with E. Hauksson and H. Qian. Moments from H. Thio of the Seismological Lab, Caltech.

## Chapter 3

### Characteristics of the Source Mechanisms

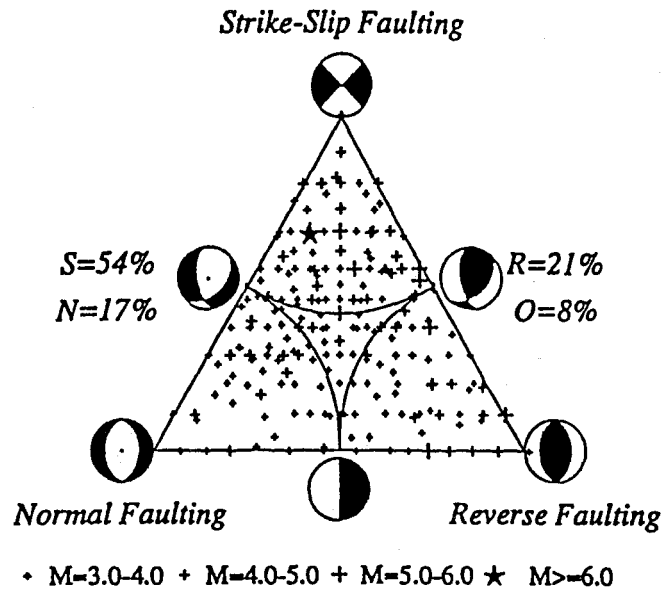
Earthquakes in southern California are diffuse in distributions and diverse in mechanisms. The first problem we are confronted with is how to measure or describe the variations quantitatively. In this chapter, we first discuss how to classify the focal mechanisms and then explore their tectonic significance.

#### 3.1 Classification of the Source Mechanisms

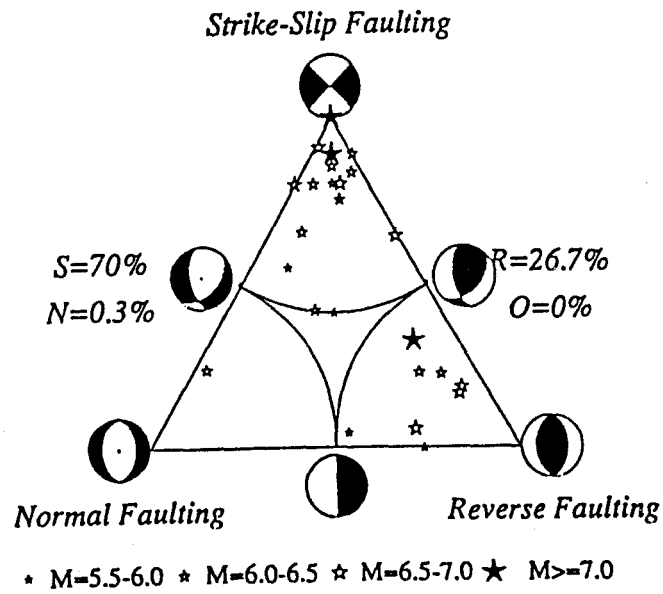
Following Frohlich and Apperson (1992), we classify focal mechanisms based on inclinations of P, T and N axes. In this method, there is no need to select a fault plane from the conjugate planes. Herein we set the threshold angle at  $45^\circ$ . That is, mechanisms with a P-axis plunge  $\geq 45^\circ$  are normal-faulting mechanisms; those with a T-axis plunge  $\geq 45^\circ$  are reverse-faulting mechanisms; those with an N-axis plunge  $\geq 45^\circ$  are strike-slip mechanisms. All others that do not belong to any one of the above groups are termed oblique-slip mechanisms.

---

Figure 3.1 Ternary diagram showing distributions of different focal mechanisms in southern California. (a) Events are  $M \geq 3.0$  from 1981 to 1991. N: normal-slip; O: Oblique-slip; S: strike-slip; and R: reverse-slip events. (b) Events are  $M \geq 5.5$ , 1918-1994. Note that the proportions of mechanisms between the short-period (1981-1991) background seismicity and the long-period (1918-1994) major earthquakes are similar, to the first order. see text for definition of the different mechanisms.



(a)



(b)

Figure 3.1

Of the 505 events of background seismicity, 54% are strike-slip, 21% reverse faulting, 17% normal faulting and the remaining 8% are oblique-slip faulting mechanisms (Figure 3.1a). Mechanisms of major earthquakes ( $M \geq 5.5$ ) between 1918 and 1994\* show similar proportions: 70% strike-slip, 26.7% reverse faulting, 2.3% normal faulting and 0.0% oblique-slip faulting (Figure 3.1b). Therefore, oblique-slip major earthquakes, as defined above, appear to be uncommon in southern California. But if we examine Figure 3.1b carefully, we can see that two of the major events are at the margin between strike-slip and oblique-slip groups (Center of Figure 3.1b). Therefore, to the first order, the proportions of mechanisms of background seismicity in the interval 1981-1991 are consistent with those of the major events in the interval 1918-1994. This is a very interesting result because it implies that about every seven major strike-slip faulting earthquakes are accompanied by about three major reverse faulting earthquakes in southern California. Spatially, the strike-slip events are the most prevalent and spread almost everywhere in the region (upper left, Figure 3.2), whereas reverse faulting events are concentrated mainly in the WTR, CTR, NIF, and WWF domains. Some are in the ETR. The normal faulting events are mainly in the SSNF domain. Some are in the BYF domain. The oblique-slip events are scattered. It is worthwhile to point out that the strike-slip events have fault planes striking more or less parallel to the general trend of the San Andreas and Garlock faults, the two prominent strike-slip faults in southern California. The reverse faulting events have fault planes striking approximately E-W, a few striking NW-SE. The normal-faulting events are relatively small both in magnitude and number (below). They strike roughly N-S (lower left, Figure 3.2). These patterns of seismic faulting are generally consistent with the surface distributions of the active faults.

---

In this classification, the period is from 1918 to 1994. But when computing the released seismic strain, the time interval is set at 1927-1994.

Figure 3.2 Spatial distributions of different types of mechanisms classified based on inclinations of P, T, and N axes. see text for detail.

Figure 3.2

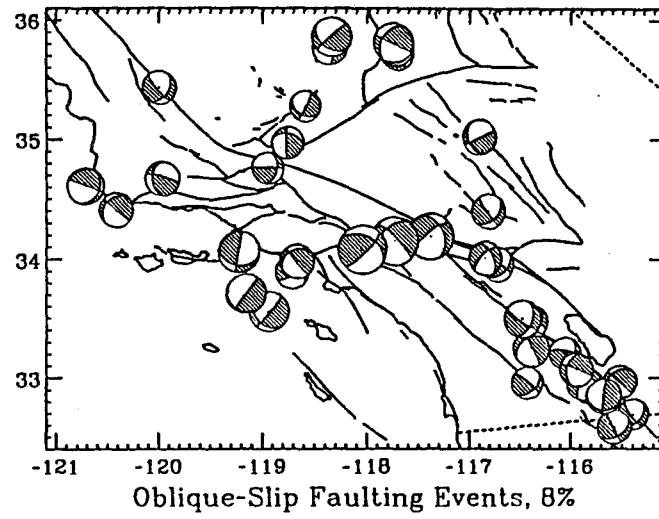
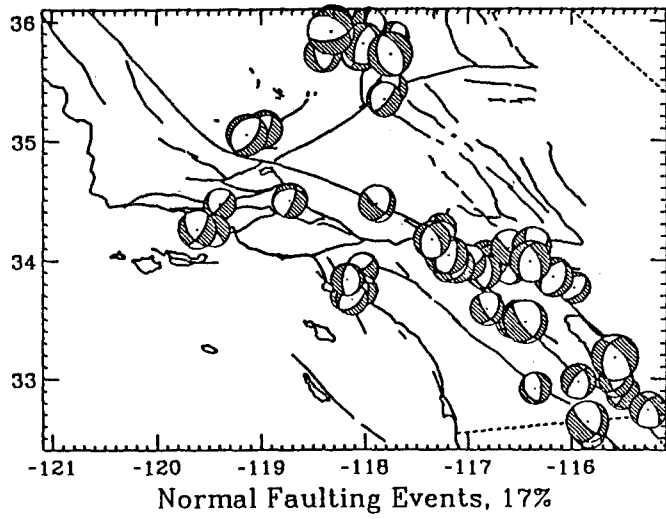
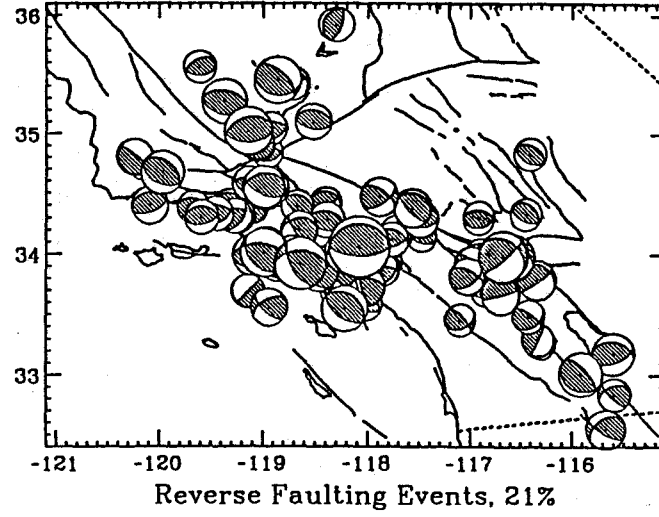
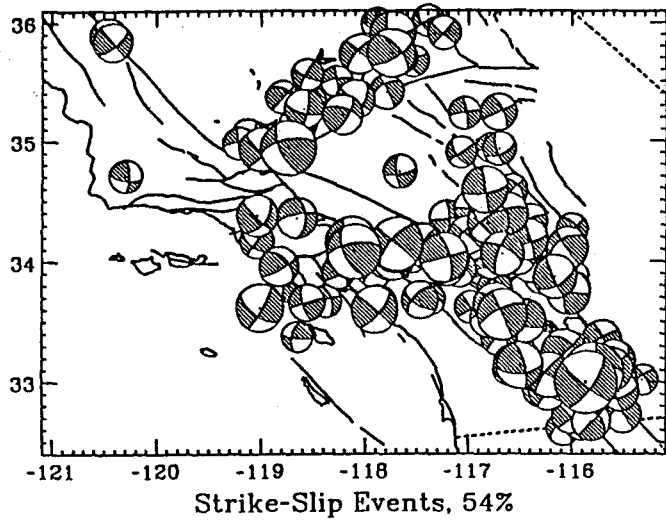
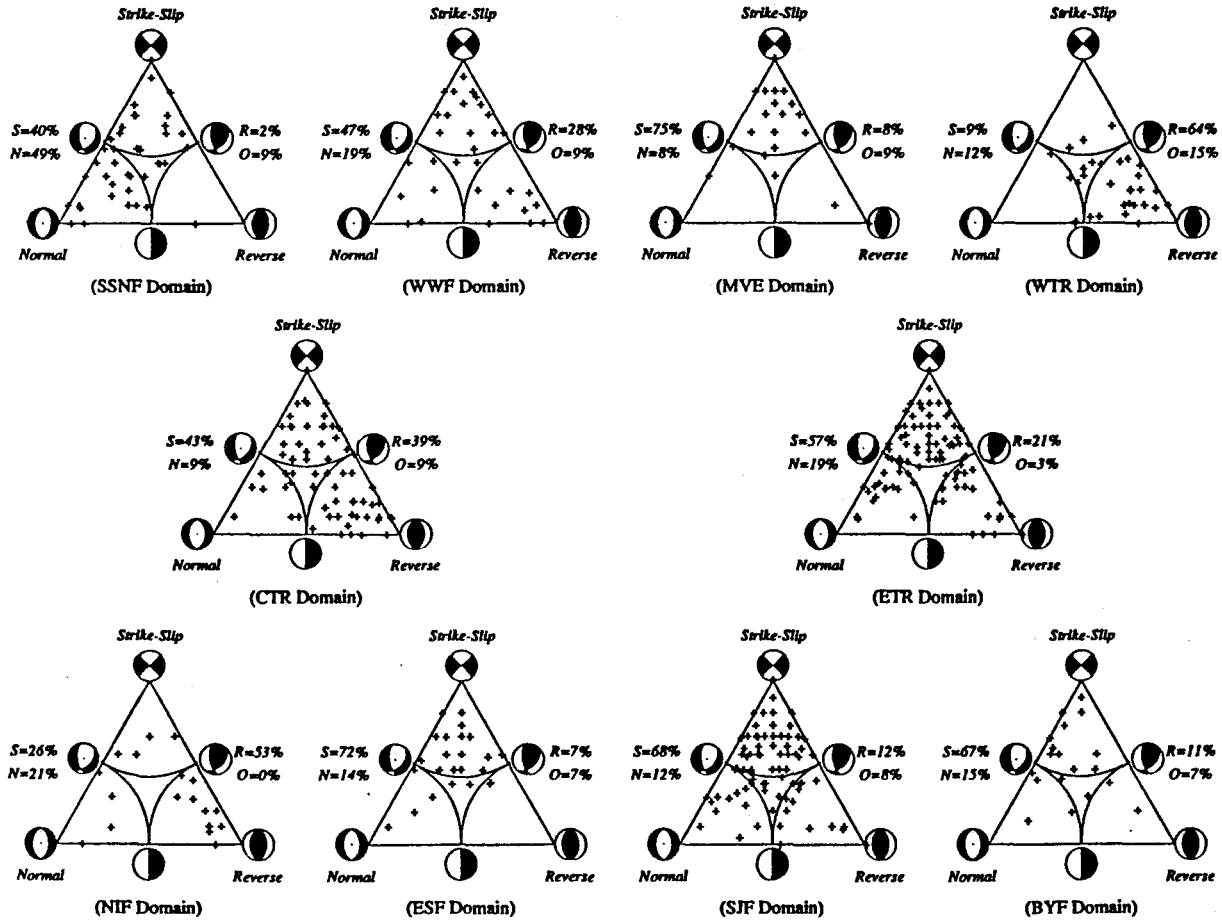


Figure 3.3



---

Figure 3.3 Ternary diagrams of focal mechanisms for individual domains.

Classification of focal mechanisms in individual domains is presented in Figure 3.3, in which distributions of different mechanisms are displayed. The largest percentage of strike-slip events, up to 75%, is in the MVE domain. The largest percentage of reverse-faulting mechanisms is in the WTR domain, up to 64%. Note that the percentage of reverse faulting events decreases eastward along the Transverse Ranges, from 64% in the WTR to only 21% in the ETR, indicating significant differences in strain fields between the two deflections of the San Andreas fault. The largest percentage of normal faulting mechanisms, up to 40%, is in the SSNF domain. And the largest percentage of oblique-slip faulting is in the WTR domain, up to 15% (Figure 3.4).

Vertically, large-magnitude events are located in the middle crust around 10 to 15 km (top of Figure 3.5). The dominant earthquakes, both in size and frequency, are strike-slip and reverse-slip faulting events. The important information from Figure 3.5 is that strike-slip and normal-slip faulting events are most frequent in the uppermost crust between 0 and 5 km, whereas the reverse-slip and oblique-slip events are most frequent between 5 and 10 km. This implies that many of the blind faults are at these depths and they deform the crust by thrusting or oblique-slip faulting that is usually not associated with clear surface traces of the faults.

If we compare the occurrence frequency of earthquakes on individual faults, we can also see that the reverse faults are associated with less frequent earthquakes than the strike-slip faults. As pointed out above, statistically, the dominant focal depths are deeper for the reverse faulting events than for the strike-slip events. This may account for the low frequency of reverse faulting events, because higher temperatures and

hence greater inelasticity can be associated with in the deep crust so that elastic strain is accumulated at a relatively low rate. If the temperature is not the major effect, then the pressure may play the role. Because the confining pressure increases downward, the resistance to failure can increase with depth in the crust. Therefore, either mechanism can make the reverse faulting earthquakes occur less frequently.

---

Figure 3.4 Comparisons of preponderance of different focal mechanisms in different domains. The strike-slip events are dominant in all domains except in the WTR domain. The WTR and NIF domains show a large percentage of reverse faulting events while the SSNF domain has the highest percentage of normal-faulting events. The oblique-slip events are generally small in number.

Figure 3.4

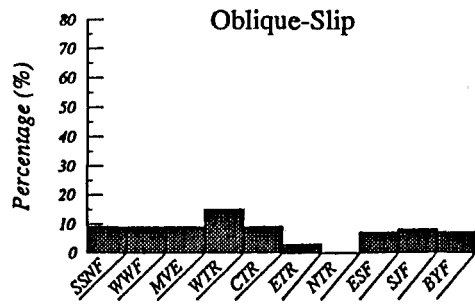
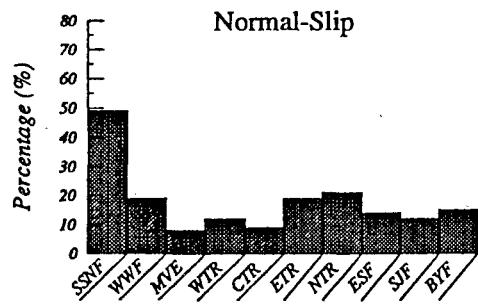
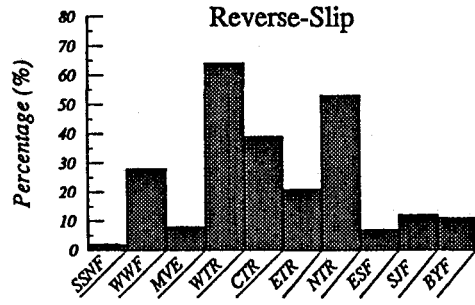
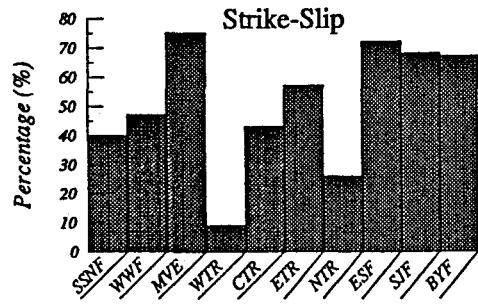
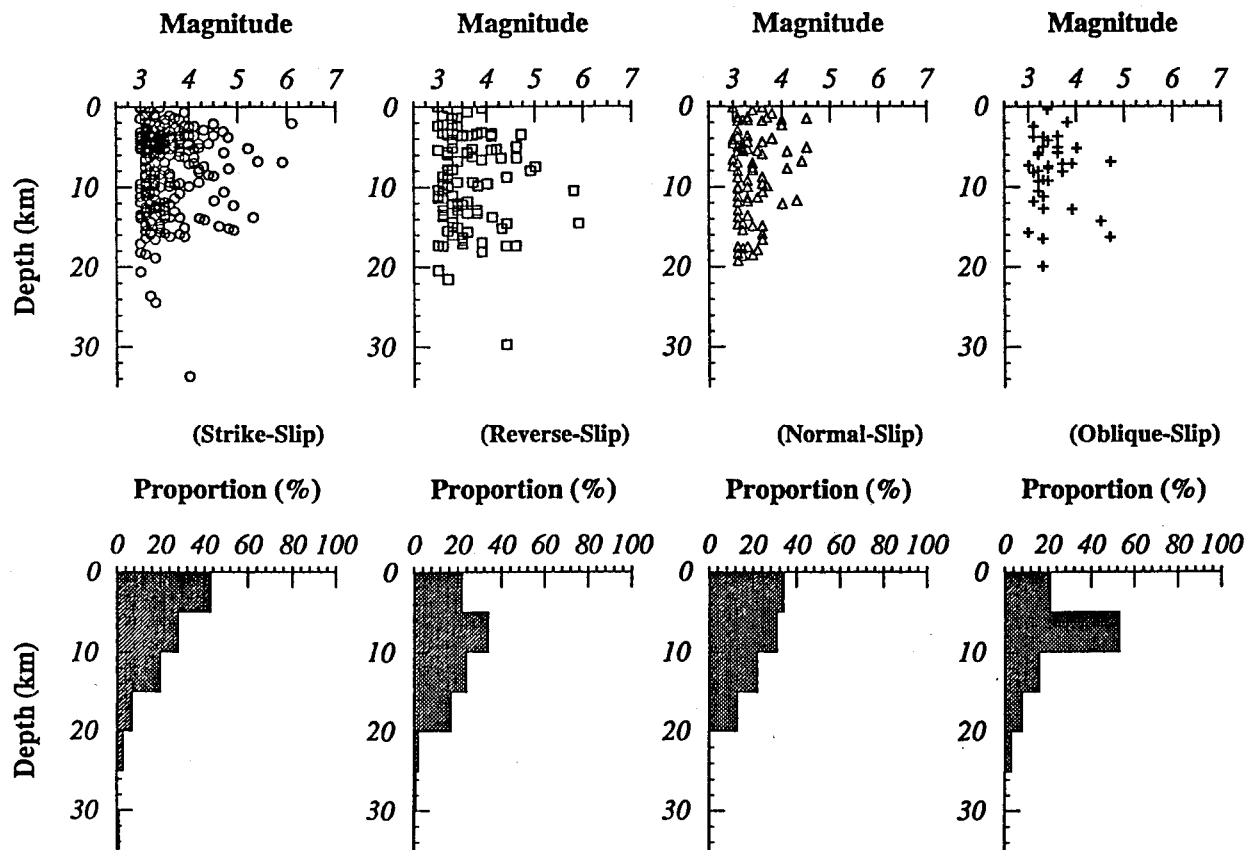


Figure 3.5



---

Figure 3.5 Depth distributions of classified focal mechanisms. The plots on the top are depth vs. magnitude. The plots at the bottom are depth histograms. It is shown that large magnitude events are in the range between 10 and 15 km. The reverse and oblique-slip events are more dominant at 5 to 10 km deep. This implies possible blind thrusts in this depth range.

### 3.2 Detachment-type Mechanisms

Detachment-type mechanisms are herein referred to fault plane solutions that have one fault plane dipping no greater than  $30^\circ$ . They are possible associated with detachment faulting in the crust. Most of the low-angle faults are buried in the middle crust and do not show clear surface expressions. Focal mechanism study is a very useful and economic way to determine them. Hadley and Kanamori (1978) were the first workers presenting evidence of earthquakes occurring on low-angle thrust faults in the west-central Transverse Ranges. Yeats (1981), from the geological point of view, suspected the regional existence of decollement(s) in the middle crust beneath the Transverse Ranges. He categorized them as flake tectonics. Webb and Kanamori (1985) extended the studies to the western and eastern Transverse Ranges and found more decollement-like mechanisms. These thrust mechanisms have been used as the supporting evidence for constructing balanced cross sections, in which many low-angle thrust faults ramp up from the major decollement as exemplified by the 1987 Whittier Narrows earthquake (see Davis et al., 1989), and the 1994 Northridge earthquake (Davis and Namson, 1994, Yeats and Huftile, 1995). Based on geological arguments and mechanisms of small earthquakes ( $M = 3 \pm$ ), we interpreted the San Gabriel Mountains in the central Transverse Ranges to be bounded by south-dipping blind thrusts to the north, and north-dipping reverse faults to the south, so that the whole mountain range is squeezed up as a result of nearly N-S compression (Huang et al., 1991, 1993a).

Table 3.1 Listed Detachment-type (dip  $\leq 30^\circ$ ) Mechanisms (1981-1991)

No.	Time	Long.(W)	Lat.(N)	$M_L$	D(km)	Dip1	Rake1	Strike1	Dip2	Rake2	Strike2	Note
1	81080611	-120.24	34.80	3.6	0.73	10	110	150	81	87	310	
2	81111100	-119.16	35.01	3.4	2.40	70	80	58	22	116	265	WK
3	81120922	-119.14	33.69	3.3	14.48	10	170	125	88	80	225	
4	81121411	-119.16	33.71	3.9	16.97	90	-80	35	10	-180	125	
5	82021619	-117.33	34.12	3.1	17.46	80	-80	60	14	-135	195	
6	82082704	-117.82	33.93	3.1	17.36	75	100	120	18	57	266	
7	83111116	-118.31	35.92	3.7	1.41	75	-100	50	18	-57	264	
8	83111412	-118.31	35.92	3.3	1.69	80	-100	55	14	-45	280	
9	84010605	-118.33	35.96	3.2	5.50	85	-90	95	5	-90	275	
10	82011604	-118.30	35.92	3.4	1.38	65	90	20	25	90	200	
11	84020520	-118.91	34.54	3.2	21.49	25	80	90	65	95	281	
12	84021114	-118.92	34.54	3.0	20.36	30	70	75	62	101	278	
13	84021416	-118.32	35.93	3.1	1.40	75	-100	50	18	-57	264	
14	84032308	-118.31	35.97	3.8	0.90	75	-90	55	15	-90	235	
15	84042122	-119.63	34.25	3.4	6.99	85	-90	275	5	-90	95	
16	84061302	-119.32	34.40	3.1	13.66	65	80	85	27	110	288	
17	84070622	-118.06	35.73	3.6	5.94	10	-160	140	87	-81	30	
18	84100507	-116.70	33.67	3.9	18.07	85	80	75	11	153	319	
19	84101800	-118.03	33.93	3.1	18.32	85	-100	50	11	-27	294	
20	84111905	-117.73	35.86	3.1	5.00	30	-60	45	64	-106	191	
21	84112608	-119.46	34.25	3.1	9.99	5	-80	150	85	-90	320	
22	85082904	-115.51	32.88	3.2	5.61	20	-160	140	83	-71	31	
23	86052311	-118.02	35.81	4.1	7.72	30	-120	350	64	-74	204	
24	87052518	-119.11	34.38	3.2	5.98	5	50	65	86	93	285	
25	87070721	-118.18	33.84	3.2	14.61	25	-110	345	67	-81	187	
26	87082506	-117.57	34.38	3.7	9.37	70	100	135	22	65	288	
27	87100114	-118.08	34.06	5.9	14.60	25	90	270	65	90	90	HJ
28	87110219	-117.82	35.34	3.4	7.88	75	-80	40	18	-123	186	
29	87112418	-115.91	33.01	4.3	6.40	25	70	115	67	99	317	CK
30	87121402	-119.05	34.90	3.3	13.22	15	90	85	75	90	265	
31	88011923	-118.06	34.08	3.5	16.26	70	90	70	20	90	250	
32	88060608	-116.33	33.30	3.2	9.84	5	90	205	85	90	25	
33	88121523	-116.54	33.48	3.3	11.78	20	-80	5	70	-94	174	
34	89020204	-118.85	33.94	3.9	6.62	20	140	120	77	74	248	
35	89071923	-116.68	33.97	3.0	11.12	65	90	45	25	90	225	
36	90051719	-115.68	32.85	3.4	7.39	20	-180	95	90	-70	5	

CK: Checked events for P-wave first arrival polarity. HJ: Hauksson and Jones (1989); WK: Webb and Kanamori (1985).

Table 3.1 lists all mechanisms that have one of the conjugate planes dipping no greater than  $30^\circ$ . Figure 3.6(a) shows their spatial distributions. 56% of these events are located in or adjacent to the Transverse Ranges. Some are in the SSNF area, and a few are in the Salton trough and in the Peninsular Ranges along the SJF fault zone. Two very impressive features are displayed in Figure 3.6. First, both reverse and normal faulting events exist (Figure 3.6a). Second, the possible low-angle faulting events are located at various depths with diverse slip directions (Figure 3.6b). There are three possible reasons to explain the first feature. First, they may reflect the roughness of the nearly flat shear surface. The undulation of the surface can provide thrust mechanisms in some areas and normal mechanisms in others. This is very similar to the nappe structure (Figure 3.7a). This mechanism may explain the events with approximately the same strikes and at about the same depth. Possible events of this kind are events 15, 24, and 34 in the WTR (Figure 3.6a). Second, the low angle faulting may occur in association with folding above a basal decollement. Interlayer or intralayer reverse slip is likely to occur at the flank of a synform where a local intensified compressional regime exists, whereas normal faulting is likely to occur at the hinge of an antiform where a local enhanced extensional regime exists (Figure 3.7b). This mechanism can explain events with the same strike but different depths. Possible events of this kind are events 19 and 31 in the CTR (Figure 3.6a). The third possibility is that the low angle faulting is transferred from major strike-slip faults, being a normal fault at the divergent end and a reverse fault at the convergent end (Figure 3.7c). This is also very likely because southern California is located in a broad transform plate boundary between the North American and Pacific plates. Many strike-slip faults within the boundary are composed of short fault segments that are aligned en echelon. Normal faults have been observed in the releasing bends (Crowell, 1974) or in the dilational jogs (Sibson, 1986), and reverse faults have been observed in the restraining bends (Crowell, 1974) or in the antidilational jogs (Sibson, 1986) of a strike-slip fault zone.

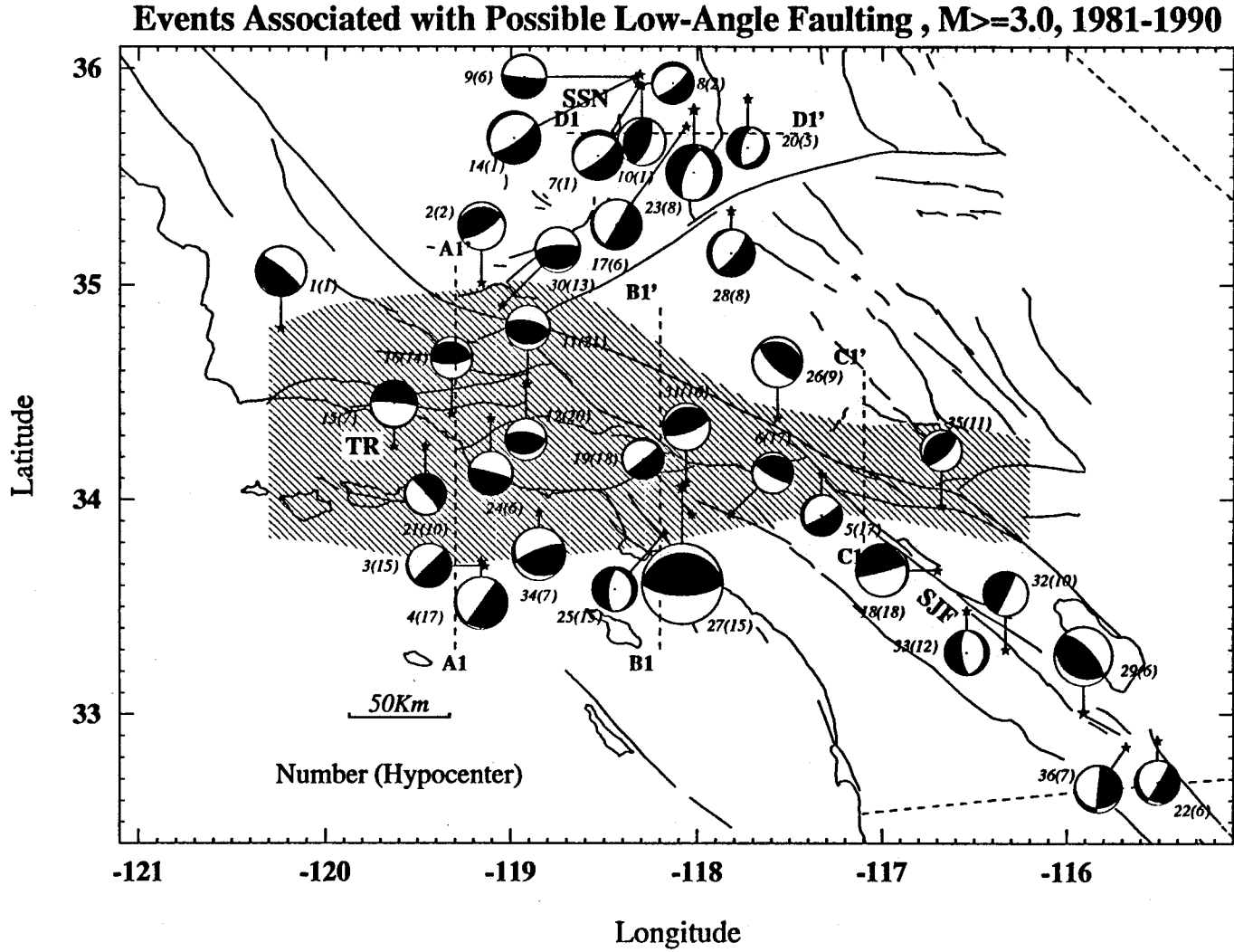
This mechanisms can explain events with strike oblique to the general trending of the strike-slip fault. Examples of this kind are in the SJF zone, such as events 23, 23, and 36 (Figure 3.6a).

In the depth dimension, the low-angle faults are generally shallow (around 5 km) in the southern Sierra Nevada (Figure 3.6b), and the motion there is primarily E-W extension (Figure 3.6a). In contrast, the Transverse Ranges are associated with deeper (more than 10 km) (Figure 3.6b) low-angle faulting events and their motions are mainly N-S contraction (Figure 3.6a). Complexity exists in the Peninsular Ranges and in the Salton Trough. It is evident from Figure 3.6b that there is no single unified, seismically-active detachment in southern California. Instead, the focal mechanisms indicate that the low-angle faults move in various directions and at different depths. Many of them do not correspond to the surface traces of active faults. But this does not exclude the possibility that all these low-angle faults are controlled by deeper large detachment(s) slipping aseismically, above which many low-angle faults branch and occasionally slip seismically.

---

Figure 3.6 (a) Map showing mechanisms associated with possible detachment structures. The numbers in parentheses adjacent to the focal mechanism numbers are hypocenters (in kilometers). 56% of the events are located in or adjacent to the Transverse Ranges as indicated by the shaded area; (b) Cross sections across the WTR, CTR, ETR, and SSNF domains, showing different levels of detachment structures based on focal mechanisms of Figure 3.6a. SCIF, Santa Cruz Island fault; ORF, Oak Ridge fault; APF, Arroyo Parida fault; SYF, Santa Ynez fault; PMF, Pine Mountain fault; SAF, San Andreas fault; PT, Pleio thrust; RF, Raymond fault; SMF, Sierra Madre fault; BF, Banning fault.

Figure 3.6(a)



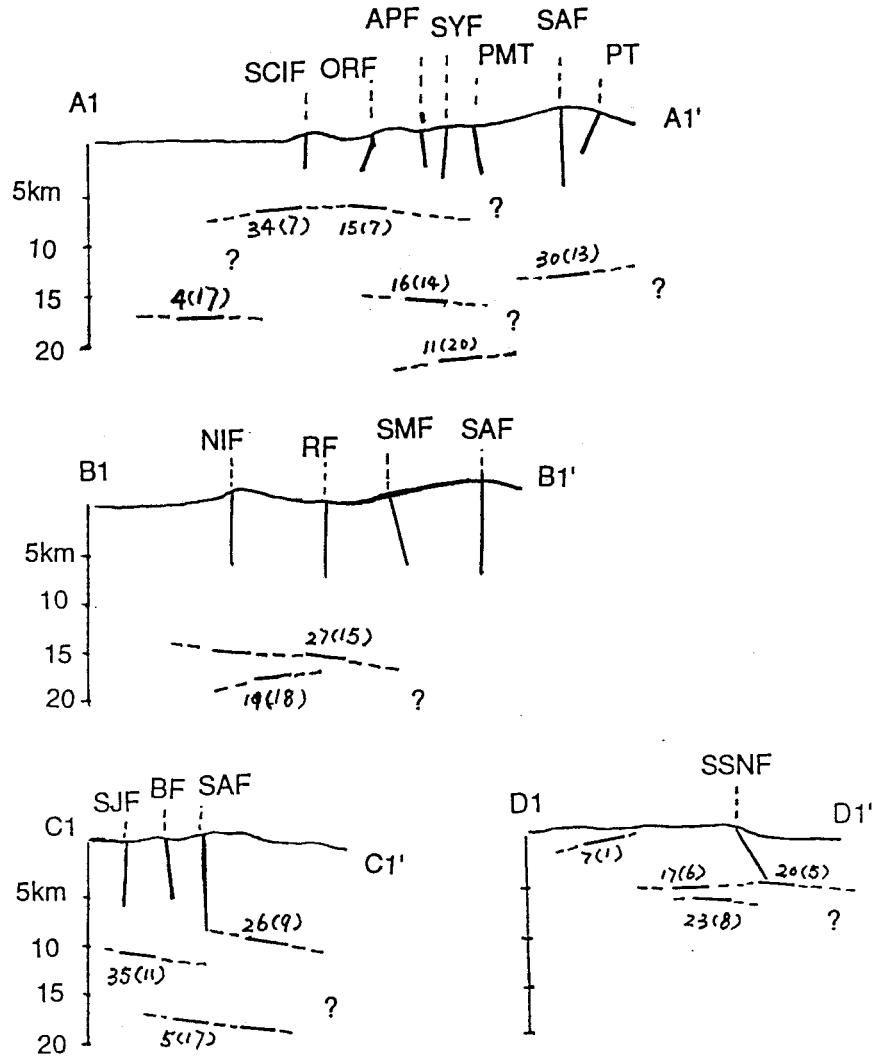


Figure 3.6(b)

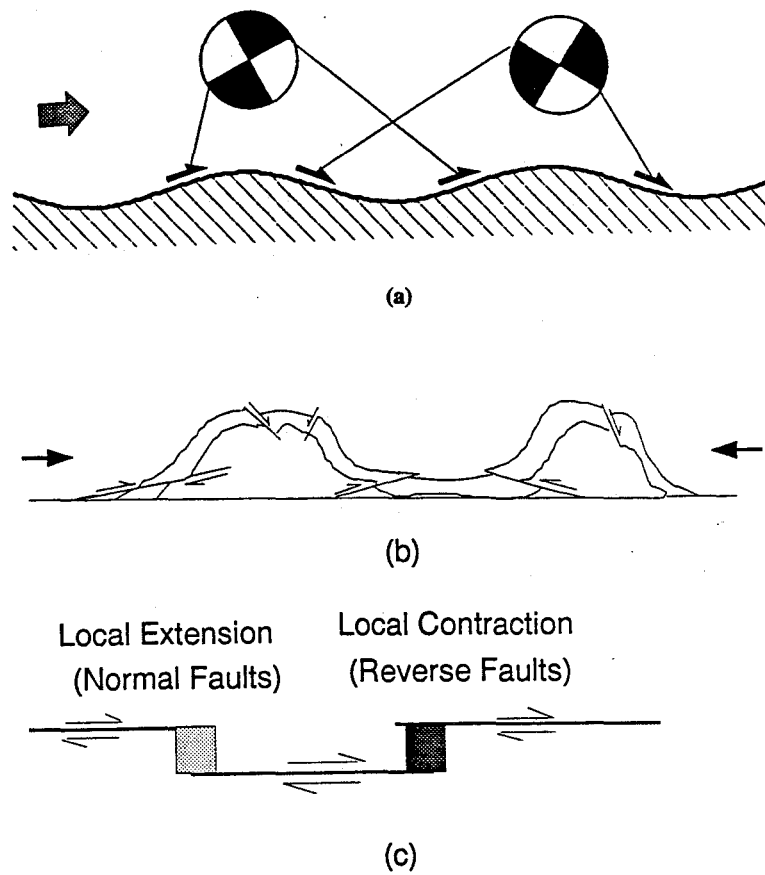


Figure 3.7 (a) Sketchy diagram illustrating the possibilities of coexistence of normal and reverse low-angle faulting mechanisms on a wavy detachment surface; (b) In association with folding above basal shear; (c) En echelon structure on a strike-slip fault can also cause both reverse and normal faults in the jog areas of a strike-slip fault zone.

In addition to the earthquake evidence, other lines of evidence also support the possible existence of detachments: the seismic reflection profiles across the Santa Maria basin and offshore (Henry et al., 1993), and the  $P_g$  velocity variations over the whole southern California region (Hearn and Clayton, 1986). The COCORP seismic profiles revealed gently south-dipping discontinuities in the upper and middle crust beneath the western Mojave block (Cheadle et al., 1986). The major discontinuity is at the middle ( $15 \pm 6$  km) crust and extends northward into the Great Basin, but is lost southward near the San Andreas fault. Cheadle et al. (1986) therefore concluded that the San Andreas fault is a vertical deep fault, while the Garlock fault is not. Recent work by Li et al. (1992), who combined COCORP and gravity data, showed that beneath the southwestern Mojave there exists a gently north-dipping ENE-striking low angle reflector at about 5-6 km depth. Unfortunately, there is no seismicity in the western Mojave Desert to permit us to determine the focal mechanisms there. If the nearly horizontal discontinuities discovered by Cheadle et al. (1986) and Li et al. (1992) are active structures, they may have slipped aseismically without generating earthquakes. This is possible because the Rand schist and Pelona schist are exposed in the north and southern parts of the western Mojave block, and the western Mojave appears to rest on the ductilely-deformable schist.

The implications of Figure 3.6 are schematically visualized in Figure 3.8. It is evident that the seismogenic zone generally is above 15 km, but locally extends down to 25 km in the Transverse Ranges, indicating that the brittle-ductile transition is deepest beneath the Transverse Ranges. Many imbricate reverse faults may be concealed beneath the thick alluvium shed off from the Transverse Ranges. Others may have never reached the surface as indicated by the large fraction of reverse fault events that do not correspond to mapped faults (previous section).

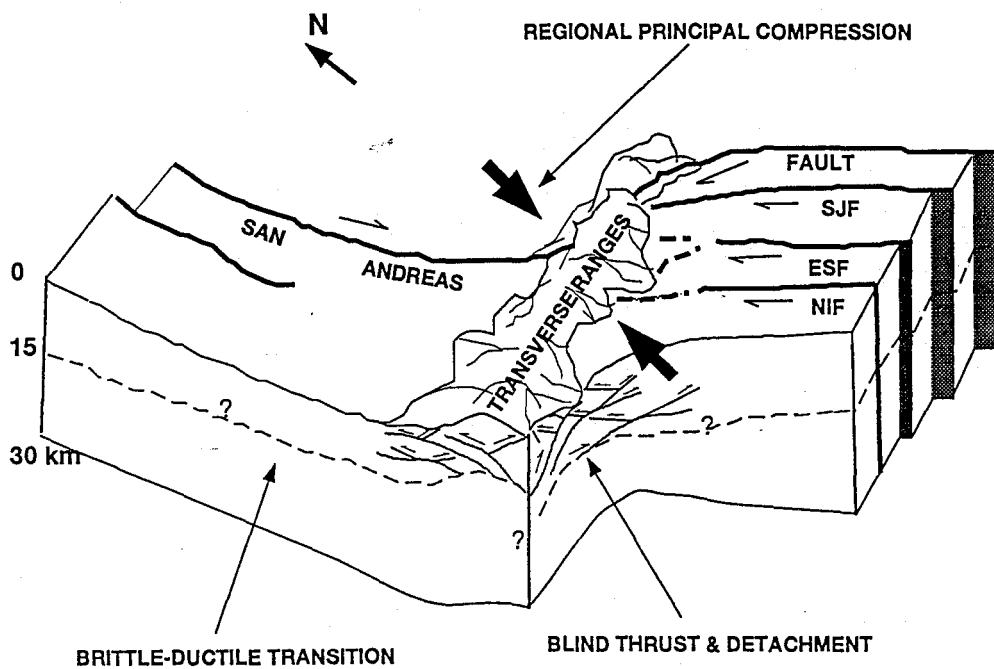


Figure 3.8 Schematic block diagram illustrating possible imbricate or cross blind thrusts beneath the Transverse Ranges. They become shallower away from the ranges. See text for detail.

The kinematic significance of the brittle-ductile transition zone is speculative. It is generally believed that the lower crust is plastic (e.g. Anderson, 1971, Sibson, 1984) and deforms ductilely (e.g. Hadley and Kanamori, 1977, Hearn and Clayton, 1986b), and hence is relatively weak to account for the general absence of seismicity (Chen and Molnar, 1983). It has been suggested that even the giant San Andreas fault may be offset by the regional decollement between the upper and lower crust (Yeats, 1981), or between crust and mantle (Hadley and Kanamori, 1978). Some people believe that the transition zone is a thick interval and the upper and lower crust are strongly coupled together to accommodate the plate motion (e.g. Bird and Rosenstock, 1984, Humphreys and Hager, 1990, Molnar, 1992), although they deform in different styles. Nevertheless, there is no doubt that the Transverse Ranges indicate shortening of the crust in an essentially N-S direction. A significant fraction of the strike-slip motions on the strike-slip faults are apparently converted into movements on reverse faults beneath the Transverse Ranges.

In summary, regional deep (10-20 km) detachment structure is most apparent from earthquakes beneath the Transverse Ranges. The possible detachments in the southern Sierra Nevada are shallow in depth and characterized by extensional rather than contractional motion. Our current data do not indicate the existence of a single unified seismically-active detachment in the seismogenic crust. If the master detachment exists, it may be below the seismogenic depth and slip aseismically.

### 3.3 Seismic Consistency

Seismic consistency (Sc) is a measure of similarity of a group of focal mechanisms (Apperson, 1991). It is defined as the ratio of scalar moment of the total moment tensor to the sum of the scalar moments of individual or normalized moment tensors, i.e.,

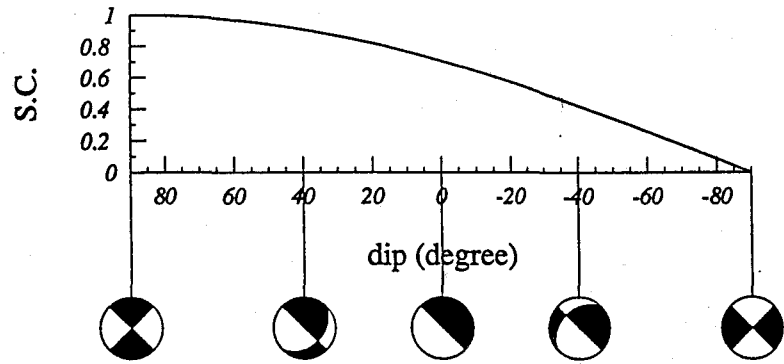
$$Sc = \frac{M_0^{\text{Sum}}}{\sum_{k=1}^N M_0^k}, \quad (3.1)$$

where  $M_0^{\text{Sum}}$  is the scalar moment of the total moment tensor.  $M_0^k$  is the scalar moment of an individual tensor.  $N$  is the total number of events and  $k$  represents the  $k$ th event.

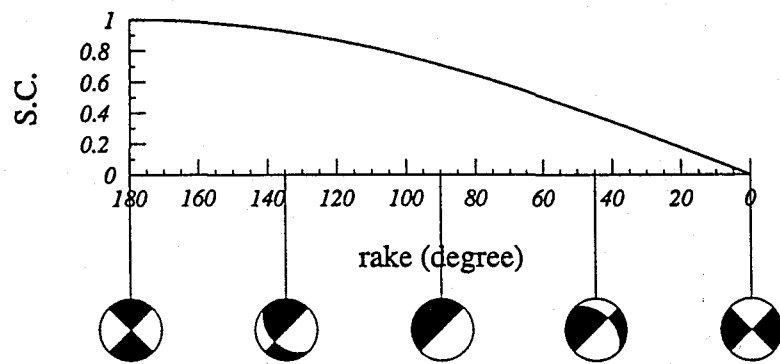
Both  $M_0^{\text{Sum}}$  and  $M_0^k$  should be calculated from the unit tensors which are normalized by their own scalar moments. When the magnitudes do not have a large range of variation, Sc may be approximated using unnormalized tensors. In the following discussions, Sc is calculated using unit tensors unless otherwise specified.

---

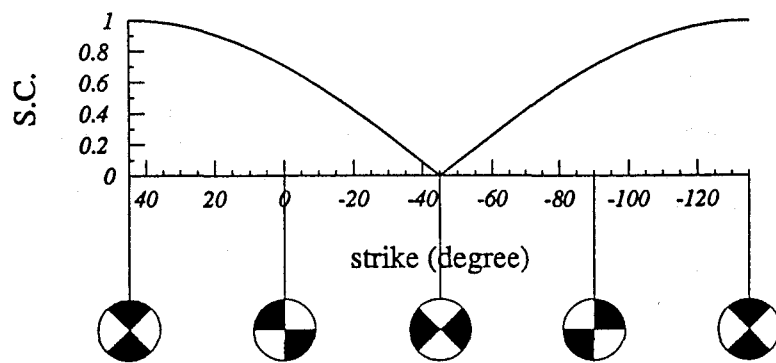
Figure 3.9 Plot showing geometric relationship between parameters of focal mechanisms and the seismic consistency (Sc). The mechanism to the leftmost of each plot is compared with those on the right. (a) Sc vs. dip; (b) Sc vs. rake; (c) Sc vs. strike.



(a)



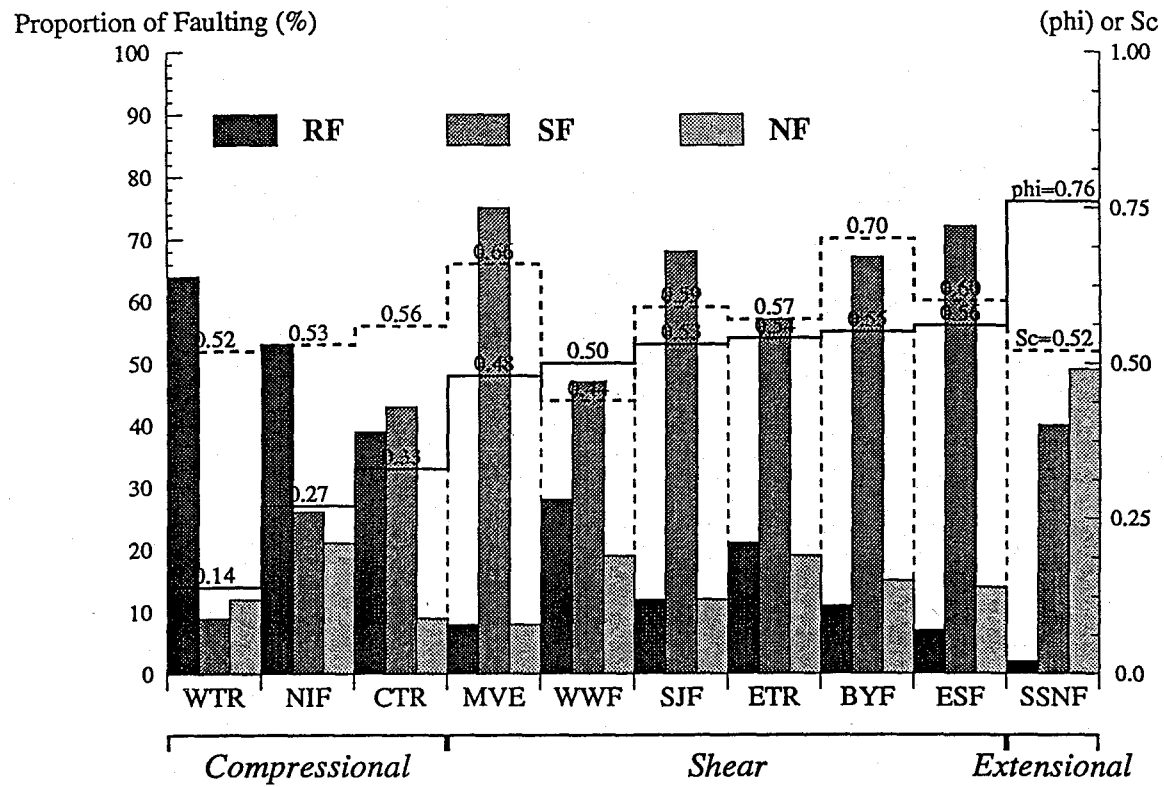
(b)



(c)

Figure 3.9

Figure 3.10



Eq.(3.1) indicates that  $Sc$  can vary from 1, representing two identical mechanisms to 0, representing two opposite mechanisms. Since  $Sc$  is related to moment tensor in a nonlinear way,  $Sc$  does not indicate whether the difference in mechanism is caused by difference in dip, rake, or strike. In other word, the same value of  $Sc$  does not necessarily correspond to the same difference of faulting mechanism in dip, rake, or strike as illustrated in Figure 3.9. In Figure 3.9, the vertical axes are  $Sc$  varying from 0 to 1, the horizontal axis is the source parameters, i.e. dip (Figure 3.9a), rake (Figure 3.9b), and strike (Figure 3.9c). The first mechanism to the left is compared to the mechanisms to the right. Graphically, the similarity of the two mechanisms can be understood as the overlapping areas that have the same polarities on the focal sphere. It can be seen that if two mechanisms are opposite, their  $Sc = 0$ , corresponding to no overlapping areas of the same polarities; if two mechanisms are identical,  $Sc = 1$ , corresponding to complete overlapping areas of the same polarities. For southern California as a whole,  $Sc$  is 0.53 from the background seismicity. For individual domains,  $Sc$  varies from 0.44 in the WWF domain to 0.70 in the BYF domain (Figure 3.10). In general, bimodal or even trimodal distributions of focal mechanisms such as in the WWF and SSNF domains correspond to small values of  $Sc$  whereas unimodal distributions such as in the MVE and BYF domains correspond to large values of  $Sc$ .

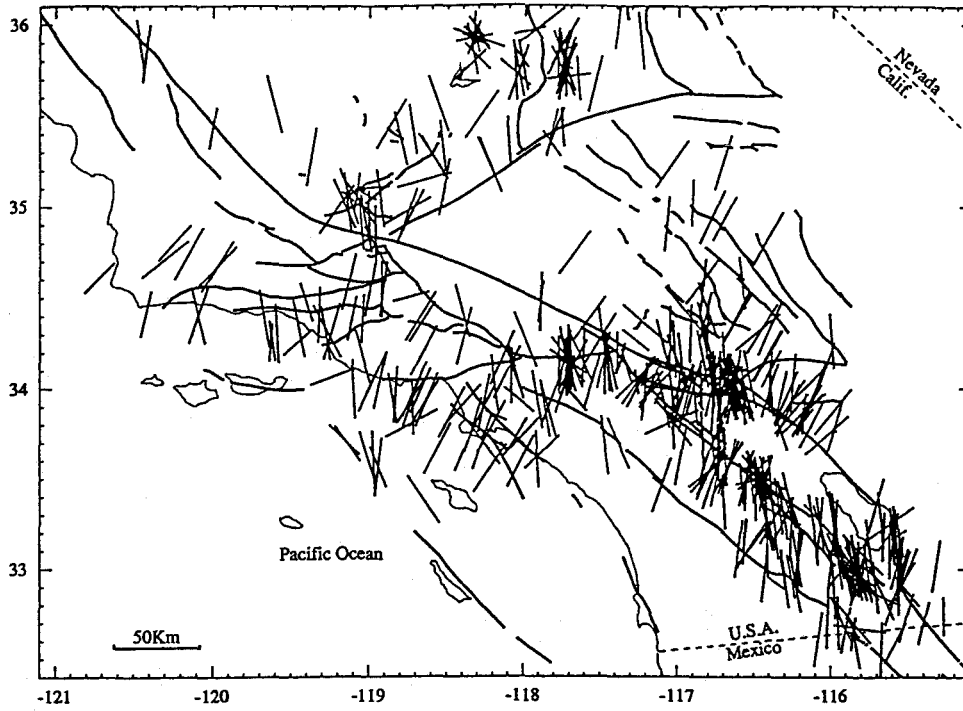
---

Figure 3.10 Plot showing the relationship between distributions of fault patterns, seismic consistency ( $Sc$ ), and the relative values of principal stresses, or the stress ratio,  $\Phi$ , in different domains.  $\Phi = (\sigma_2 - \sigma_3) / (\sigma_1 - \sigma_3)$ , where  $\sigma_1$ ,  $\sigma_2$ , and  $\sigma_3$  are the maximum, intermediate and minimum principal compressive stresses, respectively (see next Chapter 4 for detail).

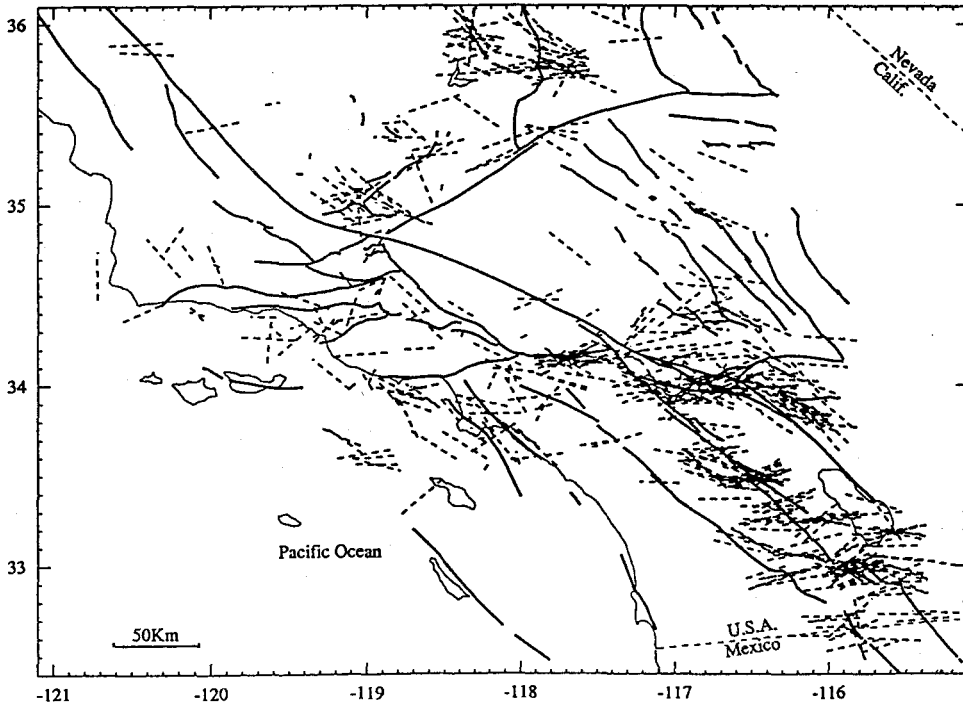
The advantage of using  $S_c$  from Eq.(3.1) is that similarity in a group of focal mechanisms is described numerically or quantitatively. The disadvantage is that the value of  $S_c$  does not indicate whether the dissimilarity in mechanisms results from the differences in strike, dip, rake, or all of these. Hence, it is more practical just to distinguish the four different types of focal mechanisms, i.e., the strike-slip, reverse-slip, normal-slip, and oblique-slip faulting mechanisms. However, we still miss the spatial orientations, even using Frohlich and Apperson's method because their method does not involve fault strikes. Therefore, it is necessary to study the strain patterns. This will be presented in the next chapter.

### **3.4 P, T, and N Axes Orientations**

Earthquake focal mechanisms are commonly represented by the principal strain axes, i.e., P, T, and N axes. These axes are not necessarily the same as the principal stress axes, although in many cases, the average directions of the P axis are close to the principal maximum compressive stress axis (next chapter). Figure 3.11 (a) shows the horizontal projection of P axes from individual earthquakes. The length of the bars is proportional to the plunge angle of the axes (the same for Figure 3.11b). It can be seen that the majority of P axes are oriented N-NW, particularly in the SJF and the ETR domains. The CTR domain shows dominant N-S directions while the WTR shows both N-NE and N-NW directions. Large scatter exists in the WWF and SNNF domains. The T axes are mainly oriented E-W and vary more widely from place to place (Figure 3.11b). In general, P axes are more stable and consistently in the N-S direction whereas the T axes are less stable, not only in orientation, but also in plunge angle (Figure 3.12). This pattern partly reflects the fact that both reverse and strike-slip faulting events coexist regionally. Even within individual domains, P axes show very stable orientation while both T and N axes vary (Figure 3.13).

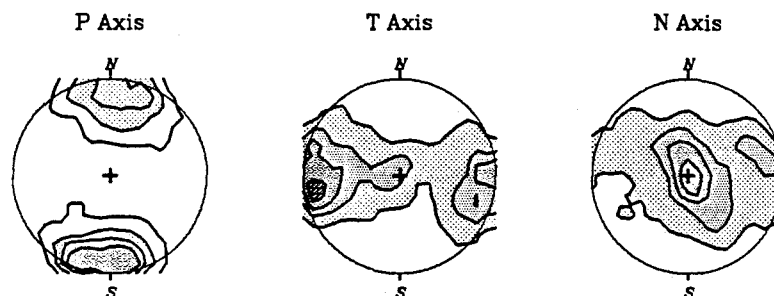


(a)



(b)

Figure 3.11 Horizontal projection of P (a) and T (b) axes from individual earthquakes. The length of bars is proportional to the plunge angles of the axes, with maximum for horizontal axes and zero for vertical axes.



$M \geq 3.0$ , 1981-1990  
Southern California ( $I=1.0\%$ )

Figure 3.12 Equal-area projection of the P, T, and N axes. It shows that P axes are persistent throughout southern California whereas T and N axes vary, both in orientation and plunge as indicated by the large girdles. I: Contour interval.

---

Figure 3.13 Equal-area projection of P, T, and N axes for each domain. Overall, the P axes are very stable, being oriented dominantly N-S whereas the T and N axes are scattered. Note the large plunge of P axes in the SSNF domain. Others are near horizontal. Earthquakes used for this figure are again the background seismicity. (a) P axis; (b) T axis; (c) N axis.

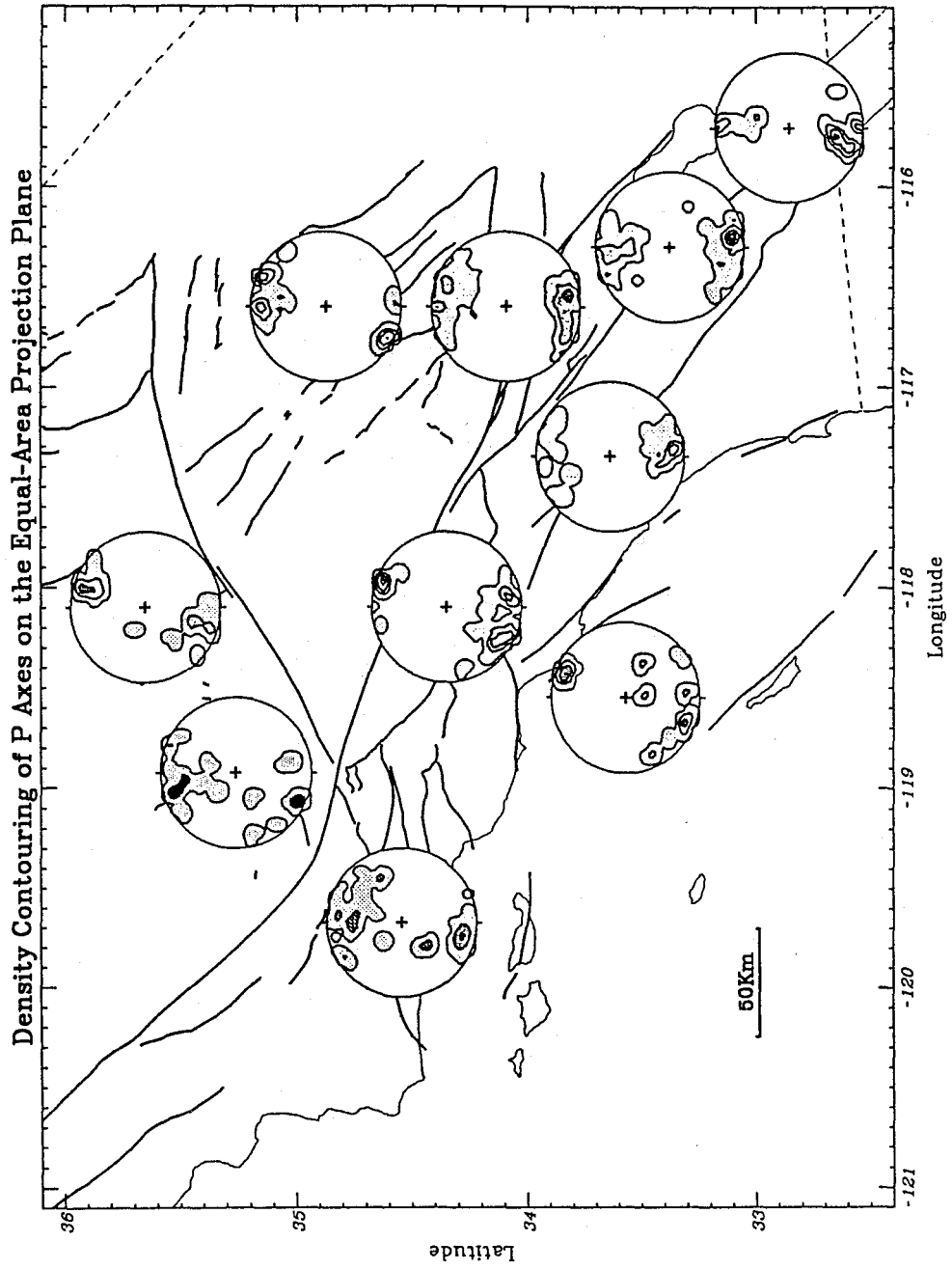
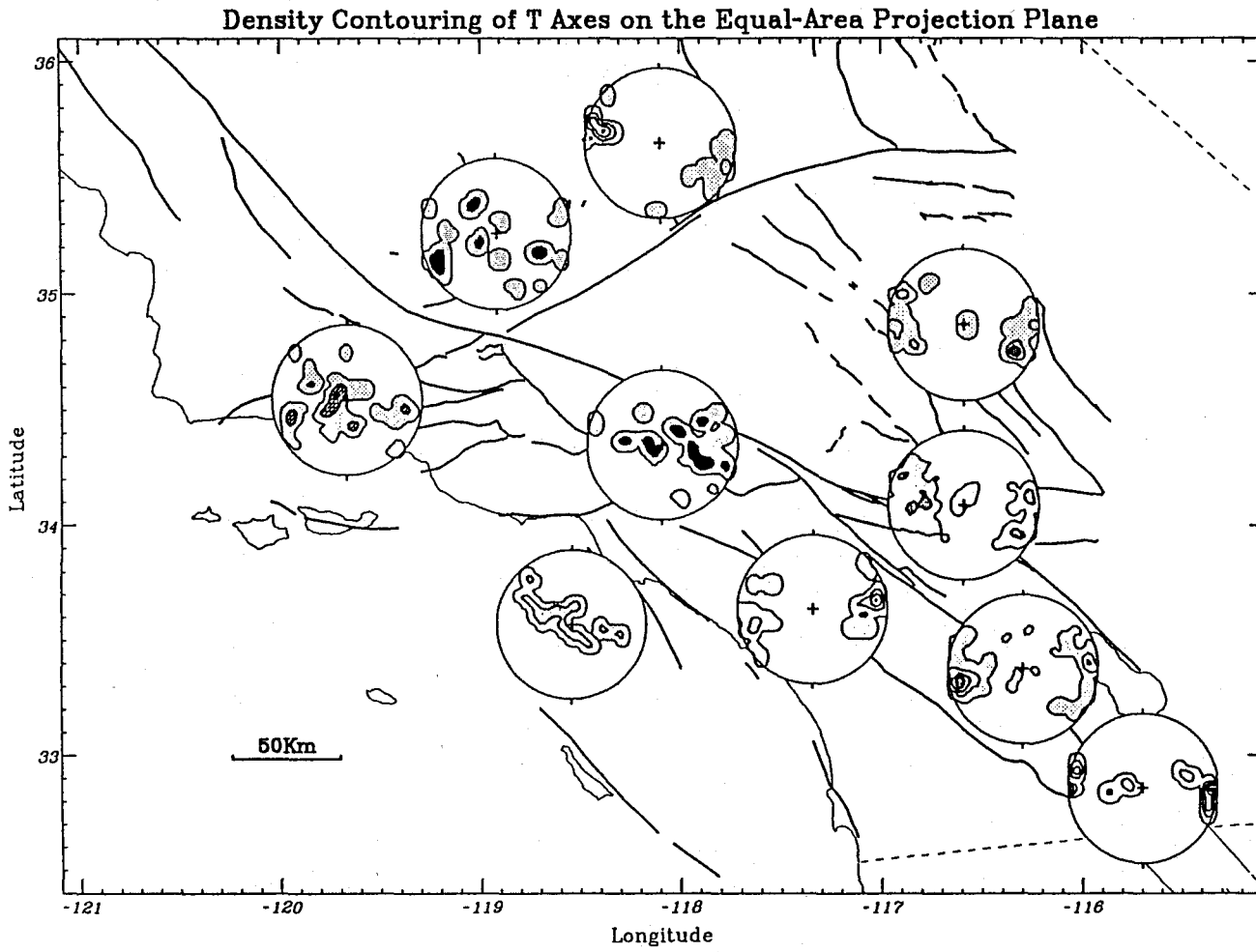


Figure 3.13 (a)

Figure 3.13 (b)



Density Contouring of N Axes on the Equal-Area Projection Plane

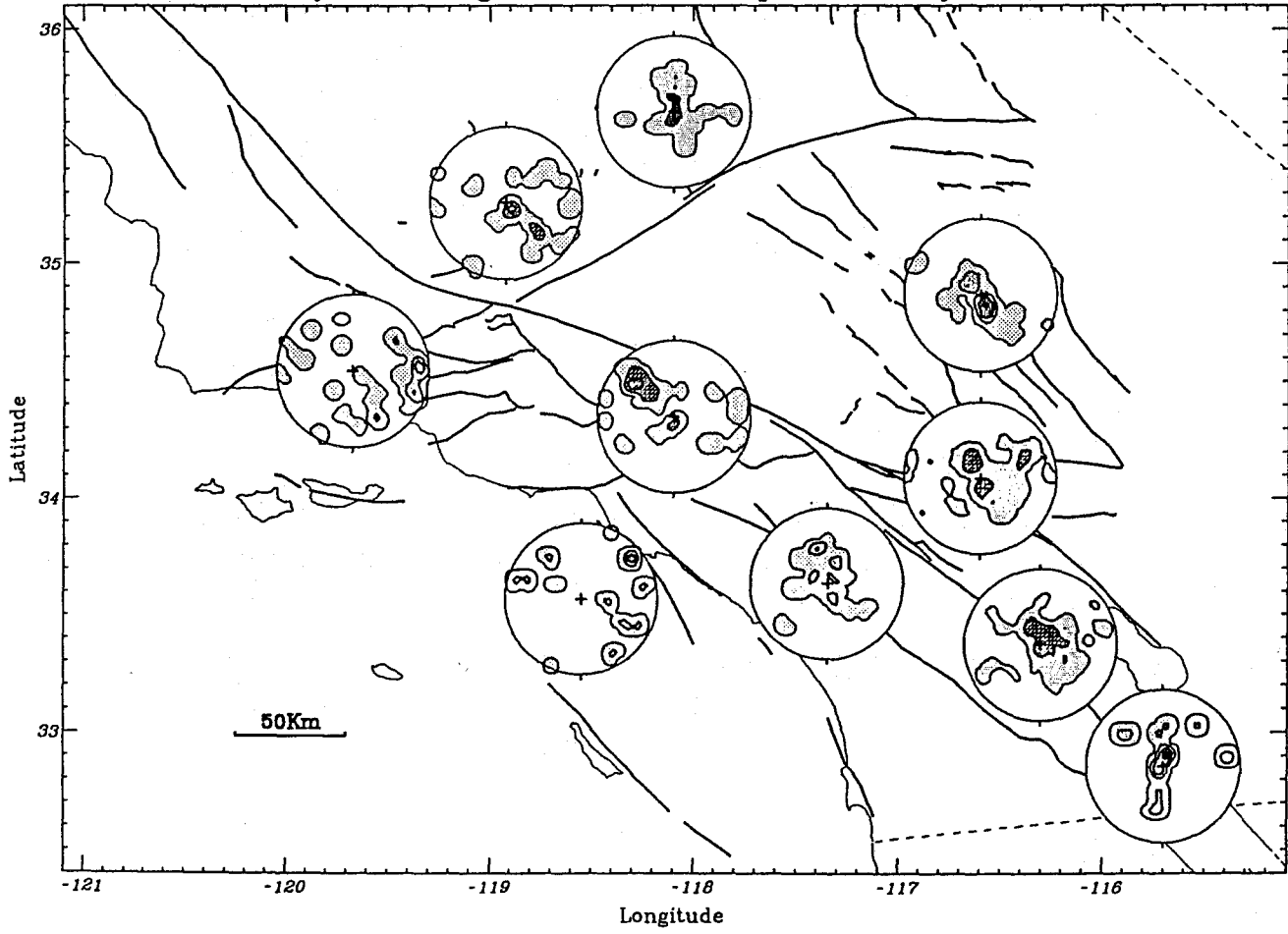


Figure 3.13 (c)

### 3.5 Summary

The characteristics of source mechanisms in southern California can be summarized as the following:

(1) The proportions of strike-slip, reverse, normal and oblique-slip faulting events for the interval 1981-1991  $3.0 \leq M \leq 6.0$  background seismicity are about 7:3:2:1. These proportions of mechanisms, to the first order, are similar to those of the interval 1918-1994  $M \geq 5.5$  earthquakes;

(2) Of the 505 fault plane solutions, 36 of them are possibly caused by slip on low-angle faults. 56% of these events are located in or adjacent to the Transverse Ranges. The depths of the possible detachments vary from 1 km in the SSNF to 20 km in the Transverse Ranges. They indicate near E-W extensional movements in the SSNF and near N-S compressional movements in the Transverse Ranges. The available fault planes solutions so far do not appear to indicate the existence of a single unified seismically-active detachment in the seismogenic crust. If the master detachment exists, it may be located below the seismogenic depth and slip aseismically;

(3) Focal mechanisms are very similar in the BYF, MVE, SJF, and ESF domains ( $Sc > 0.60$ ), but are not very similar in the WWF, WTR, NIF SSNF, CTR, and ETR domains ( $Sc < 0.60$ );

(4) Orientations of P axes are very stable while those of T and N axes are variable from place to place. P axes are nearly horizontal and oriented nearly N-S, whereas T axes are dominantly vertical and oriented nearly E-W. The neutral axes are also variable from domain to domain.

## Chapter 4

### Seismic Strain and Tectonic Stress

#### 4.1 Introduction

Two pieces of information can be extracted from the instrumentally recorded seismic data. They are (1) the total released seismic strain and (2) the regional tectonic stress field under which faulting occurs. In an isotropic and homogeneous elastic medium, strain is linearly related to stress by Hook's law. In this case, the principal axes of the stress tensor coincide with those of the strain tensor, i.e. the maximum deformation corresponds to the maximum stress. But the strain and stress we want to discuss herein are defined somewhat differently and have special meanings. The medium we deal with here is the Earth's crust that is highly heterogeneous in strength and elastic properties. We consider a uniform regional tectonic stress field under which the Earth's crust fractures. The deformation in response to the uniform tectonic stress is complex as a result of the heterogeneity of the mechanical properties of the crust. In this chapter, we examine how heterogeneous a region is by studying the differences between the strain and stress tensors. The strain used here is a measure of the total deformation of a geological domain as a whole.

The procedures we employ are the following. After determining the fault plane solutions of background seismicity in each domain, which are listed in the appendix (see also, Huang et al., 1993), we perform numerical inversions from the slip vector data to obtain the tectonic stress fields, and determine the seismic strain fields by tensorial summations of individual seismic moment tensors (see also Huang et al., 1992). These ideas are graphically illustrated in Figure 4.1 and will be explained in detail below.

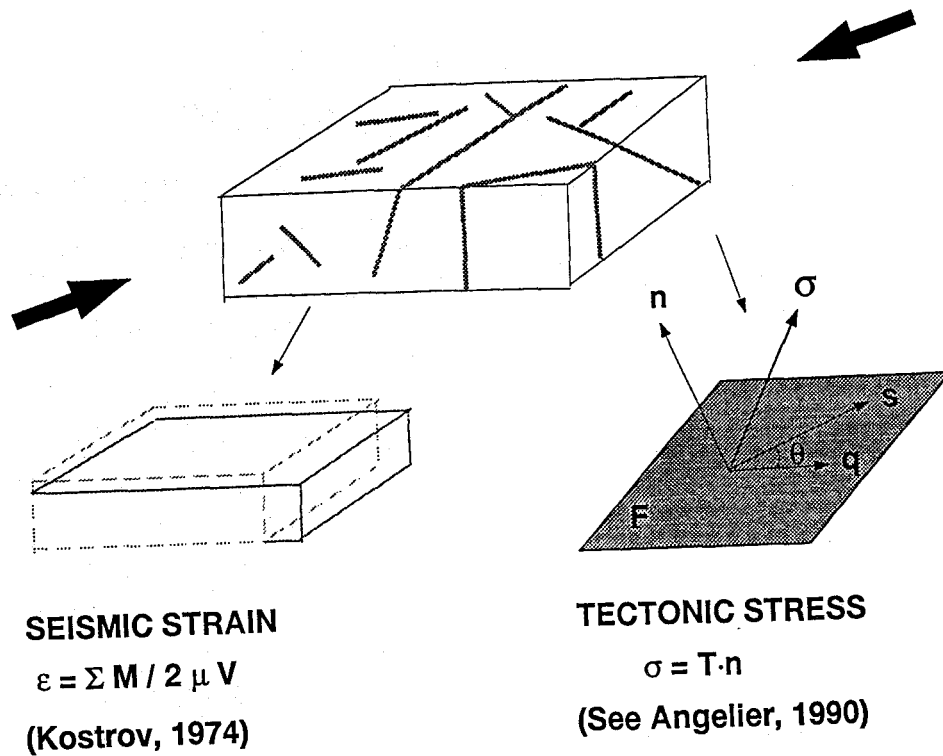


Figure 4.1 Graphic illustration of seismic strain and tectonic stress. The seismic strain is a measure of total seismic deformation averaged over a volume. The tectonic stress is the stress under which all diversely-oriented faults slip within the deforming volume.  $M_{ij}$ , seismic moment tensor;  $V$ , volume of the deforming domain;  $\mu$ , shear modulus;  $T$ , stress tensor;  $n$ , vector normal to the fault plane,  $F$ ;  $\sigma$ , stress acting on  $F$ ;  $s$  and  $q$  are observed and predicted slip vectors, respectively.

## 4.2 Seismic Strain Tensor

The seismic strain tensor  $\epsilon_{ij}$  is obtained using Kostrov's (1974) formula:

$$\epsilon_{ij} = \frac{1}{2 \cdot \mu \cdot V} \sum_{n=1}^N M_{ij}^n, \quad (4.1)$$

where  $\mu$  is the shear modulus;  $V$ , deforming volume;  $N$ , the total number of events;  $M_{ij}$ , individual seismic moment tensors. The magnitudes of deformation can be calculated from Eq.(4.1) once  $V$  is specified (Huang et al., manuscript in preparation). We herein consider orientations, only. Hence, the total moment tensor  $\sum M_{ij}$  is used to represent the strain field. The directions of the principal strain axes are then easily determined by finding the eigenvectors of  $\epsilon$ .

To display the seismic moment tensor or seismic strain tensor graphically, we use the P-wave radiation pattern plotted on the focal sphere. If the P-wave polarity is up, we use a plus symbol to represent it; if the P-wave polarity is down, we leave the sphere blank. The P-wave radiation pattern presented this way gives us an intuitive picture of how close the source is to a double-couple. For a pure double-couple source, the P-wave radiation patterns are represented by up and down quadrants separated by the two conjugate fault planes. However, when the total moment tensor is not a pure double-couple, which is usually the case, the P-wave radiation pattern may not be represented by two conjugate fault planes as exemplified in Figure 4.2.

---

Figure 4.2 Plots showing P wave radiation patterns of the total moment tensors obtained from two moment tensors of the same sizes. (a) mixture of strike-slip and normal faulting on the releasing bend of a right-lateral shear zone; (b) mixture of strike-slip and thrust faulting on the restraining bend of a right-lateral shear zone; (c) Opposite mechanisms give zero total strain as if no deformation had occurred.

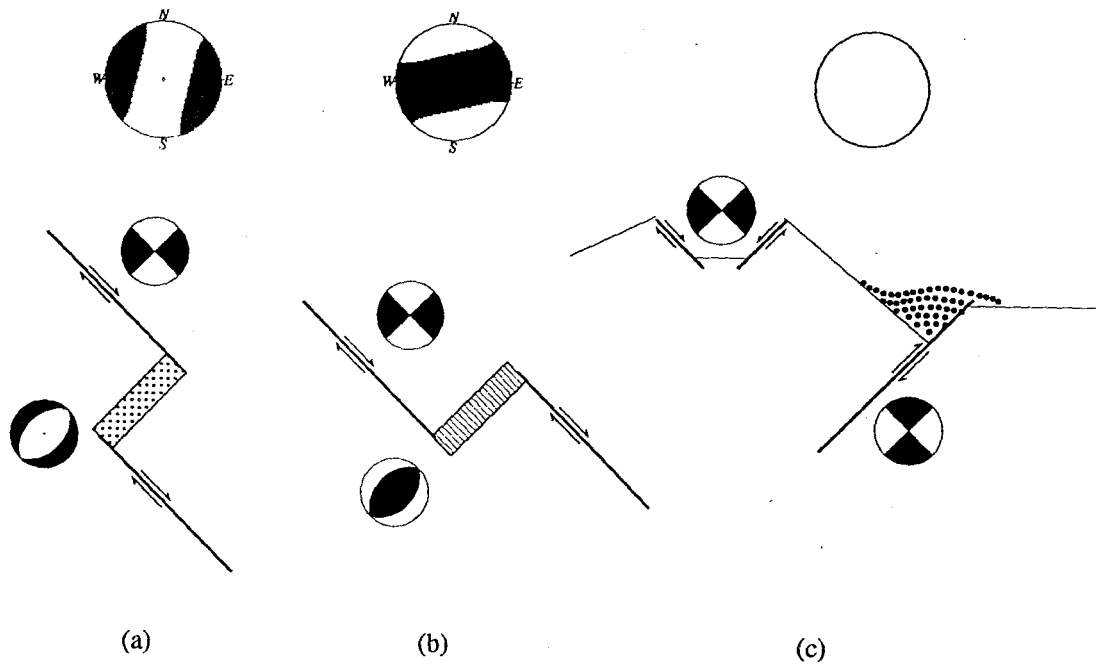


Figure 4.2

### 4.3 Tectonic Stress Tensor

Very similarly, but in a less straightforward manner, the stress tensors,  $\mathbf{T}$ , are obtained by performing numerical inversions of a group of slip vectors. By definition, the stress,  $\boldsymbol{\sigma}$ , acting on the fault plane,  $\mathbf{F}$ , is related to  $\mathbf{T}$  by

$$\boldsymbol{\sigma} = \mathbf{T} \cdot \mathbf{n} , \quad (4.2)$$

where  $\mathbf{n}$  is the vector normal to the fault plane (see Angelier, 1990). The objective for stress inversion is to find a common uniform stress field  $\mathbf{T}$  that will best fit all observed slip directions, i.e., the predicted slip vector from  $\mathbf{T}$  will have the minimum angle differences from the observed slip vectors. The basic assumption is that all faults with diverse orientations slip in response to a common stress tensor regardless of their strength (cohesion or friction). The magnitudes of slip are not important. Only the directions are involved. There are basically two algorithms used to find  $\mathbf{T}$  (see Angelier, 1984). One is a simplified linear approach (Michael, 1984, Angelier, 1990). The other is non-linear or the grid-search technique (Gephart and Forsyth, 1984). For fast inversion with appropriate resolution, we follow Angelier's (1990) method. The problem for stress inversion using fault plane solutions is to choose one of the conjugate planes. In our algorithm, fault planes that can collectively produce a minimum dispersion parameter are chosen unless we have other independent evidence to determine the actual fault planes. Absolute value of stress is not derived from the stress inversion. But the stress ratio  $\Phi$  is obtainable.  $\Phi$  is defined as  $\Phi = (\sigma_2 - \sigma_3) / (\sigma_1 - \sigma_3)$ , where  $\sigma_1$ ,  $\sigma_2$ , and  $\sigma_3$  are the maximum, intermediate, and minimum principal compressive stresses, respectively.  $\Phi$  reflects the shape of the stress ellipsoid and bears information on faulting patterns (Hill, 1982, Huang et al., 1994) (further discussion below).

#### 4.4 Physical Implications

It is clear from the above descriptions that the strain and stress tensors are derived independently, although they are from the same data set. The strain tensor determined by Eq.(4.1) represents irrotational translation and does not change regardless of which of the conjugate planes is used (see Jackson and McKenzie, 1988), whereas the stress tensor obtained from the inversions represents the deviatoric stress and is fault plane dependent. The relationship between the strain and stress tensors is linear for an isotropic and homogeneous medium, but nonlinear and complex for a nonisotropic and heterogeneous medium (see Ramsay, 1967). It is well established that under a given stress field ruptures begin first on the weak planes that require the minimum shear stress to generate slip. Therefore, comparison between seismic strain and tectonic stress tensors can provide us information on the complexity of fault geometry and variations of fault strength. If the strain and stress tensors are similar, it implies either that the fault geometry and/or strength are relatively uniform, or that the weak zones are coincidentally oriented in the direction favorable for movement under the regional tectonic stress field. On the other hand, if they are dissimilar, it means that the deforming domain is not uniform in fault geometry and significant weak zone(s) may exist. The difference between the principal strain and stress axes may be as large as  $90^\circ$  (McKenzie, 1969) (Figure 4.3).

---

Figure 4.3 Plot illustrating inconsistency of principal directions between stress and strain tensors due to the existence of weak zone(s).

### Graphic Illustration of Principal Stress and Strain Axes, and Their Relation to Faulting

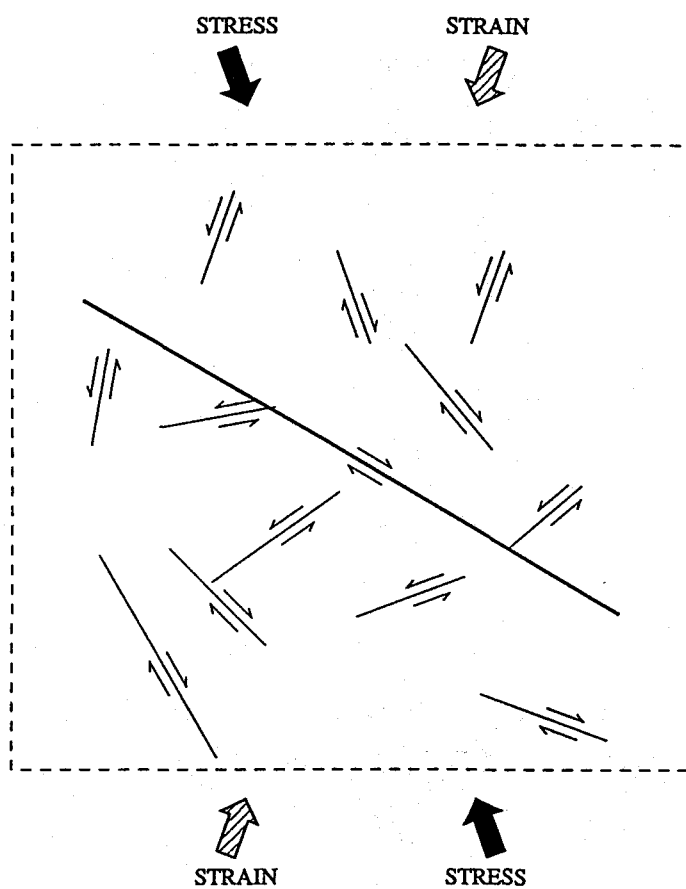


Figure 4.3

#### 4.5 Results in Southern California

For intuitive comparisons, we plot the strain tensors in terms of P-wave radiation patterns. The principal strain axes are from the best double-couple part of the total moment tensors. For the stress tensors, we plot the predicted mechanisms based on the inverted principal stress axes (Figure 4.4). We can see that the stress fields are favorable for strike-slip faulting in most of the deforming domains, but for normal and reverse faulting in the SSNF and WTR, respectively. In general, the maximum principal stress axes ( $\sigma_1$ ) are similar in all of the region, oriented  $N6^\circ E \pm 11^\circ$ . The maximum principal strain axes ( $\epsilon_1$ ) are also dominantly oriented in the N-S direction, but varying in a wider range ( $N5^\circ \pm 21^\circ$ , Table 4.1). In order to measure quantitatively the similarity of the stress and strain tensors, we use two different methods and compare their results. The first is herein termed tensor difference (TD), which is a measure of the differences of orientations (both direction and inclination) of the principal axes as defined in the footnotes of Table 4.1. TD varies from 0 to 1, corresponding, respectively, to the minimum and maximum differences of the two tensors. The second parameter is the seismic consistency (Sc) introduced by Apperson (1991), which is expressed by the ratio of the scalar moment of the total moment tensor to the sum of the scalar moments of the individual moment tensors (Apperson, 1991). Like TD, Sc also varies from 0 to 1, corresponding, respectively, to the lowest and highest consistencies of the two tensors. In general, a small TD corresponds to a large Sc and a large TD to a small Sc. But exceptions exist as for the case in the ESF domain (Figure 4.5). It should be pointed out that the same value of Sc or TD does not reflect whether the difference is caused by the dip, rake, or strike of a focal mechanism. For instance, in the WWF and ESF domains, both have about the same value of Sc ( $\approx 0.93$ ) and TD ( $\approx 0.4$ ), but the strain patterns in these two domains are very different. Reverse faulting is dominant in the WWF while strike-slip faulting is dominant in the

ESF (Figure 4.4). Therefore, the best way to compare the stress and strain tensors is to plot both Figures 4.4 and 4.5.

Table 4.1 Listed Orientations of Principal Axes

Domain	Tectonic Stress ( $\sigma$ )						Seismic Strain ( $\epsilon$ )						TD	Sc
	$\alpha_1$	$\lambda_1$	$\alpha_3$	$\lambda_3$	$\alpha_2$	$\lambda_2$	$\theta_1$	$\gamma_1$	$\theta_3$	$\gamma_3$	$\theta_2$	$\gamma_2$		
SSNF	5	46	104	8	201	43	13	5	282	7	136	81	0.39	0.9311
WWF	4	16	98	13	225	70	24	1	115	43	293	47	0.38	0.9290
MVE	15	8	284	11	139	76	26	8	296	2	188	82	0.24	0.9791
WTR	12	1	106	71	282	19	22	7	160	80	291	6	0.27	0.9425
CTR	5	2	96	24	271	66	176	10	9	80	267	2	0.55	0.8655
ETR	189	6	282	22	84	67	157	29	267	31	33	45	0.28	0.9277
NIF	197	20	290	6	35	69	10	2	110	77	279	13	0.46	0.8232
ESF	355	29	90	11	198	59	9	1	279	12	102	78	0.41	0.9327
SJF	179	1	270	8	83	82	345	13	251	17	110	69	0.19	0.9488
BYF	191	5	101	4	331	84	177	23	267	2	3	66	0.20	0.9542

$\alpha_i$ , Azimuth of  $\sigma_i$  ( $i=1, 2$ , and  $3$ );  $\lambda_i$ , Inclination of  $\sigma_i$ ;  $\theta_i$ , Azimuth of  $\epsilon_i$ ;  $\gamma_i$ , Inclination of  $\epsilon_i$ . TD, Tensor difference measured by the directional and inclinational differences of principal axes of two tensors. TD varies between 0 and 1, representing, the minimum (identical) and maximum differences of  $\sigma$  and  $\epsilon$ , respectively.  $TD = [\delta_1^2 + \delta_2^2]^{1/2} / \sqrt{2}$ , where  $\delta_1 = [ \sum_{i=1}^3 (\alpha_i - \theta_i)^2 ]^{1/2} / 90 \cdot \sqrt{3}$ ,  $\delta_2 = [ \sum_{i=1}^3 (\lambda_i - \gamma_i)^2 ]^{1/2} / 90 \cdot \sqrt{3}$ . Note that the directional difference is not the same as the azimuthal difference. The former ranges from  $0^\circ$  to  $90^\circ$  whereas the latter ranges from  $0^\circ$  to  $360^\circ$ . Sc, seismic consistency (see Apperson, 1991).

Figure 4.4

### Comparisons of Strain and Stress Tensors from Earthquakes, 81-91

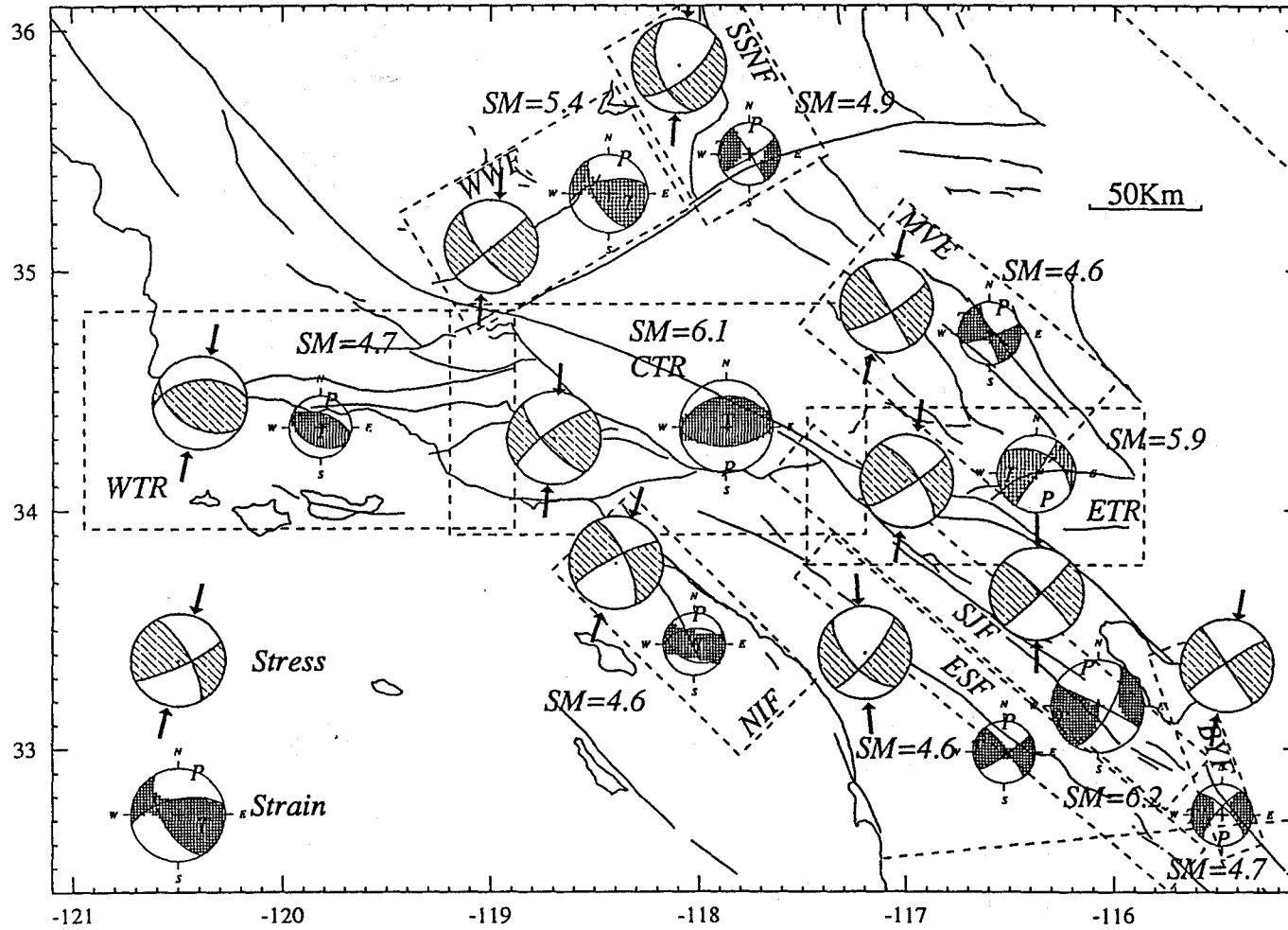


Figure 4.4 Comparison of seismic strain and tectonic stress obtained from the background seismicity ( $3.0 \leq M \leq 6.0$ , 1981-1991). SM: equivalent magnitude from the total moment tensor.

Overall, the directional differences are  $10^\circ$  to  $20^\circ$  for the compressional axes, but up to  $87^\circ$  for the extensional (CTR) and  $84^\circ$  for the neutral axes (ESF) between the stress and strain tensors (Table 4.1). Except for the SSNF domain, the inclinational differences are less than  $30^\circ$  for the compressional axes, but up to  $70^\circ$  (NIF) for the extensional and  $64^\circ$  (CTR) for the neutral axes (Table 4.1). Therefore, the compressional axes are very stable whereas the extensional and the neutral axes fluctuate.

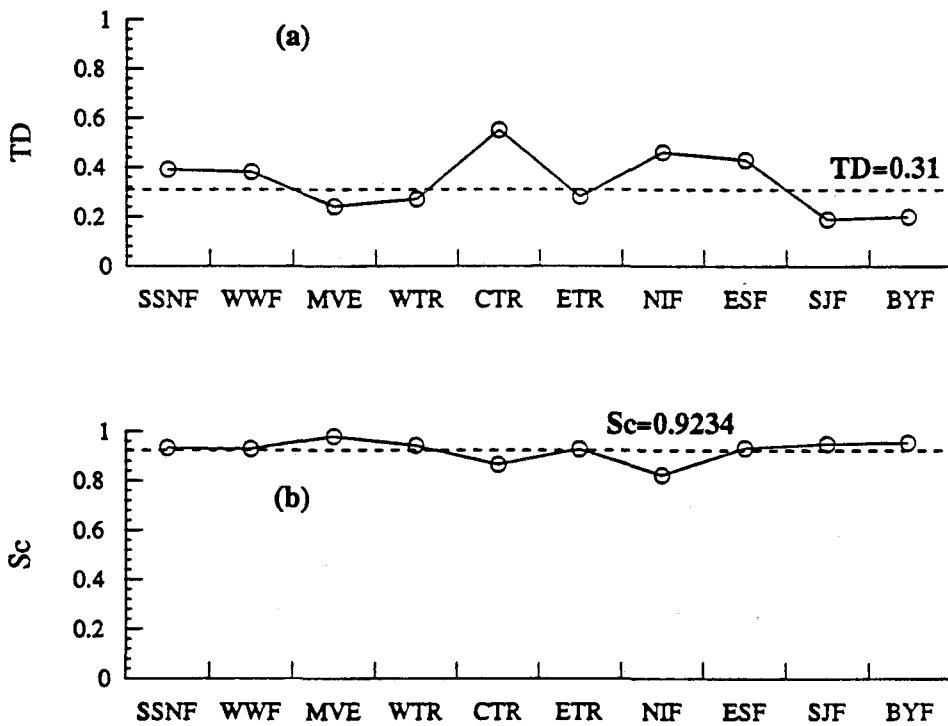


Figure 4.5 Plots showing similarities of the stress and strain tensors measured by the tensor difference (TD) (a) and the seismic consistency (Sc) (b) in each domain labeled on the horizontal axes.

#### 4.6 Geological Insights

The N-S-oriented near horizontal compression or convergence in southern California has long been recognized geologically, geophysically, and geodetically (see Hill and Dibblee, 1953; Zoback and Zoback, 1980; Mount and Suppe, 1992; Pechman, 1987; Jones, 1988; Hauksson, 1990; Savage, 1983). But we feel that it is important to distinguish seismic strain and tectonic stress, since they have different physical meanings. As early as in 1953, Hill and Dibblee, based on the nature and geometry of the San Andreas fault, Garlock fault, and the Big Pine fault, proposed two possibilities, N-S compression and NE-SW shear. They preferred the left-lateral NE-SW shear because they attempted to explain the NW-trending fold axes in the Coast Ranges, and the E-W-trending fold axes as well as the reverse faults in the Transverse Ranges. Allen (1957) noted the coexistence of strike-slip and reverse faults in the eastern Transverse Ranges, and inferred that the N-S-oriented  $\sigma_1$  was stable while  $\sigma_2$  was changeable over time. Like Hill and Dibblee, Davis and Burchfiel (1973) emphasized the role of NE-SW couple shear. The westward extension of the Death Valley and the Great Basin Province was carried out primarily on the left-lateral E-NE-striking Garlock fault, which they called an intracontinental transform fault, and caused the bending of the San Andreas fault. Weldon and Humphreys (1986) attributed the N-S compression in the Transverse Ranges to the left-stepping of the San Andreas fault, and inferred that major faults may exist offshore to account for the N-S shortening in the western Transverse Ranges. It is therefore very evident that southern California has long been subjected to N-S to N-NE regional compression. Our analysis shows that such a stress regime is still dominant, and plays an important role in the complex fault kinematics of southern California.

#### 4.7 Stress Ratio $\Phi$

By definition (see 4.3), the stress ratio  $\Phi$  can vary from 0 to 1, indicating uniaxial and biaxial compression, respectively. The values of  $\Phi$  can be obtained using earthquakes over the whole seismogenic depth range. In this case,  $\Phi$  represents an average. If the seismic data set is large enough, we can compare values of  $\Phi$  below and above 10 km depth to see whether a significant change in the state of stress with depth exists or not. The results are plotted in Figure 4.6. Except for the SSNF and MVE domains where events below 10 km are too small in number to do the inversion, all other domains can be examined this way (Figure 4.6a). Significant changes in the stress tensors are obvious in the WWF, WTR, NIF, ETR, ESF and SJF domains. The apparent changes of state of stress in the SJF and ESF domains may result from the fact that many of the events in these two domains (northern segments of the SJF and ESF) are within the ETR domain where many deep (> 10 km) events exist. Figure 4.6b shows that the values of  $\Phi$  over the whole seismogenic depth range are not a simple arithmetic average of those below and above 10 km because of the nonlinear relationship between  $\Phi$  and the stress tensor. For simplicity, the discussion below is based on the values of  $\Phi$  obtained for the whole seismogenic depth.

---

Figure 4.6 Plots showing vertical variations (below and above 10 km) of the stress tensors. (a) Predicted faulting patterns from the inverted stress tensors; (b) Variation of  $\Phi$  in individual domains. The dashed lines represent  $\Phi$  obtained using the total mechanisms throughout the seismogenic depth.

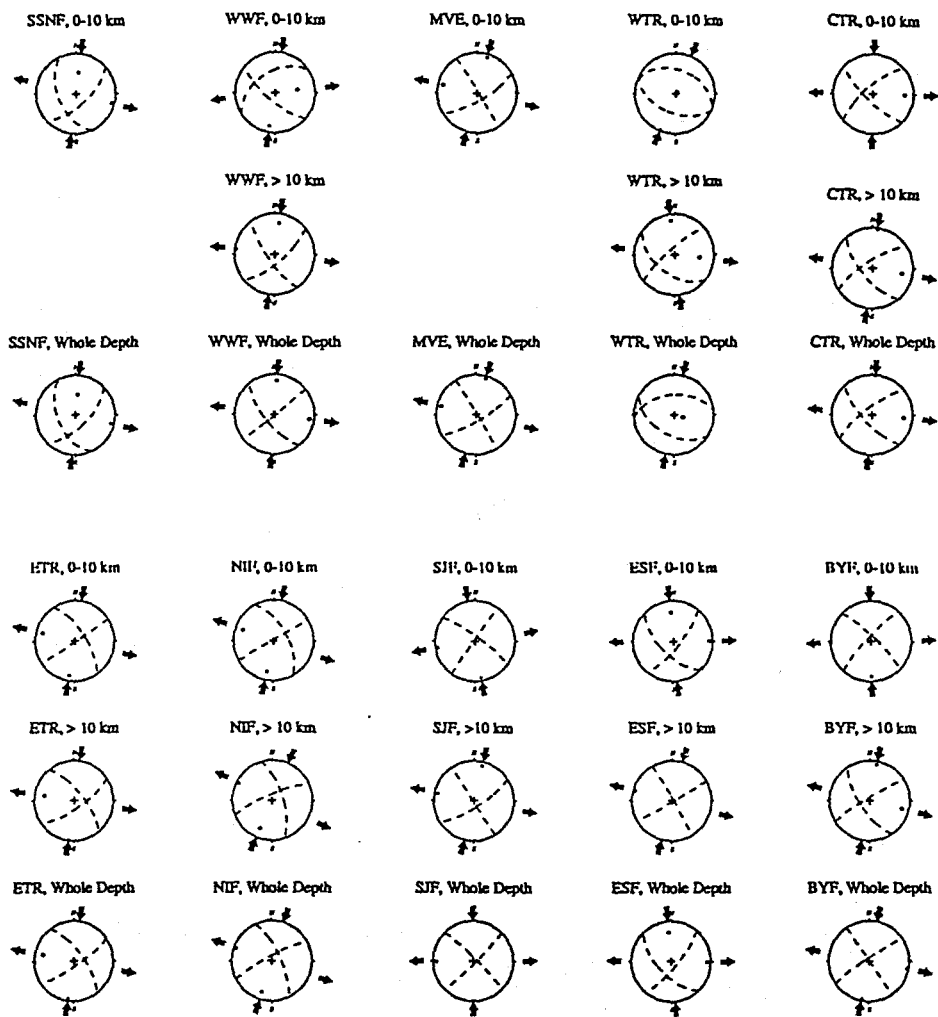
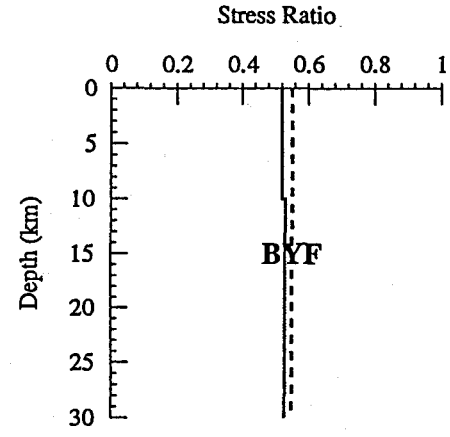
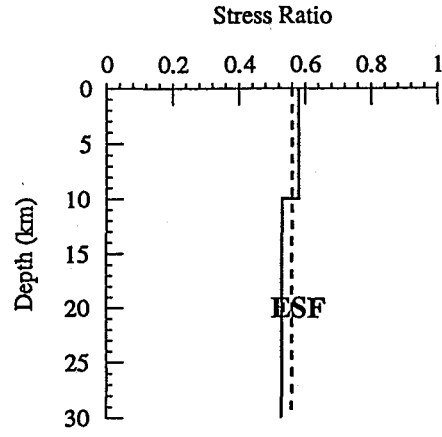
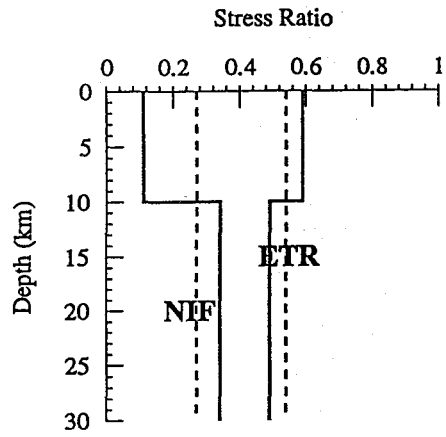
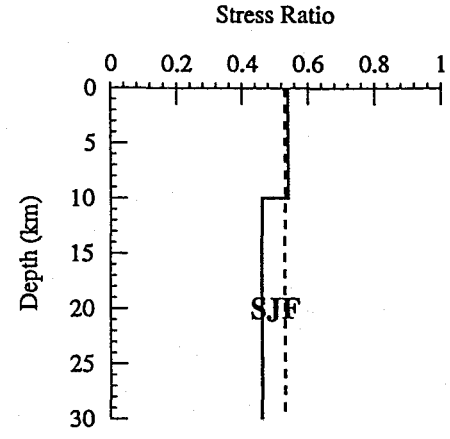
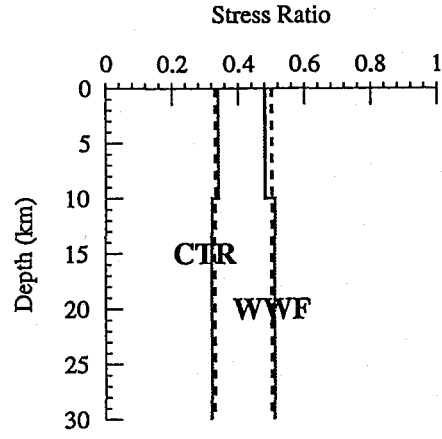
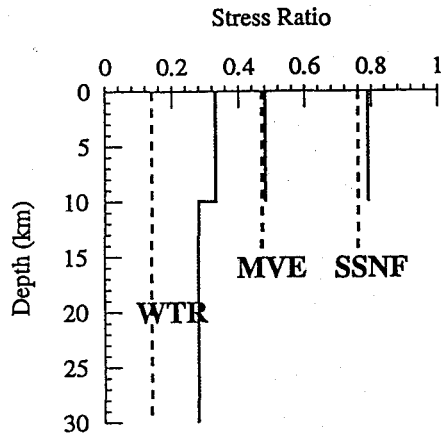


Figure 4.6 (a)

Figure 4.6 (b)



In southern California (refer to Figure 3.10), the WTR, CTR, and NIF domains show large proportions (>40%) of reverse faulting events, mixed with small fractions (<30%) of strike-slip events, and hence represent a convergent area. The SJF, MVE, WWF, ESF, BYF, and ETR domains show large proportions of strike-slip events, mixed with small but similar proportions of both reverse and normal faulting events, and hence represent a transcurrent area. Only one domain, the SSNF, shows a large fraction of normal faulting events, and hence represent a divergent area. From Figure 3.10, we can see that the convergent domains have small  $\Phi$  (<0.35) whereas the transcurrent domains have  $\Phi \approx 0.5$ . The only divergent domain, the SSNF, has a large  $\Phi$  (>0.65).

---

Figure 4.7 Schematic diagrams illustrating the relationship between  $\Phi$  and faulting patterns. The example here shows that faulting patterns can change as a result of variations of  $\sigma_2$ , for a given orientation of the principal stress axes. see text for detail.

Change of Faulting Patterns as a Result of Change in  $\sigma_2$

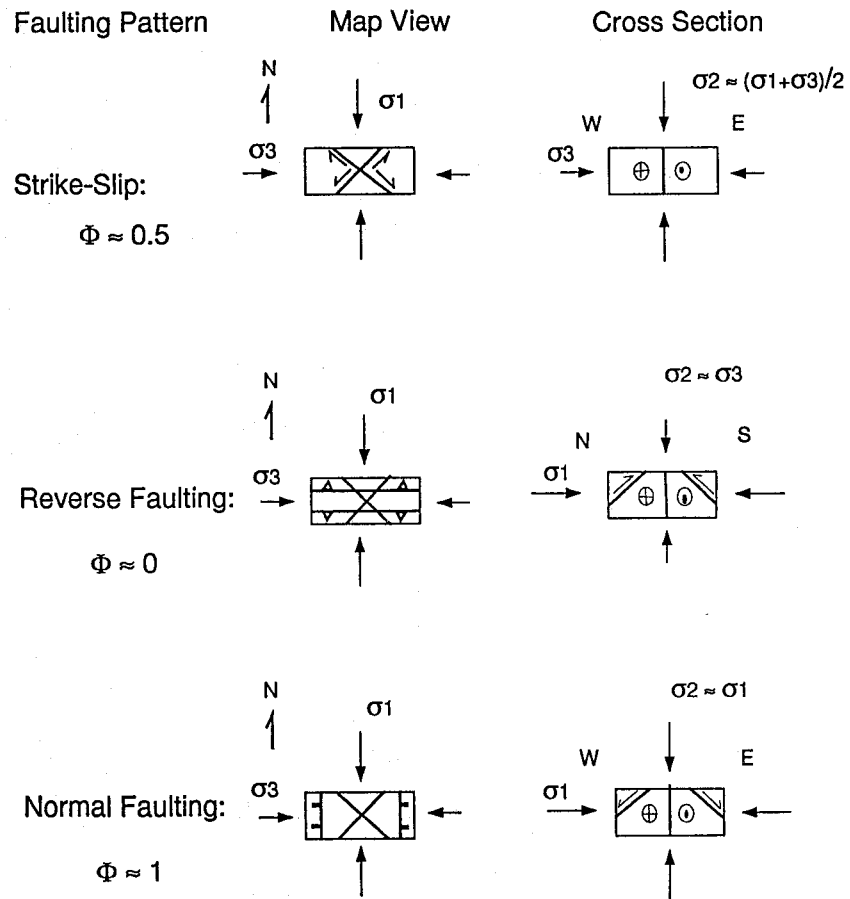


Figure 4.7

According to Anderson (1951), types of faulting depend on the orientations of the principal stress axes. If  $\sigma_1$  is vertical, normal faulting is expected; if  $\sigma_2$  is vertical, strike-slip faulting is expected; and if  $\sigma_3$  is vertical, reverse faulting is expected. In our data, none of the deforming domains shows a single type of faulting but a combination of different types of faults with one type dominant. For a given stress field, faulting patterns can change as a result of variations in  $\sigma_2$  (see also Bott, 1959).

The relationship between  $\Phi$  and faulting patterns is illustrated graphically in Figure 4.7. In the example shown in Figure 4.7,  $\sigma_1$  and  $\sigma_3$  are horizontal, oriented N-S and E-W, respectively.  $\sigma_2$  is vertical to the paper. When  $\sigma_2 \approx (\sigma_1 + \sigma_3)/2$ , or  $\Phi \approx 0.5$ , strike-slip faulting is dominant (first row of Figure 4.7). When  $\sigma_2$  decreases toward  $\sigma_3$ , the tendency of reverse faulting increases because of the increase in shear stress on the potential reverse fault planes. When  $\sigma_2 \approx \sigma_3$ , i.e.  $\Phi \approx 0$ , the potential reverse faults have similar maximum shear stress to the strike-slip faults and hence these two types of faults can slip simultaneously (middle row of Figure 4.7). Similarly, when  $\sigma_2$  increases toward  $\sigma_1$ , the tendency for normal faulting increases because of the increase in shear stress on the potential normal fault planes. When  $\sigma_2 \approx \sigma_1$ , or  $\Phi \approx 1$ , the potential normal faults have similar maximum shear stress to the strike-slip faults and hence these two types of faults can slip contemporaneously (bottom row of Figure 4.7). This relationship between  $\Phi$  and faulting patterns can also be illustrated using the 3D Mohr stress diagrams and the Coulomb failure criterion (see Hill, 1982 and below). The combination of the faulting patterns explain, to some extent, why the WWF, CTR, NIF, and SSNF domains show dissimilarities between the stress and strain tensors because their faulting patterns are complex and associated with approximately bimodal or trimodal distributions in histogram.

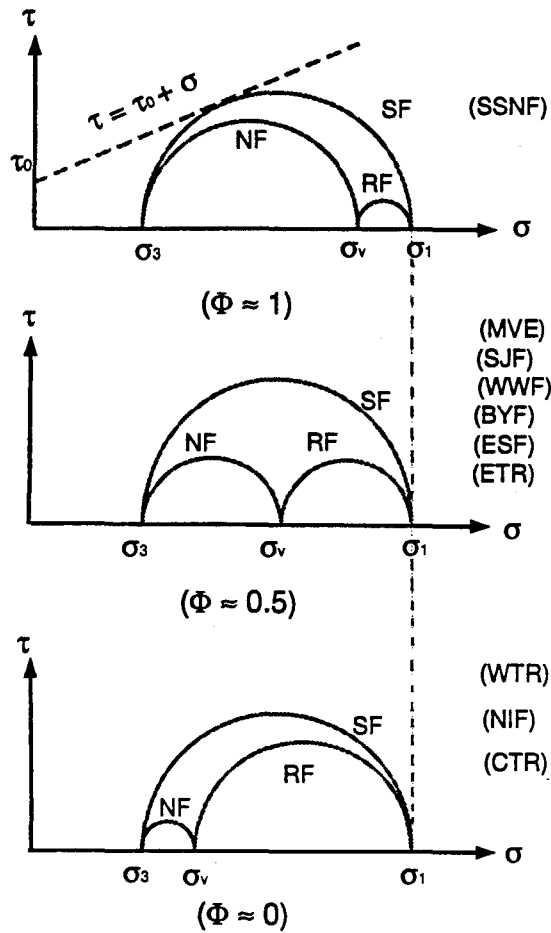


Figure 4.8 Constructed 3D-Mohr stress diagrams based on  $\Phi$  values. The stress fields show that  $\sigma_2$  is near vertical for all domains hence it is indicated by  $\sigma_v$  in these plots. (a) Assuming  $\sigma_1$  is the same and letting  $\sigma_2$  vary; (b) (Next page) Assuming  $\sigma_2$  is the same and letting  $\sigma_1$  and  $\sigma_3$  vary. In all cases, the differential stress  $\sigma_1 - \sigma_3$  is assumed to be the same.

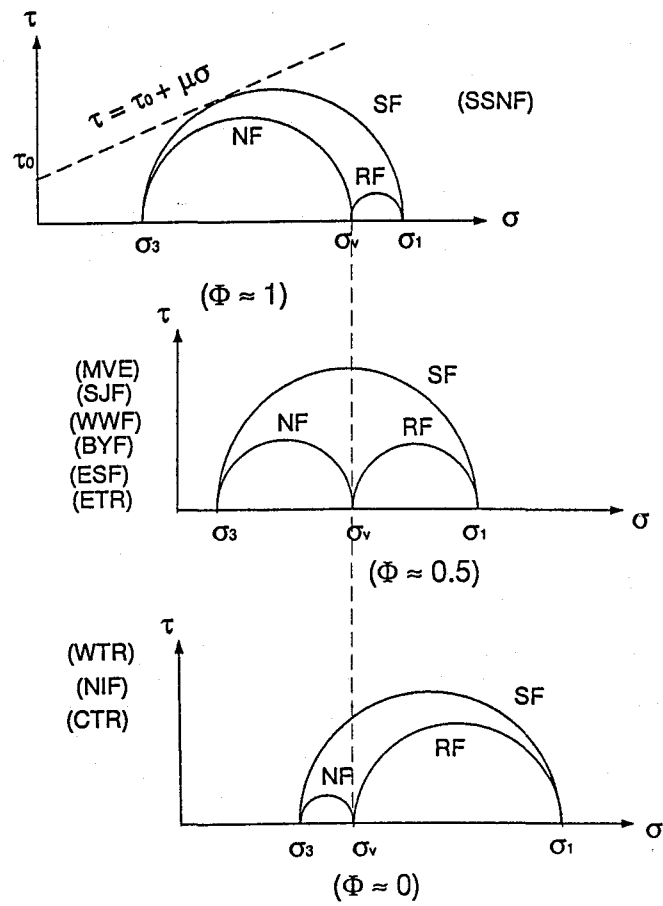


Figure 4.8 (b)

#### 4.8 Interpretations

The contemporaneous coexistence of all faulting patterns within a deforming domain indicates complexity of the state of stress and/or the inhomogeneity of mechanical properties of the crust. Since  $\sigma_1$  is consistently oriented in the N-S direction regardless of the local strike of the San Andreas fault, we can conclude that the regional tectonic stress field is very stable in orientation although it may vary in magnitude from domain to domain as implied by the variations of stress ratio  $\Phi$ . If we assume that  $\sigma_1$  is the same for all domains, that is, that southern California as a whole is regarded as being subjected to the same stress due to the motion between the North American and Pacific plates, we can then construct the Mohr diagrams as shown in Figure 4.8. Since  $\sigma_1$  and  $\sigma_3$  are nearly horizontal as we have presented above, all domains are in a state of stress that is favorable for strike-slip faults, i.e.  $\sigma_2$  near vertical. In this case, Figure 4.8(a) indicates that variations of  $\Phi$  are a result of variations in  $\sigma_2$ . The SSNF domain apparently has a larger  $\sigma_2$  whereas the WTR, NIF, and CTR domains have a smaller  $\sigma_2$ . Others have  $\sigma_2$  values in between. This, to some degree, explains the large horizontal convergence accommodated by the possible detachment structures across the Transverse Ranges (see Hadley and Kanamori, 1978; Yeats, 1981; Davis et al., 1989) and large horizontal divergence accommodated by the large-scale low-angle normal faults in the Great Basin area (see Wright, 1976; Wernicke et al., 1988).

If, however,  $\sigma_2$  is assumed to be the same for all domains, that is, difference in overburdens resulting from topography and the vertical dynamic stress are neglected, the constructed Mohr diagrams indicate that the WTR, CTR, and NIF domains have large values of  $\sigma_1$  where as the SSNF domain has a small value of  $\sigma_1$ . The values of the other domains lie in between (Figure 4.8b). In either case, domains with large  $\Phi$  could imply that the strike-slip and normal faults have similar strength and their

orientations (away from  $\sigma_1$ ) spread over about the same range. Similarly, domains with small  $\Phi$  could imply that the strike-slip and reverse faults have similar strength and their orientations spread approximately the same range as illustrated in Figure 4.9. This explains why domains with either large or small  $\Phi$  usually, though not always, have bimodal distributions of faulting patterns (refer to Figure 3.10).

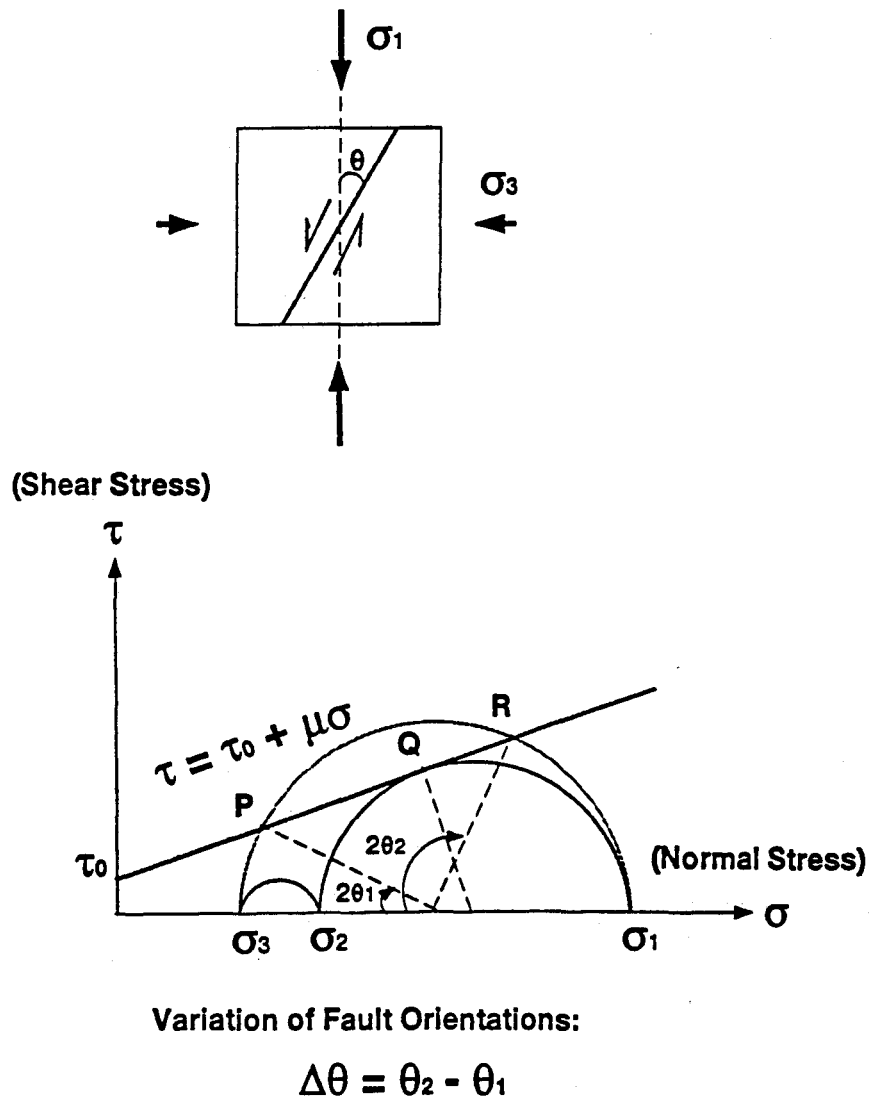


Figure 4.9 3D-Mohr diagram illustrating the relationship between faulting orientation ( $\theta$ ) and state of stress.  $\tau_0$ : internal friction;  $\mu$ : friction coefficient. Given weak zones having Coulomb strength  $\tau = \tau_0 + \mu\sigma$ , the possible range of fault orientations can be  $\Delta\theta = \theta_2 - \theta_1$ . The two big half circles imply bimodal distribution of faulting patterns.

#### 4.9 Summary

(1) The maximum principal compressional stress axes ( $\sigma_1$ ) in southern California are consistently directed N6°E  $\pm$  11° regardless of the local fault structures;

(2) The maximum principal convergent strain axes ( $\epsilon$ ) are also dominantly oriented N-S, but vary in a wider range (N5°E  $\pm$  21°);

(3) The stress and strain tensors are similar to each other for the MVE, SJF, ESF, ETR, WTR and BYF domains, but are dissimilar for the CTR, SSNF, WWF, and NIF domains;

(4) Stress ratio  $\Phi$  is smaller than 0.35 in the WTR, WWF, and CTR domains, but larger than 0.65 in the SSNF domain. Other domains have values of  $\Phi$  around 0.5;

(5) Variations of the state of stress with depth appear to exist only in or adjacent to the Transverse Ranges, where deep earthquakes are common. Other domains do not show large changes of the state of stress throughout the seismogenic depth range.

## Chapter 5

### Seismic Deformation and Geological Environment

#### 5.1 Motivation

California is host to an active continental transform fault system (see Anderson, 1971). The Pacific plate moves at a rate of 48 mm/yr (DeMets et al., 1992) northwestward relative to the North American plate. The deformation is concentrated principally within a 200 to 350 km-wide zone (see Ekström and England, 1989; Jackson and Molnar, 1992), as expressed by active faults and folds, as well as distributed earthquakes. The well-constrained Holocene slip rate on the San Andreas fault (SAF) in the Carrizo Plain is about 35 mm/yr (Sieh and Jahns, 1984). Therefore, about 70% of the deformation is attributed to the movement of the SAF at that latitude. It is believed that the rest of the deformation must be partitioned among other faults or structures (Minster and Jordan, 1984, 1987, Weldon and Humphreys, 1986; Humphreys and Weldon, 1994), differing not only in amount, but also in style (see Thatcher, 1990). Geologically, the most striking feature of the boundary is the change in strike of the SAF from its general NW-strike ( $N35^{\circ}$  to  $40^{\circ}W$ ) in central California to WNW-strike ( $N65^{\circ}$  to  $70^{\circ}W$ ) passing through the E-W-trending Transverse Ranges in southern California. This results in a significant local N-S-directed component of convergence due to the general plate motion direction, which is about  $N35^{\circ}W$  (DeMets et al., 1992). Therefore, strike-slip faulting and reverse faulting coexist in the area adjacent to the SAF as manifested by recent earthquakes, such as the 1971  $M = 6.6$  San Fernando, 1987  $M = 5.9$  Whittier Narrows, 1991  $M = 5.8$  Sierra Madre, 1992  $M = 6.1$  Joshua Tree, 1992  $M = 7.3$  Landers, and 1994  $M = 6.7$  Northridge earthquakes (chapter 2). In addition,

north across the Garlock fault is the southwestern region of the Great Basin, which is characterized by WNW-directed extension (Wright, 1976; Wernicke et al, 1988). Normal faulting mechanisms of earthquakes have been observed there (see Jones and Dollar, 1988). East of the Peninsular Ranges is north end of the Gulf of California rift, where extension is prominent (see Crowell, 1981). Therefore, southern California encompasses diverse tectonic environments that include many types of active faulting. There is little doubt that the diversity of faulting, or strain patterns, is more complex if observed in different time intervals. In this chapter we will explore the quantitative complexity by analyzing the released seismic deformation and its relation to the local geological environments.

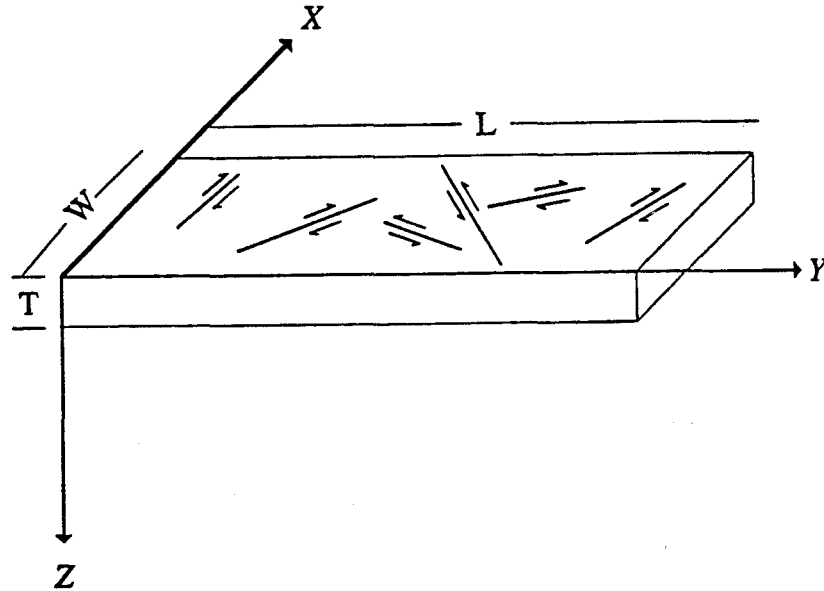


Figure 5.1 Diagram illustrating the setup of the coordinate system for computing seismic strain rates within a deforming domain. X is toward the north. Y is toward the east, and Z is downward. L, length; W, width; T, thickness. The volume is  $V=LTW$ .

In the following, I will give a brief review, as methods for seismic deformation study are briefly mentioned in the last chapter (Chapter 4). Details of these aspects can be found in other references (Jackson and Mckenzie, 1988; Frohlich and Anderson, 1992; Anderson et al., 1993). As pointed out in the last chapter, once the volume is specified in a coordinate system (Figure 5.1), Kostrov's formula (Eq. 4.1) can be used to compute the seismic strain in three dimensions. Given the time interval  $T_s$ , the seismic strain rates can be estimated as  $\dot{\epsilon} = \epsilon/T_s$ . Let  $S_x = (S_{xx}, S_{xy}, S_{xz})$ ,  $S_y = (S_{yx}, S_{yy}, S_{yz})$ ,  $S_z = (S_{zx}, S_{zy}, S_{zz})$  be the vectorial slip rates of surface whose normals are in the x, y, and z directions. From elastic mechanics, we know that the irrotational strain rate tensor is defined as:

$$\dot{\epsilon} = \frac{1}{2} \begin{bmatrix} \frac{2S_{xx}}{W} & \frac{S_{xy} + S_{yx}}{W + L} & \frac{S_{xz} + S_{zx}}{W + T} \\ \frac{S_{xy} + S_{yx}}{W + L} & \frac{2S_{yy}}{L} & \frac{S_{yz} + S_{zy}}{L + T} \\ \frac{S_{xz} + S_{zx}}{W + T} & \frac{S_{yz} + S_{zy}}{L + T} & \frac{2S_{zz}}{T} \end{bmatrix}. \quad (5.1)$$

For  $L \gg W \gg T$ , the above is approximated as:

$$\dot{\epsilon} = \frac{1}{2} \begin{bmatrix} \frac{2S_{xx}}{W} & \frac{S_{xy}}{W} & \frac{S_{zx}}{T} \\ \frac{S_{xy}}{W} & \frac{2S_{yy}}{L} & \frac{S_{zy}}{T} \\ \frac{S_{xz}}{T} & \frac{S_{zy}}{T} & \frac{2S_{zz}}{T} \end{bmatrix}. \quad (5.2)$$

The six slip components of the deforming domain are then evaluated by comparing Eqs.(5.2) and (4.1) (see Jackson and McKenzie, 1988). Since the shear components  $S_{ij}$ , where  $i \neq j$ , are obtained by approximation, they may have a larger uncertainty than the axial components. The physical meanings of the components in Eq.(5.2) are that the diagonal components can be either compression (if they are negative) or

extension (if they are positive) and the off-diagonal components represent shear. The principal strain axes are easily obtained by finding the eigenvectors of the symmetric moment tensor  $M$ . The corresponding eigenvalues will give us information on the seismic sources, such as the equivalent scalar moment (ESM), the amount of nondouble-couple percentage, which is a measure of deviation from a double-couple source (see Jost and Herrmann, 1989).

The scalar moment ( $M_0$ ) can be estimated in two ways. First, it can be obtained from wave form modeling (for large events that have well recorded seismograms). Second it can be estimated using empirical formula. For major events, we use wave form moments. For small events, we use the empirical relation between  $M_0$  and  $M_L$  or  $M_W$  formulated by Thatcher and Hanks (1973):

$$\log M_0 = 1.5M + 16.05 , \quad (5.3)$$

where  $M$  can be either  $M_L$  or  $M_W$ . Usually, the focal mechanism parameters such as rake, dip, and strike can be well constrained, but the scalar moment  $M_0$  is not well controlled. A factor of 2 error in  $M_0$  is possible. Therefore, the uncertainty of seismic slip rates is mainly caused by the error of  $M_0$  as pointed out by Molnar and Deng (1984). Jackson and McKenzie (1988) allow 0.2 unit error in magnitude, and estimate the maximum value of seismic slip rates for +0.2 error in  $M$ , and minimum value of seismic slip rates for -0.2 errors in  $M$ . This is equivalent to a factor of 0.5 to 2.0 uncertainty in the calculated seismic slip rates.

The seismic strain calculated by Eq.(4.1) is a volumetric average. For seismic slip on a single fault, we can use:

$$D = M_0/\mu S \quad (5.4)$$

(Brune, 1968), where  $M_0$  is the scalar moment;  $D$ , average slip on the fault plane;  $S$ , area of the fault plane;  $\mu$  is the same as in Eq.(4.1). Eq.(5.4) is a special case of

Eq.(5.1). Brune (1968) used Eq.(5.4) to estimate seismic slip on major faults in southern California. He suggested that if the seismic slip is smaller than geodetic or geologic displacements, then creep without generating earthquakes is implied. His conclusion was apparently based on the assumption that the seismic records represent the long-term seismic deformation. This assumption is, of course, questionable. For instance, Allen (1968) argued that historical earthquake catalogues are not long enough to provide information on seismic activity of an apparently quiet area. Scholz and Cowie (1990) also pointed out the pitfall of using short-term seismic records. Therefore, the observational time intervals are a very important parameter. We must be very careful when extrapolating from limited data, particularly when comparing slip rates averaged over different time intervals. For example, Brune (1968) obtained a 1.5 cm/yr seismic slip rate for the San Jacinto fault for the period between 1912 and 1963, whereas Thatcher and Hanks (1975) derived a seismic slip rate of 0.8 cm/yr for the period between 1890 and 1973.

We can also estimate the seismic moment rates given the slip rates on the faults, or vice versa, using Eq.(5.4). For instance, Anderson (1979) applied Eq.(5.4) to southern California, and concluded that north of the Transverse Ranges, most of the slip implied by tectonic studies can be accounted for on known faults, but over 10 mm/yr is still missed south of the Transverse Ranges. Ekström and England (1989) applied Eq.(5.1) to the whole of California. They found that seismic deformation accounted for only 10% of the plate motion between 1977 and 1987, and that large events greater than magnitude 7.0 since 1812 accounted for about 45-60% of the plate motion. It is therefore almost certain from the previous work that the total released seismic strain can not account for the total deformation. Significant deformation remains to be accounted for. Where and how does the rest of the deformation take place?

This chapter will attempt to answer the following three questions:

(1) Is the short-term seismic strain pattern consistent with geologic and geodetic measurements?

(2) To what extent can the released seismic strain account for the total deformation measured geologically or geodetically?

(3) How do we appropriately use the limited data to evaluate earthquake potential?

## **5.2 Seismic Deformation in Individual Domains**

Since seismicity is diffuse and different types of faults exist in southern California, it is necessary to examine seismic deformation domain by domain. Ten major deforming domains are divided based on the geologic structures and geographical distributions of seismicity (Figure 2.1). Two criteria are applied to the division. (1) The domain contains faults of similar nature or focal mechanisms; (2) The total rupture length associated with the observed maximum or typical larger earthquakes must be within the deforming domain. We have allowed some overlap for some adjacent domains because of the ambiguity of the domain boundaries. Applying Eq.(5.1) to each domain, we can obtain the strain rates. The results are tabulated in Table (5.1). As expected, the domains with largest earthquakes have the largest strain rates, such as the WWF, BYF, and the southern-central MVE domains. In general, the principal convergent strains from both the background seismicity and the seismicity containing many major events are near N-S, varying  $10^\circ$  to the west and  $30^\circ$  to the east of north, with the exception of the WTR, indicating persistence of the seismic strain patterns (Figure 5.2). But spatial variations of strain patterns and magnitude are obvious (see Chapter 4). The Transverse Ranges, for instance, in addition to N-S shortening, E-W

left-lateral shearing in the WTR and CTR, and E-W right-lateral shear in the ETR are significant. The amount of left-lateral shear appears to increase westward along the Transverse Ranges, indicating that little SAF-type strain was released seismically in the WTR in this century.

Table 5.1 Calculated Seismic Strain Rates

Parameters	1981-1991						1927-1991					
	11	22	33	12	13	23	11	22	33	12	13	33
SSNF	W=60 km, L=85 km											
$\dot{M}(10^{22})$	-1.93	2.71	-0.78	-1.05	-0.01	-0.49	-1.65	14.0	-12.3	-1.18	4.27	-1.14
$\dot{\bar{\epsilon}}(10^{-9}\text{yr}^{-1})$	-0.42	0.59	-0.17	-0.23	0.00	-0.11	-0.36	3.05	-2.69	-0.26	0.93	-0.25
$S^0(\text{mmyr}^{-1})$	-0.03	0.05	0.00	-0.03	0.00	0.00	-0.02	0.26	-0.04	-0.03	0.03	-0.01
$S^1(\text{mmyr}^{-1})$	0.01	0.00	0.00	0.07	0.00	0.00	0.12	0.06	-0.04	0.19	0.01	-0.03
$\phi_p(\delta_p), \phi_t(\delta_t)$	Strain: 13(5), 282(7) Stress: 5(46), 104(8)						176(71), 275(3)					
$M_{sm}(\times 10^{23})$	2.583						91.025					
$M_{em}$	4.9						5.9					
R (%)	44.7						95.7					
N	47						48					
WWF	W=60 km, L=110 km											
$\dot{M}(10^{24})$	-0.14	0.05	0.09	-0.11	-0.03	0.07	-30.7	7.91	22.8	8.17	6.93	-17.5
$\dot{\bar{\epsilon}}(10^{-7}\text{yr}^{-1})$	-0.02	0.01	0.01	-0.02	-0.01	0.01	-5.18	1.33	3.84	1.37	1.17	-2.95
$S^0(\text{mmyr}^{-1})$	-0.14	0.09	0.02	-0.21	-0.02	0.03	-31.1	14.7	5.77	16.5	3.50	-8.85
$S^1(\text{mmyr}^{-1})$	0.00	-0.16	0.02	-0.27	-0.03	0.02	-28.4	9.85	5.77	-25.6	7.46	-5.91
$\phi_p(\delta_p), \phi_t(\delta_t)$	Strain: 24(1), 115(43) Stress 4(16), 98(13)						164(11), 272(57)					
$M_{sm}(\times 10^{25})$	0.176						223.901					
$M_{em}$	5.4						7.5					
R (%)	82.2						100.0					
N	32						33					
MVE <sup>1</sup>	W=70 km, L=125 km											
$\dot{M}(\times 10^{22})$	-0.73	0.67	0.06	-0.92	-0.13	-0.12	-42.4	41.1	1.33	-34.3	4.77	-7.45

$\dot{\bar{\epsilon}}(\times 10^{-10}\text{yr}^{-1})$	-0.93	0.85	0.07	-1.17	-0.17	-0.15	-53.9	52.2	1.69	-43.5	6.06	-9.46
$S^0(\text{mmyr}^{-1})$	-0.01	0.01	0.00	-0.02	0.00	0.00	-0.38	0.65	0.00	-0.61	0.02	-0.03
$S^1(\text{mmyr}^{-1})$	-0.01	0.02	0.00	0.01	0.00	0.00	-0.37	0.64	0.00	0.63	0.00	-0.03
$\phi_p(\delta_p), \phi_t(\delta_t)$	Strain: 26(8), 296(2) Stress: 15(8), 284(11)						200(2), 290(9)					
$M_{sm}(\times 10^{24})$	0.117						35.593					
$M_{em}$	4.6						6.3					
R (%)	86.9						100.0					
N	24						28					
<hr/>												
WTR			W=100 km, L=190 km									
$\dot{M}(10^{22})$	-1.42	-0.07	1.49	-0.66	-0.44	-0.01	-44.3	-187.0	232.0	-94.4	-60.1	-194.0
$\dot{\bar{\epsilon}}(10^{-10}\text{yr}^{-1})$	-0.83	-0.04	0.87	-0.39	-0.25	-0.01	-25.9	-110.0	135.0	-55.2	-35.2	-113.0
$S^0(\text{mmyr}^{-1})$	-0.01	0.00	0.00	-0.01	0.00	0.00	-0.26	-2.08	0.20	-1.10	-0.11	-0.34
$S^1(\text{mmyr}^{-1})$	-0.01	0.00	0.00	-0.01	0.00	0.00	-0.26	-2.08	0.20	-1.10	-0.11	-0.34
$\phi_p(\delta_p), \phi_t(\delta_t)$	Strain: 22(7), 160(80) Stress: 12(1), 106(71)						66(20), 260(69)					
$M_{sm}(10^{24})$	0.165						200.907					
$M_{em}$	4.7						6.8					
R (%)	78.5						100.0					
N	33						35					
<hr/>												
CTR <sup>2</sup>			W=100 km, L=180 km									
$\dot{M}(10^{24})$	-1.37	0.10	1.27	0.11	0.49	0.02	-1.34	-0.45	1.78	-0.78	-0.29	0.21
$\dot{\bar{\epsilon}}(10^{-9}\text{yr}^{-1})$	-8.45	0.63	7.82	0.65	3.03	0.10	-8.25	-2.77	11.00	-4.82	-1.78	1.31
$S^0(\text{mmyr}^{-1})$	-0.85	0.11	0.12	0.13	0.09	0.00	-0.82	-0.50	0.17	-0.96	-0.05	0.04
$S^1(\text{mmyr}^{-1})$	-0.85	0.11	0.12	0.13	0.09	0.00	-0.82	-0.50	0.17	-0.96	-0.05	0.04
$\phi_p(\delta_p), \phi_t(\delta_t)$	Strain: 176(10), 9(79) Stress: 5(2), 96(24)						30(2), 123(80)					
$M_{sm}(10^{25})$	1.552						11.849					
$M_{em}$	6.1						6.6					
R (%)	85.3						94.4					
N	86						89					
<hr/>												
ETR <sup>3</sup>			W=70 km, L=150 km									
$\dot{M}(10^{23})$	-6.17	6.00	0.21	2.92	3.45	-5.87	-11.2	8.78	2.46	4.29	-0.19	-5.43
$\dot{\bar{\epsilon}}(10^{-9}\text{yr}^{-1})$	-6.52	6.30	0.22	3.09	3.65	-6.11	-11.9	9.29	2.61	4.54	-0.21	-5.75
$S^0(\text{mmyr}^{-1})$	-0.46	0.95	0.00	0.43	0.11	-0.18	-0.83	1.39	0.04	0.64	-0.01	-0.17
$S^1(\text{mmyr}^{-1})$	-0.46	0.95	0.00	0.43	0.11	-0.18	-0.83	1.39	0.04	0.64	-0.01	-0.17
$\phi_p(\delta_p), \phi_t(\delta_t)$	Strain: 157(29), 267(31) Stress: 189(7), 282(21)						167(4), 260(8)					
$M_{sm}(10^{24})$	9.514						79.074					
$M_{em}$	5.9						6.5					
R (%)	97.8						94.6					
N	130						131					
<hr/>												
NIF			W=50 km, L=100 km									
$\dot{M}(10^{22})$	-1.13	0.52	0.61	-0.29	-0.08	0.00	-145.0	154.0	-9.04	4.52	36.3	-0.85

$\dot{\bar{\epsilon}}(10^{-9}\text{yr}^{-1})$	-0.25	0.12	0.14	-0.06	-0.02	0.00	-32.2	34.2	-2.01	1.01	8.08	-0.19
$S^0(\text{mmyr}^{-1})$	-0.01	0.01	0.00	-0.01	0.00	0.00	-1.61	3.42	-0.03	0.10	0.24	-0.01
$S^1(\text{mmyr}^{-1})$	-0.01	0.00	0.00	0.02	0.00	0.00	0.10	0.00	0.00	3.32	0.00	0.00
$\phi_p(\delta_p), \phi_t(\delta_t)$	Strain: 10(2), 110(77) Stress: 197(20), 290(6)						179(14), 269(0)					
$M_{sm}(10^{23})$	0.897						1000.74					
$M_{em}$	4.6						6.6					
R (%)	4.2						99.9					
N	19						20					

ESF	W=25 km, L=215 km											
$\dot{M}(10^{22})$	-1.13	1.00	0.13	-0.34	0.02	-0.20	-0.17	0.15	0.02	-0.05	0.00	-0.03
$\dot{\bar{\epsilon}}(10^{-10}\text{yr}^{-1})$	-2.33	2.06	0.27	-0.69	0.03	-0.42	-0.36	0.32	0.04	-0.11	0.00	-0.06
$S^0(\text{mmyr}^{-1})$	-0.01	0.04	0.00	0.00	0.00	0.00	0.00	0.01	0.00	0.01	0.00	0.00
$S^1(\text{mmyr}^{-1})$	0.00	0.02	0.00	0.01	0.00	0.00	0.00	0.00	0.00	0.00	0.00	0.00
$S^2(\text{mmyr}^{-1})$	0.00	0.02	0.00	0.01	0.00	0.00	0.00	0.00	0.00	0.00	0.00	0.00
$\phi_p(\delta_p), \phi_t(\delta_t)$	Strain: 9(1), 279(12) Stress: 355(29), 90(11)						9(0), 279(12)					
$M_{sm}(10^{23})$	1.135						1.135					
$M_{em}$	4.6						4.6					
R (%)	85.1						85.1					
N	28						28					

SJF	W=30 km, L=230 km											
$\dot{M}(10^{24})$	-1.70	1.82	-0.12	1.21	-0.64	-0.60	-2.74	2.76	-0.02	0.46	0.09	-0.25
$\dot{\bar{\epsilon}}(10^{-8}\text{yr}^{-1})$	-2.74	2.94	-0.20	1.95	-1.04	-0.97	-4.40	4.44	-0.04	0.74	0.15	-0.40
$S^0(\text{mmyr}^{-1})$	-0.82	6.75	-0.03	1.17	-0.31	-0.29	-1.32	10.22	-0.01	0.44	0.04	-0.12
$S^1(\text{mmyr}^{-1})$	0.46	-3.07	-0.03	1.88	-0.42	-0.02	-0.01	0.14	-0.01	2.69	-0.04	-0.12
$\phi_p(\delta_p), \phi_t(\delta_t)$	Strain: 345(13), 251(17) Stress: 179(1), 270(8)						175(2), 265(5)					
$M_{sm}(10^{25})$	2.306						18.186					
$M_{em}$	6.2						6.8					
R (%)	78.9						97.2					
N	127						132					

BYF	W=20 km, L=95 km											
$\dot{M}(10^{23})$	-0.10	0.13	-0.03	0.01	0.04	-0.01	-86.9	86.9	0.00	-51.0	0.00	0.00
$\dot{\bar{\epsilon}}(10^{-9}\text{yr}^{-1})$	-0.57	0.73	-0.16	0.06	0.22	-0.05	-508.0	508.0	-0.02	-299.0	0.03	-0.01
$S^0(\text{mmyr}^{-1})$	-0.01	0.07	0.00	0.00	0.01	0.00	-10.16	48.27	0.00	-11.94	0.00	0.00
$S^1(\text{mmyr}^{-1})$	0.01	-0.04	0.00	0.01	0.00	-0.01	3.95	50.09	0.00	31.19	0.00	0.00
$\phi_p(\delta_p), \phi_t(\delta_t)$	Strain: 177(23), 268(2) Stress: 191(5), 101(4)						15(0), 105(0)					
$M_{sm}(10^{24})$	0.1204						655.05					
$M_{em}$	4.7						7.1					
R (%)	81.6						100.0					
N	27						29					

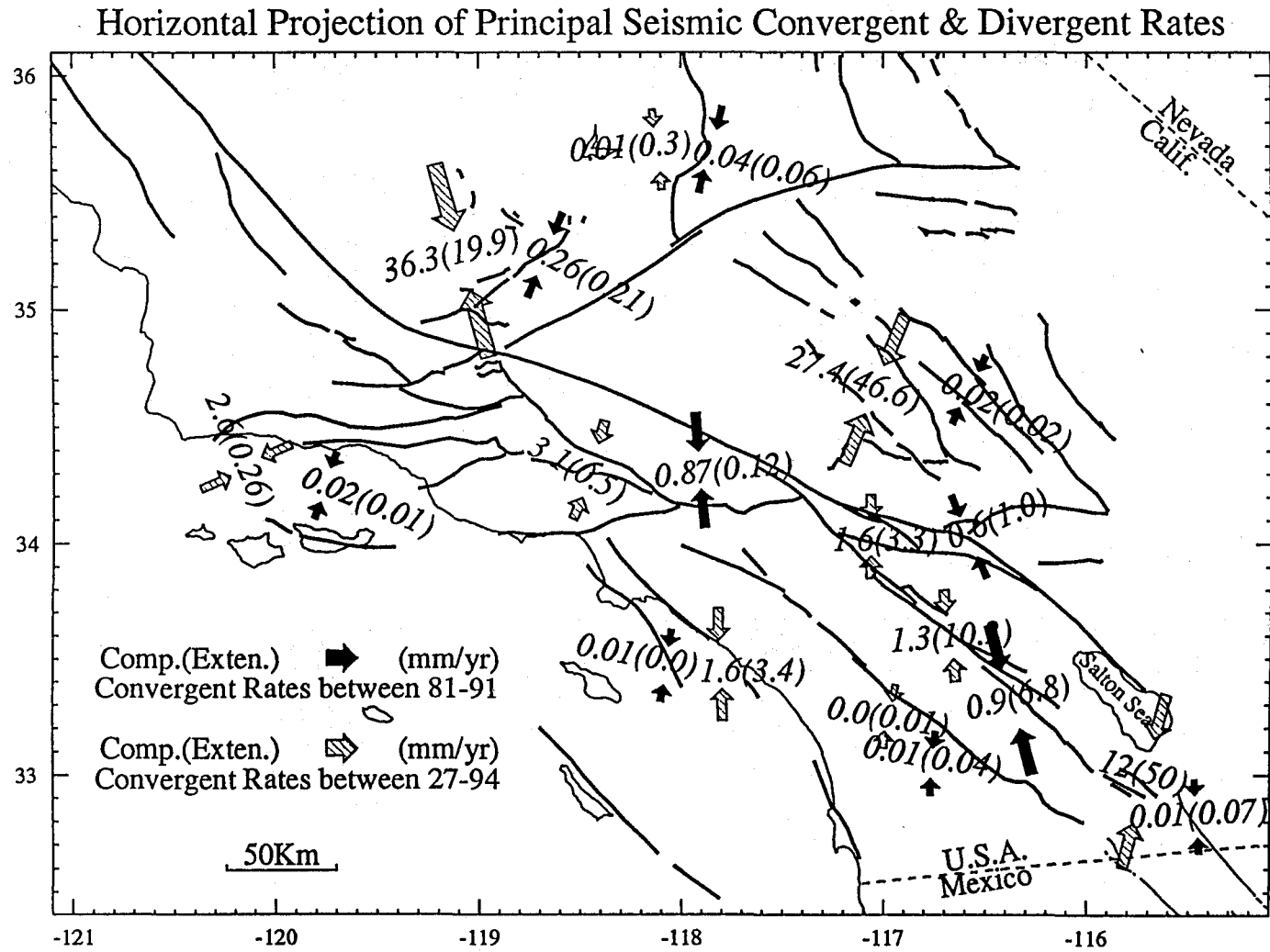
$\dot{M}$ : Moment rates (dyne.cm/yr) for the unrotated coordinate system;  $\dot{\epsilon}$ : Strain rates for the unrotated coordinate system;  $S^0$ : Seismic slip rates calculated the unrotated coordinate system, which is set up as x=North, y=East, Z=Downward;  $S^1$ : Seismic slip rates calculated for the rotated coordinate system, in which x axis is perpendicular to strike (Width), y axis is along the strike (Length), z axis remains downward. Depth is taken as 15 km for all the domains.  $\phi_p$ : Azimuth of P Axis,  $\phi_t$ : Azimuth of T axis;  $\delta_p$ : Plunge of P axis;  $\delta_t$ : Plunge of T axis;  $M_{sm}$ : Total scalar moment (dyne.cm), which is the average of the two largest eigenvalues (both are in absolute values);  $M_{em}$ : Equivalent magnitude calculated from the empirical relation of Thatcher and Hanks (1973),  $\text{Log}M_0 = 1.5M + 16.1$ ; R: Double couple percentage, which is calculated from  $(1-2\psi)*100.0$ , where  $\psi$  is  $|\eta_{\min}| / |\eta_{\max}|$  and  $\eta$  is eigenvalue from the total moment tensor (see Jost and Herrmann, 1989). N: Number of events.

1: With the occurrence of the 1992 Landers  $M_w=7.3$  earthquake, the seismic strain rates for the MVE are adjusted to as:  $S_{11}^1=-14.8$ ,  $S_{22}^1=26.6$ ,  $S_{33}^1=-0.02$ ,  $S_{12}^1=7.12$ ,  $S_{13}^1=-0.56$ ,  $S_{23}^1=-0.33$ ;

2: With the Occurrence of the 1994  $M_w=6.7$  Northridge earthquake, the seismic strain rates for the CTR are adjusted to as:  $S_{11}^1=-1.90$ ,  $S_{22}^1=-0.70$ ,  $S_{33}^1=0.34$ ,  $S_{12}^1=-1.90$ ,  $S_{13}^1=-0.16$ ,  $S_{23}^1=0.08$ ;

3: When adding the 1992 Big Bear  $M=6.5$  and 1992 Joshua Tress  $M=6.1$  events, the seismic strain rates for the ETR are adjusted as:  $S_{11}^1=-1.62$ ,  $S_{22}^1=3.28$ ,  $S_{33}^1=0.02$ ,  $S_{12}^1=0.19$ ,  $S_{13}^1=-0.14$ ,  $S_{23}^1=-0.22$ ;

Figure 5.2



---

Figure 5.2 Map showing the horizontal projection of seismic slip rates along the principal compressive and extensional axes, calculated from the total seismic moment tensors in each deforming domain. They correspond to principal convergence and divergence rates associated with earthquakes in different areas of southern California. As expected, the largest rates are associated with the largest events such as in the WWF, BYF, and MVE domains. Note also the temporal and spatial variations of the principal orientations in some domains such as in the WWF and WTR domains.

### **5.3 Geological Tour of Individual Domains**

In the following sections, we describe in detail the tectonic setting and the geological deformation in each domain. In the next section, we will assess the deformation mode and evaluate the seismic potential making comparisons among the available geologic, seismological, and geodetic data.

#### **5.3.1 SSNF Domain**

The SSNF domain is located in the western margin of the Great Basin (western part of the Basin and Range Province) (Figure 5.3). The largest event recorded is the 1946  $M=6.3$  Walker Pass earthquake located within the southern Sierra Nevada batholith. Most events of the background seismicity are not located on the major faults. Several are on the Garlock fault. Topographically, the domain is characterized by a N-S-trending uplift belt bounded by the steeply east-dipping Sierra Nevada boundary fault along its eastern base (Dibblee, 1955; Christensen, 1966; Huber, 1981). To the east is the Great Basin that is characterized by west-dipping normal faults, and NE-, NW-striking conjugate strike-slip faults (see Wright, 1976; Jones, 1987; Wernicke et al., 1988). To the west is the Great Valley in which thick Cenozoic sediments shed from the rising Sierra Nevada are accumulated (see Dibblee, 1955; Crowell, 1987). The southern side of the Sierra Nevada is bounded by the Garlock fault, on which E-W extension of the southwest Great Basin occurred, causing the bending of the San

Andreas fault (Davis and Burchfiel, 1973). The nearly E-W-directed extension of the Great Basin was not generally recognized until the late 60s and early 70s (see Wernicke et al., 1988). Wright (1976) estimated a 5% to 10% extension in the northern part of the Basin and Range Province, and up to 30% in the southern part. Minster and Jordan (1987) calculated an extension rate of  $9.7 \pm 2.1$  mm/yr along  $N56^{\circ}W \pm 10^{\circ}$ , based on integrations of neotectonic estimates, ground-based geodetic measurements, and the VLBI (very long baseline interferometer) data for the global plate tectonic model. By reconstructing profiles at the latitude of Las Vegas, Wernicke et al. (1988) determined a  $247 \pm 56$  km net extension in the direction of  $N73^{\circ}W \pm 12^{\circ}$ . According to Wernicke et al. (1988), the extension began about 20 m.y. ago, and accelerated between 5 to 15 m.y. ago, but slowed down in the past 5 m.y. with extension rate changing from 20-30 mm/yr to only about 10 mm/yr.

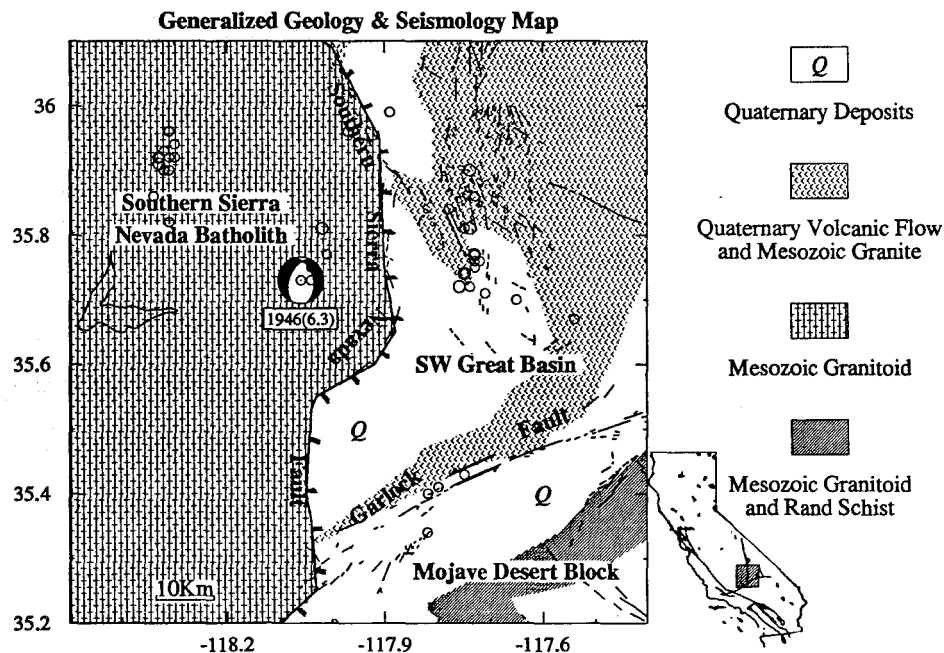


Figure 5.3 Generalized seismotectonic map of the SSNF domain.

Two major faults exist in this domain, the southern Sierra Nevada boundary fault and the western segment of the Garlock fault. The southern Sierra Nevada fault is a normal fault, bounding the Sierra Nevada uplift to the east. Topographically, it is a pronounced escarpment (Christensen, 1966). The southern Sierra Nevada itself is composed of several generations of Mesozoic granitic rocks, (e.g. Saleeby, 1981, 1988). Late Cenozoic volcanic activity was very intensive. Basaltic lava flows can be found in the lowlands such as the river canyons of the uplift, and are 3-9 m.y. old (Dalrymple, 1963). Dalrymple (1963) inferred at least 6000 ft (2 km) uplift in the past 9 m.y. (cited by Christensen, 1966, p.171-172). The uplift movement in the southern Sierra Nevada was apparently not uniform, with the eastern side rising faster than the western side and causing a westward tilting of the block (Dibblee, 1955; Christensen, 1966). Although the west-tilting uplift began as early as late Cretaceous (Dibblee, 1955), the last major uplift was accomplished in the past 3 m.y. (Christensen, 1966). The best estimate of vertical movement on the southern Sierra Nevada fault is 4000 ft (1.2 km) in the last 3 m.y. (Christensen, 1966), which yields a vertical uplift rate of 0.4 mm/yr.

The other major fault, the Garlock, is a left-lateral strike-slip fault, which bends from NE to nearly E-W as it extends into southern Death Valley. It shows up to 64 km of left-lateral displacement of dike swarms since late Tertiary time (Smith, 1962). Although there was little seismic activity on the fault in this century (see Allen et al., 1965 and Figure 5.3), geologic studies reveal that the fault slipped in the Holocene era, and could produce a large earthquake in the future (Astiz and Allen, 1983). The Holocene slip rates on the Garlock fault in this segment vary from 5 to 10 mm/yr (McGill and Sieh, 1993). The principal extensional axes from tectonic stress, seismic strain, geodetic measurements, and surface geological measurements are very similar to each other, which are oriented WNW (see Jones, 1987 and Chapter 4).

Theodolite alignment arrays across the Garlock fault in this reach between 1973 and 1983 recorded no slip within a few hundreds of meters of the fault (Louie et al., 1985), indicating temporary locking of the Garlock fault. However, trilateration measurements between 1973-1979 showed a principal extensional strain of  $0.02 \times 10^{-6}$  in the direction  $N72^\circ W$  (Savage et al., 1981), which is 1.0 mm/yr for a 50 km wide zone. But seismic strain rate is only about 0.3 mm/yr from 1927 to 1990 (Figure 5.2).

### 5.3.2 WWF Domain

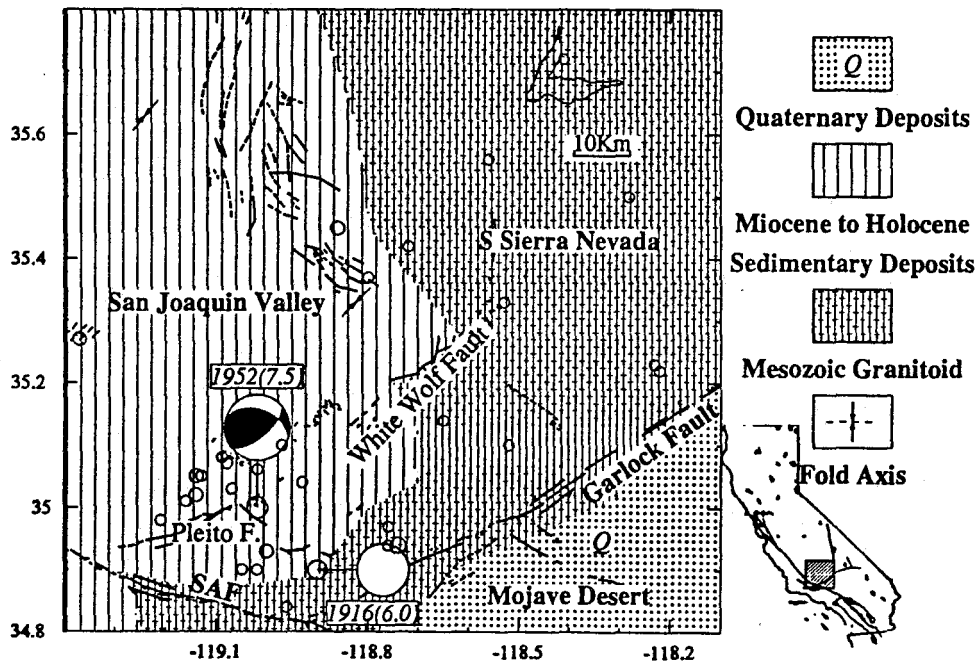


Figure 5.4 Generalized seismotectonic map of the WWF domain.

The WWF domain is located at the southeast terminus of the Great Valley (San Joaquin Valley) (Figure 5.4), where the southern Sierra Nevada, Coast Ranges, Mojave Desert, and the Transverse Ranges meet. The San Joaquin Valley is a west-tilting basin filled with thick Cretaceous-Cenozoic sediments shed from the rising Sierra Nevada to the east and southeast (see Dibblee, 1955). The rugged mountainous areas, including the Tehachapi, Bear, and San Emigdio Mountains, between the WWF and the Garlock fault have been attributed to N-S compression (Hill and Dibblee, 1953). The N-S shortening is expressed in the E-W trending reverse faults and fold axes, for instance, the Pleito thrust, the WWF, and the Wheeler Ridge. The Pleito thrust is sinuous in trace, and generally dips  $50^{\circ}$  to the south. It brought the basement complex to the surface in the elevated San Emigdio Canyon (Dibblee, 1955). The E-W-trending fold axes in the Tertiary sediments indicate that the folding was associated with the uplifting of the Tehachapi, Bear, and the San Emigdio Mountains. The total vertical displacement on the WWF is estimated as 1.5-3.0 km (Dibblee, 1955, P.30). The mapped White Wolf fault was recognized largely within the granitic basement before the 1952 earthquake. The surface rupture of the earthquake extended southward and beneath the alluvium of the southern San Joaquin Valley (Dibblee, 1955). Although the surface rupture during the 1952 earthquake did not extend southwestward into the Pleito thrust, many lines of evidence indicate that the WWF extends under the Wheeler Ridge anticline which separates the thick Plio-Pleistocene series 4,000 ft on the ridge, and 12,000 ft in the valley to the north (Dibblee, 1955), a drop of 8,000 ft (2.6 km). The recent activity of the fault was exemplified by the July 21, 1952  $M_W=7.5$  Kern County earthquake. Surface investigations following the earthquake showed that the WWF slipped 1 m vertically, and 1/2 m horizontally (Buwalda and Amand, 1955; Dibblee, 1955). The gross P-wave first motion data yielded a focal plane solution of  $320^{\circ}$  strike,  $63^{\circ}$  dip, and  $55^{\circ}$  rake angle (Gutenberg, 1955). Integrating surface geology and geodetic data, Stein and Thatcher (1981) interpreted that the dip angle of the White

Wolf fault changes from 75° on the southwest to 20° on the northeast. The amount of slip also decreases from southwest to northeast along strike. Based on offset of a Quaternary volcanic ash horizon across the fault, Stein and Thatcher (1981) determined the vertical slip rate on the WWF to be 3-9 mm/yr between 0.6-1.2 m.y. ago.\* They concluded that the long-term geologic rate is consistent with the 48-year-period geodetic rate, which was 5-10 mm/yr between 1926 and 1972. The seismic slip rates averaged over the past 65 years also show similar vertical movement (6.0 mm/yr), but the horizontal shear rate from earthquakes is much larger than the vertical rate (Table 5.1).

The slip rates on the Garlock fault were summarized in detail by Astiz and Allen (1983), who gave a best estimate of 7 mm/yr for the Holocene epoch. The geologic slip rates are determined based on offset Holocene and Pleistocene alluvial fan gravels (Carter, 1971, 1980), and Holocene tufa (Clark and Lajoie, 1974), which yields a slip rate of 8-12 mm/yr and 7 mm/yr, respectively. Astiz and Allen (1983) noted that unlike the eastern segment of the Garlock fault, the western Garlock fault has noticeably large left-lateral creep, up to 4 mm/yr over a 150-meter wide zone, and perhaps as much as 7 mm/yr over a wider zone (Keller et al., 1978, cited by Astiz and Allen, 1983, p.1724). The seismic shear rate in the past 65 years was 26 mm/yr across the 60 km-wide domain, which is about 3 times that of the geologic rate for the Garlock and the White Wolf faults combined. This is because of the contribution of the 1952 earthquake. Our time window is far from covering the earthquake cycle, which is estimated as about 170-450 years (Stein and Thatcher, 1981). Trilateration measurements between 1973-1979 showed that the principal compressional strain is oriented N13°W, with a rate of  $0.15 \times 10^{-6}$  (Savage et al., 1981). For a 60 km wide-zone, the

---

\* The vertical displacement on the WWF is controversial. For instance, Davis (1986) argued, with more stratigraphic control, that vertical separation has been insignificant since the middle Pleistocene. But everybody agrees that the vertical component is more obvious than the horizontal.

N-S geodetic convergence rate is about 9.0 mm/yr.

Oblique-slip mechanisms are predominant in the background seismicity. And P axes showed a wide range of variation in orientation (see Chapter 3). The stress tensor shows N-S principal compression, while the strain tensor shows NNE. The stress tensor is favorable for strike-slip motion, while the strain tensor is favorable for reverse or oblique-slip (see Chapter 4). Note also that the strain patterns from trilateration in the period from 1973 to 1980, and from 1973 to 1984 show NNW principal compression (Savage et al. 1981, 1986). These slightly different orientations of principal maximum convergence implies that fault geometry and strength in the WWF domain is heterogeneous. The complexity can also be seen from contemporary borehole breakouts. Castillo and Zoback (1994) show that the principal compressive stress axes from borehole measurements systematically change from NE-SW in central California to near N-S in the southern San Joaquin Valley, and to near E-W, parallel to the strike of the WWF in the vicinity of the fault. This near E-W compression is inconsistent with the regional stress field, and may, according to Castillo and Zoback, be the result of the stress drop of the Kern County earthquake.

### **5.3.3 MVE Domain**

The Mojave Desert is a triangular area bounded on the north and northwest by the Garlock fault, on the southwest by the San Andreas fault, and on the southeast by the Pinto Mountain fault. Its eastern boundary is ambiguous, and it is probably not a single fault boundary. Several kinematic models have been proposed to explain the internal structures, deformation patterns, and their relation to adjacent provinces. Garfunkle (1974) inferred 30° - 40° counterclockwise rotation of the Mojave Desert about a vertical axis since a time no earlier than the late Pliocene, based on total right-lateral

displacements on the fault systems in the central Mojave. Cummings (1976) developed a two-dimensional plastic model, and showed that the structural lines in the Mojave Desert can be simulated by a simple N-S compression across the Mojave Desert. Carter (1987) integrated paleomagnetic data and suggested that the western and southern Mojave were rotated 15° counterclockwise, and that the northeastern Mojave was rotated 40° clockwise about a vertical axis. Dokka and Travis (1990, a,b) based on field geology and available paleomagnetic data argued that the deformation in the Mojave Desert is not uniform. They divided the Mojave Desert into six domains, each of which has different deformation patterns, either in sense or in magnitude, or both. Our definition of the MVE domain is the south-central Mojave, or the II and III domains of Dokka and Travis (1990a). It encompasses several closely-spaced parallel NW-striking faults. From west to east, they are the Helendale, Lenwood, Camp Rock, West Calico and Pisgah faults (Figure 5.5). The total measured displacement on these faults is 65 km. This corresponds to a slip rate of about 7 mm/yr since the late Miocene (6-10 Ma) (Dokka and Travis, 1990, a,b). Dokka and Travis (1990, a,b) pointed out that slip on the NW-striking faults decreases northwestward as they approach the Garlock fault. They also concluded that geologic activity becomes younger westward and southward.

---

Figure 5.5 Generalized seismotectonic map of the MVE domain.

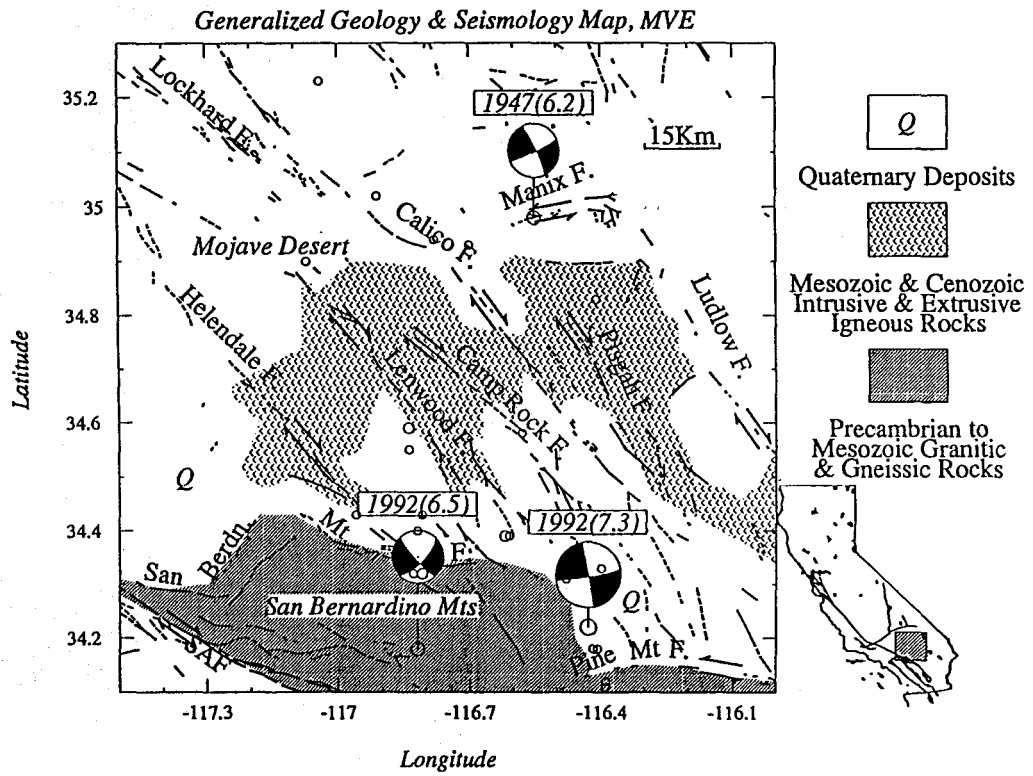


Figure 5.5

The background seismicity (1981-1990) was low and chiefly distributed in the central and southern part of the Mojave Desert (Chapter 2). Dokka and Travis (1990, a,b) proposed a major shear zone bounded by the Blackwater-Calico fault on the southwest and by the southern Death Valley fault to the northeast. They termed it the East California Shear Zone. This shear zone deflects the Garlock fault in its eastern segment, making it trend more E-W. Trilateration and triangulation measurements in Barstow demonstrate the existence of the shear zone, with as much as 6-8 mm/yr right-lateral shear (Sauber et al., 1986; Savage et al., 1990). For a 60 km wide zone, the geodetic shear rate is 12 mm/yr (Sauber et al., 1994).

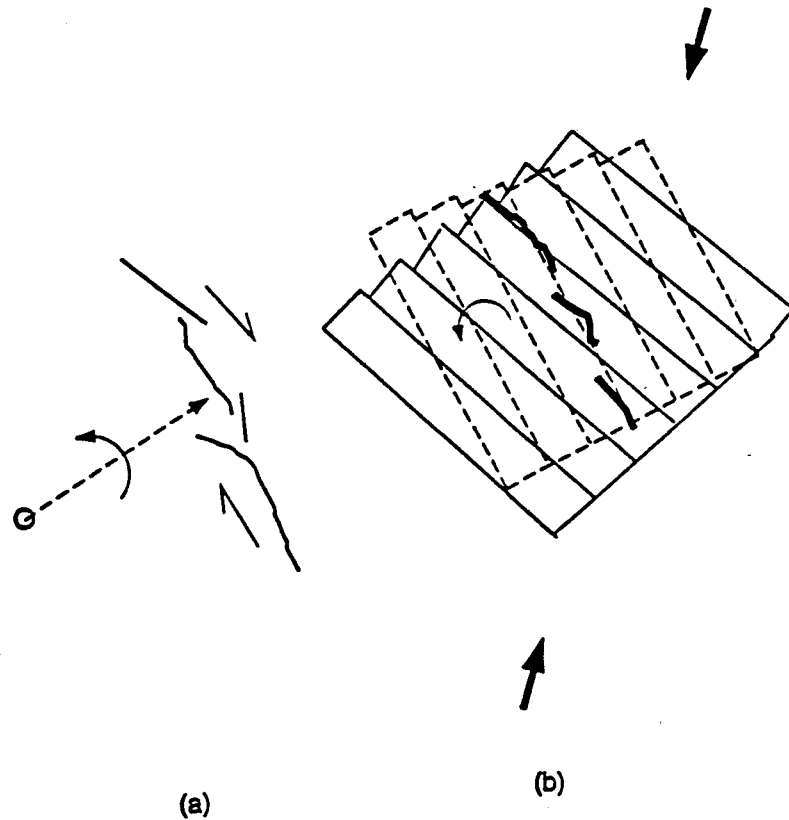


Figure 5.6 Two possible explanations for faulting associated with the Landers earthquake. (a) Counterclockwise rotation about a vertical axis; (b) Newly-born NNW-striking fault in response to the current tectonic stress field (Nur et al., 1992).

the seismic strain pattern of background seismicity in the MVE domain is dominated by strike-slip (see Chapter 4). Both the stress tensor and the strain tensor show similar orientations of the principal compressive axis (Table 5.1), which is in the N-NE direction. Both are favorable for strike-slip faulting. Focal mechanisms in the MVE have a large value of  $S_c$ , reaching 0.66. Before the 1992 Landers  $M=7.3$  earthquake, the right-lateral seismic shear strain rate was very small, less than 10% of the geologic or geodetic rates. With the occurrence of the Landers earthquake, the seismic strain rates are added up and apparently match the total deformation that is observed geologically and geodetically. Seismic shear strain rate across the 70 km-wide zone is 5.2 mm/yr for the period from 1900 to 1992 (Huang et al., 1992), or 8 mm/yr from 1934 to 1992. Apparently, elastic strain had accumulated before the Landers earthquake. Nur et al. (1992) argued, based on the consistent mechanisms of major earthquakes since 1947, that a new NNE-striking fault zone is being formed that is transforming the mapped NW-striking fault system. It appears that the Landers earthquake may also indicate the counterclockwise rotation of the southwestern side relative to the northeastern side, as implied by the curvature of the associated surface ruptures (Figure 5.6).

#### **5.3.4 WTR Domain**

The WTR domain defined in this study encompasses the Santa Barbara Channel, Ventura basin, Santa Ynez Mountains, and the Santa Maria basin (Figure 5.7). This domain is characterized by E-W-trending structures such as fold axes and fault traces. Approximately N-S compression has long been suggested from geologic studies alone (see Hill and Dibblee, 1953; Dibblee, 1982; Yeats, 1983). Weldon and Humphreys (1986) hypothesized an offshore left-stepping right-lateral shear system that is parallel to the San Andreas fault to account for the N-S shortening across the WTR. But the

development of the WTR may not be entirely due to N-S compression. Paleomagnetic data indicate that the WTR was originally trending N-S. It was rotated clockwise up to 90° in the past 16 m.y.. (Hornafius et al., 1986; Luyendyk and Hornafius, 1987). This large angle of rotation produced a series of basins adjacent to the north and south boundaries of the WTR (Luyendyk and Hornafius, 1987). Jackson and Molnar (1992), noting that the slip vectors from major earthquakes are nearly perpendicular to the San Andreas fault, proposed that the EW-trending left-lateral faults are rotated clockwise about the vertical axis in response to the N-S compression.

### Generalized Geology & Seismology Map, WTR

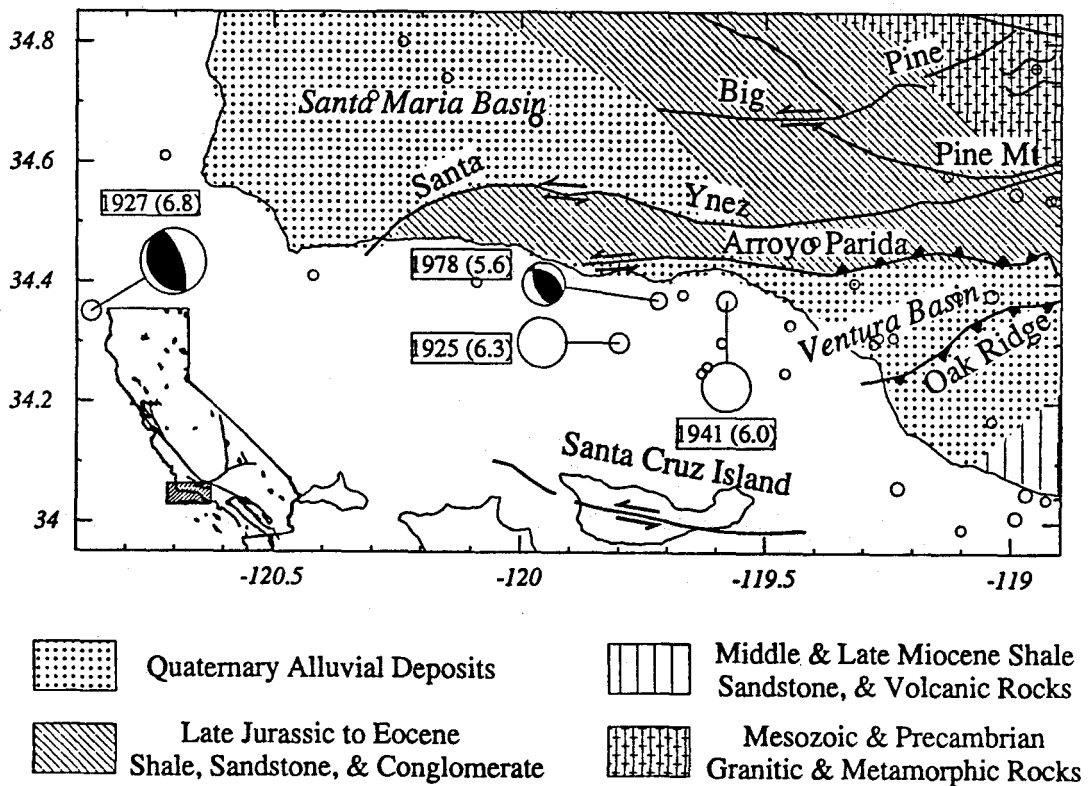


Figure 5.7 Generalized seismotectonic map of the WTR domain.

It is worthwhile to point out that the E-W-trending strike-slip faults are evidently away from the bend area of the San Andreas fault. Within the bend area, reverse faults prevail. For example, the Arroyo Parida fault connects eastward to the north-dipping Santa Cayetano, Santa Susana, and Sierra Madre faults that are all located south of the bend area of the San Andreas fault (see next section). The Malibu-Coast-Raymond fault is in general regarded as a left-lateral strike-slip fault (see Davis and Burchfiel, 1973; Campbell and Yerkes, 1976; Luyendyk and Hornafius, 1987). Recent geomorphological analysis by Dolan and Sieh (1991) indicates that this fault is segmented. The segment east of the intersection with the Newport-Inglewood fault is perhaps dominated by reverse faulting, whereas the segment west of the intersection is dominated by left-lateral faulting. The Santa Ynez fault is sinuous along its strike, and convex to the south on its eastern segment, but to the north on its western segment. The left-stepping en echelon folds along its strike indicate that this fault is a left-lateral shear zone (Sylvester and Darrow, 1979). However, Holocene activity of the Santa Ynez and Arroyo Parida faults is nebulous, and weak if it exists at all (Buchanan-Banks et al., 1975; Sylvester and Darrow, 1979).

The most important basin in the WTR is the Ventura basin, since it has a great package (up to 10-15 km thick) of Cenozoic sedimentary rocks (see Yeats, 1983; Keller and Prothero, 1987). It is bounded on the north by the north-dipping Santa Cayetano fault, on the south by the south-dipping Oak Ridge fault, and flanked by the Santa Ynez Mountains to the north and the Santa Monica Mountains to the south. The N-S convergence across the Ventura basin occurs chiefly on these two faults, with a rate as large as 23 mm/yr in the past 0.2 m.y. (Yeats, 1983). As much as 6-13 mm/yr of this may be on the Oak Ridge fault (Yeats, 1988). The Ventura basin began to form 22 m.y. ago (Crowell, 1974, 1987), and subsided rapidly in the past 2 m.y. (Yeats, 1977). It continues to sink as indicated recently by leveling (Buchanan-Banks

et al., 1975). The N-S shortening is also active. GPS work indicates a N-S shortening rate of up to  $11\pm 3$  mm/yr between 1987 and 1992 across the Ventura basin (Donnellan et al., 1993). However, the principal directions from GPS vary significantly within 20-30 km from  $N24^{\circ}W$  to  $N15^{\circ}E$  (Donnellan et al., p.21,734, their Figure 5). These observations, in my opinion, may be attributed to the heterogeneous folding of the incompetent sedimentary rocks within the basin.

The Santa Maria basin has a different history from that of the Ventura basin. In early and middle Miocene time, it was dominated by NW-striking right-lateral strike-slip faults associated with small-scale pull-apart basins. But since late Miocene time, W-NW-striking north-dipping thrusts came into being (see Luyendyk and Hornafius, 1987), the so-called Santa Maria fold and thrust belt (see Feigl et al., 1990). Geodetic measurements and interpretations by Feigl et al. (1990) indicate that the integrated convergence rate across the basin is  $7\pm 1$  mm/yr in the direction of  $N3^{\circ}E\pm 13^{\circ}$ , which is the same magnitude as in the Ventura basin, and essentially the same orientation. Restoration of a balanced cross section from the West Montalvo oil field near the Oak Ridge fault north to the San Emigdio Mountains by Namson and Davis (1988) yields a N-S convergence rate of 11.3-17.0 mm/yr in the past 2-3 m.y.. Terrace studies by Lajoie et al. (1979) suggested a Quaternary uplift rate of 4-10 mm/yr near Ventura. Based on similar data, Yerkes and Lee (1987) estimated a maximum rate of tectonic uplift along the Santa Barbara-Ventura Coast as 10 mm/yr in the past 45,000 years. It is, therefore, very evident that the WTR region has been undergoing folding and thrusting. As a result, some parts of it exhibit uplift, whereas others show subsidence.

Most earthquakes in the past decade were located south of the Santa Ynez fault (Figure 5.7). This was also true for the period between 1970 and 1975, as reported by Yerkes and Lee (1987). They were scattered in distribution with no clear correspondence to the surface faults. The total seismic strain indicates that the WTR is

dominated by reverse faulting (Chapter 4). One abnormal phenomenon in the WTR is that it has the deepest (30 km) earthquake in southern California (Chapters 3, 4). A large number of events have focal depths down to 20-30 km, which is 10 km deeper than other areas of southern California. Bryan and Jones (1992) attributed these anomalous focal depths to the downwarping of the Moho surface beneath the Ventura basin, in which up to 15 km of Cenozoic sediments are accumulated, and which has very low heat flow. They suggested that the rapid convergence of the Ventura basin is confined to the basin itself, not the whole WTR. The principal compressive axis from stress inversion is oriented N12°E, which is close to the geodetically observed shortening direction in the Santa Barbara Channel area of N25°E (Larsen et al., 1993). The magnitude of strain is, however, quite different between geodesy and seismology. Slip rates from summed seismic moments, both in the last 10 and 65 years, are one order of magnitude smaller than those from geodesy and geology. The N-S seismic shortening is only 0.26 mm/yr in the past 65 years whereas the E-W left-lateral shear is 1.1 mm/yr (Table 5.1).

### 5.3.5 CTR Domain

---

Figure 5.8 Seismicity ( $M \geq 1.0$ , 1975-1991) and major earthquakes from 1971 to 1994 in the CTR domain. Shading shows two seismic zones in which seismicity has been concentrated. The north branch is termed here "the southern mountain frontal fault" system because it bounds the San Gabriel and Pine Mountains. The southern branch is "the southern range frontal fault system" because it bounds the southern Transverse Ranges. Note the approximately equal spacing of epicenters of major earthquakes in the shaded zones.

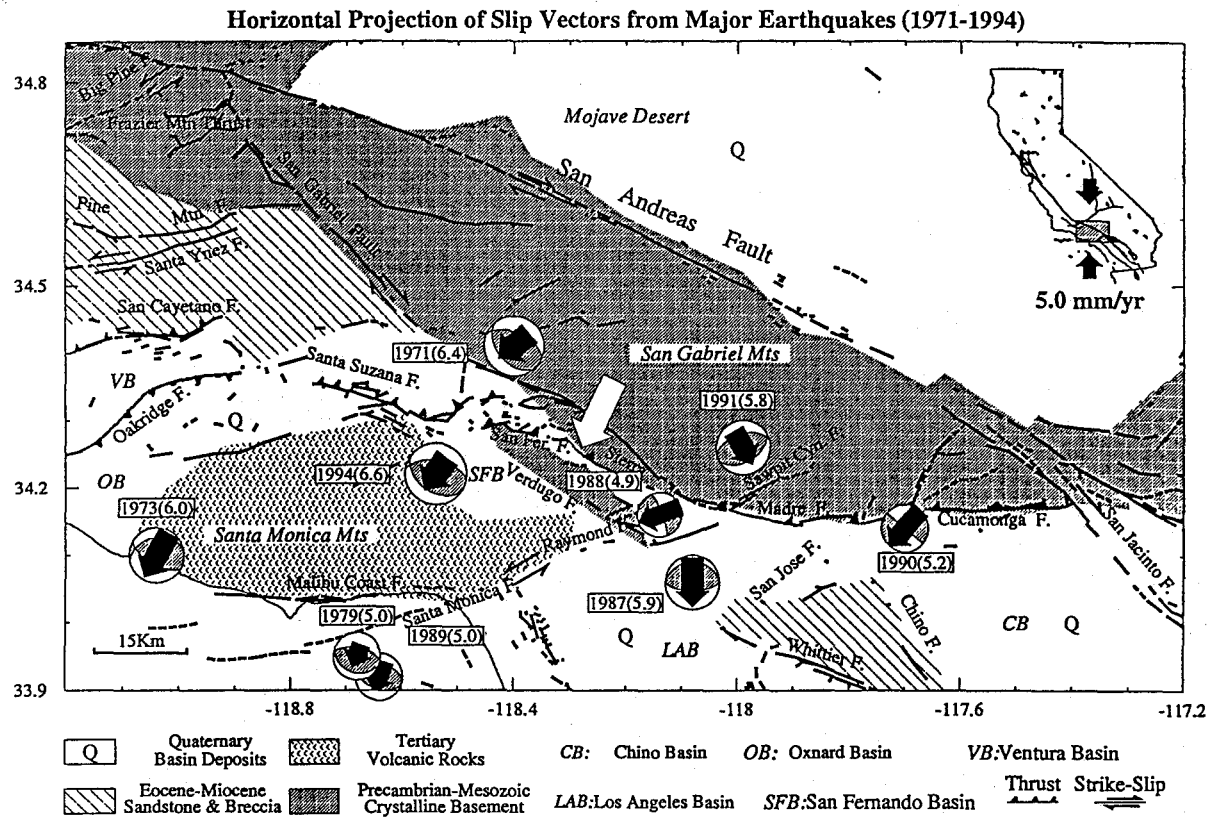


The CTR domain is one of the most seismically active areas in southern California in the past two decades. Several major earthquakes have struck this domain and caused severe damage (Figure 5.8). Among these are the 1971  $M_L=6.4$  San Fernando, the 1987  $M_L=5.9$  Whittier Narrows, the 1988  $M_L=4.8$ , Pasadena, the 1988  $M_L=4.6$  and 1990  $M_L=5.2$  Upland, the 1991  $M_L=5.8$  Sierra Madre, and the 1994  $M_w=6.7$  Northridge earthquakes. Both reverse and strike-slip mechanisms coexist in this domain. The 1988 Pasadena earthquake (Jones et al., 1990; Ma and Kanamori, 1991), and the 1988 and 1990 Upland earthquakes (Hauksson and Jones, 1991a) are strike-slip mechanisms, while the 1971 San Fernando (Whitcomb et al., 1973), the 1987 Whittier Narrows (Hauksson and Jones, 1989), the 1991 Sierra Madre (Dreger and Helmberger, 1991; Hauksson and Jones, 1991b; Huang et al., 1991), and the 1994 Northridge earthquakes are reverse mechanisms. Some reverse faults on which earthquakes have occurred do not reach the surface and hence their histories of activity are difficult to assess. Typical examples are the Whittier Narrows (Davis et al., 1989) and the Northridge earthquakes (Davis and Namson, 1994; Yeats and Huftile, 1995). Davis et al. (1989) proposed that a major detachment exists at a depth of about 15 km, gently dipping to the north. Slip on this detachment creates propagation folding south of the San Gabriel Mountains and a number of ramp-flat structures. The N-S shortening rate for the past 2.2-4.0 m.y. from the N-S balanced cross section between Palos Verdes Hills and the San Andreas fault is at least 4-7 mm/yr, and possibly between 5-14 mm/yr (Davis et al., 1989). However, the N-S convergent seismic rates in the past 10 and 65 years are only about 0.8 mm/yr. It is only about 1.9 mm/yr even if we take the 1994 Northridge earthquake into account (Table 5.1).

---

Figure 5.9 Horizontal projection of slip vectors associated with major earthquakes, CTR. The slip vectors indicate the motion of northern (either northeastern or northwestern) blocks relative to the southern blocks. The open arrow is the average slip direction which is S26°W.

Figure 5.9



Strain partitioning among major fault zones is obvious. Seismicity was mainly concentrated in two zones (Figure 5.8), the southern mountain frontal fault system (Santa Cayetano-Santa Susana-Sierra Madre-Cucamonga) (Huang et al., 1991), or the Santa Ynez-San Gabriel zone of Namson and Davis (1988), and the southern range frontal fault system (the Malibu Coast-Raymond Hill) (Huang et al., 1991), or the Santa Monica zone of Namson and Davis (1988). We gave different names to these zones because we think they are more compatible with the regional structure. It appears in Figure 5.8 that epicenters of major earthquakes are approximately equally spaced along these two zones, for instance, between San Fernando and Pasadena, between Pasadena and Malibu, between Pasadena and Upland. Geologically, Campbell and Yerkes (1976) inferred a 60-90 km left-lateral strike-slip displacement on the Malibu Coast fault based on regional studies. Topographically, the northern side of the southern mountain frontal fault system is a high region with a sinuous and discrete topographic discontinuity along the strike. The basement rocks were brought up by reverse faults and rapid erosion deposited thick alluvial fans at the foothills. The N-S convergent rate in the past 13,000 years across the Cucamonga fault is estimated at least 5 mm/yr (Matti et al., 1985), and possibly 10 mm/yr (Morton and Matti, 1987).

---

Figure 5.10 Earthquakes and focal mechanisms adjacent to the San Andreas fault, Mojave segment. Most of them are from Jones (1988). The numbers adjacent to the focal mechanisms correspond to the events listed in Table 5.2.

Figure 5.10

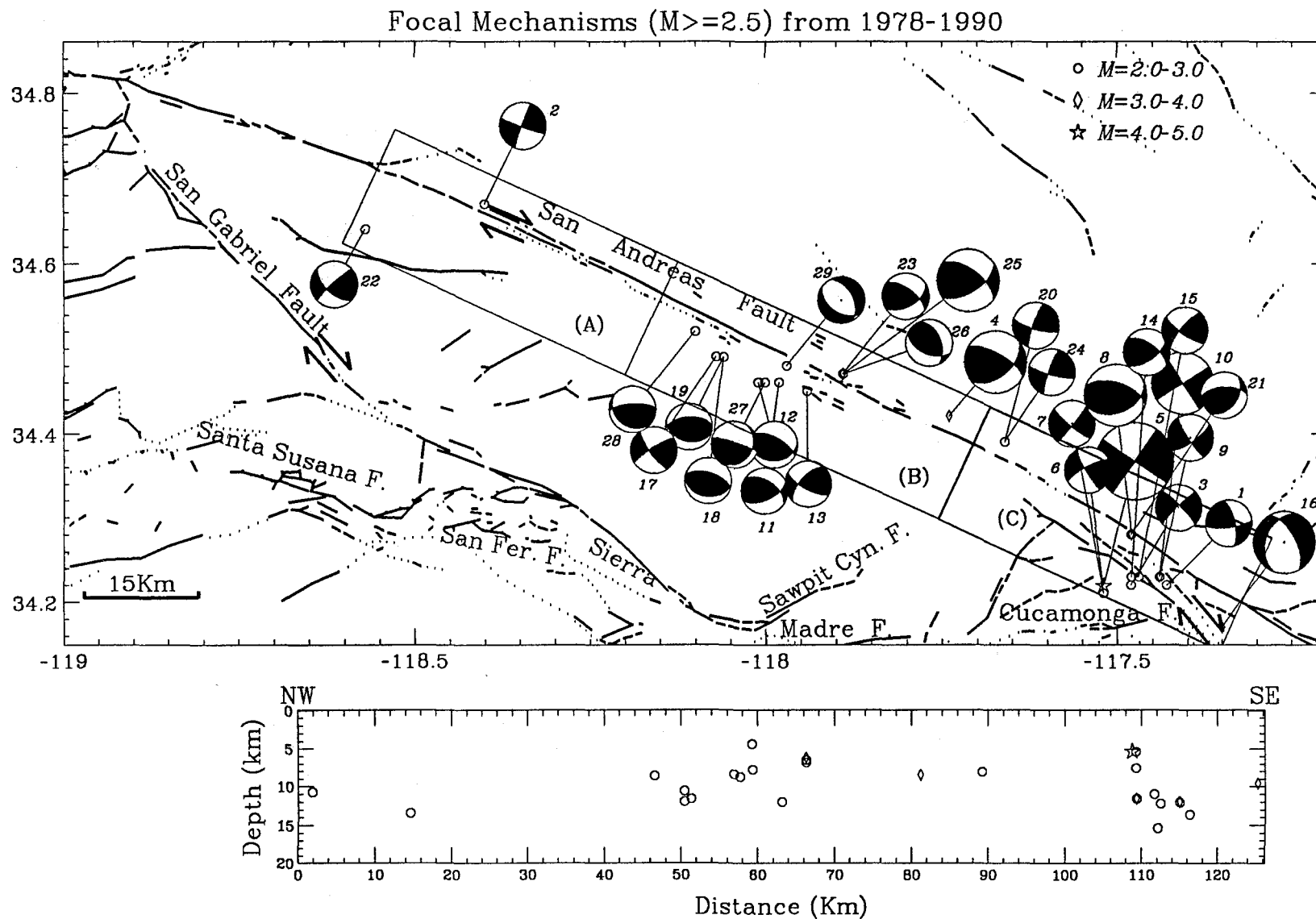


Table 5.2 Listed Events with Known Focal Mechanisms (78-90)

No.	Yr	Mon	Dy	Hr	Mit	Long.	Lat.	M	Dep	Dip	Rake	Stk	Ref.
1	78	08	13	21	48	-117.43	34.22	2.8	13.60	68	163	346	LJ
2	78	11	07	00	28	-118.40	34.67	2.6	13.40	85	176	110	LJ
3	79	06	03	18	24	-117.48	34.22	2.8	15.40	82	186	316	LJ
4	79	08	28	08	57	-117.74	34.42	3.9	8.50	67	136	299	LJ
5	79	10	19	12	22	-117.52	34.22	4.1	5.30	90	180	305	LJ
6	79	10	19	12	28	-117.52	34.21	2.6	5.40	83	167	150	LJ
7	79	10	19	12	30	-117.52	34.21	2.7	7.60	80	185	130	LJ
8	79	12	20	20	31	-117.48	34.28	3.2	11.60	56	115	288	LJ
9	81	10	05	10	42	-117.44	34.23	2.8	12.10	82	195	147	LJ
10	81	10	05	17	43	-117.44	34.23	3.0	12.00	90	180	327	LJ
11	81	10	24	19	10	-117.98	34.46	2.7	7.80	52	136	304	LJ
12	82	03	25	18	08	-118.01	34.46	2.6	8.39	30	60	85	
13	82	08	12	21	01	-117.94	34.45	2.8	12.00	70	150	120	LJ
14	83	01	31	15	38	-117.48	34.23	2.8	11.00	60	145	305	LJ
15	83	10	24	19	01	-117.47	34.23	2.6	12.20	75	165	125	LJ
16	83	12	29	19	46	-117.35	34.17	3.6	9.60	40	311	200	LJ
17	84	02	25	01	17	-118.07	34.49	2.5	10.60	75	170	145	
18	84	02	25	01	41	-118.06	34.49	2.6	11.60	60	95	287	LJ
19	84	04	14	02	27	-118.07	34.49	2.9	11.90	56	80	267	LJ
20	85	02	11	19	85	-117.66	34.39	2.6	8.10	76	170	106	LJ
21	85	04	12	09	44	-117.48	34.28	2.6	11.60	61	121	268	LJ
22	85	06	01	11	31	-118.57	34.64	2.8	10.70	60	172	134	LJ
23	85	07	08	23	24	-117.89	34.47	2.7	6.50	63	137	307	LJ
24	85	07	19	16	17	-117.66	34.39	2.8	8.1	80	169	106	LJ
25	85	10	31	19	54	-117.89	34.47	3.7	6.20	60	143	306	LJ
26	85	10	31	20	23	-117.89	34.47	2.7	6.80	49	120	337	LJ
27	88	01	11	01	48	-118.00	34.46	2.5	8.74	25	20	35	
28	88	11	14	06	58	-118.10	34.52	2.5	8.58	25	130	110	
29	90	08	06	07	41	-117.97	34.48	2.8	4.36	45	-110	125	

LJ: Lucy Jones (1988). Depths are in kilometers.

Since the slip vectors (Figure 5.9) from major earthquakes trend SSW-NNE, oblique to the E-W-striking fault, both N-S-shortening and E-W left-lateral shearing coexist. For example, the 1971 San Fernando earthquake was associated with 1 m north side up, 1.5-2.0 m left-lateral slip of the northern block relative to the southern block on the San Fernando fault (Kamp et al., 1971; Sharp, 1975). Two fold and thrust belts in the Los Angeles basin area were geologically recognized (Davis et al., 1989) and seismically interpreted (Hauksson, 1991). The one on the northeast is termed the Elysian Park fold and thrust belt. The one on the southwest is called the Torrance-Wilmington fold and thrust belt. This indicates that the N-S shortening across the CTR is not only partitioned in the surface reverse fault zones, but also in the concealed fault systems. The N-S seismic convergence can be seen adjacent to the San Andreas fault in the Mojave segment (Jones, 1988; Huang et al., 1993a), in the central Los Angeles basin, and the southern front of the San Gabriel Mountains (Pechmann, 1987; Hauksson; 1991; Huang et al., 1991), and on the offshore area, such as the Santa Monica bay area (Hauksson and Saldiver, 1989; Hauksson, 1991; Huang et al., 1991). The coexistence of thrust and strike-slip faulting events in the Santa Monica bay area led Hauksson and Saldiver (1989) to conclude that this area is a transitional zone from Peninsula Ranges province where NW-striking strike-slip faults dominate, to the Transverse Ranges province where E-W-striking reverse faults prevail.

Both the seismic stress tensor and the strain tensor for the past 10 years yield a similar N-S directed horizontal principal compression (Chapter 4). But the strain pattern indicates the prevalence of thrust events. Principal compressive strain axes from geodesy show variations between NNW and NNE (Cline et al., 1984). The seismic strain tensor from the past 10 years is oriented N-NW, but NNE for the past 65 years (Table 5.1). Therefore, the maximum convergent strain is approximately in the N-S direction, with about 20° variation around it.

The San Andreas fault in the Transverse Ranges has been relatively quiet in seismicity during the observational time. No earthquakes with magnitude greater than 4.5 have been recorded within 15 km zone of the fault since 1978 (e.g. Jones, 1988) when the southern California seismic network began to expand to its current operation. With the dense seismic network, we are able to determine the fault plane solutions for events with magnitudes even smaller than 3.0 (Table 5.2, Figure 5.10 and Appendix). Of the 29 events between 1978 and 1990 on the San Andreas fault in this segment, 41% of them exhibit reverse faulting mechanisms (Figure 5.11). This large fraction of E-W-trending reverse faulting events can not be attributed to the motion on the San Andreas fault. Instead, they imply concealed thrust faults beneath the San Gabriel Mountains. Geologically, the only exposed thrust fault in this area is the ancient Vincent thrust (Figure 5.12). But the Vincent thrust does not show recent activity. Figure 5.12 indicates that the crystalline rocks of the San Gabriel Mountains appear to be rootless, resting on the Pelona Schist on the Vincent thrust (Ehlig, 1982, Huang et al., 1993a).

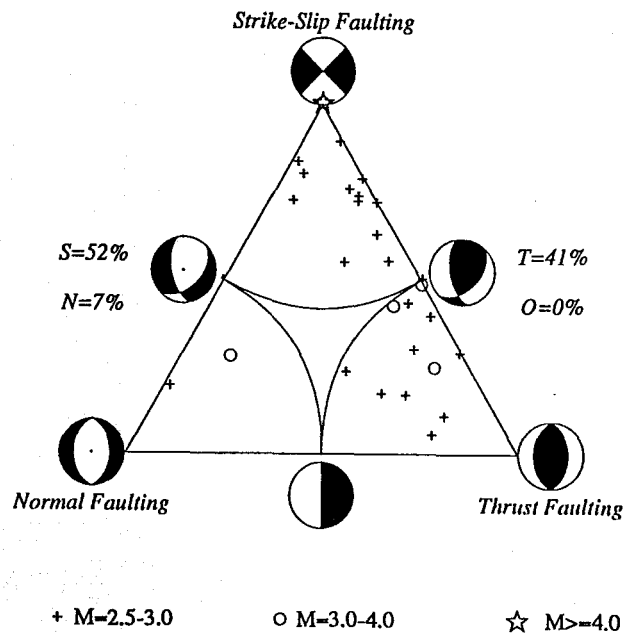
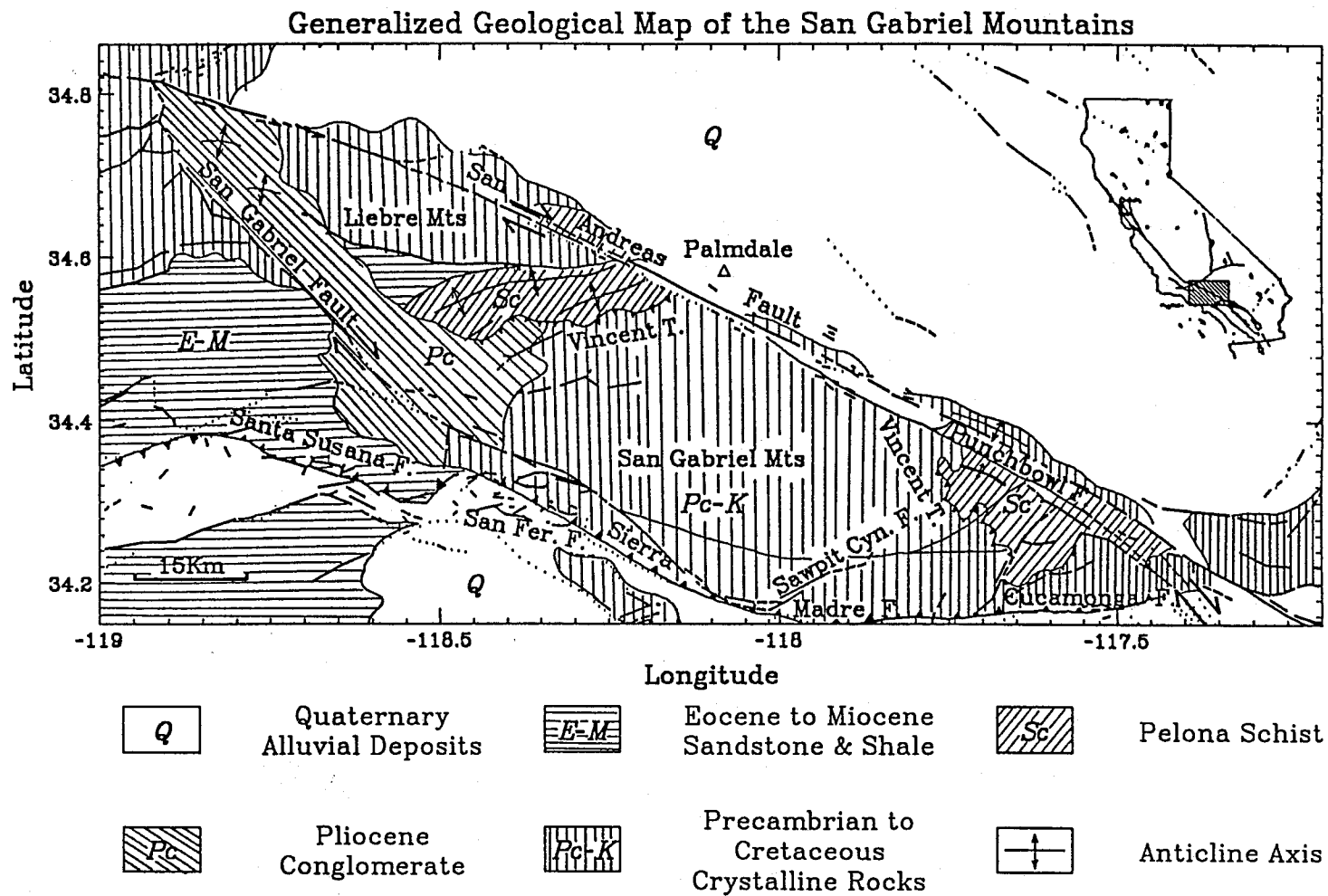


Figure 5.11 Ternary diagram for earthquakes adjacent to the San Andreas fault, Mojave segment.

Figure 5.12



---

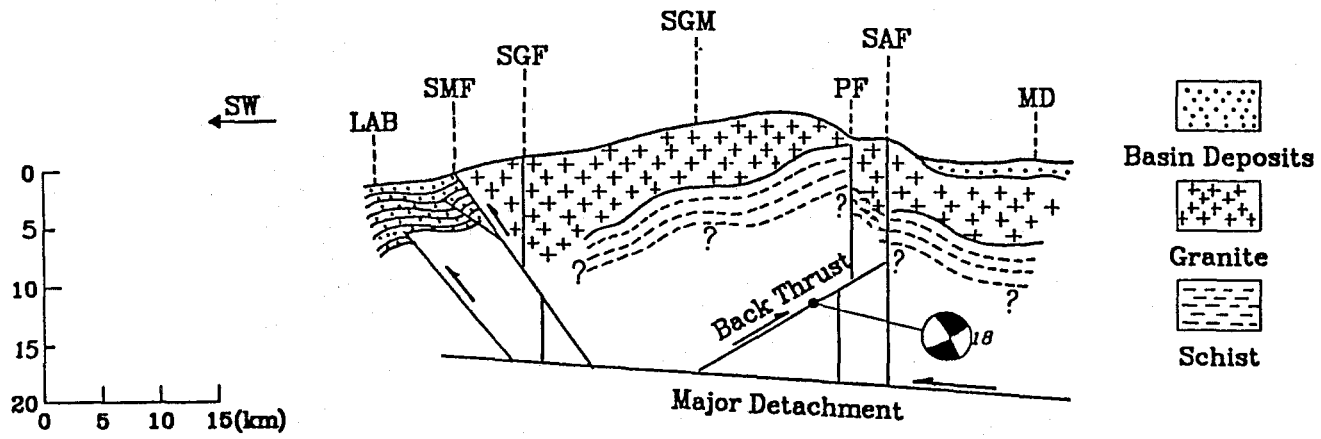
Figure 5.12 Generalized geologic map of the San Gabriel Mountains. The San Gabriel Mountains are bounded by the San Andreas fault on the northeast, by the Vincent thrust on the east and west, and by the Sierra Madre and Cucamonga thrust on the south. The granitic and gneissic mountains apparently rest on the Pelona schist. Compiled from Jennings (1977), Ehlig (1982), and Meisling and Weldon (1989).

To explain these abnormal focal mechanisms, we construct a N-S cross section across the San Gabriel Mountains and part of the Los Angeles basin (Figure 5.13). We visualize that the San Gabriel Mountains are bounded by south-dipping concealed faults on the north and north-dipping faults on the south. Because of the N-S compression, the deformation is partitioned by folding in the basement (Silver, 1991), as well as in the basin (Bullard et al., 1993). As the major detachment slips southward (Davis et al. 1989), the mountains are squeezed, being forced upward and expanding southward.

---

Figure 5.13 Schematic cross section across the San Gabriel Mountains. LAB: Los Angeles basin; MVE: Mojave Desert; PF: Punchbowl fault; SAF: San Andreas fault; SGF: San Gabriel fault; SMF: Sierra Madre fault. Most of the deformation on the back thrust may be inelastic or in the form of small earthquakes. As the major detachment moves southward, the San Gabriel Mountains are squeezed up, expanding southward, and rising northward.

Figure 5.13



Generalized Cross Section across the SGM

Cline et al. (1984) integrated geodetic data since 1870, and found a N-S shortening rate of 1.6 cm/yr between Vernon and Palmdale (their figure 5, p.289) across the CTR. VLBI data from 1984 to 1989 indicate that JPL is moving 34.8 mm/yr N42°W relative to the North American plate (Ward, 1990), from which a N-S convergent rate of 26 mm/yr can be resolved. According to Ward (1990), the SAF at point 34.1°N, 117°W (near the Cajon Pass) has a slip rate of  $25.0 \pm 1.1$  mm/yr in the direction of  $52^\circ \pm 3^\circ$ W. He concluded that north of the Los Angeles basin, a rate of 8 mm/yr convergence normal to the SAF could be produced. Therefore, much of the deformation appears to be within the Los Angeles basin, in which 6-7 km-thick marine and nonmarine deposits from the Miocene to the present are accumulated (Yerkes et al., 1965, Wright, 1991). Therefore, the northern part of the CTR is perhaps characterized by more elastic deformation, and the southern part by more inelastic deformation.

### 5.3.6 ETR Domain

The ETR is located in the eastern bend area of the San Andreas fault. The San Andreas fault there splays into two branches that continue southeastward from the master fault. The northern branch is called the Mill Creek fault (northwestern segment) or the Mission Creek fault (southeastern segment). The southern branch is the Banning fault (Figure 5.14). The ETR domain defined here encompasses the whole of the San Bernardino Mountains, San Gorgonio Pass, and Cajon Pass. The right-lateral Holocene slip rate on the San Andreas fault at Cajon Pass is about 25 mm/yr (Weldon and Sieh, 1985), 25-35 mm/yr in the southern Indio Hills for the Quaternary era (Keller et al., 1982). According to Allen (1957), the Banning fault is an E-W-striking north-dipping fault, evidently showing reverse slip with a displacement of at least 5,000 ft (1.5 km) in the Quaternary time. Holocene right-lateral displacement is nebulous but late Pliocene and Pleistocene right-lateral strike-slip movements total about 5

miles (8 km). Holocene activity appears to occur a few hundreds of meters south of the Banning fault in the San Gorgonio Pass - the San Gorgonio Pass fault system (Matti et al., 1985). This E-W-trending fault system may have a N-S convergence rate as large as 10 mm/yr (Matti et al., 1985).

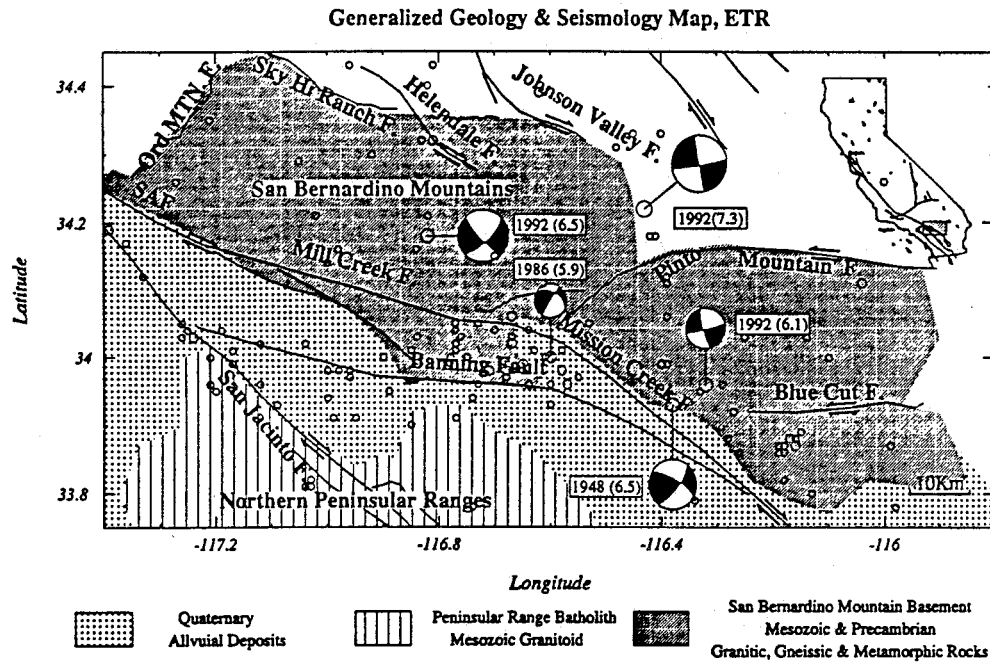


Figure 5.14 Generalized seismotectonic map, ETR domain.

North of the Mill Creek fault are the San Bernardino Mountains. Many fold axes in the basement rocks and the Miocene sediments are mapped adjacent and parallel to the San Andreas fault. According to Meisling and Weldon (1989), the most significant one is the West San Bernardino Arch near Cajon Pass on the northeastern side of the San Andreas fault. These fault-parallel folds imply post-Miocene fault-normal compression. Weldon and Springer (1988) found that many recent normal faults exist in the wedge between the San Andreas and the San Jacinto faults. They pointed out that these diverse secondary structures adjacent to the San Andreas fault may account for the diverse focal mechanisms found by Jones (1988) in the San Andreas fault zone of the San Bernardino segment.

Seismicity is mainly concentrated in the wedge area bounded by the Mission Creek fault, Banning fault and the San Jacinto fault (Figure 5.14). This probably implies that the surface faults are not vertical but dip either southward or northward. One important feature of the seismicity in this domain is that there appears to be a linear distribution of seismicity off of the San Andreas fault, but parallel to its general strike, north from Indio into the south-central Mojave Desert. These mechanisms are consistently strike-slip (see Chapter 4). They may imply a continuous NW-striking fault in the crystalline basement that is not observable on the surface. Many events in the ETR have focal depths down to 20 km (Chapter 2). Furthermore, the focal depths deepen southward across the San Andreas fault (see also Nicholson et al., 1986a). After analyzing microseismic activity, Nicholson et al. (1986, a,b) inferred that rotation and right-lateral strike-slip translation coexist in the ETR area. The largest event in the background seismicity is the 1986  $M_L=5.9$  Palm Springs earthquake. It was a strike-slip event (Jones et al., 1986, Figure 5.14). The tectonic stress tensor and the seismic strain tensor from the background seismicity are very similar (Chapter 4). The principal compressive axes from these two tensors both trend N-NE (Table 5.1). Both the

stress tensor and the strain tensor are favorable for strike-slip movements. The maximum convergent strain direction documented from trilateration between 1973 and 1984 is N16°W at Cajon Pass (Savage et al., 1986), which is about 20° different from the maximum convergence direction obtained from the total seismic moment tensor (Table 5.1).

Little creep was recorded geodetically in this segment of the San Andreas fault, although Keller et al. (1978) reported some aseismic slip (with large uncertainties) from alignment arrays at several places on the San Andreas fault in this domain. Trilateration surveys in the Cajon Pass area between 1974 and 1984 showed a principal convergence rate of  $0.19 \times 10^{-6}$  in the direction of N16°W (Savage et al., 1986), which is about 9 mm/yr for a width of 50 km. In the western Mojave or the northern San Bernardino Mountains, triangulation measurements show a principal strain of  $0.08 \times 10^{-6}$  /yr between 1943 and 1982 in the direction of N86°W (Savage et al., 1990), which gives a N-S convergence rate of 4 mm/yr across a 50 km wide zone. These geodetic rates appear to be within the range of geologic rates (5-10 mm/yr) estimated by Matti et al. (1985). Seismic data between 1927-1991 showed a N-S shortening rate of 0.8 mm/yr. Adding the 1992 M=6.1 Joshua Tree and the Big Bear M=6.5 earthquakes, the N-S seismic convergence rate increases to 1.6 mm/yr (Table 5.1). Considering the fact that the Landers ruptures were extended northwestward into the Mojave, although the epicenter was in the ETR, it is reasonable to believe that the N-S seismic shortening rate across the ETR should be somewhat greater than 1.6 mm/yr.

### 5.3.7 NIF Domain

The NIF domain encompasses two NW-striking faults, the NIF and the Palos Verdes Hills fault (Figure 5.15). The NIF bounds the Los Angeles basin on the southwest. Perhaps, it separates the greenschist facies basement on the NE from the

blueschist facies on the southwest (Yeats, 1973). It is a right-lateral strike-slip fault as indicated by the en echelon fold axes along the fault zone (Yerkes et al., 1965, Wright, 1987). However, its accumulative horizontal displacement is nebulous since no good piercing points have been found. Based on a paleomagnetic rotation model, Luyendyk and Hornafius (1987) estimate 60 km of right-lateral displacement since Miocene time on the NIF to accommodate the opening of the Los Angeles basin. Ziony and Yerkes (1985) inferred a Quaternary rate of 1 mm/yr (cited by Hauksson, 1987). The documented vertical slip on the NIF ranges from 0.1 to 6.0 mm/yr (Clark et al., 1984, cited by Wesnousky, 1986). One thing worthwhile to point out is that seismicity between 1977-1985 showed that the state of stress along the fault is segmented (Hauksson, 1987). The northern segment showed vertical minimum principal stress, a stress state favorable for reverse faulting, while the southern segment showed vertical intermediate principal stress, a stress state favorable for strike-slip faulting. Structurally, the Palos Verdes Hills is an antiform with its axis plunging NW and SE (Yerkes et al., 1965). It is the only place onshore where the Catalina schist crops out (e.g. Yeats, 1981).

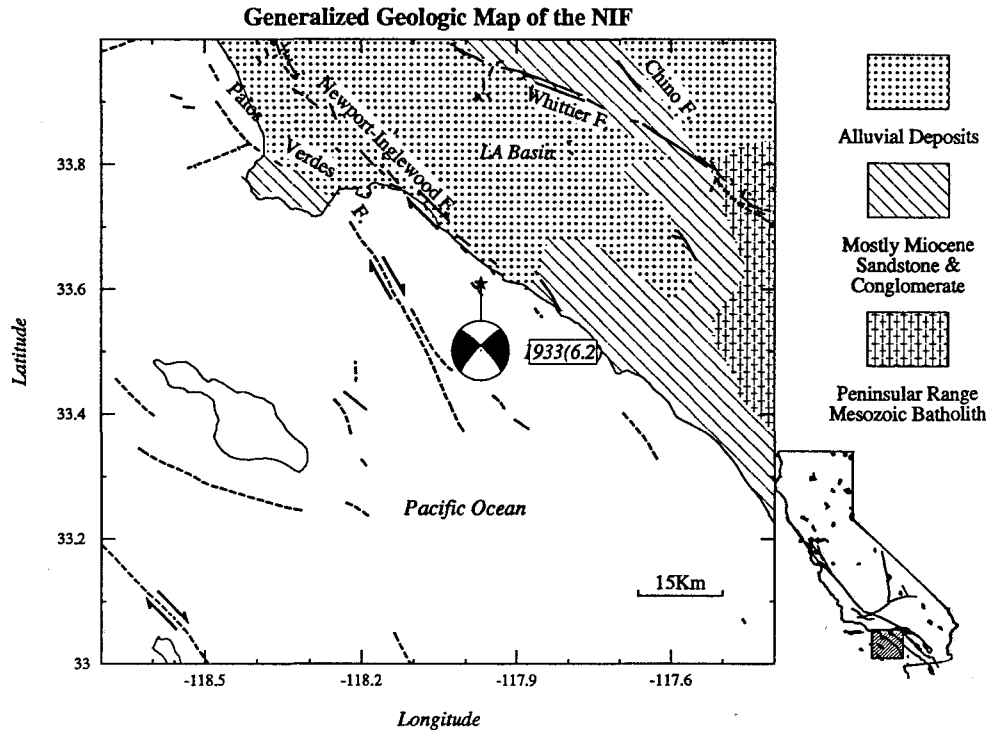


Figure 5.15 Generalized seismotectonic map, NIF domain.

Seismicity in the period from 1981-1991 shows a large number of reverse events (Chapter 3). These events are chiefly located in the thrust belt, the Torrance-Wilmington fold and thrust belt (See Hauksson, 1990). The majority of slip vectors from fault plane solutions are directed N-S. The stress tensor and strain tensor are similar only in their principal compressive axis, but not in the pattern of faulting (Chapter 4). The N-NE orientation of principal compressive strain is very consistent with geodetic measurements reported by Cline et al. (1984). The seismic slip rates and vertical movements are very small from the background seismicity, but right-lateral slip rate is significant for the past 65 years due to the contribution of the 1933 Long Beach M=6.3 earthquake, reaching 3.3 mm/yr between 1927 and 1991 (Table 5.1). The mechanism indicates that the earthquake was associated with faulting on a simple right-lateral fault, the NIF, striking  $315^{\circ}$ , dipping  $80^{\circ}$  to the northeast (Hauksson and Gross, 1990). The associated N-S shortening is 1.6 mm/yr averaged over the period between 1927 and 1991 (Table 5.1). Geodetic surveys between 1870 and 1978 across the NIF domain indicate a principal convergent strain rate of  $0.24 \times 10^{-6}$ /yr in the direction of  $N21^{\circ}E$  (Cline et al., 1984). The N-S convergence rate is therefore  $0.22 \times 10^{-6}$ /yr, which is about 11 mm/yr for a 50 km wide zone.

### **5.3.8 ESF Domain**

The Elsinore fault is actually a family of NW-striking right-lateral faults. They extends north from the gulf rifting in Mexico to the Los Angeles basin, where it splays into two branches. The southwestern branch is the Whittier fault; the northeastern branch is the Chino fault. Like the San Jacinto fault, it is not continuous but consists of a number of short fault strands. It is suggested from microseismicity studies that the dip of the northern segment of the Elsinore fault changes with depth, from vertical to  $70^{\circ}$  SW beneath the Santa Ana Mountains (Hull and Nicholson, 1992). The reported

Quaternary slip rates vary from 0.6 to 9 mm/yr, and apparently vary along the strike (Pinault and Rockwell, 1984, 1985; Millman and Rockwell, 1985; Wesnousky, 1986). The background seismicity is relatively low. The largest earthquake was the 1910  $M=6.0$  located on the northern segment (Figure 5.16). The maximum principal compressive axes from stress tensor and strain tensor are very close, both in a N-S direction (Chapter 4), with about  $10^\circ$  difference. Focal mechanisms in this domain are dominantly strike-slip, being consistent with surface geology. However, the seismic strain rates are very small: 0.01 mm/yr (Table 5.1).

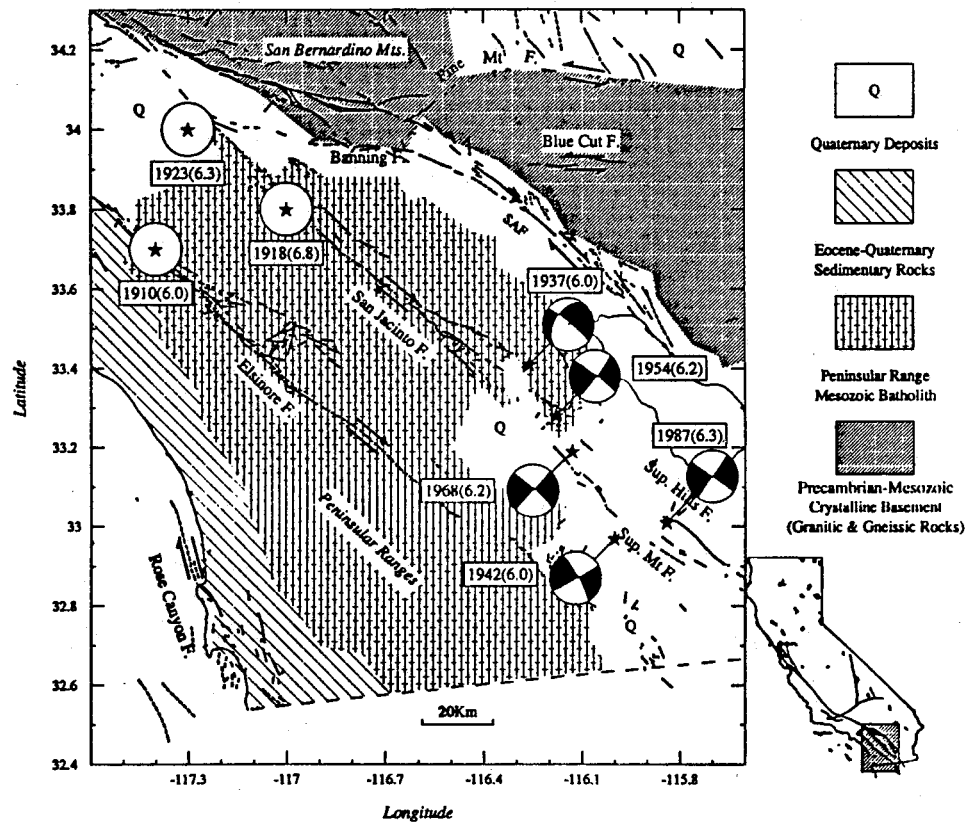


Figure 5.16 Generalized seismotectonic map, ESF and SJF domains.

### 5.3.9 SJF Domain

This domain contains the whole San Jacinto fault zone, composed of several individual short faults, arranged en echelon and generally striking NW (Figure 5.16). As many as nine sections can be identified (Wesnousky, 1986). It is developed in the Peninsular Range batholith and has displaced the batholith more than 24 km since the Pliocene (Sharp, 1967; Hill, 1988). Wesnousky (1986) gave a very detailed summary of the slip rates on the San Jacinto fault. The right-lateral slip rates in the past 0.73 m.y. in the fault zone are estimated as 8-12 mm/yr by Sharp (1981), based on offset Quaternary alluvium. Sharp (1981) also pointed out that variable slip rates existed in the San Jacinto fault in the Holocene time. For example, slip rates were 2.8-5.0 mm/yr in the past 400 years, but 1.4-2.0 mm/yr between 400 and 6,000 years ago. In the northern reach of the fault, the Holocene slip rate is only about 1.7-3.3 mm/yr (Wesnousky et al., 1991). Geodetic measurements are frequently cited for their consistency with the geologic analysis in this fault zone. For instance, following the 1940 Imperial Valley earthquake, triangulation surveys indicate a right-lateral slip rate of 2.4 cm/yr between 1940-1954 (Whitten, 1956). Trilateration measurements and interpretations between 1969-1975, and 1973-1981 yield a slip rate of 11-18 mm/yr (Savage and Prescott, 1976; King and Savage, 1983).

In terms of frequency of moderate earthquakes, the San Jacinto fault was the most seismically active fault in southern California in this century (see Allen et al., 1965; Thatcher et al., 1975; Sanders and Kanamori, 1984). There have been 7  $M \geq 6.0$  earthquakes since the beginning of this century (see Figure 2.3), an average recurrence interval of less than 20 years (see Hutton et al., 1991; Sander, 1993). Using the major events, Brune (1968) calculated a seismic slip rate of 15 mm/yr in the time interval 1912-1963 on the San Jacinto fault. Thatcher et al. (1975) used the same technique, but a longer period (1890-1973), and determined a seismic slip rate of 8 mm/yr. Our

volumetric average shows 1.9 mm/yr between 1981 and 1990, and 2.7 mm/yr between 1927 and 1991 (Table 5.1), in the direction of NW-SE, approximately parallel to the general trend of the San Jacinto fault. The differences among these three calculations are attributed to the difference in the techniques used for the measurement and in the observational time intervals. Our rates are from the tensorial sum of all seismic moments and are dependent on orientations of the coordinate system and the parameters of the focal mechanisms. Both Brune (1968) and Thatcher et al. (1975) made a reasonable assumption that all events have the same mechanisms (pure strike-slip) with slip vectors parallel to the strike of the fault. Our rates are best understood as the integrated or total brittle shear deformation across the width of the fault zone.

Aseismic creep does not seem to be common on the San Jacinto fault. Alignment arrays measurements by Keller et al. (1978) show some creep on the fault, but with large uncertainties. Sanders and Kanamori (1984), based on seismicity analysis and other geodetic data, argued that virtually no aseismic slip appears on the Anza segment of the San Jacinto fault. The seismic strain pattern indicates that the SJF domain is dominated by strike-slip mechanisms (Chapter 4). But small-scale stress heterogeneity in the Anza area is observed (Hartse et al., 1994). Some microearthquakes are not strike-slip mechanisms and they are distributed off the master fault trace in the southern segment of the SJF zone (Peterson et al., 1991). In general, the principal compressive axes from strain tensor and stress tensor differ by  $15^\circ$ , with the axis from the stress tensor oriented N-S, and that from the strain tensor oriented  $N15^\circ W$  (Table 5.1, and Chapter 4). But they are all favorable for strike-slip faulting. Geodetically, between 1973 and 1980, the maximum shortening strain was oriented  $N8^\circ E$  (Savage et al., 1981), but between 1973 and 1984, it was almost N-S (Savage et al., 1986), indicating temporal variations of strain. The approximate horizontal N-S-oriented  $\sigma_1$  and E-W-oriented  $\sigma_3$  could promote slip on both NW and NE-striking conjugate strike-slip

faults, as observed during the 1987 Superstition Hills earthquakes (Magistrale et al., 1989; Wald et al., 1990).

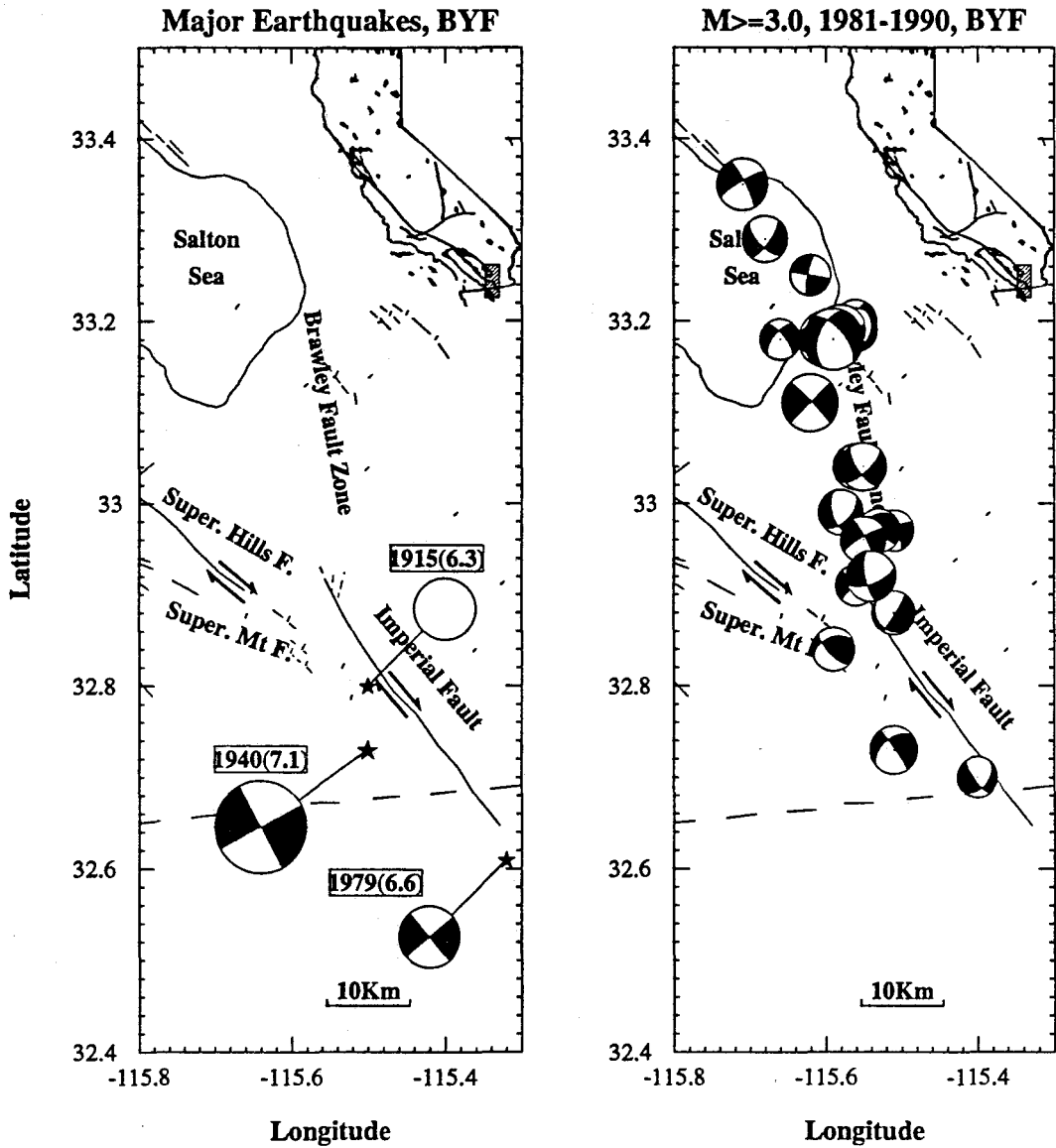


Figure 5.17 Generalized seismotectonic map, BYF domain.

### 5.3.10 BYF Domain

The BYF domain encompasses the Imperial fault and Brawley fault zones. The Imperial fault strikes NW, whereas the Brawley fault strikes N-NW. The BYF appears to connect the San Andreas fault to the north in the Salton Sea, and the Imperial fault to the south. Geologists first recognized the Imperial fault from the displacement during the 1940  $M_W=7.1$  Imperial Valley earthquake (Buwalda and Richter, 1941). The Brawley fault was not recognized until an earthquake swarm occurred in 1975 (Johnson and Hadley; 1976, Sharp, 1976). The background seismic strain field indicates that the BYF domain is dominated by strike-slip with a few normal faulting events (Chapter 4). The principal compressive axes from both the stress tensor and strain tensor are all nearly in the N-S direction. Geodetically, trilateration and triangulation surveys between 1977 and 1984, and between 1973 and 1989 show that the maximum convergent strain axis is oriented  $N5^\circ E$  (Savage et al., 1986, Lisowski et al., 1991). Two major events occurred on the Imperial fault in the past 65 years. The 1940  $M=7.1$  event was centered in the U.S. territory. The 1979 event  $M_W = 6.6$  was centered in the Mexican territory (Figure 5.17). The 1940 event was associated with a surface rupture length of 62 km with a maximum right-lateral displacement of 5.8 m. The 1979 event was associated with a rupture length of only 31 km with a maximum right-lateral displacement of 0.6-0.7 m (Sharp, 1982). Only the northern segment of the Imperial fault was reactivated during the 1979 earthquake. The aftershocks were mainly along the Brawley fault zone, showing activity migrating northward (Johnson et al., 1982). Seismic strain rates from the background seismicity are very small. The calculated right-lateral slip rate is 0.1 mm/yr (Table 5.1). However, because of the contribution of the 1940 and 1979 events, the right-lateral slip rate is as large as 31 mm/yr between 1927-1991, with no discernible vertical movements. As a matter of fact, the geodetic measurements across the valley also indicate a large right-lateral shear rate,  $5.9 \pm 1.0$

mm/yr from GPS between 1988 and 1989 (Larsen and Reilinger, 1992), and  $3.7 \pm 0.1$  mm/yr from trilateration between 1973 and 1989 (Lisowski et al., 1991). Obviously, these short-term rates are influenced by the 1987 Supperstition Hills and the 1979 Imperial Valley earthquakes. According to Louie et al. (1985), postseismic slip after the 1979 earthquake can be more than 50% of the coseismic slip on the Imperial fault (their figure 7, p. 821). They estimated a constant aseismic slip up to 5 mm/yr. This indicates that geodetic strain rates actually bear a large fraction of non-seismic deformation.

In summary, it is evident that the current seismic strain is a continuation of the geological deformation because all the seismic strain patterns are consistent with the geological observations. Therefore, geology is the first step toward our understanding of the seismic activity. But, the deformation rates obtained by these two fields are quite different. This is not surprising and can be explained. The following section will explore the causes.

## 5.4 Comparison of Seismic, Geodetic and Geologic Data

### 5.4.1 Problems of the Comparisons

In this section we compare the deformation rates obtained from geology, geodesy, and seismology. The purpose of the comparison is to investigate the deformation modes, i.e., seismic vs. aseismic. It is important to know, before making comparisons, how these deformation rates are measured, and what they really represent. Two questions must be answered before the comparison: (1) What is the observational time interval over which the deformation rates are averaged? (2) What is the dimension or volume in which the deformation rates are measured? We will show that if these questions are ignored, comparisons among geologic, geodetic, and seismologic deformation rates will not make any sense.

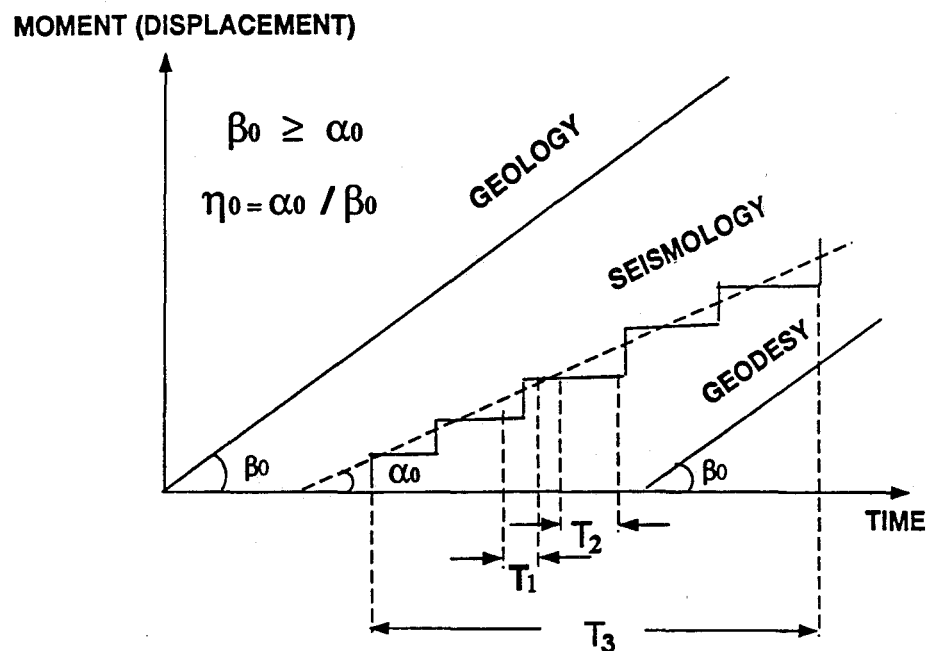


Figure 5.18 Schematic diagram illustrating differences in deformation rates obtained from seismology, geology, and geodesy. see text for explanations.

The first question is illustrated in Figure 5.18. Geologic rates are averaged over  $10^3$  to  $10^6$  or longer years while seismic rates are usually averaged over less than a few hundreds of years for available records, rarely up to  $2-3 \times 10^3$  years; geodetic rates are based on even shorter intervals, within one or two centuries at the most. Precise measurements were carried out only over the past few decades. Both geology and geodesy measure the accumulative deformation that is the sum of seismic and aseismic contributions either expressed by displacements on faults or by distributed strain in the crust. Therefore, they should be greater than or equal to the seismic deformation if all of them are measured in the same time range and share the same time origin. If the time interval of collection of seismic data is long enough (encompassing many major events in a deforming domain) ( $T_3$  in Figure 5.18), then the apparent seismic deformation rate,  $\alpha$ , may be a good approximation of the long-term seismic rate,  $\alpha_0$ . However, when the observational time interval,  $T_s$ , of the seismic data is short, which is usually the case,  $\alpha$  would be either greater than  $\alpha_0$  when  $T_s$  brackets one or a group of clustered major events ( $T_1$  in Figure 5.18), or approaches 0 when  $T_s$  brackets no major event ( $T_2$  in Figure 5.18). That is,  $\alpha$  is not a true measure of the long-term seismic strain rate as indicated in Figure 5.19.

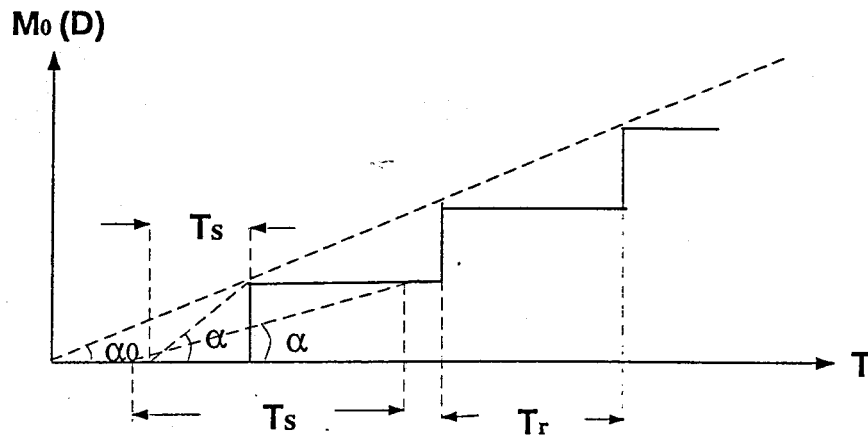


Figure 5.19 Diagram showing the relationship among the observational time interval,  $T_s$ , the average occurrence interval  $T_r$ , and the short-term and long-term seismic strain rates,  $\alpha$  and  $\alpha_0$ , respectively.  $\alpha$  usually is not a good estimator of  $\alpha_0$  if  $T_s < T_r$ .

For the second question raised above, we need to keep in mind that displacements on fault planes within a deforming domain are the minimum deformation across a deforming zone because they do not include the deformation distributed on other structures such as folds and concealed faults. Geodetic deformation is usually represented by the relative changes of station positions separated by some distance. Seismic strain calculated from tensorial summations of individual seismic moment tensors within a deforming zone also gives the total deformation across the zone from one side to the other. Therefore, for the same time interval, the geodetic measurement should yield the largest value whereas the seismic deformation can be either greater than geological deformation, if many major earthquakes occur in the concealed faults, or smaller than the geologic deformation if some of the faults have slipped aseismically. Another reason why the seismic strain rates determined from earthquake data can be different from the geodetic and geologic rates is that seismic strain is averaged over a volume. This volume could be different from the volume in which geodetic strains are measured. We need to make corrections to the measured seismic strain rate so that we can compare them with those obtained geodetically.

#### **5.4.2 Assessment of Deformation Mode**

Listed in Table 5.3 are principal strain rates obtained geodetically in each domain. Table 5.4 compares the horizontal principal strain rates determined seismologically and geodetically. Figure 5.20 is a map view of the data listed in Table 5.4. It can be seen from Figure 5.20 that the orientations of compressional and extensional axes determined from seismic data are generally in good agreement with those from geodetic data. This is especially the case for the compressional axes. This suggests that we can use the magnitudes of the strain rates determined for each domain to investigate the mode of deformation. Furthermore, both the seismological and geodetic data share

approximately the same time scale and are obtained within a similar size of the deforming volume. Therefore, in the following, we choose to compare the total strain rates from both seismology and geodesy. These rates can be expressed as  $\dot{\epsilon}^S = [(\dot{\epsilon}_1^S)^2 + (\dot{\epsilon}_2^S)^2]^{1/2}$  and  $\dot{\epsilon}^G = [(\dot{\epsilon}_1^G)^2 + (\dot{\epsilon}_2^G)^2]^{1/2}$ , where  $\dot{\epsilon}^S$  and  $\dot{\epsilon}^G$  are the total seismic and geodetic strains rates, respectively. The subscripts indicate the two horizontal components of the principal strain rates. Using the values listed in Table 5.4 and our calculated seismic strain rates, we can estimate  $\eta' = \dot{\epsilon}^S / \dot{\epsilon}^G$  for each deforming domain. The results are tabulated in the right column of Table 5.4. Values of  $\eta'$  in Table 5.4 are computed without considering the differences in the deforming sizes between the geodetic and seismic domains. In general, the domain sizes used for determination of the seismic strain rates are 30 to 60% larger than those of the geodetic network used. For purposes of the present discussion, we make a correction for this difference by multiplying  $\eta'$  by 2. The corrected  $\eta'$  is denoted by  $\eta$  in Table 5.4 and plotted in Figure 5.21. Although this correction is very crude, it is adequate for the present discussion. Table 5.4 shows that the apparent fraction of seismic deformation  $\eta$  thus computed for WWF, MVE and BYF domains exceeds 1. This is not unreasonable because a large earthquake happened to occur in these domains within the time interval we observed. As mentioned earlier,  $\eta$  does not represent the real fraction of seismic deformation, because the seismological observational time interval,  $T_s$ , is short and does not cover the whole earthquake cycle. Because of the short seismological observations, it is thus impossible to estimate the true fraction of seismic deformation,  $\eta_0$  as illustrated in Figure 5.19. With this difficulty in mind, we interpret the data as follows. For simplicity, we assume that major earthquakes with similar sizes occur in an average interval of  $T_r$ . If clustering events occur within a relatively short time period, we treat them as a single large earthquake and  $T_r$  represents the time interval between the two clusters. This treatment is based on the observed seismic activity in each deforming domain. Figure 5.22 shows the time history of the energy release for each domain.

Since small events contribute little energy compared to large events, the curve of accumulated energy changes only when a large event occurs. They look like a step function. Most domains have had one or two major events or event clusters in this century. Some domains appear to have relatively regular recurrence intervals of major events, such as in the San Jacinto fault, eastern Transverse Ranges, and possibly the Brawley fault zone. The CTR domain shows clustering activity between 1971 and 1994. The inter-event interval  $T_r$  is different from the repeat time of earthquakes on the same segment of a fault. It is the time interval between major activities in the domain as a whole. If the observational time interval does not contain a major earthquake, it is then impossible to make any useful inference from  $\eta$ ; the data base is just insufficient. However, if the time interval contains one major event or cluster,  $\eta_0$  can be given by

$$\eta_0 = (T_s/T_r)\eta . \quad (5.5)$$

In general, if the time interval includes  $N$  size-similar major events, Eq. (5.5) becomes

$$\eta_0 = (T_s/N \cdot T_r)\eta . \quad (5.6)$$

If  $N \gg 1$ , i.e.  $T_s$  is much longer than the time scale of earthquake cycles, then  $T_s = N T_r$ , and  $\eta$  is a good approximation of  $\eta_0$ . Unfortunately,  $N=0$ , or 1 for most of the studied domains. Only in the SJF and the ETR domains  $N$  can be 2 or larger. With this limitation, we cannot discuss this problem in a deterministic sense. Thus we will first consider this problem by asking a question "Can  $\eta_0 = 1$ ?".

Table 5.3 Listed Geodetic Strain Rates Used for the Comparisons

Domain	Location	Time Interval	Contraction		Extension		References
			Az	R( $\mu\text{yr}^{-1}$ )	Az	R( $\mu\text{yr}^{-1}$ )	
SSNF	W. Garlock F.	1973-1984	12	0.11	102	0.07	Savage et al., (1990)
	Owens Valley	1974-1988	14	0.05	104	0.07	Savage et al., (1990)
WWF	Tehachapi Mts.	1973-1984	348	0.12	78	0.07	Savage et al., (1986)
MVE	Barstow	1979-1989	12	0.06	102	0.07	Savage et al., (1990)
	W. Mojave	1934-1982	4	0.08	94	0.08	Savage et al., (1990)
WTR*	Santa Maria Basin	1879-1987	17	0.13	107	0.06	Feigl et al., (1990)
	Santa Barbara Channel	1970-1988	25	0.14	115	0.02	Larson et al., (1993)
CTR	San Fernando Valley	1870-1978	22	0.34	112	0.10	Cline et al., (1984)
	San Pedro	1870-1978	21	0.24	112	0.08	
	Wilson Peak	1870-1978	2	0.54	92	0.04	
	E. Los Angeles	1870-1978	3	0.07	93	0.05	
ETR	Cajon Pass	1974-1988	344	0.19	74	0.16	Savage et al., (1986)
	N. San Bernardino Mts.	1934-1982	4	0.08	94	0.08	Savage et al., (1990)
NIF	San Pedro	1870-1978	21	0.24	111	0.08	Cline et al., (1984)
ESF	E. Los Angeles	1870-1978	3	0.07	93	0.05	Cline et al., (1984)
SJF*	Anza	1973-1984	359	0.15	89	0.15	Savage et al., (1986)
	Salton	1972-1984	5	0.16	95	0.18	
BYF*	Salton	1972-1981	2	0.22	92	0.14	Savage (1983)

\* For the WTR domain, the Ventura basin shows a very complex pattern of deformation, according to Donnellan et al. (1993). The orientations of principal compression vary from N24°E to N15°W, and the maximum rate reaches 0.6  $\mu\text{yr}$  between 1987 and 1992. For the southern SJF and the BYF domains, Johnson et al. (1994) present more data to show that these domains have principal strain orientations of near N-S, and average contraction rates of 0.11  $\mu\text{yr}$  between 1973 and 1991.

Table 5.4 Comparison of Principal Strain Rates from Seismology and Geodesy

Domain	Seismic Strain				Geodetic Strain*				$\eta'$	$\eta$
	Contraction ( $\dot{\epsilon}_1^S$ )		Extension ( $\dot{\epsilon}_2^S$ )		Contraction ( $\dot{\epsilon}_1^G$ )		Extension ( $\dot{\epsilon}_2^G$ )			
	Az	R ( $\mu\text{yr}^{-1}$ )	Az	R ( $\mu\text{yr}^{-1}$ )	Az	R ( $\mu\text{yr}^{-1}$ )	Az	R ( $\mu\text{yr}^{-1}$ )		
SSNF	176	$0.31(\times 10^{-3})$	275	$3.00(\times 10^{-3})$	13	0.08	103	0.07	0.03	0.06
WWF	164	$5.41(\times 10^{-1})$	272	$1.56(\times 10^{-1})$	348	0.12	72	0.16	2.82	5.64
MVE	33	$2.22(\times 10^{-1})$	303	$2.24(\times 10^{-1})$	8	0.07	98	0.08	3.0	6.00
WTR	66	$1.37(\times 10^{-2})$	260	$1.21(\times 10^{-2})$	21	0.14	111	0.04	0.13	0.26
CTR	19	$1.87(\times 10^{-2})$	94	$1.82(\times 10^{-2})$	12	0.30	102	0.01	0.09	0.18
ETR	0	$2.31(\times 10^{-2})$	267	$2.19(\times 10^{-2})$	354	0.14	84	0.12	0.017	0.34
NIF	179	$3.22(\times 10^{-2})$	269	$3.42(\times 10^{-2})$	21	0.24	111	0.08	0.19	0.38
ESF	9	$0.38(\times 10^{-4})$	279	$0.34(\times 10^{-4})$	3	0.07	93	0.05	<0.01?	?
SJF	175	$4.46(\times 10^{-2})$	265	$4.50(\times 10^{-2})$	2	0.16	92	0.17	0.27	0.54
BYF	15	$5.89(\times 10^{-1})$	105	$5.89(\times 10^{-1})$	2	0.22	92	0.14	3.2	6.40

Az: Azimuth in degrees; R: Strain rates in  $\mu$  strain/yr;  $\eta'$ : Raw seismic fraction of deformation without considering the error resulting from the difference of the deforming volumes between seismology and geodesy. It is calculated as  $\eta = \dot{\epsilon}^S / \dot{\epsilon}^G$ , where  $\dot{\epsilon}^S$  and  $\dot{\epsilon}^G$  are total seismic and geodetic strains rates, respectively. They are calculated as  $\dot{\epsilon}^S = [(\dot{\epsilon}_1^S)^2 + (\dot{\epsilon}_2^S)^2]^{1/2}$  and  $\dot{\epsilon}^G = [(\dot{\epsilon}_1^G)^2 + (\dot{\epsilon}_2^G)^2]^{1/2}$ .  $\eta$ , corrected  $\eta'$  based on the adjustment of the size of the domains. see text for detail.

\*Geodetic strain rates are obtained mostly from triangulation and GPS. When a domain has several geodetic measurements, the average is taken for the comparison.

Figure 5.20 Horizontal projection of principal axes from seismology and geodesy. (a) Principal compressive axes; (b) Principal extensive axes. The number adjacent to the arrows are strain rates in  $\mu$  strain/yr.



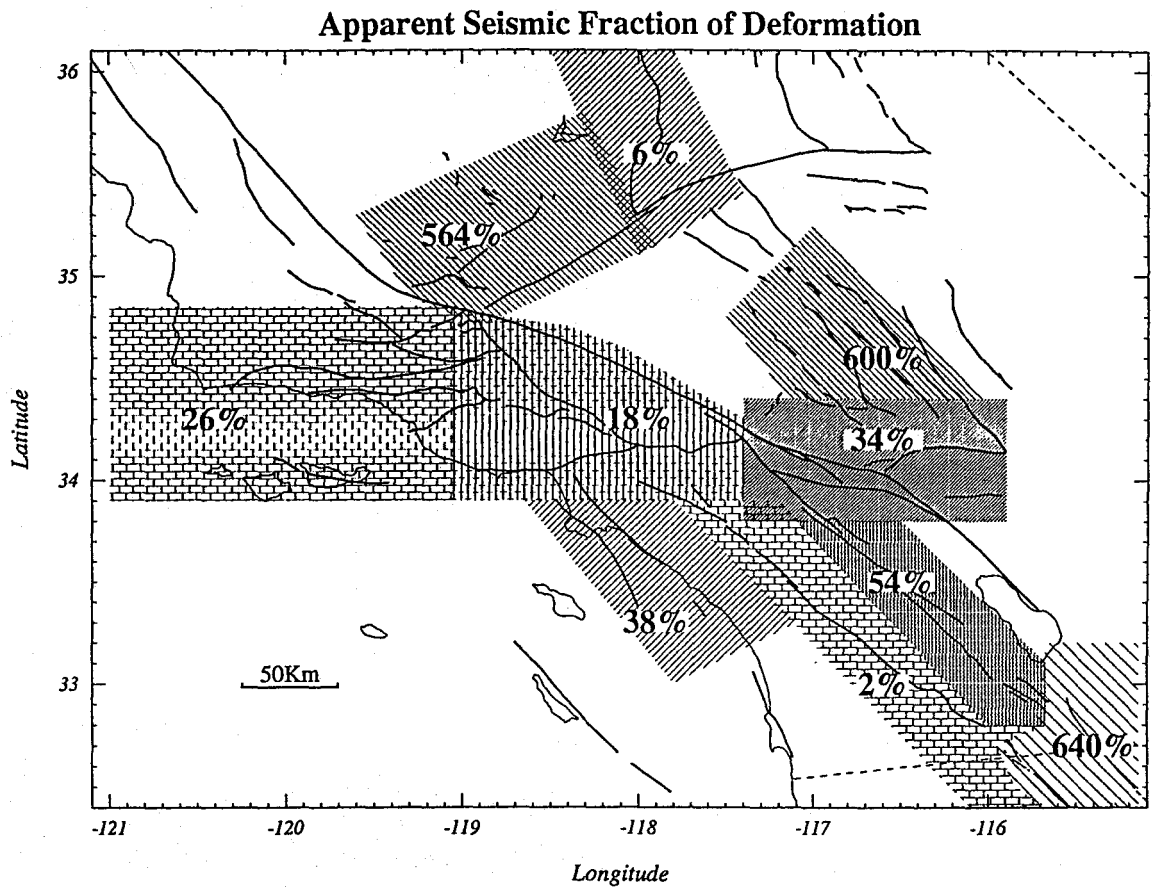


Figure 5.21 Apparent seismic fraction of deformation (SFOD) in each domain obtained from comparisons of principal strain rates between seismology and geodesy.

For the WWF domain  $\eta=5.64$ . The 1952 Kern County earthquake is the major contributor to the seismic deformation in this domain. The reason why  $\eta$  is much greater than 1 is that, as Eq.(5.6) indicates,  $T_s$  is much smaller than  $T_r$ . For  $\eta_0$  to be equal to 1, i.e. completely seismic deformation, Eq.(5.6) indicates that  $T_r$  must be of an order of 370 years. Although the repeat time of the 1952 Kern County type earthquake is not well determined, Stein and Thatcher (1981) suggested an interval in the range of 170-450 years. This suggests that the deformation in this domain could be primarily seismic.

Similarly, for the MVE domain, the 1992 Landers earthquake dominates the seismic strain budget. If the repeat time of the Landers type earthquake in this domain as a whole is about 390 years, then  $\eta_0$  can be approximately equal to 1, i.e. deformation is primarily seismic. Sauber et al. (1994) estimated a 3,500 to 5,000 year recurrence interval for the Landers type earthquake. Considering the existence of many related active faults in the eastern Mojave desert,  $T_r=390$  years for the entire domain does not seem to be unreasonable. If this is the case, the slip in the MVE domain can be considered primarily seismic.

A similar argument can be made for the BYF domain. The main contributor is the 1940 Imperial Valley earthquake. If  $T_r$  is about 420 years or so,  $\eta_0$  can be 1. Geologically, Clerk et al. (1984) (cited by Wesnousky, 1986) reported a minimum recurrence interval of 700 years for the 1940-type earthquakes. They set it as the minimum value because no slip was obvious for at least 700 years prior to the 1940 earthquake. Therefore, with  $\eta$  in Table 5.4, we have  $\eta_0$  around 0.6.

---

Figure 5.22 Plots showing seismic energy release with time in each domain. The bottom plot is for the whole of southern California. see text for interpretation.

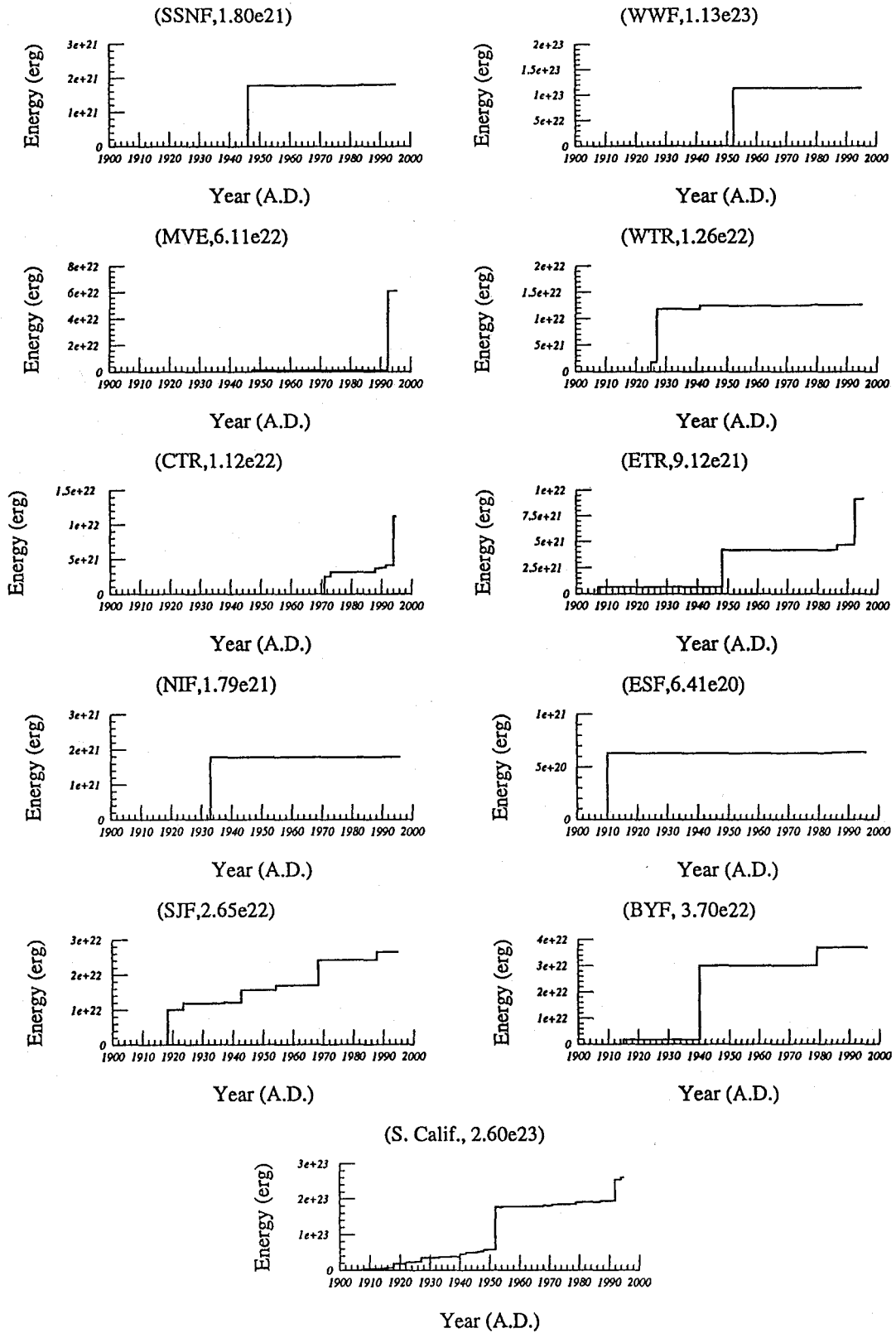


Figure 5.22

For the SJF domain,  $N > 1$  so that  $\eta$  can be a good approximation of  $\eta_0$ . Thus the value of  $\eta$  in Table 5.4 suggests about 50 % aseismic deformation, but if the 1918 earthquake is included,  $\eta$  is about 0.8 which, within the uncertainty of our method, suggests that the deformation in the SJF could be predominantly seismic.

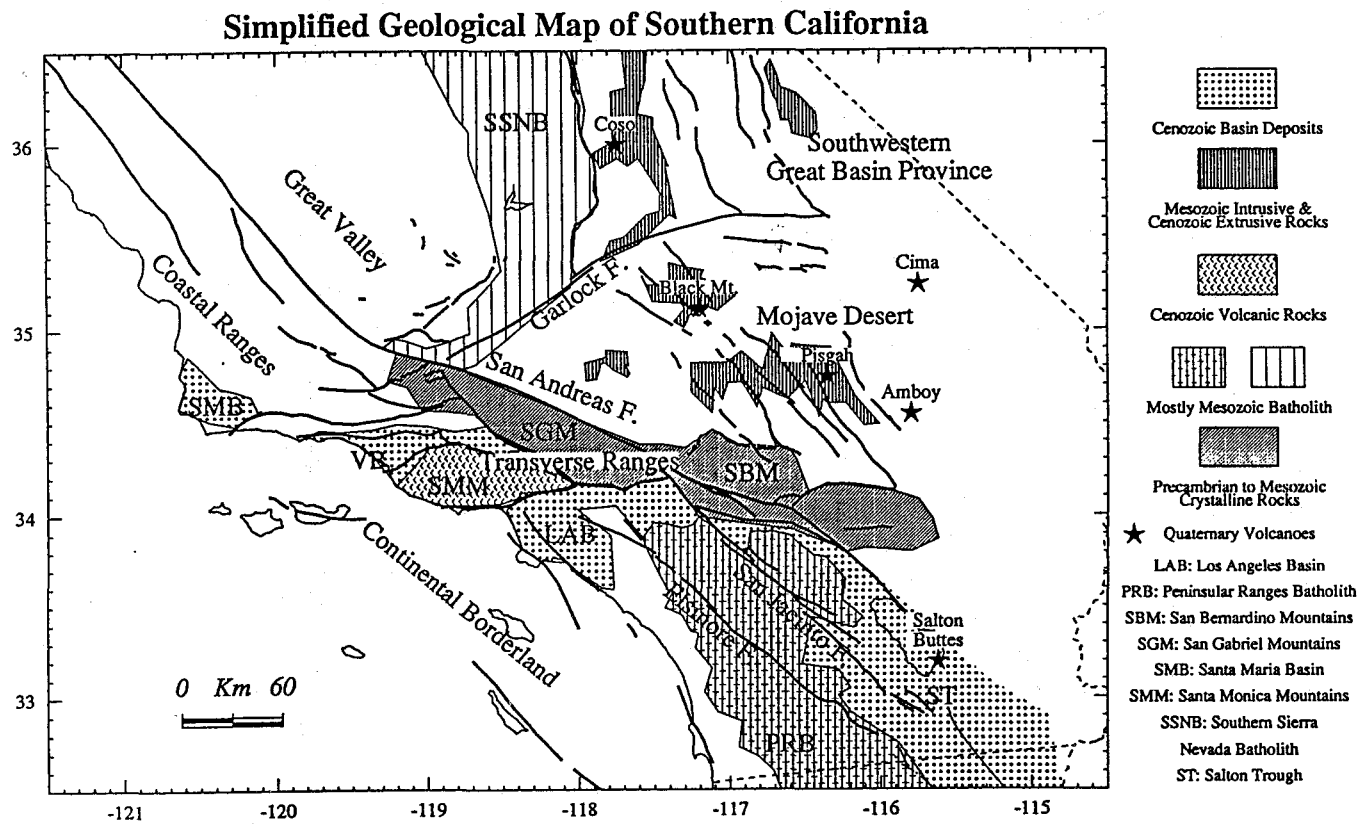
For other regions,  $\eta$  is less than 0.4 suggesting either that the observational time interval we use does not include major earthquakes, or that large fractions of aseismic slip exist. For these domains, because of the limited seismological data base, we cannot make useful estimations of the seismic behavior. We then seek to examine in the following discussion the geological environment in each deforming domain in order to gain some insights.

As we have shown above, the deformation could be completely seismic for the WWF, MVE, and SJF domains. Geological evidence supporting this inference is that the basement rocks in the SJF and MVE domains are primarily granitic or crystalline batholithic rocks that are relatively rigid and susceptible to brittle seismic deformation (Figure 5.23). The WWF domain is more complicated because it involves the deep sedimentary trough of the San Joaquin Valley to the north and the crystalline basement to the south. If our correlation of crystalline basement with seismic behavior is valid, we can suspect that a large fraction of seismic deformation exists at least in the southern WWF domain. By the same reasoning, deformation in the ETR and ELS domains which are developed in the brittle crystalline batholithic basement may be primarily seismic and we may anticipate future earthquakes if the deformation deficit estimated in Table 5.4 is real.

---

Figure 5.23 Simplified geologic map of southern California, largely from Jennings (1977).

Figure 5.23



Like the WWF domain, the NIF and CTR domains are highly heterogeneous in lithology and structure (Figure 5.23). The CTR domain defined here contains part of the deep Los Angeles basin on the south, the crystalline San Gabriel Mountains on the north with ductilely deformed Pelona schist beneath it. Beneath the CTR and perhaps south of it, the deepest known basement rocks are primarily Pelona schist, which was ductilely deformed prior to the mid-Tertiary. They have been brought up to the surface by subsequent basement folding and faulting. These rocks are apparently emplaced on the inferred active deep, ductile decollement beneath the San Gabriel Mountains (Huang et al., 1993a). The NIF is associated with a major fold in the western Los Angeles basin (Yerks et al., 1965; Wright, 1991). Therefore, the CTR and NIF domains have similar geological environments to that of the WWF. If the interpretation for the WWF domain can be applied to the CTR and NIF domains, future major earthquakes in these domains are very likely.

It has been noted that earthquakes in southern California tend to nucleate in the high-velocity areas in the middle crust (Lees and Nicholson, 1993). But the reverse situation does not seem to be true. That is, low velocity zones do not necessarily exclude seismic deformation. For instance, the Brawley and Imperial fault domains are located near the northern region of the extending Gulf of California and are associated with a low velocity zone in the middle crust (10-20 km) (Zhao and Kanamori, 1992). As mentioned above the deformation in the BYF domain can be largely seismic, if  $T_r$  is of the order of 500 years. However, if  $T_r$  is much longer than 500 years, aseismic deformation must be involved.

The geological environment in the SSNF domain is somewhat similar to the WWF domain because it involves batholithic rocks in the western part and a valley in the eastern part. The WTR domain is a special one, both geologically and seismologically. Geologically, it has the deepest Neogene sedimentary basins (see also Yeats,

1983) such as the Ventura-Santa Barbara and Santa Maria basins. Seismologically, it records the deepest earthquakes in the Ventura basin (up to 32 km), indicating a deep cold environment (Bryant and Jones, 1992). The less competent sedimentary rocks tend to deform by ductile folding, but they may intermittently fail by brittle faulting at the later stages of continuous folding. Therefore, it is possible for earthquakes to occur.

However, while seismic deformation is possible, aseismic deformation is not excluded. The aseismic deformation can be either in the form of continuous volumetric deformation or continuous creep on individual weak fault planes. One of the observations supporting aseismic slip is the uneven distribution of seismicity on the fault planes. It has been pointed out that major earthquakes that contribute large slip are predominantly located at depths between 5 and 15 km, where deformation is believed to be seismic (see Bakun et al., 1986, King et al., 1984). The stable frictional slip in the uppermost crust can be attributed to the existence of unconsolidated material and/or thick gouge zones (e.g. Marone and Scholz, 1988). Chinnery (1970), noting that fault displacements associated with a major earthquake represent only a small fraction of the total slippage of a deforming zone measured by geodetic techniques, inferred that aseismic slip must have occurred either away from or beneath the causative fault prior to or following the major earthquake. Allen (1968) suggested that the serpentinite in the Franciscan formation might be responsible for the constant creep on the San Andreas fault in central California. Aseismic deformation can occur also on weak subduction zones or between two decoupled plates, whereas seismic deformation occurs on the strong subduction zones or between two coupled plates (Kanamori, 1977).

## 5.5 Concluding Remarks

Geologic, geodetic, and seismic deformation rates are usually obtained on different time scales and they have different physical meanings. Therefore, they need not be the same. Geologic and geodetic rates measure the total deformation contributed by both seismic and aseismic slip. In addition to the differences in time scale, geologic rates usually represent slip rates on individual faults whereas geodetic rates are integrated deformation rates over an area with or without obvious surface faults. Therefore, geodetic rates contribute information on deformation in the deep crust. Seismic deformation is the deformation associated with earthquakes. It can be averaged over a single fault or over a deforming volume.

Analysis of seismic deformation in a deforming domain has the advantage of relating individual faults to the regional deformation. We found that seismic strain patterns represented by the principal axes and the focal mechanisms are generally very similar to those from geodesy and geology. Therefore, the current seismic activity can be considered a continuation of the geological deformation.

Since we do not have a long-term seismological data base, quantitative evaluation of the deformation mode or the seismic behavior is very difficult. Caution must be exercised in applying the apparent seismic fraction of deformation to evaluations of seismic potential. In southern California, there are some indications that seismic deformation accounts for the total deformation in the domains that are typically associated with cold and rigid batholithic rocks or high seismic velocity anomalies such as in the SJF, southern Central MVE, WWF, and possibly the ETR domains. However, it must be pointed out that areas with low seismic velocity anomalies do not necessarily exclude earthquakes as seen in the BYF domains.

Appendix

Table A1 Earthquakes of  $M \geq 3.0$  in Southern California (1981-1991)

No.	YMnDHMt	Log.	Lat.	$M_L$	Depth	Dip	Rake	Stk	Pa	Pd	Ta	Td	Refs
1	8104010205	116.82	33.59	3.3	11.39	40	-30	35	18.3	50.3	264.8	18.3	
2	8104200137	116.70	33.37	3.5	13.93	70	-170	315	176.8	20.9	269.6	7.3	
3	8104250211	115.62	33.11	4.2	5.13	85	-179	315	179.9	3.5	270.1	3.5	
4	8104302009	116.50	33.52	3.1	14.90	75	-40	195	148.8	38.5	-109.1	14.8	
5	8105020211	117.78	35.84	3.4	5.39	50	-10	60	26.4	33.3	281.7	21.1	
6	8105022150	116.30	32.93	3.3	5.73	80	-150	305	171.0	28.1	73.9	13.0	
7	8105060556	118.04	33.74	3.1	5.00	55	-140	0	210.5	51.1	302.8	1.9	EH
8	8106030529	117.61	34.15	3.1	13.61	70	0	225	181.8	14.0	88.2	14.0	
9	8106041151	117.47	33.68	3.6	12.15	65	150	120	172.2	1.2	81.3	38.3	
10	8106120606	118.66	34.36	3.9	15.07	55	-160	0	213.5	37.1	312.8	12.0	
11	8106121102	115.98	33.25	3.8	3.66	80	0	220	175.4	7.1	84.6	7.1	
12	8106161216	116.26	33.86	3.1	1.20	75	-154	357	220.4	28.1	127.1	6.1	LJ
13	8106220731	115.97	33.24	3.1	3.95	80	-30	230	184.0	28.1	-78.9	13.0	
14	8107051030	117.72	35.76	3.1	4.93	35	-90	20	110.0	80.0	290.0	10.0	
15	8107061953	117.86	33.87	3.1	8.67	25	50	50	349.9	24.3	207.1	60.4	
16	8107181248	116.67	33.56	3.0	11.95	89	0	255	-150.0	0.0	120.0	0.0	
17	8107250624	116.78	33.48	3.0	1.52	80	-170	335	199.1	14.1	289.1	0.1	
18	8107260613	118.65	35.14	3.6	5.29	85	150	205	-104.8	16.9	157.3	24.4	
19	8107292128	116.51	33.14	3.4	5.83	65	150	160	-147.8	1.2	121.3	38.3	
20	8107292337	118.73	33.80	3.2	3.50	65	30	295	62.8	1.2	153.7	38.3	
21	8108061110	120.24	34.80	3.6	0.73	10	110	150	42.7	35.5	215.5	54.3	
22	8108280142	115.68	33.29	3.4	4.54	65	-160	135	354.0	31.2	86.8	4.6	
23	8109040028	116.56	33.15	3.9	16.16	75	-40	50	3.8	38.5	105.9	14.8	
24	8109160119	118.97	33.60	3.4	14.59	60	30	50	357.8	2.7	265.4	41.3	
25	8109251413	116.85	34.01	3.3	20.00	50	-153	-29	179.0	44.5	281.1	12.0	WK
26	8109281057	117.10	33.46	3.1	8.66	45	30	70	19.2	14.5	272.2	48.6	
27	8110132014	116.14	34.03	3.3	8.50	60	-150	10	225.4	41.3	317.8	2.7	
28	8110171947	116.07	33.24	3.8	4.43	85	-170	320	184.9	10.6	94.2	3.5	
29	8110210537	116.77	33.51	3.3	4.70	85	-180	155	19.9	3.5	110.1	3.5	
30	8110231915	119.01	33.62	4.6	14.90	60	-170	125	343.4	27.4	80.9	14.3	
31	8111102234	119.14	35.02	4.7	3.55	50	100	90	172.9	4.5	52.5	81.1	
32	8111110029	119.16	35.01	3.4	2.40	70	80	58	155.7	24.4	311.9	63.7	WK
33	8112092258	119.14	33.69	3.3	14.48	10	170	125	324.3	42.5	124.8	45.9	
34	8112141132	119.16	33.71	3.9	16.97	89	80	215	314.9	44.1	115.1	44.1	
35	8112240223	116.77	34.01	3.3	18.90	76	31	-5	123.1	10.5	219.6	31.6	WK,LJ
36	8202020540	116.45	33.47	3.1	6.84	80	-160	320	184.6	21.2	92.0	6.6	

No.	YMnDHMt	Log.	Lat.	M <sub>L</sub>	Depth	Dip	Rake	Stk	Pa	Pd	Ta	Td	Refs
37	8202040007	115.76	32.98	3.2	4.81	65	20	40	351.8	4.6	259.0	31.2	
38	8202070810	118.10	35.35	3.8	6.19	50	-10	30	356.4	33.3	251.7	21.1	
39	8202161910	117.33	34.12	3.1	17.46	80	-80	60	342.0	54.0	141.5	34.3	
40	8202221406	116.39	34.12	3.1	3.69	50	-60	50	27.3	67.5	119.3	0.8	
41	8202250519	116.39	34.11	3.8	4.00	63	-141	169	26.9	45.8	-67.6	4.3	WK
42	8203220853	116.22	33.06	4.4	4.60	75	0	215	171.0	10.5	79.0	10.5	
43	8204050114	118.94	33.56	3.6	13.26	65	140	130	-173.0	6.5	90.4	45.3	
44	8204131102	118.97	34.05	4.0	9.56	60	90	115	-155.0	15.0	25.0	75.0	
45	8204271542	117.73	35.77	4.0	5.53	80	160	150	-162.0	6.6	105.4	21.2	
46	8204291533	118.94	33.56	3.9	12.81	85	-60	40	338.5	42.2	105.0	33.3	
47	8205251344	118.22	33.55	4.4	14.58	55	90	125	-145.0	10.0	35.0	80.0	
48	8205311542	118.41	35.72	3.6	10.57	40	-70	10	22.7	75.6	265.9	6.6	
49	8206090328	116.89	33.95	3.2	16.00	80	153	-55	-5.0	11.1	259.5	26.0	WK
50	8206152349	116.67	33.56	4.9	12.28	70	0	245	201.8	14.0	108.2	14.0	
51	8206160014	116.67	33.56	3.3	12.68	80	10	240	194.1	0.1	104.1	14.1	
52	8206271121	116.43	32.96	3.1	2.63	40	10	45	6.8	27.6	252.4	38.4	
53	8207041244	117.73	35.77	3.6	5.12	80	50	40	159.9	24.2	273.0	41.0	
54	8207070844	116.70	34.15	3.6	13.80	86	-168	131	356.1	11.3	-95.0	5.6	WK
55	8207290550	118.72	33.94	3.6	11.75	60	130	150	-147.2	6.6	113.1	55.4	
56	8207310057	117.73	35.75	3.1	5.17	70	-170	160	21.8	20.9	114.6	7.3	
57	8208031638	116.42	33.26	3.6	3.87	75	20	35	166.7	2.9	258.0	24.6	
58	8208050402	116.41	33.26	3.3	3.64	75	20	35	166.7	2.9	258.0	24.6	
59	8208101837	115.54	32.92	3.7	13.13	65	-20	70	31.0	31.2	298.2	4.6	
60	8208211020	116.41	33.26	3.2	3.30	80	-20	205	160.4	21.2	-107.0	6.6	
61	8208262228	115.99	33.27	3.4	3.59	75	0	35	351.0	10.5	259.0	10.5	
62	8208270425	117.82	33.93	3.1	17.36	75	100	120	-158.1	29.3	43.7	58.8	
63	8210011429	117.75	35.74	4.8	7.71	70	30	60	-172.1	5.2	281.6	35.0	
64	8210012210	117.76	35.72	4.4	6.79	50	-100	330	187.5	81.1	67.1	4.5	
65	8210150957	118.65	34.20	3.5	3.50	70	120	140	-152.0	19.5	87.8	54.8	
66	8210171123	119.28	34.30	3.0	0.02	30	40	45	350.9	22.7	220.8	57.1	
67	8210191427	115.99	33.27	3.2	3.68	80	10	40	354.1	0.1	264.1	14.1	
68	8210191712	117.73	35.76	3.2	5.17	89	179	495	180.0	0.0	90.0	0.0	
69	8210241923	119.23	34.06	4.0	5.18	35	0	100	70.2	35.4	309.8	35.4	
70	8210290920	117.74	35.72	3.2	5.06	35	-50	20	24.8	62.9	261.8	15.6	
71	8211101121	116.67	34.06	4.2	9.40	65	-159	298	157.0	31.2	249.8	4.6	WK,LJ
72	8211211722	115.98	32.88	3.1	1.97	89	160	490	176.8	14.0	83.2	14.0	
73	8211261230	118.96	34.84	3.1	12.90	42	69	75	359.7	4.8	251.1	75.3	LJ
74	8212091015	117.12	34.02	3.0	20.64	85	30	275	44.8	16.9	142.7	24.4	
75	8212221246	116.56	33.47	3.1	11.08	50	-20	45	14.8	39.8	271.4	15.6	
76	8212231820	117.75	35.74	3.0	10.21	80	-160	110	334.6	21.2	-118.0	6.6	
77	8212300400	118.83	33.96	3.8	1.65	75	40	60	-175.9	14.8	286.2	38.5	

No.	YMnDHMt	Log.	Lat.	M <sub>L</sub>	Depth	Dip	Rake	Stk	Pa	Pd	Ta	Td	Refs
78	8212310907	117.74	35.81	4.1	6.28	80	10	240	194.1	0.1	104.1	14.1	
79	8212311956	117.75	35.81	3.6	6.03	65	170	295	159.9	10.8	254.8	24.2	
80	8301040303	117.75	35.81	3.9	7.14	85	130	115	173.8	28.6	59.7	37.0	
81	8301071343	117.75	35.74	3.6	8.75	65	-40	225	185.4	45.3	-78.0	6.5	
82	8301080719	117.45	34.13	4.1	5.18	85	-10	215	170.1	10.6	-99.2	3.5	
83	8301080730	117.75	35.74	3.1	8.75	55	-50	30	359.4	58.1	92.9	2.2	
84	8301152337	116.29	33.36	3.1	9.91	65	-160	300	159.0	31.2	251.8	4.6	
85	8301240338	115.94	32.98	3.4	7.13	40	-140	340	171.1	56.5	284.0	14.4	
86	8301281454	118.72	33.94	3.8	13.28	40	90	110	20.0	5.0	200.0	85.0	
87	8301311019	115.32	33.02	3.0	4.04	70	-20	230	188.8	28.0	98.4	0.8	
88	8309122133	117.04	35.23	3.2	15.83	85	-10	260	215.1	10.6	-54.2	3.5	
89	8309200008	116.21	33.06	3.5	4.57	89	170	500	185.4	7.1	94.6	7.1	
90	8309230135	118.56	35.56	3.1	3.08	75	170	115	340.7	3.7	71.9	17.6	
91	8309301224	115.83	32.93	3.2	5.85	85	120	310	15.0	33.3	248.5	42.2	
92	8310071040	116.96	33.98	3.1	13.60	60	19	64	16.6	8.9	280.6	33.6	WK
93	8310191400	118.33	35.92	4.0	1.72	75	-120	25	261.0	50.8	137.8	24.1	
94	8310212244	118.33	35.91	4.5	1.49	60	-120	75	295.9	62.1	-173.9	10.2	
95	8310232335	119.02	35.06	3.1	12.90	66	-89	26	298.0	69.0	115.2	21.0	WK
96	8310251116	118.34	35.86	3.8	1.99	40	170	130	348.2	27.6	102.6	38.4	
97	8310282128	116.21	33.06	3.0	4.71	89	-170	495	0.4	7.1	269.6	7.1	
98	8310290638	116.61	34.00	3.4	11.86	55	30	25	333.1	6.7	236.6	44.0	
99	8310302002	118.32	35.90	3.6	1.81	45	-80	20	16.5	82.9	282.9	0.4	
100	8311071232	118.31	35.92	3.7	1.41	75	-100	50	306.3	58.8	148.1	29.3	
101	8311111636	115.88	32.96	3.3	5.07	75	-50	200	149.9	44.9	-98.9	19.9	
102	8311111715	115.89	32.96	3.8	4.69	75	-40	210	163.8	38.5	-94.1	14.8	
103	8311141257	118.31	35.92	3.3	1.69	80	-100	55	313.0	54.0	153.5	34.3	
104	8311150504	115.55	33.04	3.5	11.92	70	-160	145	6.2	28.0	96.6	0.8	
105	8311151102	115.56	33.04	3.3	11.47	70	-30	45	3.4	35.0	97.1	5.2	
106	8311180955	117.21	34.00	3.1	16.44	75	-150	320	184.0	31.6	88.3	9.1	
107	8312051841	118.33	35.92	3.1	1.30	65	-130	340	202.2	52.2	97.6	11.1	
108	8312060120	116.41	34.83	3.2	0.20	45	90	120	-150.0	0.0	180.0	90.0	
109	8312060910	116.21	33.06	3.2	4.76	80	10	55	9.1	0.1	279.1	14.1	
110	8312130140	116.15	33.89	3.4	4.29	70	-180	160	23.2	14.0	116.8	14.0	
111	8312181756	118.01	35.77	3.3	4.23	65	-160	310	169.0	31.2	261.8	4.6	
112	8312182051	116.08	32.61	3.2	5.40	89	150	500	189.1	20.7	90.9	20.7	CK
113	8312200115	116.30	32.95	3.5	1.57	85	160	305	-7.5	10.3	259.2	17.6	
114	8312272134	116.13	33.80	3.1	2.70	82	-147	161	28.2	28.0	-70.4	15.8	LJ
115	8312290723	118.31	35.90	3.3	1.27	50	-60	10	347.3	67.5	79.3	0.8	
116	8312291946	117.36	34.17	3.6	9.60	40	-48	200	194.4	62.2	81.7	11.5	LJ
117	8312310209	116.21	33.06	3.0	5.00	80	-20	235	190.4	21.2	-77.0	6.6	
118	8401060500	118.33	35.96	3.2	5.50	85	-90	95	5.0	50.0	-175.0	40.0	

No.	YMnDHMt	Log.	Lat.	M <sub>L</sub>	Depth	Dip	Rake	Stk	Pa	Pd	Ta	Td	Refs
119	8401130941	117.26	34.05	3.2	15.64	70	20	275	226.6	0.8	136.2	28.0	
120	8401151754	116.45	34.33	3.1	2.21	55	80	115	-147.8	9.5	350.7	77.4	
121	8401160406	118.30	35.92	3.4	1.38	65	90	20	110.0	20.0	290.0	70.0	
122	8401201207	117.97	35.96	3.3	9.17	40	-80	50	82.7	81.6	312.9	5.4	
123	8401250526	116.15	33.89	3.0	4.09	50	-100	20	237.5	81.1	117.1	4.5	
124	8402010639	116.80	33.53	3.1	0.09	85	0	70	25.1	3.5	294.9	3.5	
125	8402022147	116.85	33.90	3.3	17.45	50	-80	5	327.5	81.1	87.9	4.5	
126	8402042247	117.97	35.96	3.5	5.50	25	-40	65	76.8	56.4	297.7	26.7	
127	8402052039	118.91	34.54	3.2	21.49	25	80	90	7.5	20.3	200.3	69.3	
128	8402070333	119.27	34.31	3.3	1.46	50	50	35	332.1	2.3	238.1	60.4	
129	8402111425	118.92	34.54	3.0	20.36	30	70	75	359.6	16.3	212.5	70.8	
130	8402141618	118.32	35.93	3.1	1.40	75	-100	50	306.3	58.8	148.1	29.3	
131	8402231734	116.15	33.89	3.7	4.89	50	-20	80	49.8	39.8	306.4	15.6	
132	8402280608	116.82	34.40	3.4	9.34	45	-10	45	14.3	35.9	265.1	24.4	
133	8402290207	116.10	33.14	4.3	7.37	55	-30	25	353.4	44.0	256.9	6.7	
134	8403121017	119.02	34.90	3.5	13.50	83	168	303	-10.9	3.4	258.3	13.4	LJ
135	8403161953	116.73	33.70	3.0	18.21	75	-140	135	1.2	38.5	-100.9	14.8	
136	8403230824	118.31	35.97	3.8	0.90	75	-90	55	325.0	60.0	145.0	30.0	
137	8403311916	118.30	35.94	3.6	0.11	35	-90	10	100.0	80.0	280.0	10.0	
138	8404010717	116.41	33.11	3.9	6.16	75	40	235	-0.9	14.8	101.2	38.5	
139	8404080104	118.31	35.96	3.2	1.66	50	-90	45	315.0	85.0	135.0	5.0	
140	8404181319	118.38	33.67	3.1	2.58	60	-170	-15	203.4	27.4	300.9	14.3	CK
141	8404212223	119.63	34.25	3.4	6.99	85	-90	275	185.0	50.0	5.0	40.0	
142	8404220553	119.62	34.26	3.7	9.95	50	-150	145	352.2	46.5	93.5	10.6	
143	8404231431	115.51	32.97	3.0	9.56	75	-10	245	201.9	17.6	110.7	3.7	
144	8404262244	115.27	32.74	3.6	15.93	60	-40	215	179.6	48.3	-87.8	2.3	
145	8404291219	115.53	32.97	3.2	10.60	85	120	130	-165.0	33.3	68.5	42.2	
146	8405030947	116.40	34.33	3.3	2.89	75	10	250	204.3	3.7	113.1	17.6	
147	8405071932	119.97	34.67	4.2	5.31	45	80	115	32.1	0.4	298.5	82.9	
148	8406102019	116.18	33.82	3.1	5.60	38	-42	43	36.9	58.7	280.6	15.1	CK,LJ
149	8406112221	116.62	34.39	4.0	2.61	75	160	160	-151.7	2.9	117.0	24.6	
150	8406120027	118.99	34.55	4.1	13.75	60	110	115	-169.4	12.8	65.8	68.3	
151	8406130233	119.32	34.40	3.1	13.66	65	80	85	-177.5	19.4	335.5	68.4	
152	8406131500	118.31	35.98	3.0	0.11	55	-70	5	325.7	71.8	80.9	8.0	
153	8406242157	116.33	33.95	3.5	6.86	70	-10	235	193.2	20.9	100.4	7.3	
154	8406300634	116.61	34.39	3.4	3.41	85	160	165	-147.5	10.3	119.2	17.6	
155	8407022108	116.48	34.31	3.2	2.04	75	0	95	51.0	10.5	319.0	10.5	
156	8407041300	117.20	33.95	3.2	14.62	50	-100	150	7.5	81.1	-112.9	4.5	
157	8407061200	118.06	35.73	3.9	6.33	75	-10	220	176.9	17.6	85.7	3.7	
158	8407062214	118.06	35.73	3.6	5.94	10	-160	140	310.1	47.6	111.5	40.9	
159	8407091551	118.67	34.39	3.1	1.07	60	100	130	-147.3	14.4	64.9	73.1	

No.	YMnDHMT	Log.	Lat.	M <sub>L</sub>	Depth	Dip	Rake	Stk	Pa	Pd	Ta	Td	Refs
160	8407091909	116.80	33.54	3.2	0.55	80	-150	185	51.0	28.1	-46.1	13.0	
161	8407091931	116.80	33.54	3.0	0.16	75	-20	250	207.0	24.6	-61.7	2.9	
162	8407121217	116.39	33.48	3.2	9.40	45	10	35	354.9	24.4	245.7	35.9	
163	8407180213	119.08	35.07	3.2	15.37	45	-30	30	7.8	48.6	260.8	14.5	
164	8407251843	116.73	34.05	3.4	3.90	77	-166	137	0.5	18.3	90.6	0.2	LJ
165	8408060814	116.71	33.98	4.3	15.20	50	30	60	8.5	10.6	267.2	46.5	
166	8409111248	116.42	33.49	3.2	8.81	30	30	60	12.9	25.8	244.4	52.1	
167	8409192111	119.97	34.67	3.4	0.37	40	160	180	43.9	22.7	157.9	44.2	
168	8409300923	116.58	33.47	3.1	11.87	65	-140	135	354.6	45.3	-102.0	6.5	
169	8410011437	119.07	35.03	3.2	23.64	85	-170	100	324.9	10.6	-125.8	3.5	
170	8410020938	119.24	34.31	3.3	2.16	50	140	140	17.0	6.1	115.3	53.4	
171	8410031249	118.67	33.98	3.3	12.82	85	120	140	-155.0	33.3	78.5	42.2	
172	8410050737	116.70	33.67	3.9	18.07	85	80	75	174.1	39.2	334.2	49.1	
173	8410071544	116.07	33.26	3.0	3.20	60	-160	100	316.5	34.3	52.2	8.3	
174	8410090601	117.00	33.94	3.0	17.30	30	20	45	4.7	29.4	237.2	47.2	
175	8410102122	116.50	33.14	4.5	8.64	60	20	85	37.2	8.3	301.5	34.3	
176	8410162218	117.03	33.81	3.3	15.01	40	80	45	322.1	5.4	192.3	81.6	
177	8410180057	118.03	33.93	3.1	18.32	85	-100	50	309.2	49.1	149.1	39.2	
178	8410222028	118.52	35.10	3.5	3.67	55	90	100	-170.0	10.0	10.0	80.0	
179	8410250759	116.84	34.03	3.1	19.22	35	-140	15	198.5	57.1	319.9	18.6	
180	8410261720	118.99	34.01	4.6	5.03	60	70	280	24.4	12.8	149.2	68.3	
181	8411031502	120.30	34.71	3.2	6.35	65	20	100	51.8	4.6	319.0	31.2	CK
182	8411050259	117.43	34.14	3.4	3.43	75	-10	210	166.9	17.6	75.7	3.7	
183	8411080943	118.26	33.91	3.2	8.90	75	20	60	-168.3	2.9	283.0	24.6	EH
184	8411190502	117.73	35.86	3.1	5.00	30	-60	45	71.6	66.7	293.2	17.8	
185	8411240402	116.61	34.39	3.4	2.44	85	-160	165	30.8	17.6	-62.5	10.3	
186	8411260818	119.46	34.25	3.1	9.99	5	-80	150	229.0	49.9	50.8	40.1	
187	8412142128	117.84	33.88	3.1	9.62	50	120	95	164.3	0.8	72.3	67.5	
188	8501020524	116.53	34.05	3.8	9.50	79	166	301	-12.4	1.9	257.0	17.6	LJ
189	8501181724	115.99	33.87	3.1	13.25	85	0	85	40.1	3.5	309.9	3.5	
190	8501190030	116.40	33.99	3.8	2.87	65	-179	335	197.2	17.4	292.8	17.4	
191	8501190324	116.39	33.99	3.5	3.30	72	-20	218	176.0	26.6	-93.6	0.7	LJ
192	8501211405	116.39	33.99	3.1	2.99	40	-120	355	172.6	69.3	285.9	8.5	
193	8501221138	116.78	33.99	3.2	17.70	40	-130	350	175.0	62.9	287.6	11.2	
194	8501250528	116.40	33.99	3.6	3.05	65	-30	220	181.3	38.3	-87.8	1.2	
195	8501251350	117.09	33.93	3.4	15.20	89	-20	215	168.2	14.0	261.8	14.0	
196	8501260641	119.04	34.17	3.3	24.37	55	-180	125	344.3	23.9	85.7	23.9	
197	8502031748	115.67	32.55	3.8	3.37	70	130	120	-178.1	15.5	73.5	48.7	
198	8502080658	118.86	35.45	4.6	17.44	35	60	100	31.3	13.2	264.8	68.5	
199	8502100920	118.04	35.73	3.5	7.94	85	0	65	20.1	3.5	289.9	3.5	
200	8502101359	116.28	33.88	3.6	1.10	80	-169	160	24.1	14.1	114.1	0.1	LJ

No.	YMnDHMt	Log.	Lat.	M <sub>L</sub>	Depth	Dip	Rake	Stk	Pa	Pd	Ta	Td	Refs
201	8502151626	117.48	34.15	3.0	2.37	55	100	110	-167.2	9.5	54.3	77.4	
202	8502152326	116.40	33.99	4.0	2.33	55	-120	335	187.8	65.1	85.8	5.5	
203	8502160042	116.40	33.99	3.4	0.52	60	-50	220	183.1	55.4	-77.2	6.6	
204	8502190509	116.98	34.16	3.3	11.50	70	-20	215	173.8	28.0	83.4	0.8	
205	8502191637	116.77	34.04	3.1	12.50	89	179	480	165.0	0.0	75.0	0.0	LJ
206	8502210754	116.42	33.48	3.1	8.45	85	40	40	166.1	23.0	270.8	31.0	
207	8502280442	116.29	33.96	3.7	11.43	55	-180	165	24.3	23.9	125.7	23.9	
208	8503131719	116.06	33.21	3.1	3.90	75	130	280	-18.9	19.9	229.9	44.9	
209	8504010613	117.39	36.01	3.2	0.06	85	40	240	6.1	23.0	110.8	31.0	
210	8504030404	119.04	34.38	4.0	33.69	80	-140	135	3.7	34.8	-100.1	19.0	
211	8504080109	118.93	34.04	3.4	9.38	65	50	75	-167.4	11.1	297.2	52.2	
212	8504282223	117.04	34.02	3.1	13.13	89	160	485	171.8	14.0	78.2	14.0	
213	8505062314	119.37	35.27	4.4	29.70	40	90	100	10.0	5.0	190.0	85.0	
214	8505140242	116.31	33.31	3.1	9.51	65	-170	130	350.2	24.2	85.1	10.8	
215	8505141735	116.80	33.53	3.7	1.36	75	-160	0	223.0	24.6	131.7	2.9	
216	8505251550	116.64	33.96	3.2	14.20	65	142	317	13.0	5.5	277.7	43.9	LJ
217	8506021501	120.09	34.40	3.4	3.48	45	70	95	19.0	1.7	282.1	75.9	
218	8506030205	116.10	34.00	3.3	9.41	85	-10	65	20.1	10.6	110.8	3.5	
219	8506030653	116.00	33.03	3.5	4.10	75	170	320	185.7	3.7	276.9	17.6	
220	8506051000	115.58	32.99	3.3	13.65	55	-40	45	14.5	51.1	282.2	1.9	
221	8506051810	116.34	33.35	3.7	9.67	70	0	35	351.8	14.0	258.2	14.0	
222	8506071806	120.09	34.40	3.6	5.84	60	80	70	167.3	14.4	315.1	73.1	CK
223	8506100058	116.82	34.21	3.3	12.26	89	-10	215	169.6	7.1	260.4	7.1	
224	8506101250	117.38	33.69	3.1	6.84	89	-30	205	155.9	20.7	254.1	20.7	
225	8506210050	117.17	33.99	3.3	16.59	70	-140	350	213.2	42.0	113.5	10.7	
226	8506291823	116.55	33.48	3.4	12.53	89	20	230	3.2	14.0	96.8	14.0	
227	8507161757	116.84	34.55	3.9	0.67	89	-170	500	5.4	7.1	274.6	7.1	
228	8508060345	117.75	35.43	3.1	8.03	60	-140	140	355.4	48.3	-97.2	2.3	
229	8508140612	116.91	35.02	3.4	7.67	30	-180	155	1.6	37.8	128.4	37.8	
230	8508220021	117.74	35.90	4.5	2.06	80	-20	75	30.4	21.2	123.0	6.6	
231	8508290455	115.51	32.88	3.2	5.61	20	-160	140	321.3	48.3	104.8	35.6	
232	8508290759	116.81	34.32	4.1	6.98	70	30	235	2.9	5.2	96.6	35.0	
233	8509051433	116.96	33.97	3.0	17.10	80	10	65	19.1	0.1	289.1	14.1	
234	8509190735	119.40	34.47	3.1	10.20	30	-160	150	342.2	47.2	109.7	29.4	
235	8510022344	117.24	34.03	4.8	15.18	89	-20	255	-151.8	14.0	301.8	14.0	
236	8510170949	115.56	32.91	3.0	5.23	85	0	225	180.1	3.5	89.9	3.5	
237	8510280445	115.40	32.70	3.0	15.79	45	-20	40	13.7	42.1	265.3	19.2	
238	8510311954	117.89	34.47	3.7	6.20	60	143	306	1.6	0.9	270.7	46.2	LJ
239	8510311955	117.89	34.47	3.6	4.44	35	-20	25	7.7	45.9	247.3	26.1	
240	8512162347	117.89	35.99	3.1	3.81	55	30	105	53.1	6.7	316.6	44.0	
241	8512300454	120.00	35.43	3.3	9.25	75	-130	140	10.1	44.9	-101.1	19.9	

No.	YMnDHMt	Log.	Lat.	M <sub>L</sub>	Depth	Dip	Rake	Stk	Pa	Pd	Ta	Td	Refs
242	8601120941	118.53	35.33	3.1	7.48	75	-150	310	174.0	31.6	78.3	9.1	
243	8602170212	116.04	34.11	4.0	9.94	85	140	145	-161.1	23.0	94.2	31.0	
244	8602171058	115.55	32.96	3.3	10.65	80	-180	140	4.6	7.1	95.4	7.1	
245	8603092241	117.77	34.12	3.3	5.14	55	70	75	179.1	8.0	294.3	71.8	
246	8603170043	116.98	33.62	3.1	14.71	80	0	55	10.4	7.1	279.6	7.1	
247	8603200649	118.33	33.79	3.2	10.06	35	100	115	17.8	10.4	168.3	78.1	
248	8604050650	118.01	33.73	3.6	15.65	50	30	275	223.5	10.6	122.2	46.5	
249	8604051721	115.71	33.35	3.8	4.08	80	-10	240	195.9	14.1	105.9	0.1	
250	8604210635	117.78	35.84	3.4	6.17	80	-40	50	1.3	34.8	105.1	19.0	
251	8605190412	118.40	33.90	3.0	5.42	70	120	155	-137.0	19.5	102.8	54.8	
252	8605231141	118.02	35.81	4.1	7.72	30	-120	350	143.4	66.7	281.8	17.8	
253	8605310142	116.61	34.10	3.5	11.31	35	-20	25	7.7	45.9	247.3	26.1	
254	8606031414	116.34	33.79	3.8	9.85	80	70	55	161.6	32.1	302.4	51.0	
255	8606181413	116.74	33.94	3.5	17.08	80	60	55	168.8	28.7	294.1	46.5	
256	8607050324	119.09	35.08	3.2	18.63	55	-130	25	235.6	58.1	142.1	2.2	
257	8607051411	117.65	35.70	3.1	9.75	60	-150	140	355.4	41.3	87.8	2.7	
258	8607081009	116.58	33.98	4.4	8.76	70	50	45	163.1	15.5	271.5	48.7	
259	8607081011	116.67	34.02	4.1	3.74	45	80	60	337.1	0.4	243.5	82.9	
260	8607150317	116.90	34.00	3.1	13.41	60	90	105	-165.0	15.0	15.0	75.0	
261	8607172035	116.65	33.99	4.6	6.44	45	70	90	14.0	1.7	277.1	75.9	
262	8607240158	116.55	33.97	3.3	7.92	65	60	55	166.5	14.8	282.2	58.6	
263	8607250544	118.40	34.42	3.0	10.42	70	70	60	165.2	22.5	301.1	60.0	
264	8607310450	116.63	34.01	3.1	10.53	65	30	35	162.8	1.2	253.7	38.3	
265	8608020505	116.67	34.03	3.1	2.87	89	-20	230	-176.8	14.0	276.8	14.0	
266	8608021136	116.70	34.04	3.4	12.94	70	120	120	-172.0	19.5	67.8	54.8	
267	8608241248	115.90	32.98	3.2	5.70	70	50	50	168.1	15.5	276.5	48.7	
268	8608281632	116.27	33.92	3.2	7.42	50	10	75	33.3	21.1	288.6	33.3	
269	8608290644	120.46	35.89	3.6	16.24	75	-30	35	351.0	31.6	86.7	9.1	
270	8608290746	116.60	33.96	3.7	5.34	55	90	75	165.0	10.0	345.0	80.0	
271	8609280706	116.58	34.01	3.2	10.93	55	30	30	338.1	6.7	241.6	44.0	
272	8610150228	116.57	33.96	4.1	5.36	50	80	80	177.1	4.5	297.5	81.1	
273	8610150819	119.21	34.98	3.2	1.83	85	170	170	-144.2	3.5	125.1	10.6	
274	8610290815	120.15	34.74	3.1	3.34	55	70	105	-150.9	8.0	324.3	71.8	CK
275	8611130512	116.73	33.96	3.3	11.29	40	20	50	6.1	22.7	252.1	44.2	
276	8612271913	116.55	33.51	3.0	11.24	80	-20	240	195.4	21.2	-72.0	6.6	
277	8612291605	115.79	33.01	3.5	5.37	80	170	320	185.9	0.1	275.9	14.1	
278	8701010825	116.64	34.04	3.4	12.36	85	70	65	172.6	36.9	314.5	46.3	
279	8701031801	116.48	33.50	3.7	7.14	45	-20	20	353.7	42.1	245.3	19.2	
280	8701150746	116.77	34.02	3.1	10.50	40	50	65	2.6	11.2	250.0	62.9	
281	8701241405	115.55	32.96	3.4	15.70	80	-10	240	195.9	14.1	105.9	0.1	
282	8702212315	117.45	34.14	4.0	7.13	65	20	45	356.8	4.6	264.0	31.2	

No.	YMnDHMt	Log.	Lat.	M <sub>L</sub>	Depth	Dip	Rake	Stk	Pa	Pd	Ta	Td	Refs
283	8702270620	117.71	35.71	3.1	8.29	85	-60	325	263.5	42.2	30.0	33.3	
284	8703011853	116.77	33.91	3.1	18.39	80	40	60	-175.1	19.0	288.7	34.8	
285	8704030533	117.26	34.03	3.3	9.98	55	-120	140	352.8	65.1	-109.2	5.5	
286	8705251818	119.11	34.38	3.2	5.98	5	50	65	12.1	41.1	198.6	48.7	
287	8705291516	118.19	33.70	3.0	6.64	65	-60	170	122.8	58.6	-121.5	14.8	CK
288	8705302306	116.18	33.87	3.3	4.39	40	-100	15	162.3	81.6	292.1	5.4	
289	8706011918	116.18	33.86	3.6	4.41	65	-40	225	185.4	45.3	-78.0	6.5	
290	8706070915	115.90	32.66	3.3	5.90	75	-140	325	191.2	38.5	89.1	14.8	
291	8706081229	118.21	33.78	3.3	12.10	55	70	105	-150.9	8.0	324.3	71.8	
292	8706140816	116.18	33.86	3.8	3.98	40	-100	25	172.3	81.6	302.1	5.4	
293	8706210856	115.81	32.67	3.7	2.74	89	140	225	277.5	27.0	172.5	27.0	
294	8706290620	116.19	33.86	3.3	4.15	89	-160	180	46.8	14.0	313.2	14.0	
295	8707050457	115.66	33.18	3.0	4.63	70	-150	320	181.6	35.0	87.9	5.2	
296	8707060223	116.65	33.98	3.3	7.69	70	130	105	166.9	15.5	58.5	48.7	
297	8707071318	117.07	34.90	3.1	9.87	89	30	235	5.9	20.7	104.1	20.7	
298	8707072107	118.18	33.84	3.2	14.61	25	-110	345	113.6	67.2	270.0	21.1	
299	8707081655	118.27	33.70	3.6	5.59	50	70	95	-161.0	3.1	300.3	74.5	CK
300	8707090042	118.27	33.70	3.4	6.79	50	80	45	142.1	4.5	262.5	81.1	
301	8707190501	119.45	34.33	3.3	5.24	45	70	65	349.0	1.7	252.1	75.9	
302	8708090312	118.36	35.77	3.4	4.29	80	-130	355	228.0	41.0	114.9	24.2	
303	8708141057	118.72	35.42	3.3	11.11	80	70	65	171.6	32.1	312.4	51.0	
304	8708171837	116.92	34.30	3.2	3.47	40	80	85	2.1	5.4	232.3	81.6	
305	8708190940	118.02	33.59	3.2	7.82	55	80	110	-152.8	9.5	345.7	77.4	
306	8708240012	116.98	33.98	3.1	15.53	89	-20	505	98.2	14.0	191.8	14.0	
307	8708250627	117.57	34.38	3.7	9.37	70	100	135	-142.7	24.4	61.1	63.7	
308	8708281922	118.56	33.66	3.5	5.09	70	-180	165	28.2	14.0	121.8	14.0	
309	8709201842	119.59	34.30	3.3	4.41	55	80	80	177.2	9.5	315.7	77.4	
310	8710011442	118.08	34.06	5.9	14.60	25	90	270	180.0	20.0	0.0	70.0	HJ
311	8710041059	118.11	34.08	5.3	13.81	60	150	155	27.2	2.7	119.6	41.3	
312	8710131559	117.21	33.96	3.8	13.84	50	0	45	7.5	27.0	262.5	27.0	
313	8711021921	117.82	35.34	3.4	7.88	75	-80	40	323.7	58.8	121.9	29.3	
314	8711240154	115.79	33.08	5.9	6.91	85	30	5	134.8	16.9	232.7	24.4	
315	8711240253	115.83	33.03	4.7	3.14	80	-179	305	169.6	7.1	260.4	7.1	
316	8711241315	115.86	33.00	6.1	2.09	70	-10	35	353.2	20.9	260.4	7.3	
317	8711241534	115.58	32.59	3.3	16.63	40	-10	55	27.6	38.4	273.2	27.6	
318	8711241850	115.91	33.01	4.3	6.40	25	70	115	40.0	21.1	243.6	67.2	CK
319	8711242041	116.84	33.71	3.3	15.96	55	80	80	177.2	9.5	315.7	77.4	
320	8711250417	115.95	33.05	3.5	2.11	75	150	105	156.7	9.1	61.0	31.6	
321	8711251354	115.83	32.98	4.1	2.40	89	-10	205	159.6	7.1	250.4	7.1	
322	8711251501	115.81	32.99	3.1	3.28	80	-10	210	165.9	14.1	75.9	0.1	
323	8711260156	115.84	32.99	4.0	2.59	75	20	15	146.7	2.9	238.0	24.6	

No.	YMnDHMt	Log.	Lat.	M <sub>L</sub>	Depth	Dip	Rake	Stk	Pa	Pd	Ta	Td	Refs
324	8711270922	115.82	33.00	3.9	3.49	80	40	55	179.9	19.0	283.7	34.8	
325	8711280039	115.82	32.98	4.3	2.89	65	30	25	152.8	1.2	243.7	38.3	
326	8712020403	115.83	32.99	4.5	3.58	85	-180	125	349.9	3.5	80.1	3.5	
327	8712031904	115.90	33.00	4.0	2.43	65	0	20	337.8	17.4	242.2	17.4	
328	8712052036	118.28	35.50	3.1	5.26	75	0	260	216.0	10.5	124.0	10.5	
329	8712081845	115.88	33.00	3.4	2.35	85	160	85	132.5	10.3	39.2	17.6	
330	8712131502	115.71	32.90	3.3	4.95	80	-30	220	174.0	28.1	-88.9	13.0	
331	8712140230	119.05	34.90	3.3	13.22	15	90	85	355.0	30.0	175.0	60.0	
332	8712170726	116.67	33.98	3.2	8.42	65	50	45	162.6	11.1	267.2	52.2	
333	8712250100	116.41	34.18	3.3	2.87	85	10	75	-150.8	3.5	299.9	10.6	
334	8712251815	115.75	33.12	3.5	4.70	89	160	485	171.8	14.0	78.2	14.0	
335	8712312134	116.42	34.18	3.9	2.31	75	10	75	29.3	3.7	298.1	17.6	
336	8801050730	115.83	32.99	3.0	3.84	65	170	95	319.9	10.8	54.8	24.2	CK
337	8801192315	118.06	34.08	3.5	16.26	70	90	70	160.0	25.0	340.0	65.0	
338	8801220052	117.03	33.82	3.5	16.37	50	40	55	358.0	6.1	259.7	53.4	
339	8801230055	117.82	35.40	3.1	8.84	70	-30	235	193.4	35.0	-72.9	5.2	
340	8802010609	118.80	35.37	3.2	14.52	50	170	305	166.7	21.1	271.4	33.3	
341	8802060806	116.99	33.91	3.5	16.72	40	30	65	15.2	18.3	261.7	50.3	
342	8802111525	118.05	34.08	4.7	16.26	75	50	45	163.9	19.9	275.1	44.9	
343	8802172356	116.12	33.26	3.5	3.83	85	-160	305	170.8	17.6	77.5	10.3	
344	8802280502	115.84	32.63	3.3	5.30	50	-100	240	97.5	81.1	-22.9	4.5	
345	8802280752	115.85	32.64	4.1	5.57	70	-120	135	7.2	54.8	-113.0	19.5	
346	8802291525	116.25	34.03	3.1	5.50	75	10	50	4.3	3.7	273.1	17.6	
347	8803011343	115.97	33.26	3.0	3.64	85	20	40	172.5	10.3	265.8	17.6	
348	8803100200	116.70	34.93	3.3	0.86	75	-150	165	29.0	31.6	-66.7	9.1	
349	8803140009	117.80	35.41	3.4	8.42	50	-10	235	201.4	33.3	96.7	21.1	
350	8803261454	118.71	33.99	3.8	12.88	45	70	100	24.0	1.7	287.1	75.9	
351	8804011852	116.23	32.92	3.6	8.73	80	-180	125	349.6	7.1	80.4	7.1	
352	8804141303	116.31	33.27	3.1	8.69	80	110	130	-156.6	32.1	62.6	51.0	
353	8805151753	117.47	34.12	3.3	8.06	89	0	225	-180.0	0.0	90.0	0.0	
354	8805161645	116.76	34.03	3.1	11.38	65	50	50	167.6	11.1	272.2	52.2	
355	8805171938	116.26	33.24	4.2	5.12	80	-10	45	0.9	14.1	270.9	0.1	
356	8805230523	116.02	32.72	3.4	0.06	75	0	45	1.0	10.5	269.0	10.5	
357	8805240755	116.78	34.00	3.4	14.88	70	30	65	-167.1	5.2	286.6	35.0	
358	8806040031	117.12	33.96	3.6	16.57	45	-60	35	24.3	68.9	284.2	3.8	
359	8806060806	116.33	33.30	3.2	9.84	5	90	205	115.0	40.0	295.0	50.0	
360	8806102306	118.74	34.94	5.4	6.83	65	150	155	-152.8	1.2	116.3	38.3	
361	8806122122	117.55	34.04	3.2	7.36	80	150	145	-163.9	13.0	99.0	28.1	
362	8806181322	116.95	33.91	3.5	16.42	45	30	65	14.2	14.5	267.2	48.6	
363	8806251748	115.98	33.78	3.2	5.16	55	10	60	17.0	17.8	276.2	30.4	
364	8806261504	117.74	34.15	4.7	6.91	80	-130	315	188.0	41.0	74.9	24.2	

No.	YMnDHMt	Log.	Lat.	M <sub>L</sub>	Depth	Dip	Rake	Stk	Pa	Pd	Ta	Td	Refs
365	8807020026	116.45	33.48	4.3	11.72	30	-40	20	24.2	57.1	254.1	22.7	
366	8807030206	117.00	33.98	3.4	18.48	65	-40	60	20.4	45.3	117.0	6.5	
367	8808252000	115.86	32.71	3.0	0.04	80	-170	95	319.1	14.1	49.1	0.1	
368	8809082316	118.97	35.10	3.5	17.86	70	-110	25	266.1	60.0	130.2	22.5	
369	8809121324	118.47	33.86	3.9	3.22	40	130	145	27.4	11.2	140.0	62.9	
370	8809171550	119.61	35.56	3.2	7.96	45	110	90	346.0	1.7	82.9	75.9	CK
371	8809270519	116.58	34.58	3.1	2.54	89	-40	225	172.5	27.0	277.5	27.0	
372	8810011756	118.39	34.28	3.4	12.01	40	90	105	15.0	5.0	195.0	85.0	
373	8810091247	117.67	34.74	3.3	3.67	75	-20	80	37.0	24.6	128.3	2.9	
374	8810191344	118.76	34.94	3.8	5.13	85	0	65	20.1	3.5	289.9	3.5	
375	8810192247	115.60	33.18	4.1	3.42	55	70	70	174.1	8.0	289.3	71.8	
376	8810302002	120.72	34.61	3.6	5.69	25	-170	30	225.1	43.8	359.5	36.1	
377	8811050523	116.83	34.32	3.0	5.33	80	-10	30	345.9	14.1	255.9	0.1	
378	8811052350	117.19	34.04	3.6	14.92	55	-110	10	229.3	71.8	114.1	8.0	
379	8811061526	116.77	34.05	3.0	13.40	65	0	220	177.8	17.4	82.2	17.4	
380	8811080434	115.67	32.87	3.2	12.95	85	0	20	335.1	3.5	244.9	3.5	CK
381	8811170543	116.49	33.42	3.3	7.00	85	30	50	179.8	16.9	277.7	24.4	
382	8811211104	115.98	33.77	3.1	2.96	50	-90	45	315.0	85.0	135.0	5.0	
383	8811222023	118.76	34.97	3.1	8.34	80	130	180	-119.9	24.2	127.0	41.0	
384	8811230625	115.95	33.07	3.3	3.93	85	-130	290	165.3	37.0	51.2	28.6	
385	8811251914	118.31	35.82	3.0	4.57	35	-150	125	315.7	51.4	76.4	22.1	
386	8812031138	118.14	34.16	4.9	15.40	89	-9	429	23.7	7.1	114.4	5.6	MK
387	8812152319	116.54	33.48	3.3	11.78	20	-80	5	78.4	64.5	267.2	25.2	
388	8812160553	116.68	33.98	4.9	7.97	80	60	50	163.8	28.7	289.1	46.5	
389	8812172346	118.13	33.67	3.1	11.19	55	-90	50	320.0	80.0	140.0	10.0	
390	8901052132	116.00	34.26	3.1	3.64	60	-179	315	175.9	20.7	274.1	20.7	
391	8901190653	118.64	33.92	5.0	7.47	60	130	150	-147.2	6.6	113.1	55.4	
392	8902020451	118.85	33.94	3.9	6.62	20	140	120	351.0	30.6	138.9	55.1	
393	8902032348	115.59	33.18	3.2	4.72	80	150	120	171.1	13.0	74.0	28.1	CK
394	8902141543	119.14	35.05	4.0	12.07	60	-90	40	310.0	75.0	130.0	15.0	
395	8902151350	115.85	33.02	3.8	3.65	89	-20	210	163.2	14.0	256.8	14.0	
396	8902161351	117.73	34.01	3.2	3.88	75	10	245	199.3	3.7	108.1	17.6	
397	8902161917	115.59	33.18	3.4	4.77	70	-30	230	188.4	35.0	-77.9	5.2	
398	8902170610	119.13	35.05	3.2	12.24	75	20	30	161.7	2.9	253.0	24.6	
399	8902180717	117.73	34.02	4.1	3.63	80	160	150	-162.0	6.6	105.4	21.2	
400	8902250100	118.63	33.93	3.8	9.82	65	50	85	-157.4	11.1	307.2	52.2	
401	8903031643	116.27	33.38	3.1	11.10	75	0	30	346.0	10.5	254.0	10.5	
402	8903031646	118.59	35.27	3.8	5.61	75	-20	10	327.0	24.6	58.3	2.9	
403	8903040534	116.26	32.96	3.2	9.01	60	-30	25	349.6	41.3	257.2	2.7	
404	8903062216	115.59	33.18	4.5	5.08	50	-40	200	175.3	53.4	77.0	6.1	
405	8903070743	115.59	33.18	4.0	4.72	80	140	305	0.1	19.0	256.3	34.8	

No.	YMnDHMt	Log.	Lat.	M <sub>L</sub>	Depth	Dip	Rake	Stk	Pa	Pd	Ta	Td	Refs
406	8903211204	119.10	33.99	3.9	0.15	40	80	80	357.1	5.4	227.3	81.6	
407	8903242316	115.58	33.19	3.7	3.58	55	70	70	174.1	8.0	289.3	71.8	
408	8903261322	115.80	32.94	3.1	3.81	80	-30	185	139.0	28.1	-123.9	13.0	
409	8903290929	119.00	34.93	4.3	14.08	70	-10	40	358.2	20.9	265.4	7.3	
410	8904072007	117.91	33.60	4.5	11.68	70	0	40	356.8	14.0	263.2	14.0	
411	8904090729	117.10	34.25	3.2	8.05	65	-30	205	166.3	38.3	-102.8	1.2	
412	8905070607	117.91	33.93	3.5	4.27	70	170	125	350.4	7.3	83.2	20.9	
413	8905130202	118.93	35.04	3.3	12.13	35	80	75	352.2	10.4	201.7	78.1	
414	8905220249	116.78	34.94	3.0	3.70	75	170	160	25.7	3.7	116.9	17.6	
415	8905251240	120.42	35.84	3.8	10.83	70	0	50	6.8	14.0	273.2	14.0	
416	8906010933	117.17	34.01	3.5	12.35	75	-20	65	22.0	24.6	113.3	2.9	
417	8906011423	117.27	34.26	3.0	4.12	60	-50	165	128.1	55.4	-132.2	6.6	
418	8906042133	116.84	34.59	4.5	2.16	75	0	80	36.0	10.5	304.0	10.5	
419	8906082142	118.59	35.27	3.0	7.45	85	-50	25	329.7	37.0	83.8	28.6	
420	8906121657	118.19	34.02	4.4	17.43	60	100	90	172.7	14.4	24.9	73.1	
421	8906280020	116.48	33.49	3.1	14.69	50	-120	10	212.7	67.5	120.7	0.8	
422	8907192346	116.68	33.97	3.0	11.12	65	90	45	135.0	20.0	315.0	70.0	
423	8908091342	116.52	33.50	3.3	5.97	65	-160	135	354.0	31.2	86.8	4.6	
424	8908122019	117.50	34.27	3.0	11.41	40	80	115	32.1	5.4	262.3	81.6	
425	8908301839	116.60	33.93	3.1	13.76	45	-150	350	192.2	48.6	299.2	14.5	
426	8908311730	118.04	35.75	3.1	3.15	80	30	220	-11.1	13.0	86.0	28.1	
427	8909020539	116.45	33.51	3.2	8.09	35	-170	115	318.7	40.5	79.0	30.6	
428	8909041753	116.25	33.34	3.2	10.26	70	-160	120	341.2	28.0	71.6	0.8	
429	8909090849	115.95	32.70	3.1	0.21	75	-160	315	178.0	24.6	86.7	2.9	
430	8909130125	118.95	34.76	3.1	11.86	40	10	10	331.8	27.6	217.4	38.4	
431	8909151320	117.49	34.29	3.5	12.24	50	100	90	172.9	4.5	52.5	81.1	
432	8909182210	117.54	35.67	3.1	5.81	80	30	245	13.9	13.0	111.0	28.1	
433	8910081758	116.46	33.49	3.1	6.47	55	-150	135	346.6	44.0	83.1	6.7	
434	8911060340	115.59	33.19	3.2	4.53	75	-30	225	181.0	31.6	-83.3	9.1	
435	8911110835	118.65	33.38	3.0	4.58	80	150	95	146.1	13.0	49.0	28.1	
436	8911121713	116.75	34.00	3.0	13.90	85	30	45	174.8	16.9	272.7	24.4	
437	8912022316	116.74	33.64	4.2	13.92	60	20	45	357.2	8.3	261.5	34.3	
438	8912061915	117.04	33.81	3.4	15.11	45	90	155	-115.0	0.0	180.0	90.0	
439	8912161521	119.13	34.58	3.3	7.85	35	120	125	13.7	13.2	140.2	68.5	
440	8912180627	116.03	33.74	4.2	7.73	75	-179	185	49.0	10.5	141.0	10.5	
441	8912220303	116.69	33.62	3.4	13.19	65	20	45	356.8	4.6	264.0	31.2	
442	8912250321	117.24	35.91	3.3	9.81	80	-180	130	354.6	7.1	85.4	7.1	
443	8912280941	117.39	34.19	4.5	14.29	75	-50	230	179.9	44.9	-68.9	19.9	
444	8912311253	116.45	33.49	3.0	7.41	50	-120	145	347.7	67.5	-104.3	0.8	
445	9001012259	115.83	32.56	3.3	3.74	60	-140	315	170.4	48.3	77.8	2.3	
446	9001020950	116.77	33.65	3.5	12.50	70	-30	35	353.4	35.0	87.1	5.2	

No.	YMnDHMT	Log.	Lat.	M <sub>L</sub>	Depth	Dip	Rake	Stk	Pa	Pd	Ta	Td	Refs
447	9001031154	116.39	33.25	3.6	5.77	40	-10	235	207.6	38.4	93.2	27.6	
448	9001110122	118.22	35.22	3.9	3.64	70	30	30	157.9	5.2	251.6	35.0	
449	9001172327	118.27	33.87	3.6	15.71	50	140	150	27.0	6.1	125.3	53.4	
450	9001191239	118.23	35.23	3.8	3.63	80	-10	20	335.9	14.1	245.9	0.1	
451	9002050051	116.46	33.51	3.6	8.26	75	30	25	153.3	9.1	249.0	31.6	
452	9002170346	117.21	34.35	3.5	4.58	80	0	355	310.4	7.1	219.6	7.1	
453	9002181553	116.46	33.51	4.2	8.10	70	170	105	330.4	7.3	63.2	20.9	
454	9002181554	116.46	33.51	3.3	7.90	65	170	95	319.9	10.8	54.8	24.2	
455	9002282343	117.70	34.14	5.2	5.20	70	0	220	176.8	14.0	83.2	14.0	HJ
456	9003010034	117.70	34.13	4.0	3.53	89	160	495	181.8	14.0	88.2	14.0	
457	9003010323	117.71	34.16	4.7	10.55	80	-160	320	184.6	21.2	92.0	6.6	
458	9003021726	117.69	34.15	4.7	5.66	70	-10	20	338.2	20.9	245.4	7.3	
459	9003030348	116.84	34.16	3.0	13.74	75	30	40	168.3	9.1	264.0	31.6	
460	9003041645	117.68	34.12	3.6	3.59	85	-170	345	209.9	10.6	119.2	3.5	
461	9003061801	117.69	34.16	3.6	9.88	89	0	220	175.0	0.0	85.0	0.0	
462	9003080625	117.71	34.14	3.7	8.12	80	-50	175	122.0	41.0	-124.9	24.2	
463	9003101840	115.51	32.73	3.5	15.81	85	-140	325	195.8	31.0	91.1	23.0	
464	9003121126	117.70	34.13	3.4	3.89	85	-10	45	0.1	10.6	90.8	3.5	
465	9003172301	116.71	35.24	3.6	9.38	70	-179	335	198.2	14.0	291.8	14.0	
466	9003181356	117.71	34.15	3.3	8.96	75	-170	100	323.1	17.6	54.3	3.7	
467	9004021213	116.19	33.87	3.1	1.75	45	-50	55	40.6	62.0	297.8	6.7	
468	9004070107	116.16	33.87	4.2	4.61	55	-10	60	23.8	30.4	283.0	17.8	
469	9004160821	117.72	34.11	3.4	4.03	85	-150	320	187.7	24.4	89.8	16.9	
470	9004170847	117.73	34.17	3.3	13.54	89	179	485	170.0	0.0	80.0	0.0	
471	9004171411	117.72	34.11	3.4	4.15	89	20	225	358.2	14.0	91.8	14.0	
472	9004172232	117.72	34.11	4.8	3.80	89	170	495	180.4	7.1	89.6	7.1	
473	9004181432	116.17	33.88	4.0	4.84	75	20	75	-153.3	2.9	298.0	24.6	
474	9004200324	117.72	34.12	3.6	3.68	85	60	65	-180.0	33.3	306.5	42.2	
475	9004230930	116.39	34.06	3.1	3.54	85	-160	135	0.8	17.6	-92.5	10.3	
476	9004241127	116.16	33.88	3.8	4.70	75	170	345	210.7	3.7	301.9	17.6	
477	9005101425	116.36	33.20	3.1	10.72	60	-170	315	173.4	27.4	270.9	14.3	
478	9005171932	115.68	32.85	3.4	7.39	20	-180	95	293.9	41.6	76.1	41.6	
479	9005260728	120.42	34.41	3.4	0.23	89	120	490	193.4	37.8	66.6	37.8	
480	9005311739	116.96	34.43	3.6	3.14	89	0	185	140.0	0.0	50.0	0.0	
481	9006090005	115.59	32.84	3.2	15.50	70	130	135	-163.1	15.5	88.5	48.7	
482	9006170608	117.25	34.04	3.8	15.87	89	-10	260	-145.4	7.1	305.4	7.1	
483	9007200840	117.72	34.18	3.3	4.13	50	100	100	-177.1	4.5	62.5	81.1	
484	9008010417	115.56	33.19	3.2	4.57	35	-70	25	54.8	73.8	280.7	11.4	
485	9008052127	116.42	33.33	4.0	3.65	80	0	45	0.4	7.1	269.6	7.1	
486	9008091315	119.67	34.38	3.2	5.57	55	60	60	170.8	5.5	272.8	65.1	CK
487	9008290321	116.60	33.11	3.2	12.73	60	160	140	7.8	8.3	103.5	34.3	

No.	YMnDHMt	Log.	Lat.	M <sub>L</sub>	Depth	Dip	Rake	Stk	Pa	Pd	Ta	Td	Refs
488	9008310338	116.07	33.25	4.4	8.54	85	40	45	171.1	23.0	275.8	31.0	
489	9009021020	117.00	34.14	3.4	15.26	65	30	30	157.8	1.2	248.7	38.3	
490	9009120636	116.75	33.49	3.2	11.86	75	-20	55	12.0	24.6	103.3	2.9	
491	9009122207	117.71	34.13	3.1	3.53	80	-180	120	344.6	7.1	75.4	7.1	
492	9009151901	117.05	34.29	3.3	2.12	80	-10	225	180.9	14.1	90.9	0.1	
493	9010090402	118.72	33.89	3.2	6.13	75	50	60	178.9	19.9	290.1	44.9	
494	9010181721	117.88	33.64	3.8	2.89	70	-150	5	226.6	35.0	132.9	5.2	
495	9010250300	116.51	33.52	3.4	14.91	65	-140	5	224.6	45.3	128.0	6.5	
496	9010310103	117.63	34.17	3.0	10.24	80	10	200	154.1	0.1	64.1	14.1	
497	9011051414	116.35	32.92	3.1	6.97	35	-120	140	304.8	68.5	71.3	13.2	CK
498	9011071107	116.74	33.78	3.4	9.97	50	-20	230	199.8	39.8	96.4	15.6	
499	9011090711	116.81	34.43	3.5	4.26	80	0	25	340.4	7.1	249.6	7.1	
500	9011151333	115.93	32.72	3.3	1.29	85	-40	25	334.2	31.0	78.9	23.0	
501	9011171434	118.73	34.50	3.4	7.55	75	-120	20	256.0	50.8	132.8	24.1	
502	9011180506	115.62	33.25	3.0	4.27	89	-10	460	54.6	7.1	145.4	7.1	
503	9012131859	115.56	33.20	3.1	3.97	70	-30	210	168.4	35.0	-97.9	5.2	CK
504	9012171744	117.02	34.21	3.7	4.89	70	0	220	176.8	14.0	83.2	14.0	
505	9106281099	117.99	34.26	5.8	10.53	45	80	60	337.1	0.4	243.5	82.9	SM

YMnDHMt: Year, Month, Day, Hour, Minute; Pa: P Axis Azimuth; Pd: P Axis plunge; Ta: T Axis Azimuth; Td: T Axis Plunge; CK: Events rechecked; EH: E. Hauksson (1987); LJ: L. Jones (1988); MK: Ma and Kanamori (1991); HJ: Hauksson and Jones (1989); WK: Webb and Kanamori (1985); SM: the 1991 Sierra Madre earthquake, mechanism from E. Hauksson (personal Communication).

Figure A1 Focal mechanisms and P-wave first motion data. The numbers below each mechanisms are first line, year-month-day, longitude, latitude; second line, depth (km), dip, rake, strike. The same for Figure A2.

Figure A1

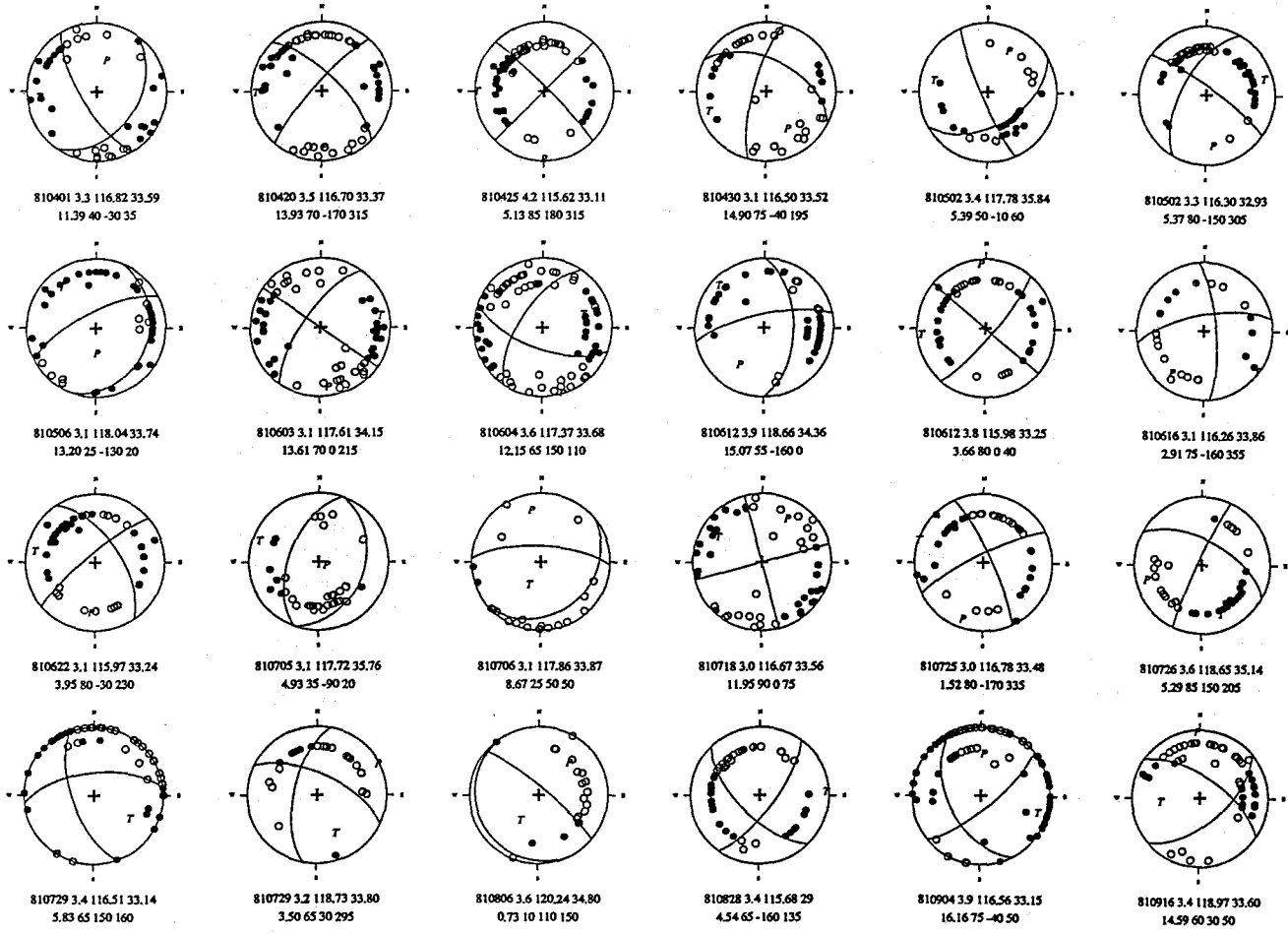


Figure A1 (continued)

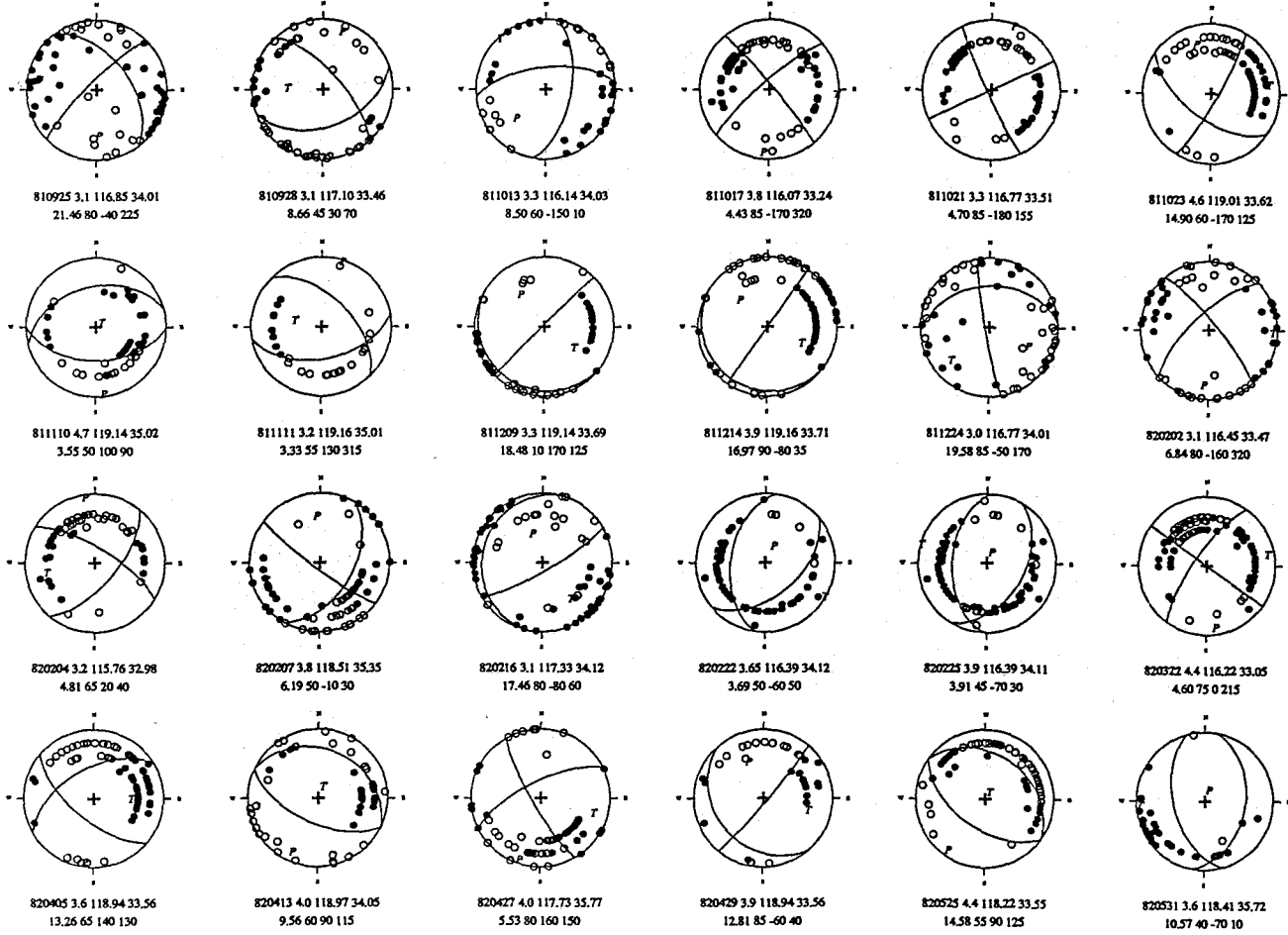


Figure A1 (continued)

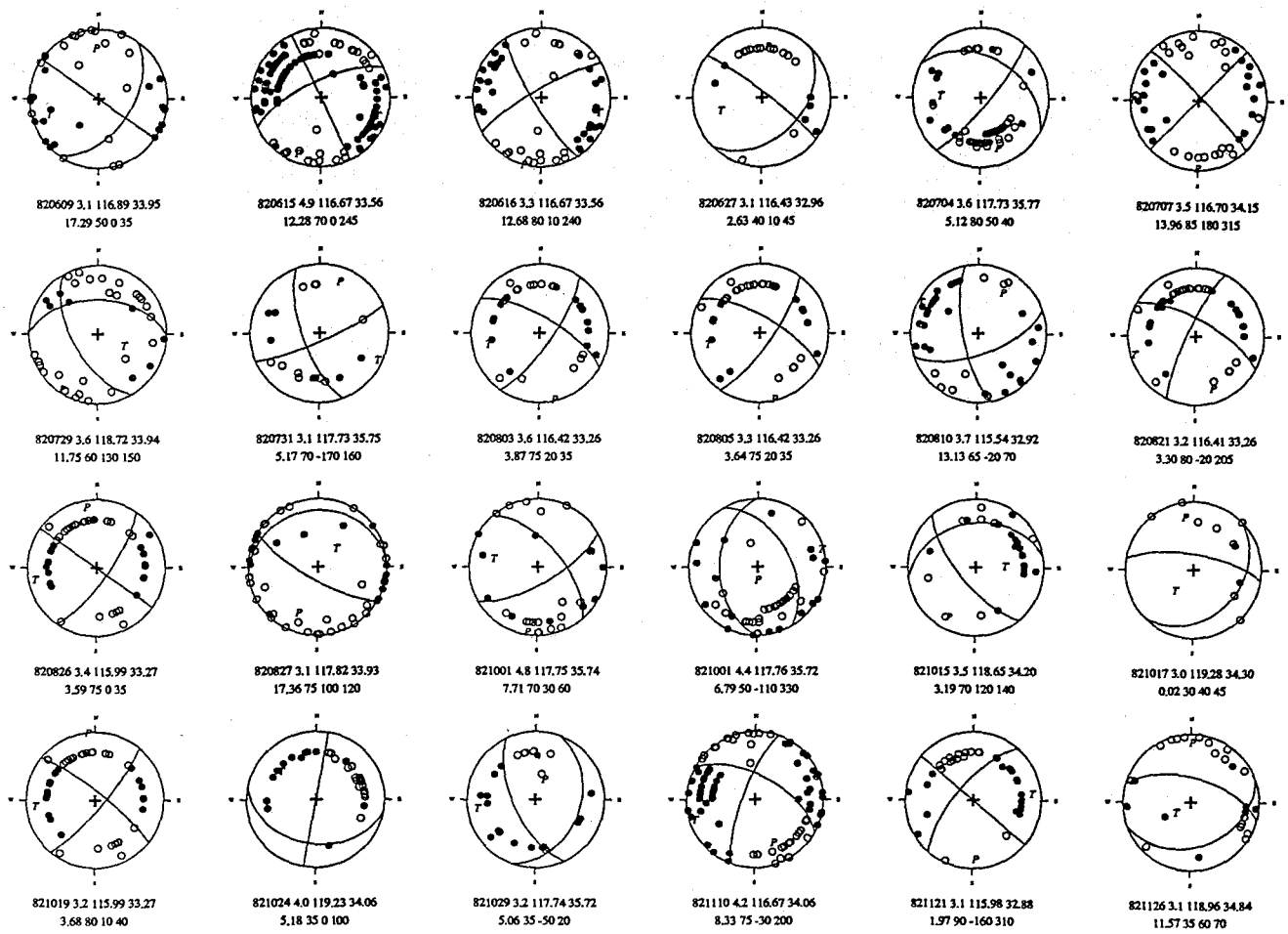


Figure A1 (continued)

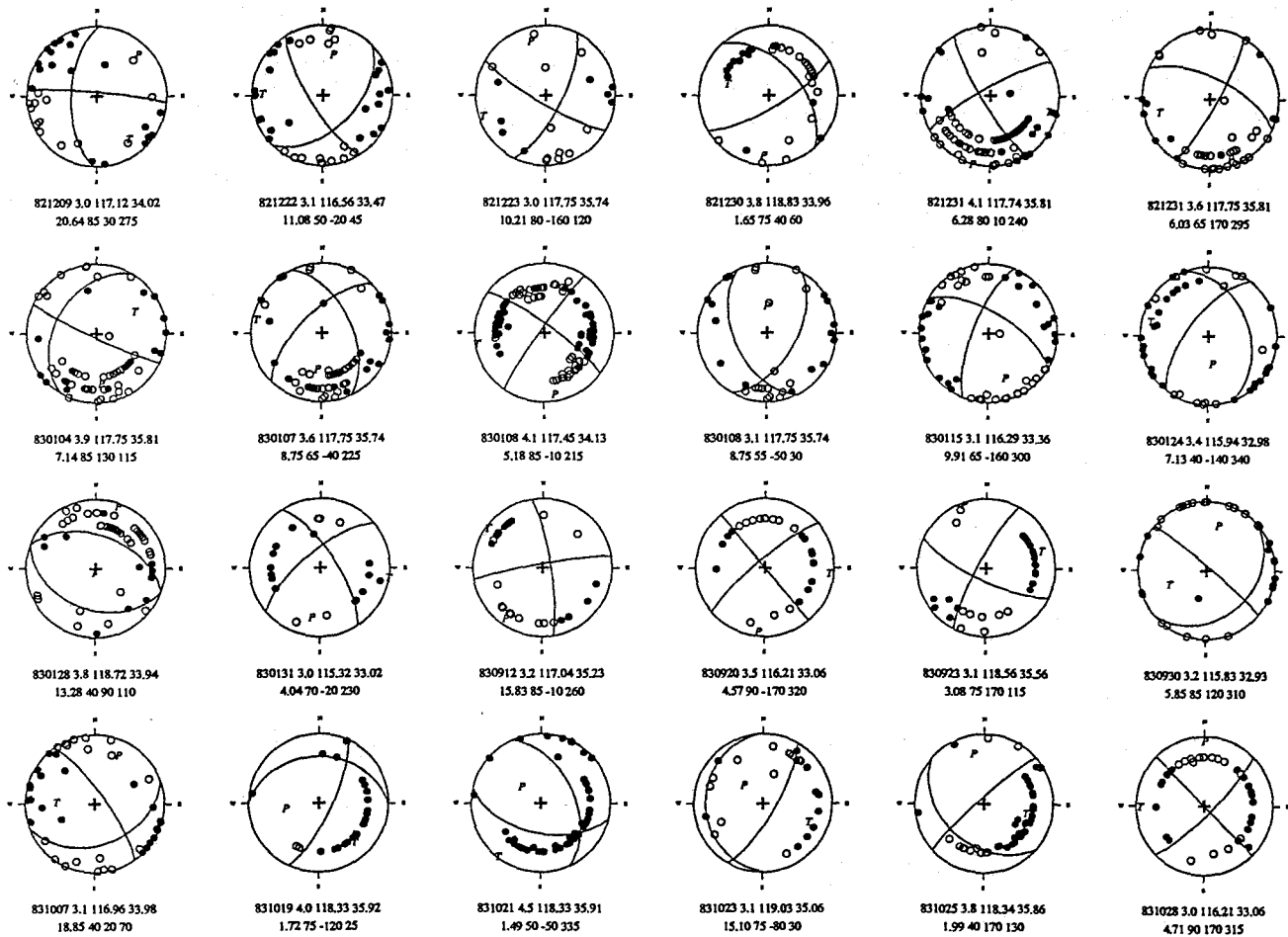


Figure A1 (continued)

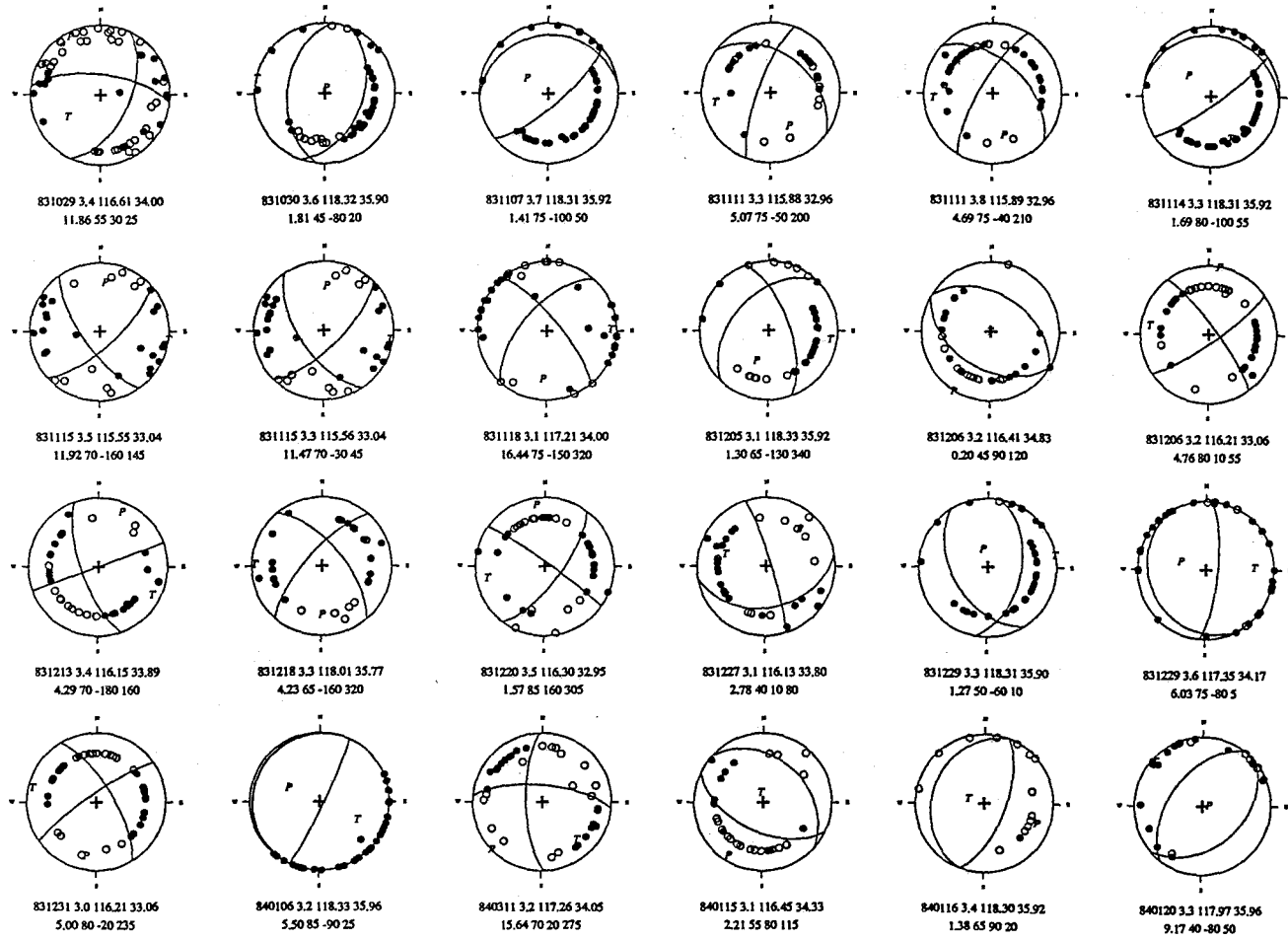


Figure A1 (continued)

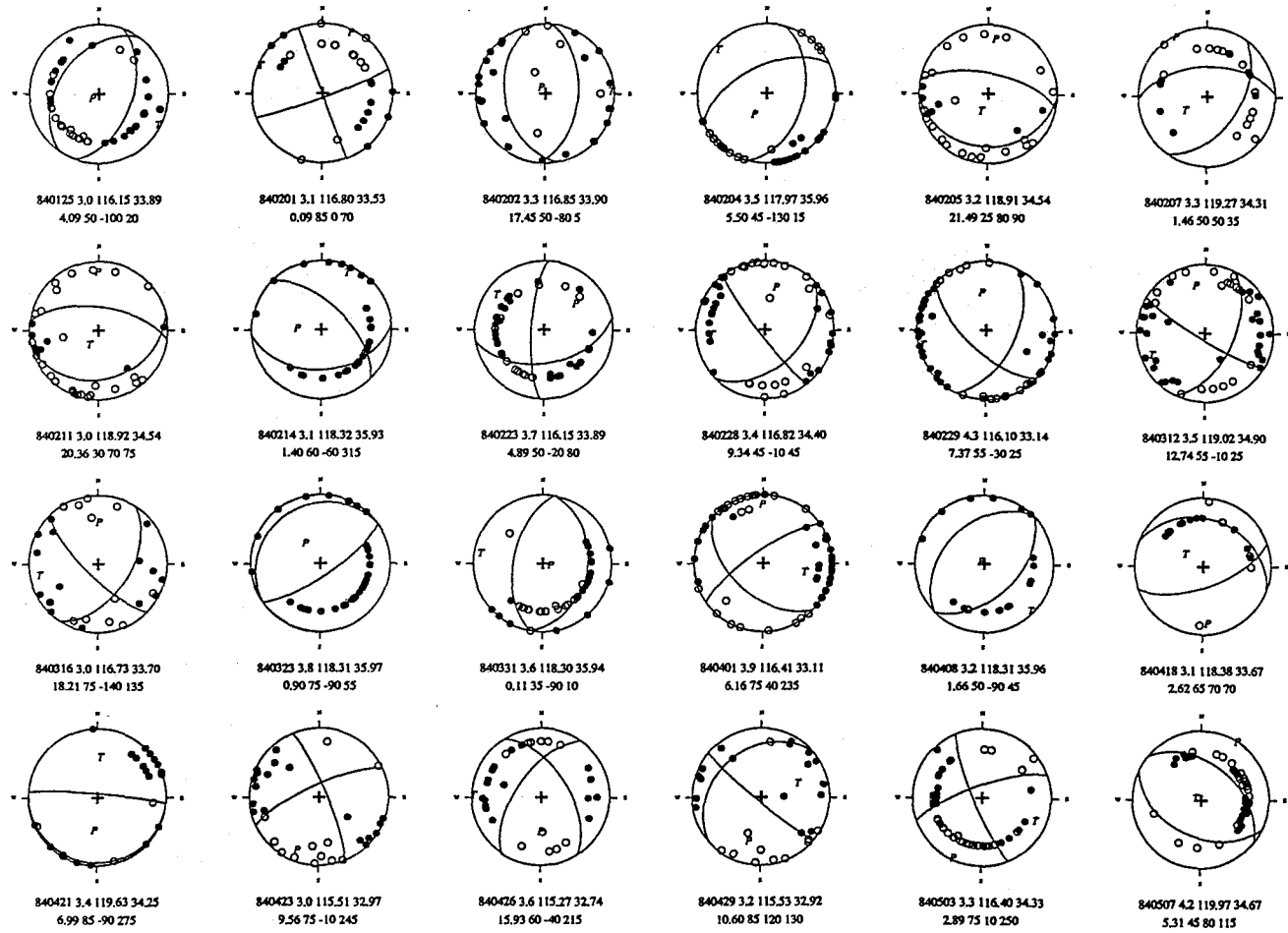


Figure A1 (continued)

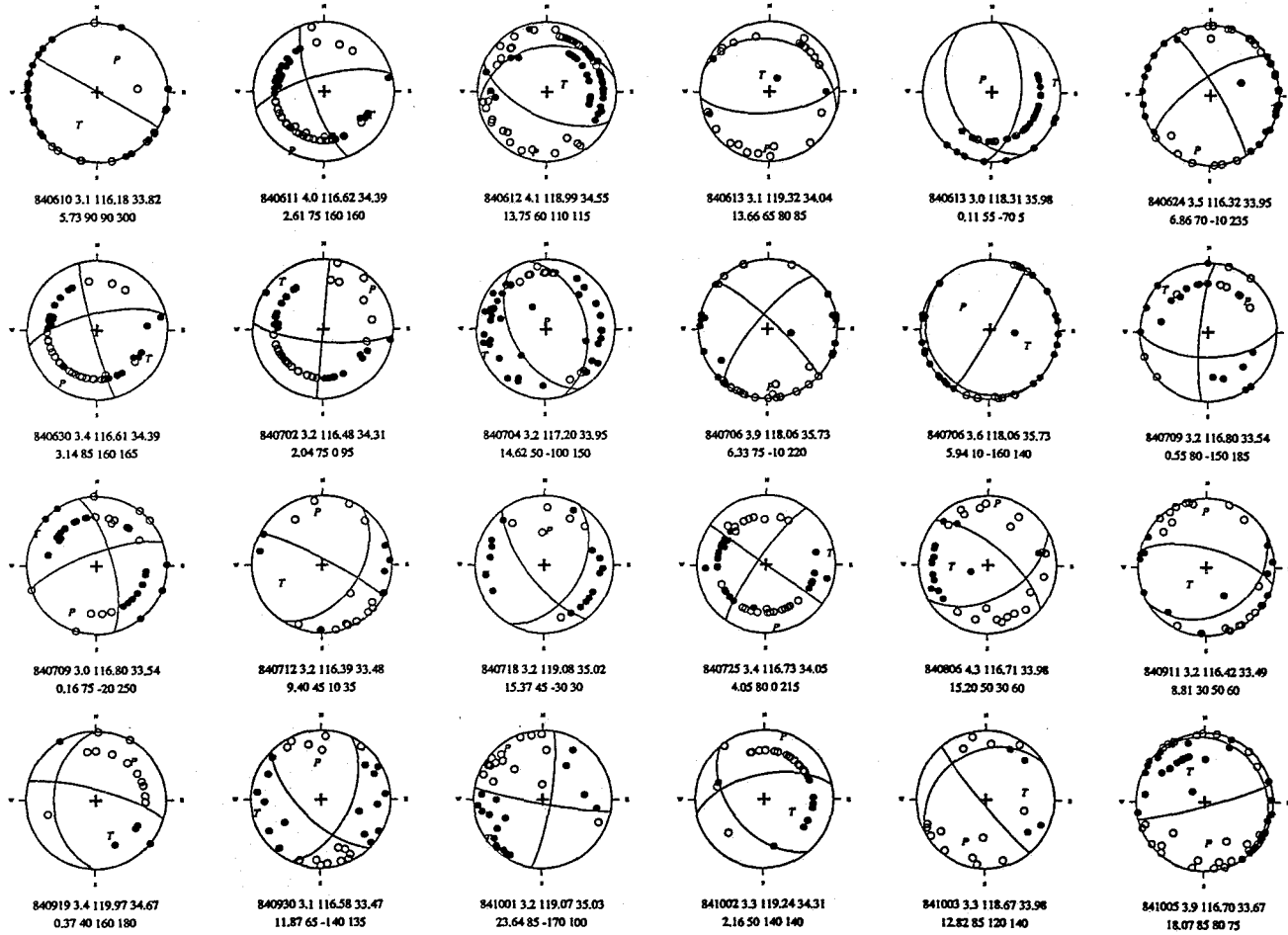


Figure A1 (continued)

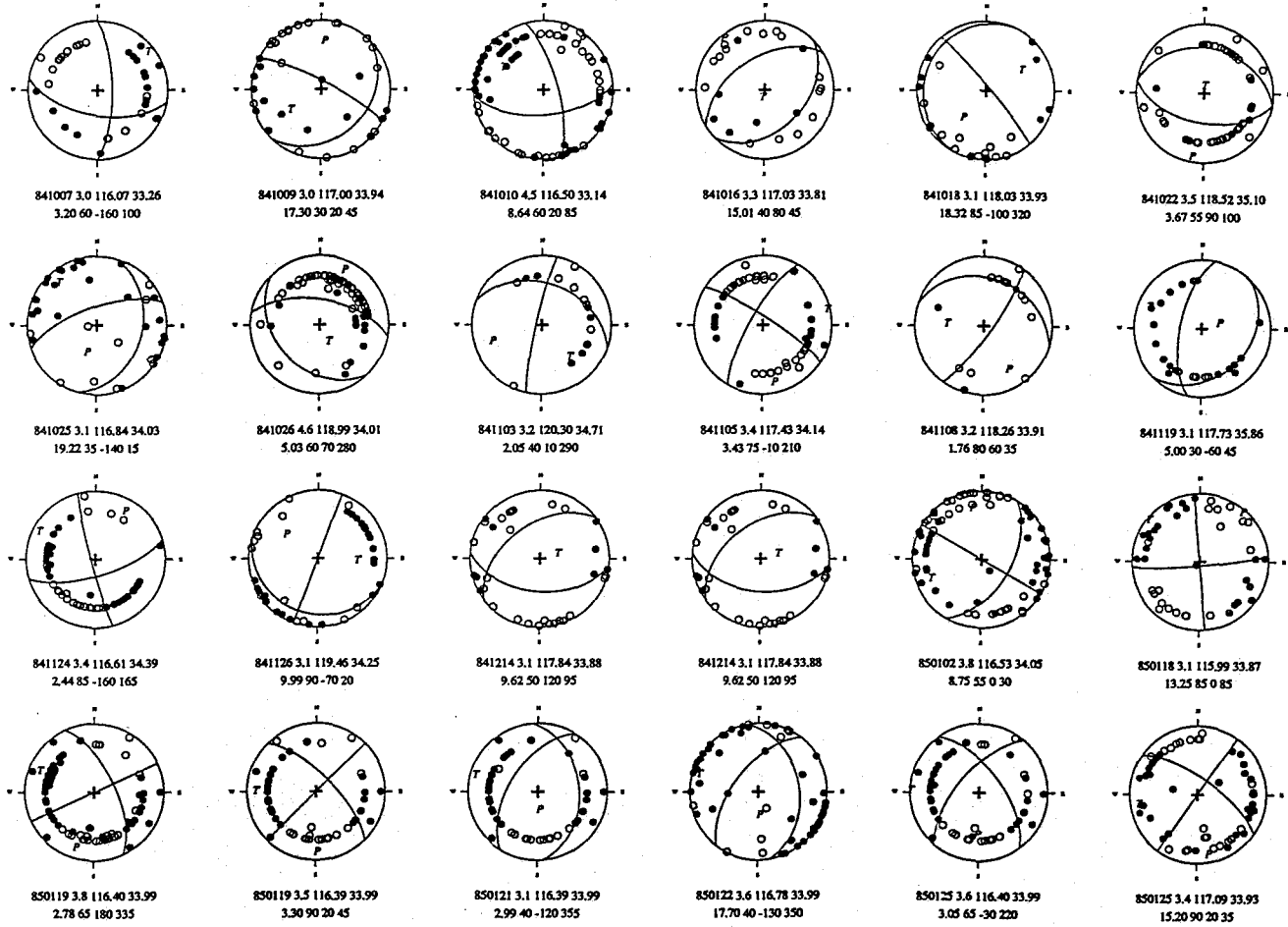


Figure A1 (continued)

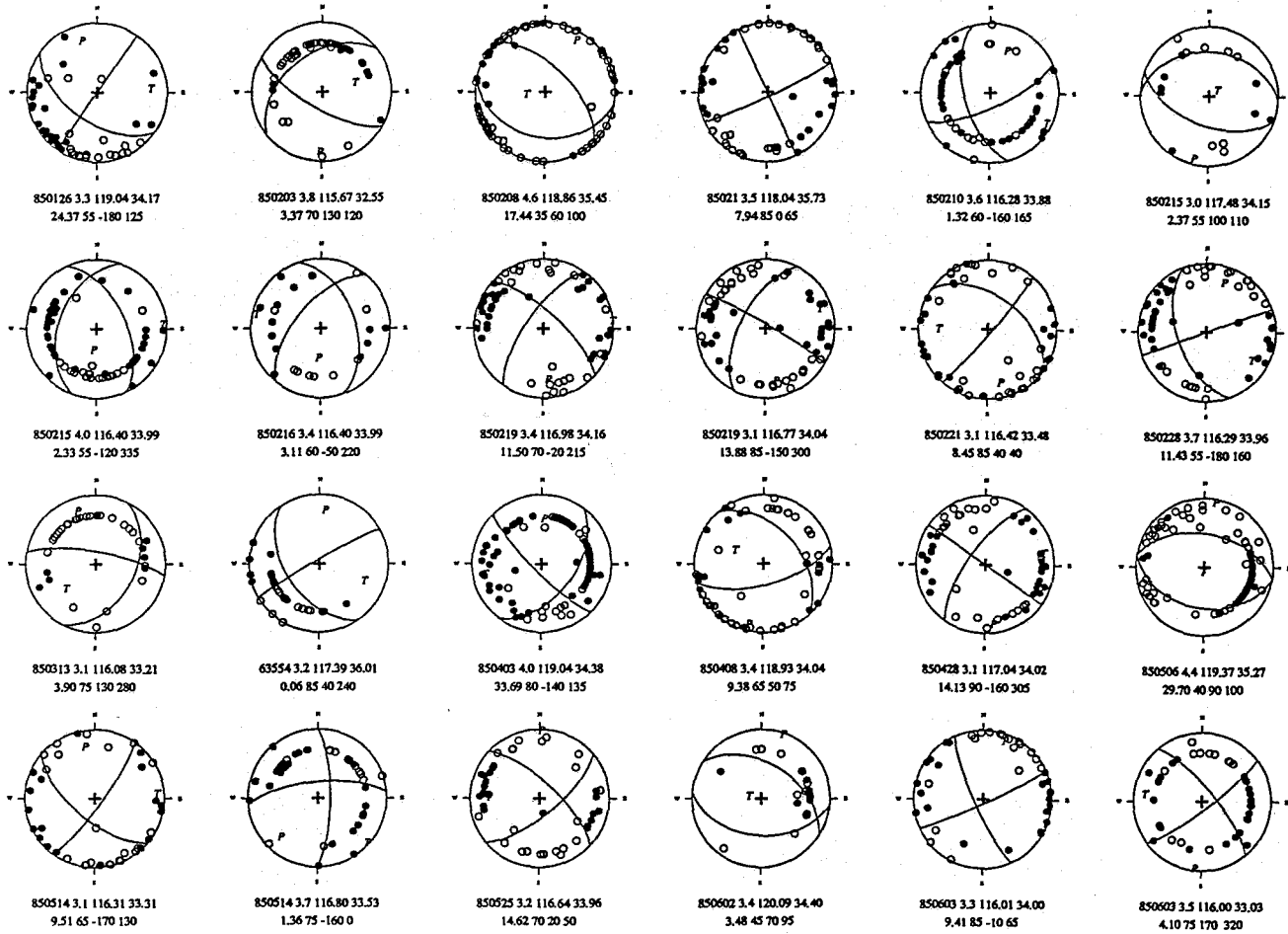


Figure A1 (continued)

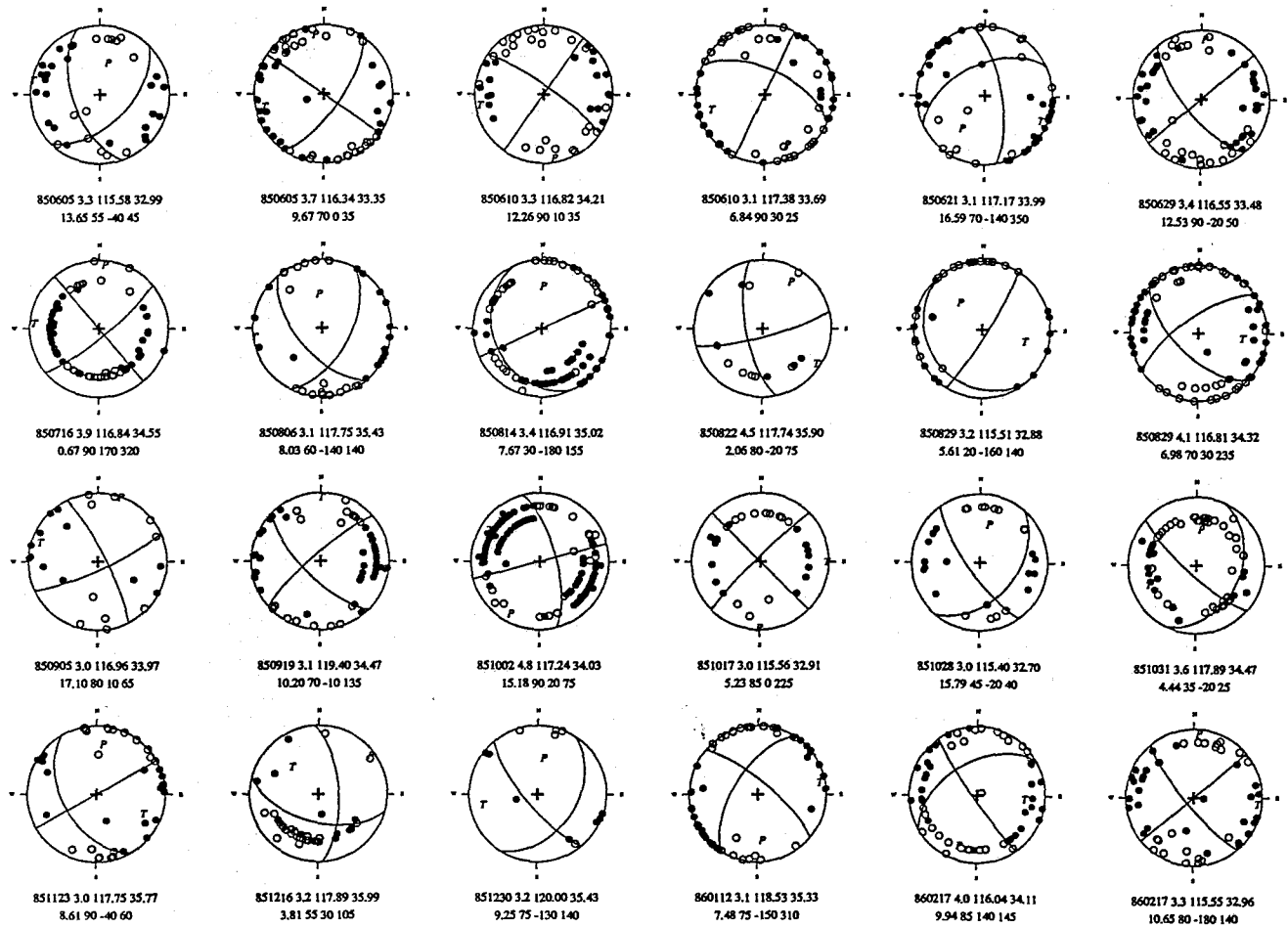


Figure A1 (continued)

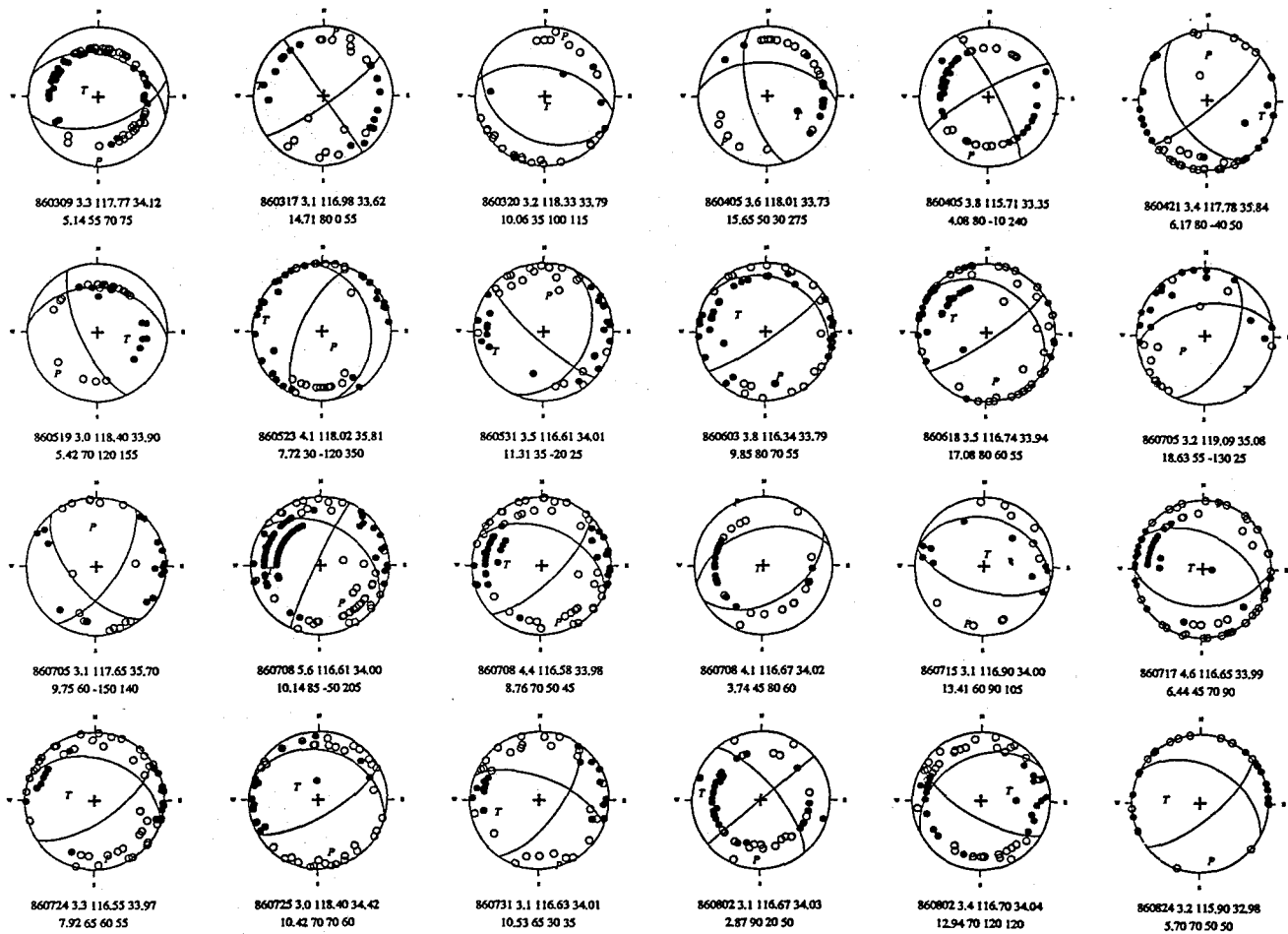


Figure A1 (continued)

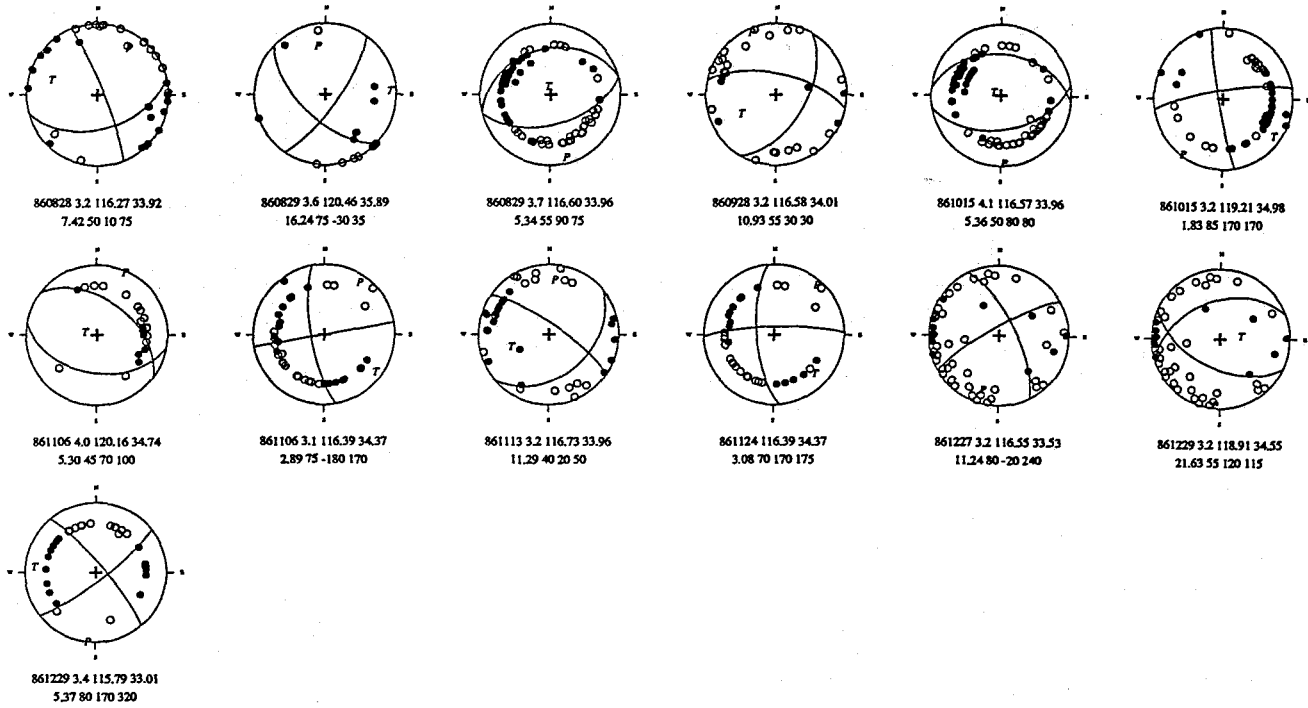


Figure A1 (continued)

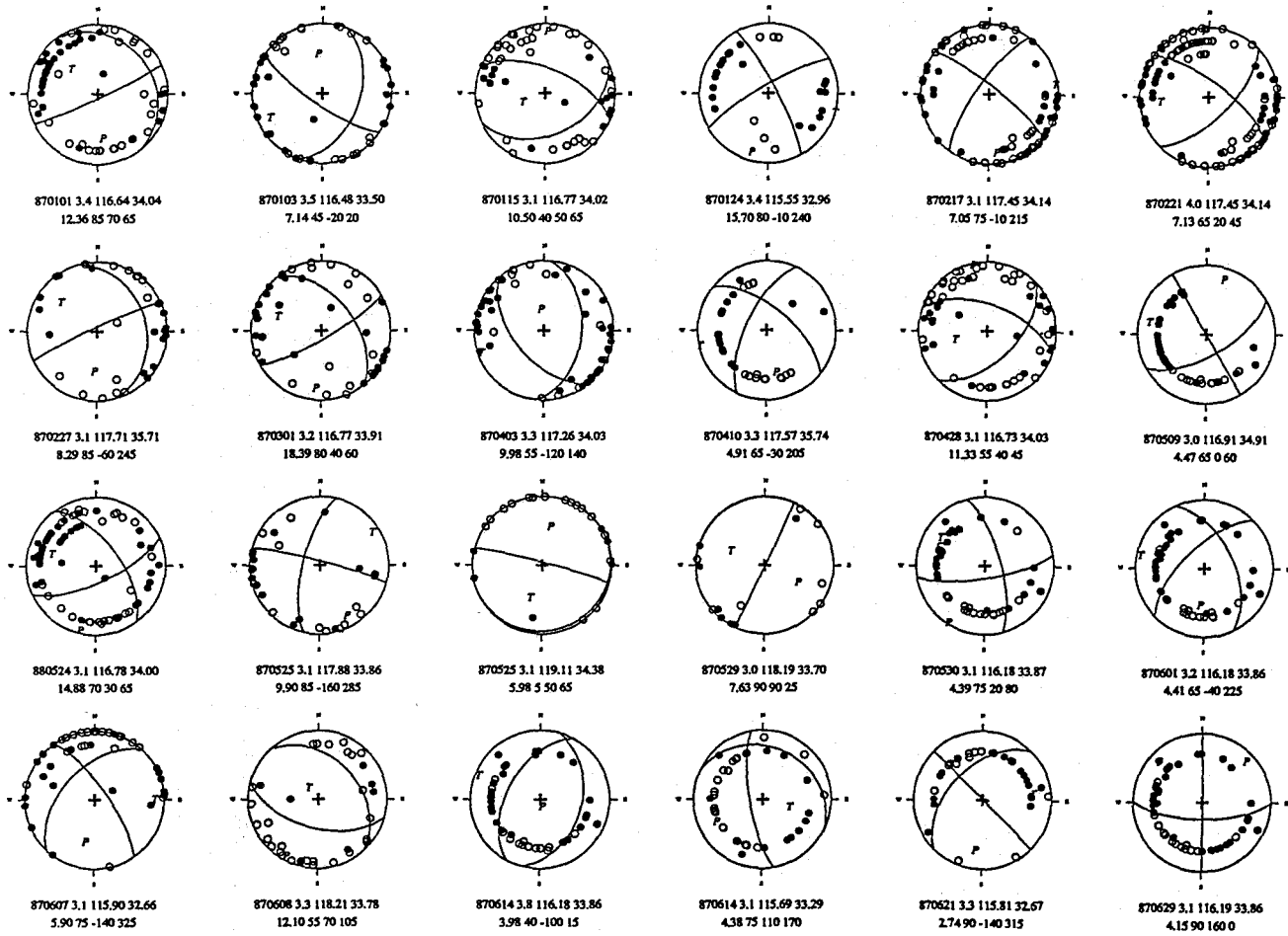


Figure A1 (continued)

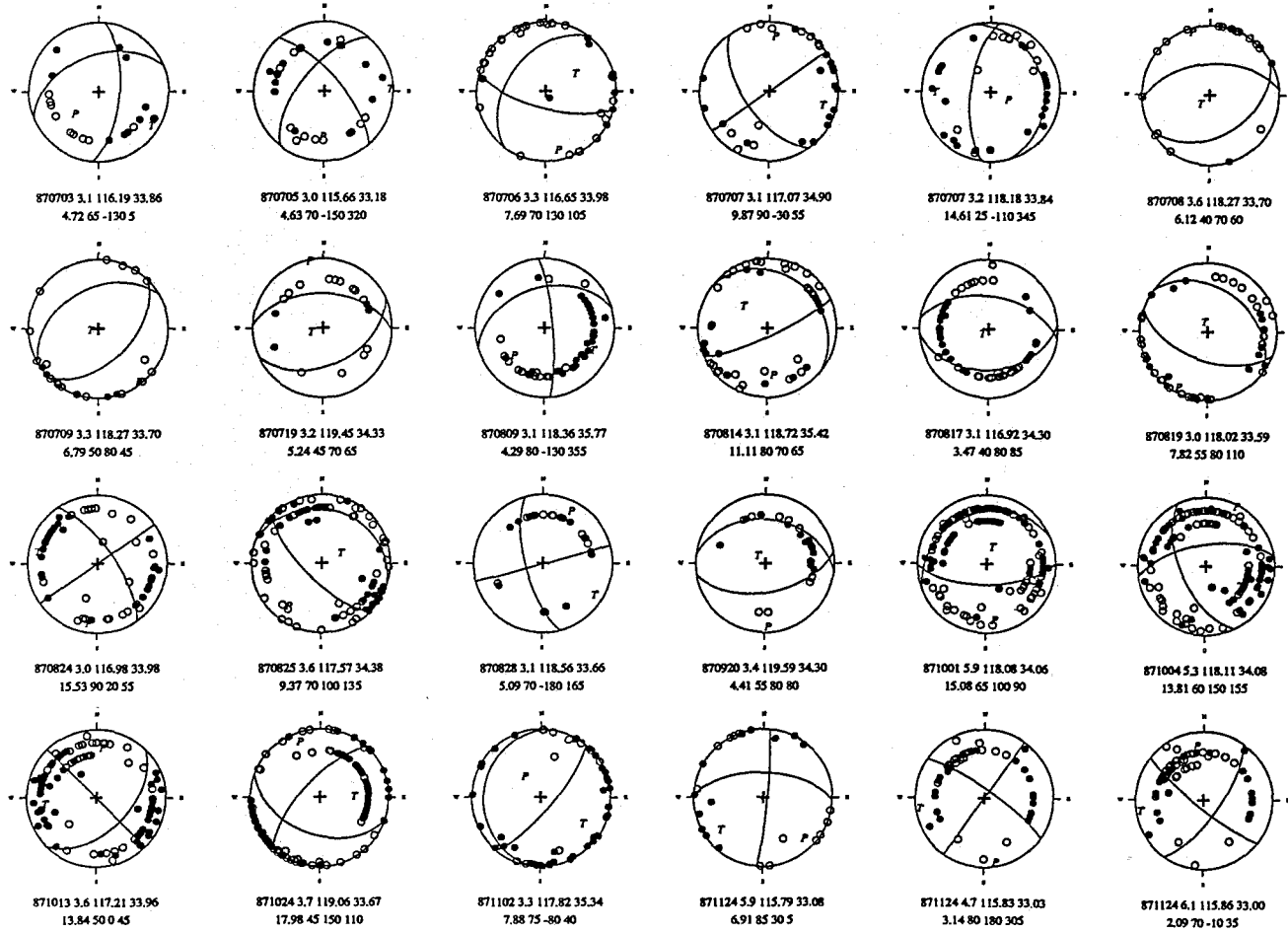


Figure A1 (continued)

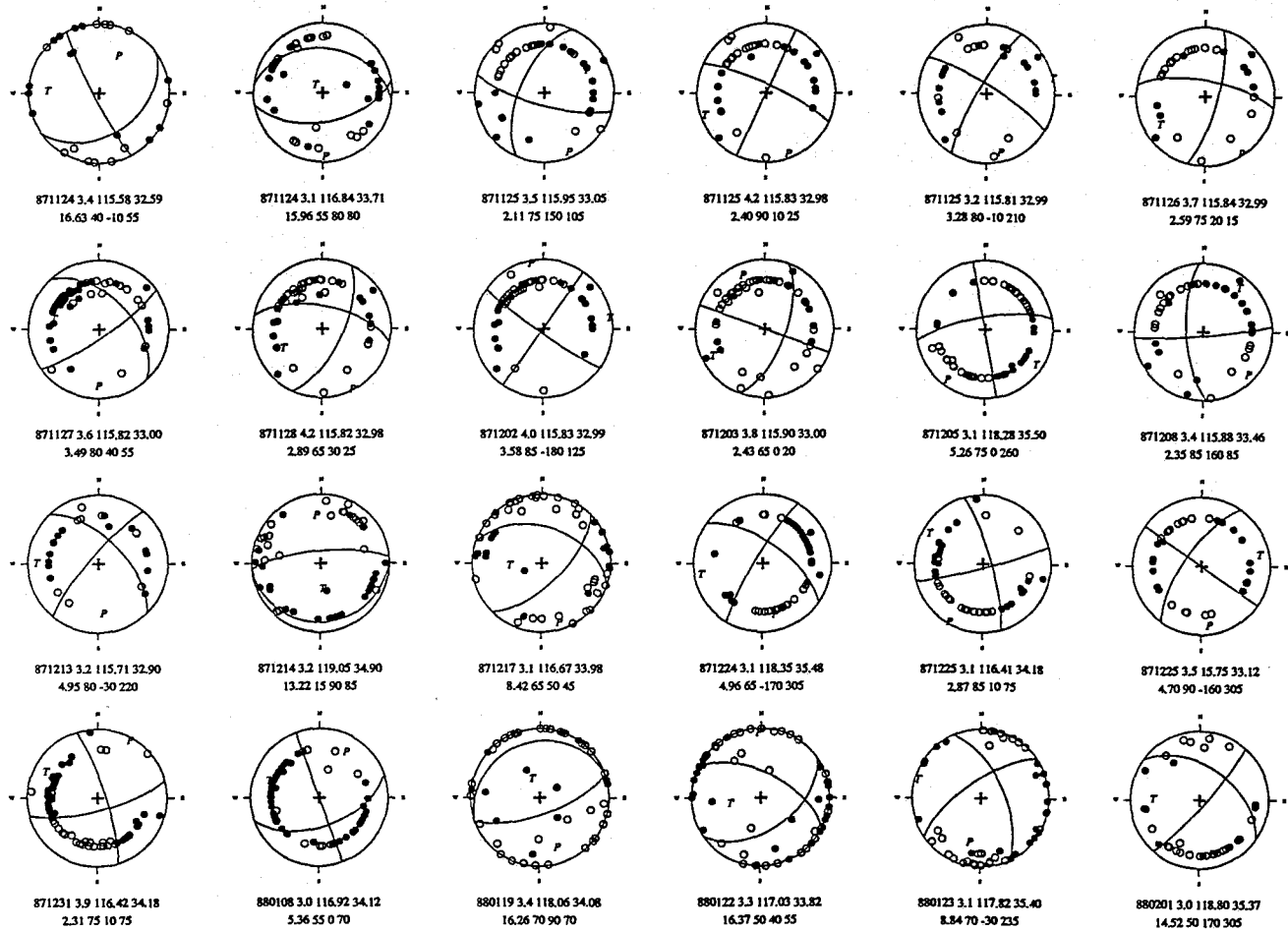


Figure A1 (continued)

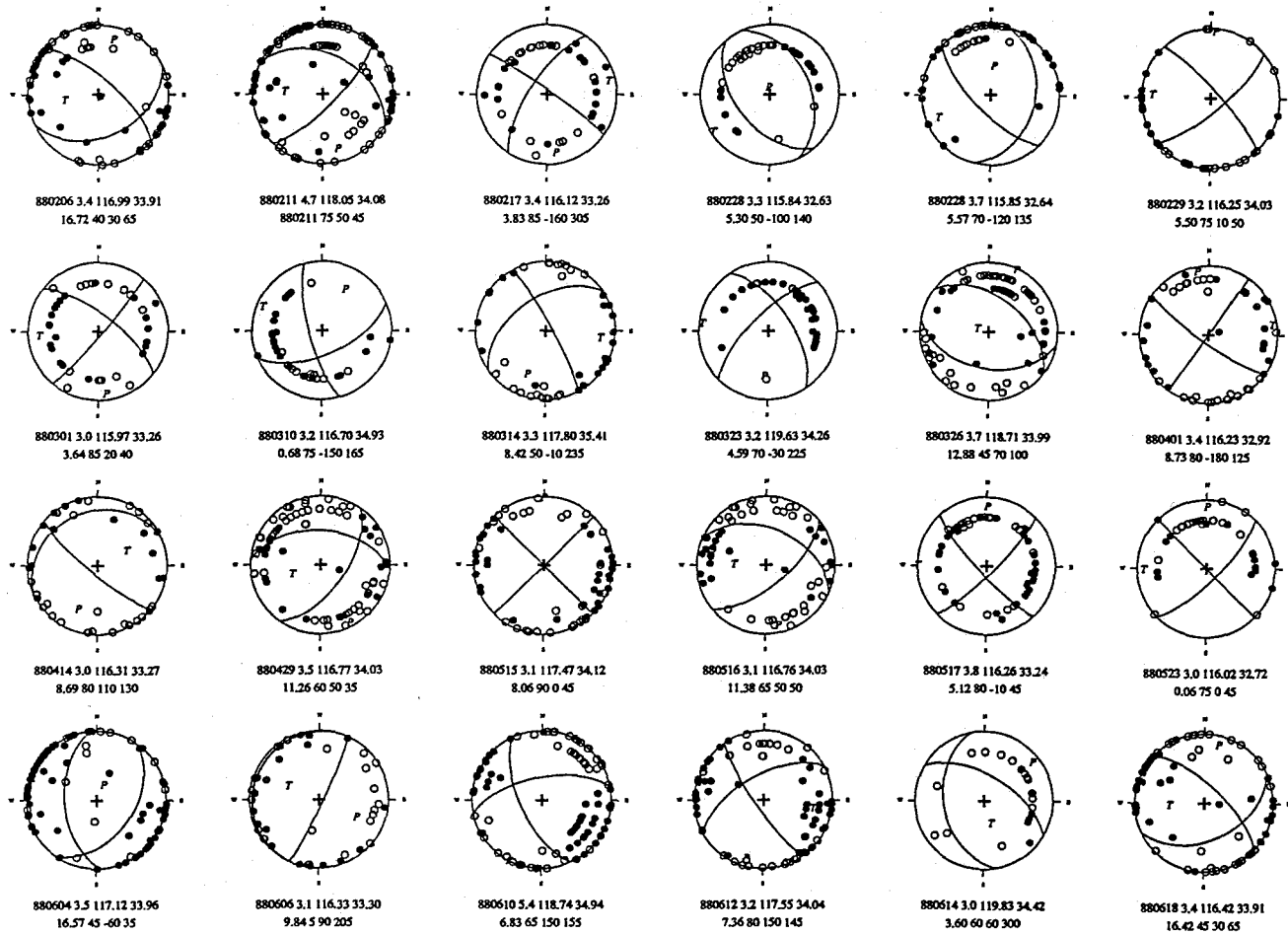


Figure A1 (continued)

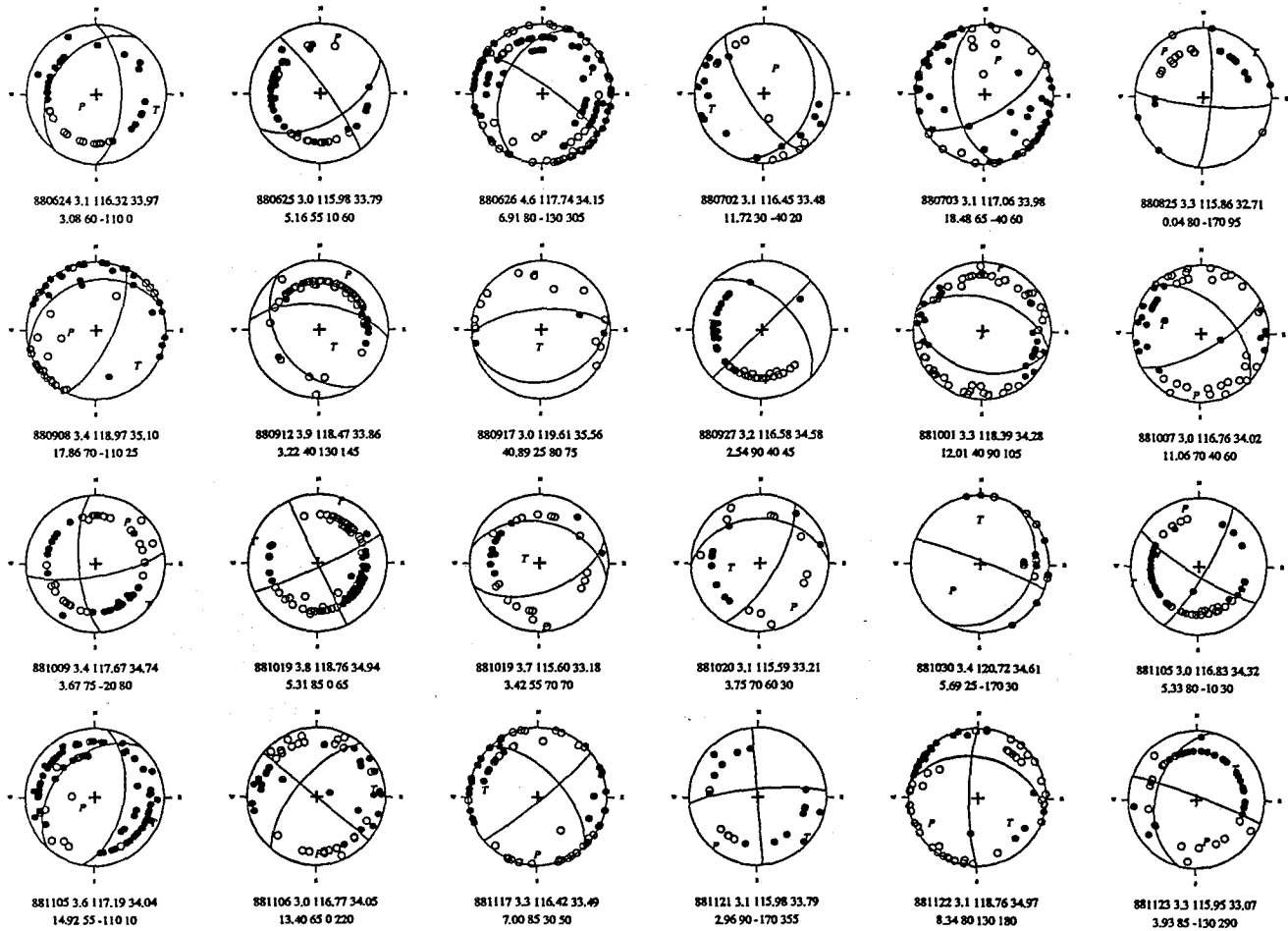


Figure A1 (continued)

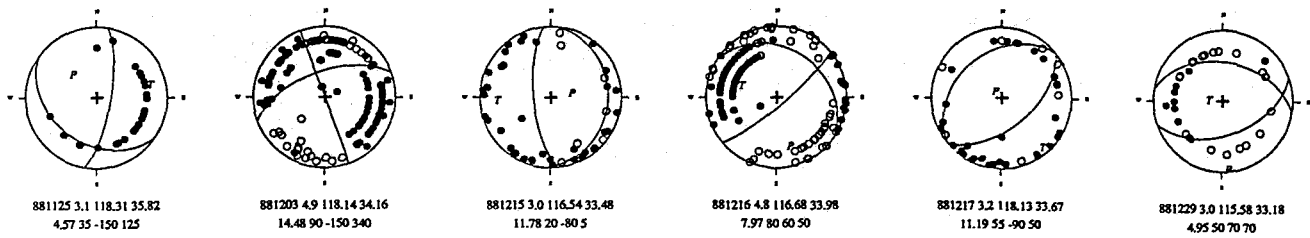


Figure A1 (continued)

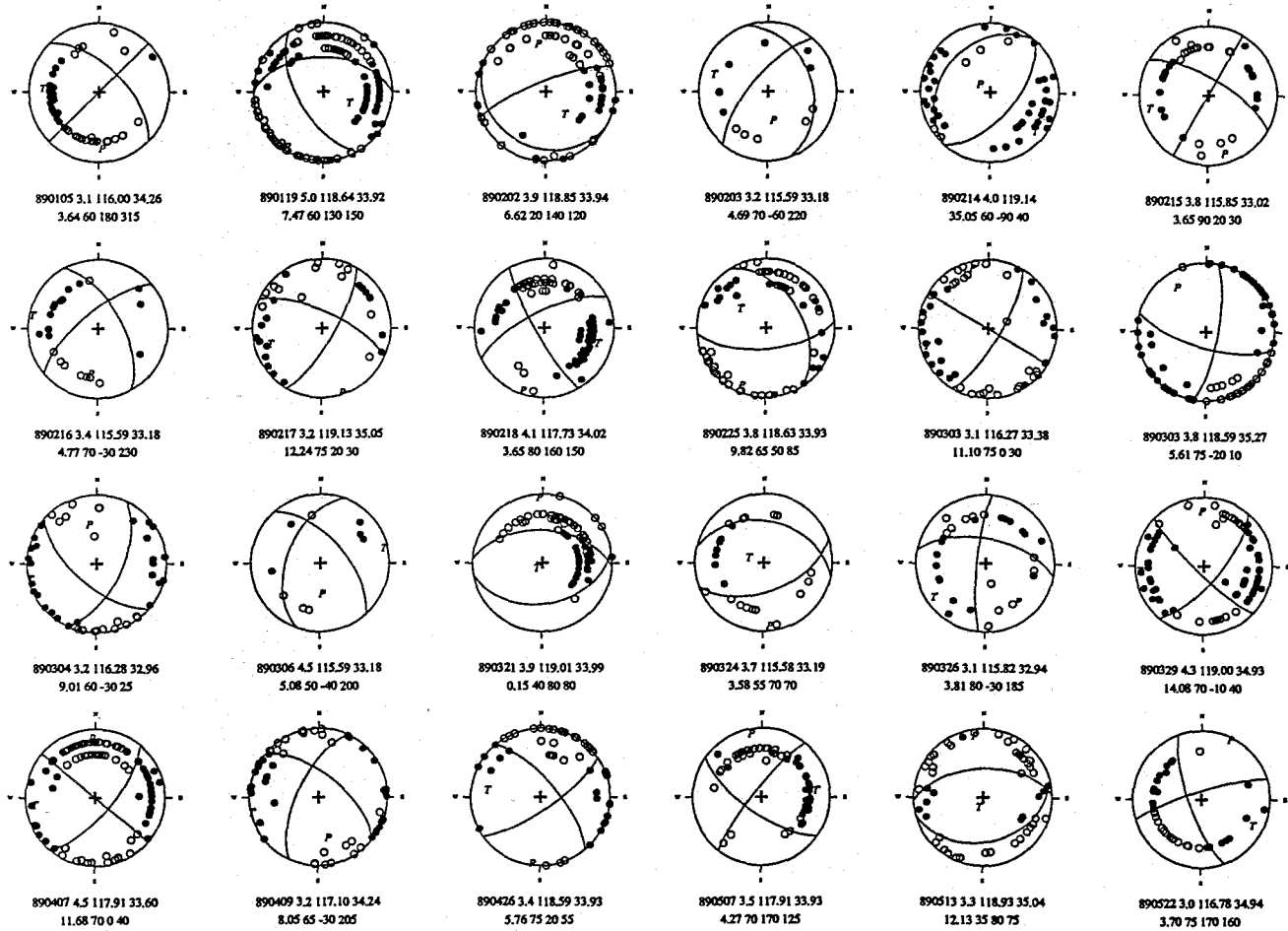


Figure A1 (continued)

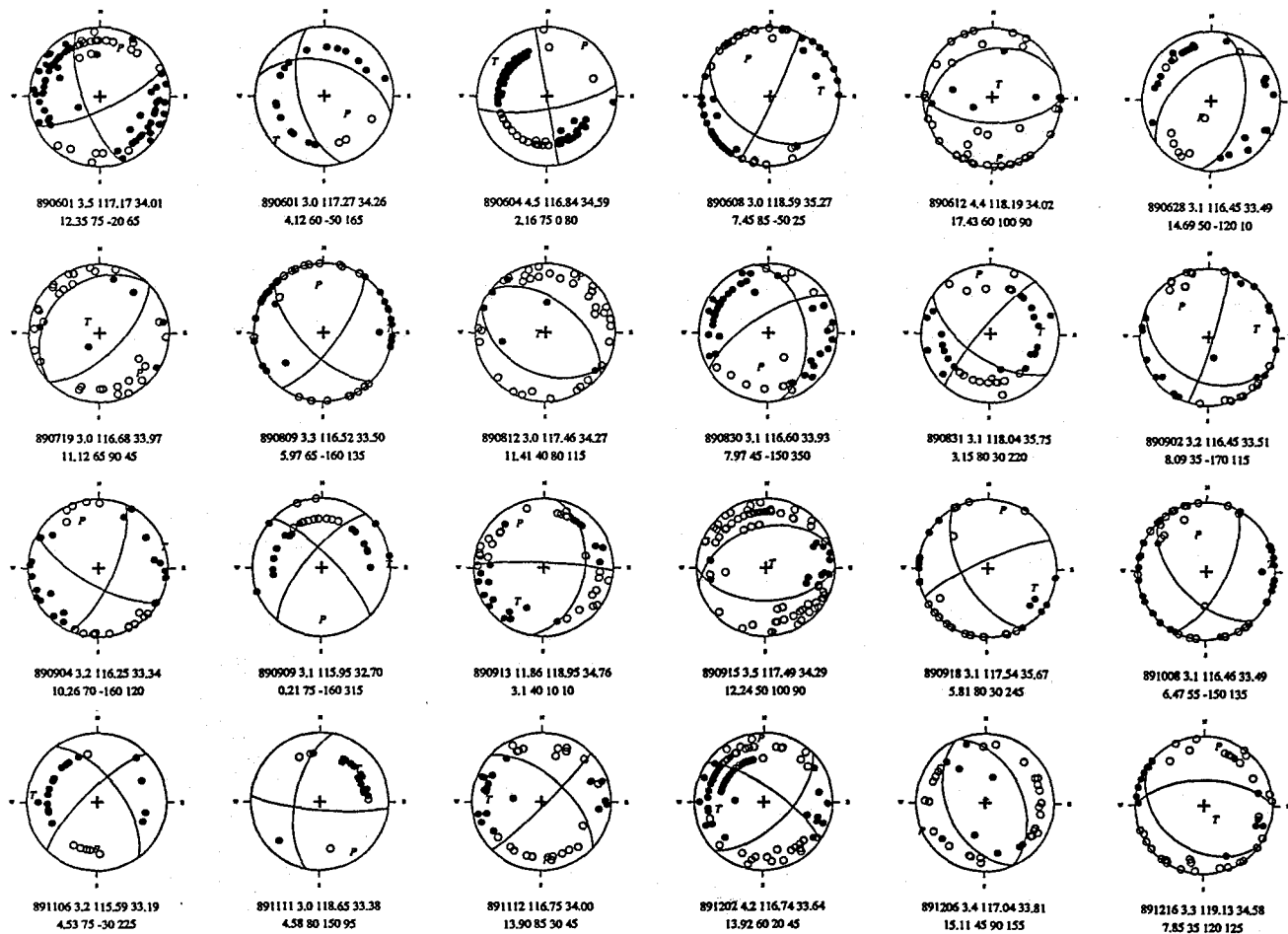


Figure A1 (continued)

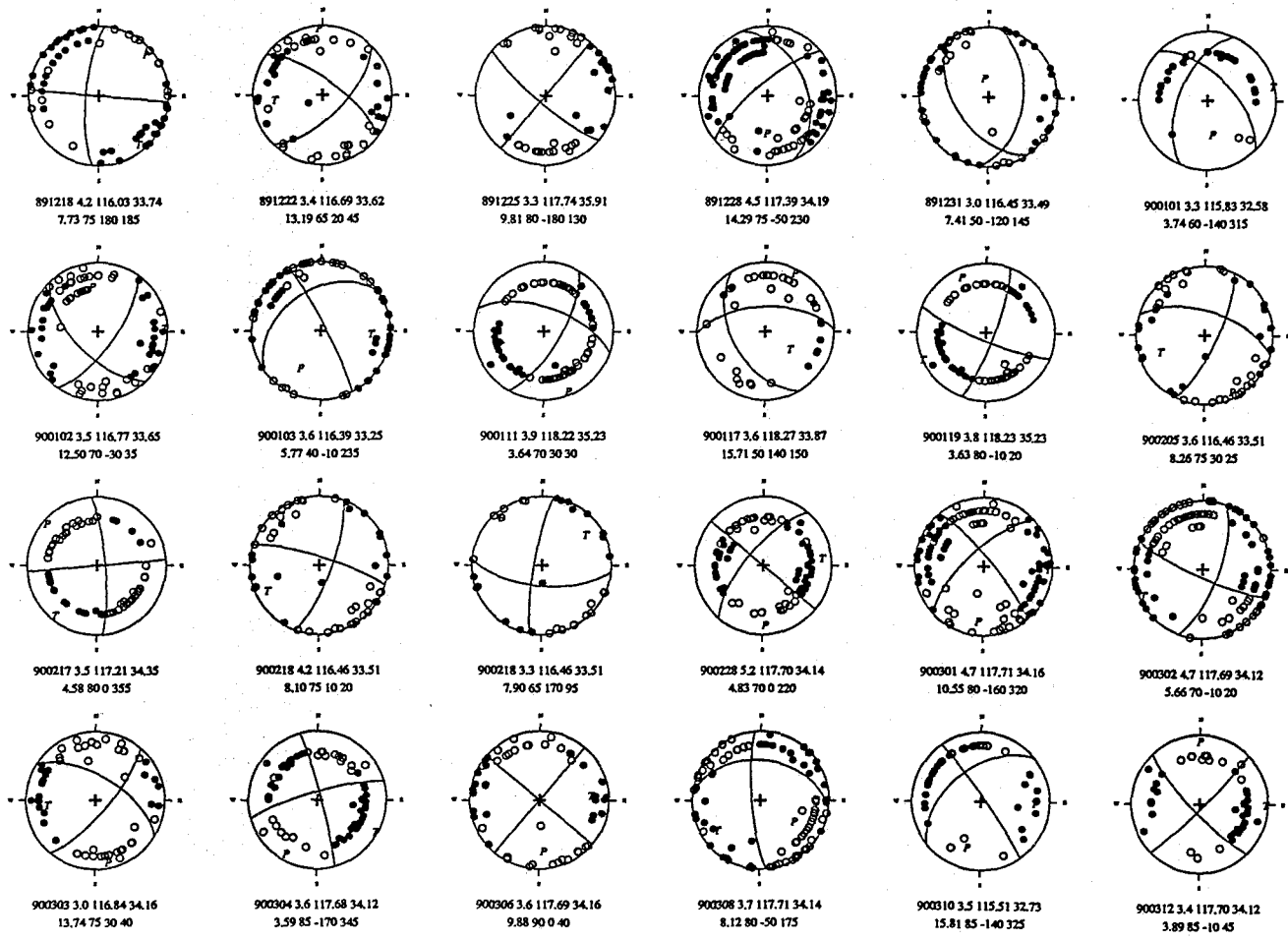


Figure A1 (continued)

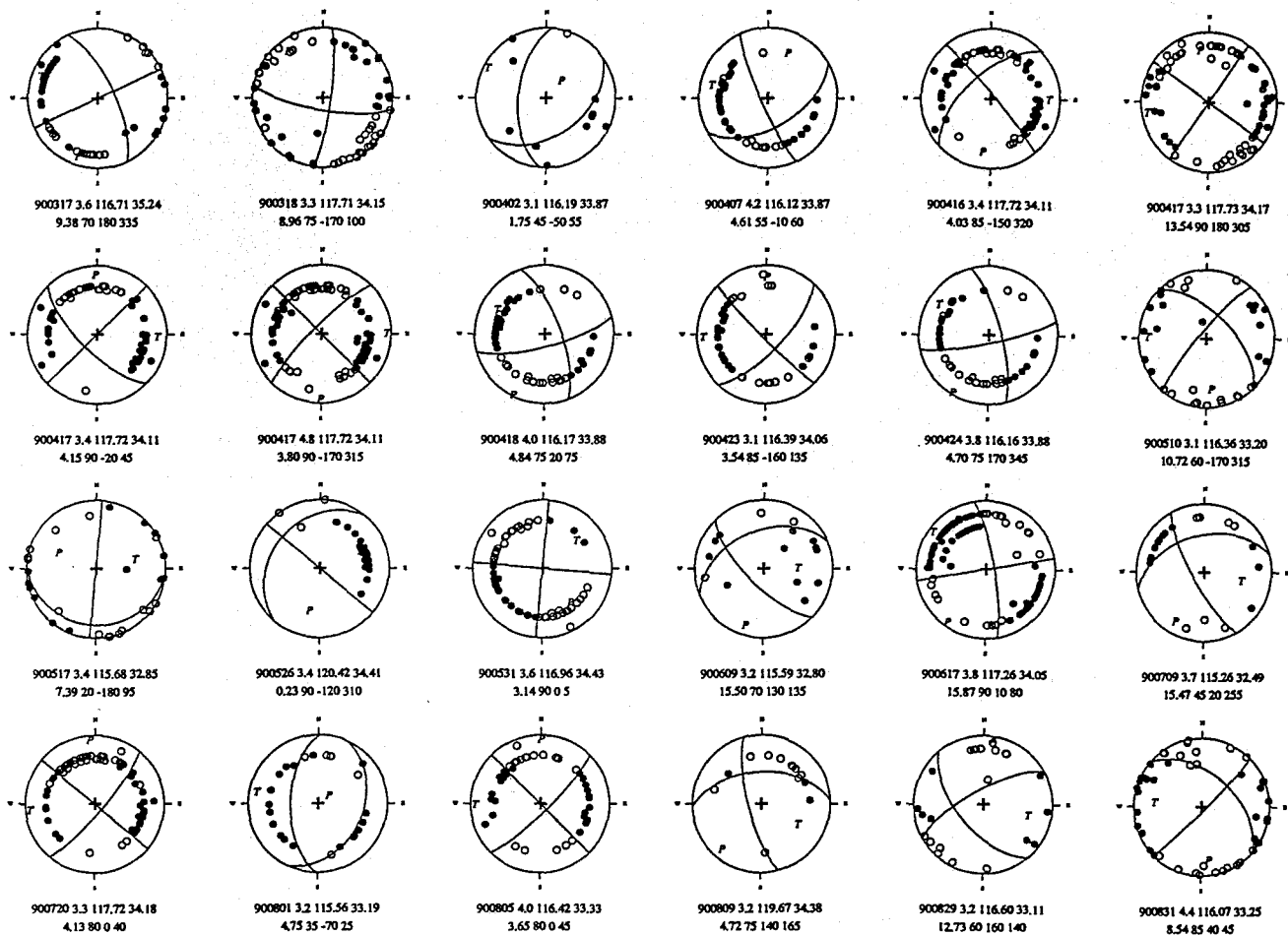
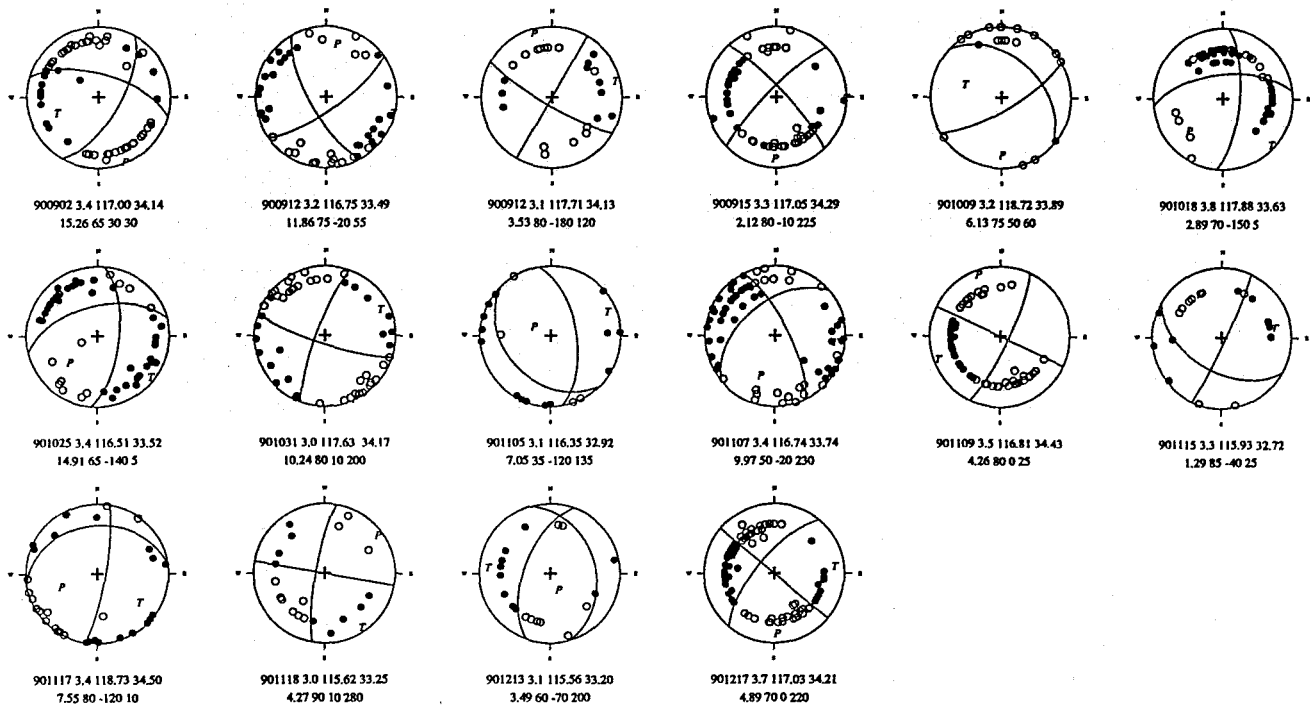


Figure A1 (continued)



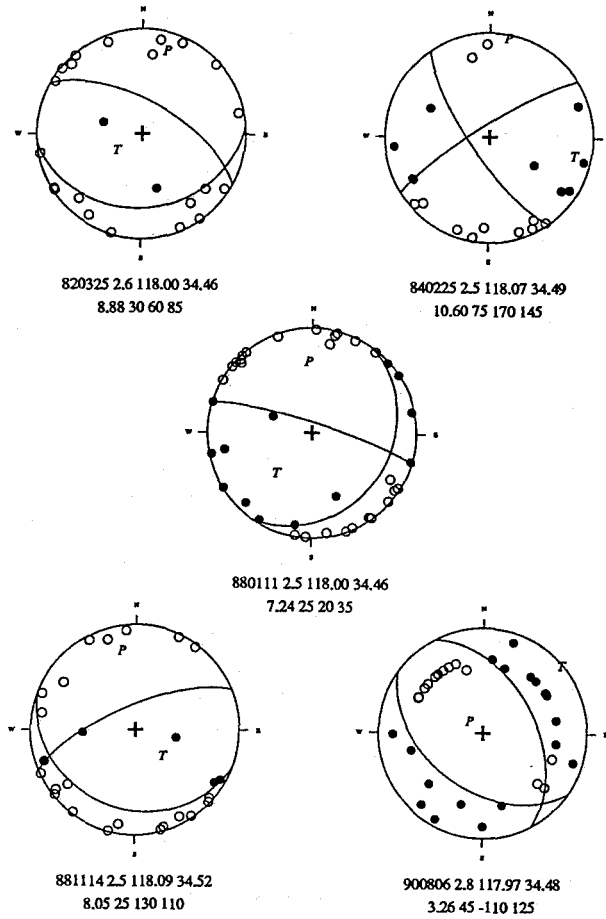


Figure A2 Focal mechanisms for the San Andreas fault, San Gabriel Mountains segment. These data are used for the discussion in Section 5.3.5.

## Bibliography

- Aki, K., Generation and propagation of G waves from the Niigata earthquake of June 16, 1964, 2, Estimation of earthquake moment, released energy, and stress-drop from the G wave spectrum, *Bull. Earthquake Res. Inst. Tokyo Univ.*, **44**, 23-88, 1966.
- Allen, C.R., San Andreas fault zone in San Gorgonio Pass, southern California: *Geol. Soc. Amer. Bull.*, **68**, 315-350, 1957.
- Allen, C.R., The tectonic environments of seismically active and inactive areas along the San Andreas fault system, In: Proceedings of Conference on Geological Problems of the San Andreas Fault System, edited by W.R. Dickenson and A. Grantz, *Stanford University Publications in Geological Sciences*, **11**, 70-82, 1968.
- Allen, C.R., 1975, Geological criteria for evaluating seismicity, *Bull. Geol. Soc. Am.* **86**, 1041-1057, 1975.
- Allen, C.R., T.C. Hanks, and J.H. Whitcomb, Seismological studies of the San Fernando earthquake and their implications, *Bull., Calif. Div. Mines Geol.*, **196**, 257-262, 1975.
- Anderson, D.L., The San Andreas fault, *Scientific American*, **225**, 53-68, 1971
- Anderson, E.M., *The Dynamics of Faulting and Dyke Formation with Applications to Britain*, Oliver and Body, Edinburgh, 206pp., 1951.
- Anderson, J.G., Estimating the seismicity from geological structure for seismic-risk studies, *Bull., Seismol. Soc. Amer.* **69**, 135-158, 1979.
- Anderson, J.G., M. Ellis, C. Depolo, Earthquake rate analysis, *Tectonophysics*, **218**, 1-21, 1993.
- Angelier, J., Determination of the mean principal directions of stresses for a given fault population, *Tectonophysics*, **56**, T17-T26, 1979.
- Angelier, J., Tectonic analysis of fault slip data sets, *J. Geophys. Res.*, **89**, 5835-5848,

1984.

- Angelier, J., Inversion of field data in fault tectonics to obtain the regional stress--III: A new rapid direct inversion method by analytical means, *Geophys. J. Int.*, **103**, 363-376, 1990.
- Apperson, K.D., Stress fields of the overriding plate at convergent margins and beneath active volcanic arcs, *Science*, **254**, 670-678, 1991.
- Bakun, W.H., G.C.P. King, and R.S. Cockerham, Seismic slip, aseismic slip, and the mechanics of repeating earthquakes on the Calaveras fault, California, In: Earthquake Source Mechanics, eds. by S. Das, J. Boatwright, and C.H. Scholz, Maurice Ewing, Geophysical Monograph 37, *Amer. Geophys. Union*, Washington D.C., **6**, 195-207, 1986.
- Bent, A.L., and D. V. Helmberger, A re-examination of historic earthquakes in the San Jacinto fault zone, California, *Bull. Seismol. Soc. Amer.*, **81**, 2289-2309, 1991.
- Bird, P., and R.W. Rosenstock, Kinematics of present crust and mantle flow in southern California, *Geol. Soc. Amer. Bull.*, **95**, 946-957, 1984.
- Bott, M.H., Mechanics of oblique slip faulting, *Geol. Mag.*, **96**, 109-117, 1959.
- Brune, J.N., Seismic moment, seismicity and rate of slip along major fault zones, *J. Geophys. Res.*, **73**, 777-784, 1968.
- Bryant, A.S., L.M. Jones, Anomalous deep crustal earthquakes in the Ventura basin, southern California, *J. Geophys. Res.*, **97**, 437-447, 1992.
- Buchanan-Banks, J.M., R.O. Castle, J.I. Ziony, Elevation changes in the central Transverse Ranges near Ventura, California, *Tectonophysics*, **29**, 113-125, 1975.
- Bullard, T.F. and W.R. Lettis, Quaternary fold deformation associated with blind thrust faulting, Los Angeles basin, California, *J. Geophys. Res.*, **98**, 8349-8369, 1993.
- Buwalda, J.P., and C.F. Richter, Imperial Valley earthquake of May 18, 1940[abs.]: *USGS Prof. Paper*, **787**, 105-111, 1941.
- Buwalda, J.P., and P. St. Amand, Geological effects of the Arvin-Tehachapi

- earthquake, *Bull. Calif. Div. Mines. Geol.*, **171**, 41-56, 1955.
- Campbell, R.H., R.F. Yerkes, Cenozoic evolution of the Los Angeles basin area--  
Relation to plate tectonics, In: Aspects of the Geologic History of the Continental  
Borderland, edited by D.G. Howell, *Amer. Assoc. of Petrol. Geologists  
Miscellaneous Publication*, **24**, 541-558, 1976.
- Carter, B., Quaternary displacements on the Garlock zone, California, *EOS, Trans.,  
AGU*, **52**, 350, 1971.
- Carter, B., Possible Pliocene inception of lateral displacement on the Garlock fault,  
California, Abstracts with Programs, Cordilleran Section, *Geol. Soc. Amer.*, **12**,  
**101**, 1980.
- Carter, J.N., B.P. Luyendyk, and R.R. Terres, Neogene clockwise rotation of the  
eastern Transverse Ranges, California, suggested by paleomagnetic vectors, *Geol.  
Soc. Amer. Bull.*, **98**, 199-206, 1987.
- Castillo, D.A. and M.D. Zoback, Systematic variations in stress state in the southern  
San Joaquin Valley: Inferences based on well-bore data and contemporary  
seismicity, *AAPG Bull.*, **76**, 1257-1275, 1994.
- Cheadle, M.J., B.L. Czuchra, T. Byrne, C.J. Ando, J.E. Oliver, L.D. Brown, S.  
Kaufman, P.E. Malin, and R.A. Phinney, The deep crustal structure of the Mojave  
Desert, California, from COCORP seismic reflection data, *Tectonics*, **5**, 292-320,  
1986.
- Christensen, M.N., Late Cenozoic crustal movements in the Sierra Nevada of  
California, *Geol. Soc. Am. Bull.*, **77**, 163-182, 1966.
- Clark, M.M., A. Grantz, and M. Rubin, Holocene activity of the Coyote Creek fault as  
recorded in sediments of Lake Cahuilla, *USGS Prof. Paper*, **787**, 112-130, 1972.
- Clark, M.M., and K.R. Lajoie, Holocene behaviour of the Garlock fault, Abstracts with  
Programs, Cordilleran Section, *Geol. Soc. Amer.*, **6**, 156-157, 1974.
- Clark, M.M., K.K. Harms, J.J. Lienkaemper, D.S. Harwood, K.R. Lajoie, J.C. Matti,

- J.A. Perkins, M.J. Rymer, A.M. Sarna-Wojcicki, R.V. Sharp, J.D. Sims., J.C. Tinsley and J.I. Ziony, Preliminary slip-rate table for late Quaternary faults of California, *U.S. Geol. Surv. Open File Rep.*, 84-106, 12pp, 1984.
- Cline, M.W., R.A. Snay, and E.L. Timmerman, Regional deformation of the earth model for the Los Angeles region, California, *Tectonophysics*, **107**, 279-314, 1984.
- Coffman, J.L., and C.A. von Hake, Earthquake history of the United States (revised through 1970), *National Oceanic and Atmospheric Administration Publication* 41-1, 208pp., 1973.
- Crowell, J.C., Origin of late Cenozoic basins in southern California, In: *Tectonics and Sedimentation, Society of Economic Paleontologists and Mineralogists Special Publication, No.22*, 190-204, 1974.
- Crowell, J.C., An outline of the tectonics history of southeastern California, In: *The Geotectonic Development of California, Rubey Volume*, edited by W.G. Ernst, *Prentice-Hall, Englewood Cliffs, N.J.*, 583-600, 1981.
- Crowell, J.C., Late Cenozoic basins of onshore southern California: Complexity is the hallmark of their tectonic history, In: *Cenozoic Basin Development of Coastal California, Rubey Volume VI*, edited by R.V. Ingersoll and W.G. Ernst, *Prentice-Hall, Englewood Cliffs, N.J.*, 207-241, 1987.
- Cummings, D., Theory of plasticity applied to faulting, Mojave Desert, southern California, *Geol. Soc. Amer. Bull.*, **87**, 720-724, 1976.
- Dalrymple, G.B., Potassium-argon dates of some Cenozoic volcanic rocks of the Sierra Nevada, California, *Geol. Soc. Amer. Bull.*, **76**, 379-390, 1963.
- Davis, G.A., and B.C. Burchfiel, Garlock fault--An intracontinental transform structure, southern California, *Geol. Soc. Amer. Bull.*, **84**, 1407-1422, 1973.
- Davis, T., A structural outline of the San Emigdio Mountains, in: *Geologic Transect across the Western Transverse Ranges*, T. L. Davis and J. S. Namson eds., *Society*

- of Economic Paleontologists and Mineralogists*, 23-32, 1986.
- Davis, T.L., Namson, J. and Yerkes, R.F., A cross section of the Los Angeles area: seismically active fold and thrust belt, the 1987 Whittier Narrows earthquake and earthquake hazard, *J. Geophys. Res.*, **94**, 9644-9664, 1989.
- Davis, T.L. and J.S. Namson, A balanced cross section of the 1994 North Ridge earthquake, southern California, *Nature*, **372**, 167-169, 1994.
- DeMets, C., R.G. Gordon, D.F. Argus, and S. Stein, Current plate motions, *Geophys. J. Int.*, **101**, 425-478, 1990.
- Dibblee, T.W., Jr., Geology of the southeastern margin of the San Joaquin Valley, *Div. of Mines of Calif. Bull.*, **171**, 23-34, 1955.
- Dibblee, T.W. Jr., Geology of the Alamo Mountain, Frazier Mountain, Lockwood Valley, Mount Pinos, and Cuyama Badlands areas, southern California, 57-77; Geology of the Santa Monica Mountains and Simi Hills, southern California, 94-130, In: *Geology and Mineral Wealth of the California Transverse Ranges*, edited by D.L. Fife and J.A. Minch, *South Coast Geological Society, Inc.*, 1982.
- Dokka, R. K. and C. J. Travis, Late Cenozoic strike-slip faulting in the Mojave Desert, California, *Tectonics*, **9**, 311-340, 1990(a).
- Dokka, R. K. and C. J. Travis, Role of the eastern California shear zone in accumulating Pacific-North American plate motion, *Geophys. Res. Lett.*, **17**, 1323-1326, 1990(b).
- Dolan, J.F., and K.E. Sieh, Structural style and geomorphology of the Santa Monica-Hollywood fault: Constrains on kinematics of recent movement, *EOS, Trans. AGU*, **72**, 319-320, 1991.
- Dollar, R.S., and D.V. Helmberger, Body wave modeling using a master event for the sparsely recorded 1946 Walker Pass, California earthquake, *EOS, Trans.* **66**, 946, 1985.
- Donnellan, A., B.H. Hager, R.W. King, and T.A. Herring, Geodetic measurement of

- deformation in the Ventura basin region, southern California, *J. Geophys. Res.*, **98**, 21,727-21,739, 1993.
- Donnellan, A., B.H. Hager, and R.W. King, Discrepancy between geological and geodetic deformation rates in the Ventura basin, *Nature*, **366**, 333-336, 1993.
- Doser, D.I., and H. Kanamori, Long period surface waves of four western United States earthquakes recorded by the Pasadena strainmeter, *Bull. Seismol. Soc. Amer.*, **77**, 236-243, 1987.
- Doser, D.I., A re-examination of the 1947 Manix, California, earthquake sequence and comparison to other sequences within the Mojave block, *Bull. Seismo. Soc. Am.*, **80**, 267-277, 1990(a).
- Doser, D.I., Source characteristics of earthquakes along the southern San Jacinto and Imperial fault zones (1937 to 1954), *Bull. Seismo. Soc. Am.*, **80**, 1099-1117, 1990(b).
- Doser, D. I., Historic earthquakes (1918 to 1923) and an assessment of source parameters along the San Jacinto fault system, *Bull. Seismo. Am.*, **82**, 1786-1801, 1992.
- Dreger, D, and D. Helmberger, Source parameters of the Sierra Madre Earthquake from regional and local body waves, *Geophys. Res. Lett.*, **18**, 1991.
- Ehlig, P.L., Cause of distribution of Pelona, Rand, and Orocopia schists along the San Andreas and Garlock faults, in Proceedings of Conf. on Geol. Prob. of San Andreas Fault System, W.R. Dickinson and A. Grantz eds., *Geol. Sci. Stanford Univ. Pub.*, 294-306, 1968
- Ehlig, P.L., The Vincent thrust: Its nature, paleogeographic reconstruction across the San Andreas fault and bearing on the evolution of the Transverse Ranges, in: Geology and Mineral Wealth of the California Transverse Ranges, D.L. Fife and J.A. Minch eds., *South Coast Geological Society, Inc.*, p.370-379, 1982
- Ekström, G., and P. England, Seismic strain rates in regions of distributed continental

- deformation, *J. Geophys. Res.*, **94**, 10,231-10,257, 1989.
- Feigl, K.L., R.W. King, and T.H. Jordan, Geodetic measurements of tectonic deformation in the Santa Maria fold and thrust belt, California, *J. Geophys. Res.*, **95**, 2679-2699, 1990.
- Frohlich, C. and K.D. Apperson, Earthquake focal mechanisms, moment tensors, and the consistency of seismic activity near plate boundaries, *Tectonics*, **11**, 279-296, 1992.
- Garfunkle, Z., Model for the late Cenozoic tectonic history of the Mojave Desert, California, and for its relation to adjacent region, *Geol. Soc. Amer. Bull.*, **85**, 1931-1944, 1974.
- Gephart, J.W., and D.W. Forsyth, An improved method for determining the regional stress tensor using earthquake focal mechanism data: Application to the San Fernando earthquake sequence, *J. Geophys. Res.*, **89**, 9305-9320, 1984.
- Gilbert, L.E., C.H. Scholz, and J. Beavan, Strain localization along the San Andreas fault: Consequences for loading mechanisms, *J. Geophys. Res.*, **99**, 23,975-23,984, 1994.
- Gutenberg, B., The first motion in longitudinal and transverse waves of the main shock and the direction of slip, *Calif. Div. of Mines Bull.*, **171**, 165-170, 1958.
- Hadley, D.M and H. Kanamori, Seismic structure of the Transverse Ranges, California, *Geol. Soc. Am. Bull.*, **88**, 1469-1478, 1977.
- Hadley, D.M and H. Kanamori, Recent seismicity in the San Fernando region and tectonics in the west-central Transverse Ranges, California, *Seism. Soc. Am. Bull.*, **68**, 1449-1457, 1978.
- Hanks, T.C., Thatcher, W., and Hileman, J.A., Seismic moments of the large earthquakes of the southern California region, 1890-1973, *Geol. Soc. Am. Bull.*, **86**, 1131-1139, 1975.
- Hartse, H.E., M.C. Fehler, R.C. Aster, J.S. Scott, and F.L. Vernon, Small-scale

- heterogeneity in the Anza seismic gap, southern California, *J. Geophys. Res.*, **99**, 6801-6818, 1994.
- Hauksson, E., Seismotectonics of the Newport-Inglewood fault zone in the Los Angeles basin, southern California, *Bull. Seismo. Soc. Amer.*, **77**, 539-561, 1987.
- Hauksson, E. and Jones, L.M., The 1987 Whittier Narrows earthquake sequence in Los Angeles, southern California: seismological and tectonic analysis, *J. Geophys. Res.*, **94**, 9569-9589, 1989.
- Hauksson, E., Earthquakes, faulting, and stress in the Los Angeles basin, *J. Geophys. Res.*, **95**, 15,365-15,394, 1990.
- Hauksson, E., and S. Gross, Source parameters of the 1933 Long Beach earthquake, *Bull. Seismo. Soc. Amer.*, **81**, 81-98, 1991.
- Hauksson, E., and L.M. Jones, The 1988 and 1990 Upland earthquakes: Left-lateral faulting adjacent to the central Transverse Ranges, *J. Geophys. Res.*, **96**, 8143-8165, 1991.
- Hearn, T.M. and R.W., Clayton, Lateral velocity variations in southern California. I. Results for the upper crust from  $P_g$  waves, *Bull. Seismo. Soc. Am.*, **76**, 495-509, 1986a.
- Hearn, T.M. and R.W. Clayton, Lateral velocity variations in southern California. II. Results for the lower crust from  $P_n$  waves, *Bull. Seismo. Soc. Am.*, **76**, 511-520, 1986b.
- Helmberger, D. V., P. G. Somerville, and E. Garnero, The location and source parameters of the Lompoc, California earthquake of 4 November, 1927, *Bull. Seismo. Soc. Amer.*, **82**, 1678-1709, 1992.
- Hileman, J.A, Allen, C.R. and Nordquist, J.M., Seismicity of the southern California region, 1 January, 1932 to 31 December 1972, Pasadena, *Seismological Laboratory, California Institute of Technology*, 487pp, 1973.
- Hill, D.P., Contemporary block tectonics: California and Nevada: *J. Geophys. Res.*, **87**,

5433-5450, 1982.

- Hill, I.R., San Jacinto intrusive complex, 1. Geology and mineral chemistry, and a model for intermittent recharge of tonalitic magma chambers, *J. Geophys. Res.*, **93**, 10,325-10,348, 1988.
- Hill, M.L., and T.W. Dibblee, Jr., San Andreas, Garlock, and Big Pine faults, California--A study of character, history, and tectonic significance of their displacements, *Geol. Soc. Amer. Bull.*, **64**, 443-458, 1953.
- Holt, W.E., J.F. Ni, T.C. Wallace, and A.J. Haines, The active tectonics of the eastern Himalayan syntaxis and surrounding region, *J. Geophys. Res.*, **96**, 14,595-14,623, 1991.
- Holt, W.E. and A.J. Haines, Velocity fields in deforming Asia from the inversion of earthquake-related strain, *Tectonics*, **12**, 1-20, 1993.
- Huang, W., H. Kanamori, and L.T. Silver, Seismic strain rates for the period 1981-1990, central Transverse Ranges, California, *EOS, Trans. AGU*, **72**, 320, 1991.
- Huang, W., H. Kanamori, and L. T. Silver, Seismic strain rates and state of tectonic stress in southern California determined from earthquakes for the periods of 1981-1990, and 1900-1992, *EOS, Trans. AGU*, **73**, p.119, 1992.
- Huang, W, L. T. Silver, and H. Kanamori, Non-SAF type focal mechanisms adjacent to the SAF, Mojave segment: implications for blind thrust beneath the San Gabriel Mountains, southern California, In: *Continental Earthquakes* (Selected Papers of II Int. Conf. on Continental Earthquakes), 405-416, *Seismological Press*, Beijing, P.R. of China, 1993a.
- Huang, W., H. Kanamori, and L. T. Silver, Background seismicity and major earthquakes in south California, *EOS, Trans. Amer. Geophys. Union*, **74**, 192, 1993b.
- Huber, N.K., Amount and timing of late Cenozoic uplift and tilt of the central Sierra Nevada, California--Evidence from the upper San Joaquin River basin, *U.S. Geol.*

- Surv. Prof. Paper*, **1197**, 1-28, 1981.
- Hull, A.G. and C. Nicholson, Seismotectonics of the northern Elsinore fault zone, southern California, *Bull. Seismo. Soc. Am.*, **82**, 800-818, 1992.
- Humphreys, E.D. and B.H. Hager, A kinematic model for the late Cenozoic development of southern California crust and upper mantle, *J. Geophys. Res.*, **95**, 19,747-19,762, 1990.
- Humphreys, E.D. and R.J. Weldon, Deformation across the western United States: A local estimate of Pacific-North America transform deformation, *J. Geophys. Res.*, **99**, 19,975-20,010, 1994.
- Hutton, L.K., C.R. Allen, A.C. Blanchard, S.A. Fisher, P.T. German, D.D. Given, C.E. Johnson, V.D. Lamanuzzi, B.A. Reed, K.J. Richter, and K.M. Watts, Southern California array for research on local earthquakes and the teleseismism (SCARLET) Caltech-USGS monthly preliminary epicenters for October 1979 through December 1979, *Seismol. Lab., Div. of Geol. & Plan. Sci., Calif. Inst. of Tech.*, Pasadena, 54pp, 1980.
- Hutton, L. K., L. M. Jones, E. Hauksson, and D. D. Given, Seismotectonics of southern California, in: Neotectonics of North America, D. B. Slemmons, E. R. Engdahl, M. D. Zoback, and D. D. Blackwell eds., Decade Map Volume, *Geol Soc. Am.*, Chapter **9**, p.133-152, 1991
- Jackson, J. and D. Mckenzie., The relationship between plate motions and seismic moment tensors, and rates of active deformation in the Mediterranean and middle East, *Geophys. J.*, **93**, 45-73, 1988.
- Jackson, J. and P. Molnar, Active faulting and block rotations in the western Transverse Ranges, California, . *Geophys. Res.*, **95**, 22,073-22,087, 1990.
- Jackson, J. J. Haines, and W. Holt, A comparison of satellite laser ranging and seismicity data in the Aegean region, *Geophys. Res. Lett.*, **21**, 2849-2852, 1994.
- Jennings, C. W., Geologic Map of California, scale 1:750,000, *Williams & Heintz Map*

*Corporation*, 1977.

- Johnson, C.E., and D.M., Hadley, Tectonic implications of the Brawley earthquake swarm, Imperial Valley, California, January, 1975, *Seismol. Soc. Amer. Bull.*, **66**, 1133-1144, 1976.
- Johnson, C. and L. K. Hutton, Aftershocks and preearthquake seismicity, In: The Imperial Valley, California, Earthquake of October 15, 1979, *USGS, Prof. Paper*, **1254**, 59-76, 1982.
- Johnson, H.O, D.C. Agnew, and F.K. Wyatt, Present-day crustal deformation in southern California, *J. Geophys. Res.* **99**, 23,951-23,974, 1994.
- Jones, C.J., Is extension in Death Valley accommodated by thinning of the mantle lithosphere between the Sierra Nevada, California? *Tectonics*, **6**, 449-473, 1987.
- Jones, L.M., and R.S. Dollar, Evidence of Basin-and-Range extensional tectonics in the Sierra Nevada: The Durrwood Meadow swarm, Tulare county, California (1983-1984), *Bull. Seismol. Soc. Amer.*, **76**, 439-461, 1986.
- Jones, L.M., L.K. Hutton, Given, D.D., and Allen, C.R., The North Palm Springs, California, earthquake sequence of July 1986, *Bull. Seismo. Soc. Am.*, **76**, 1830-1837, 1986.
- Jones, L., Focal mechanisms and the state of stress on the San Andreas fault in southern California, *J. Geophys. Res.*, **93**, 8869-8891, 1988.
- Jones, L.M., K.E. Sieh, E. Hauksson, and L.K. Hutton, The 3 December 1988 Pasadena, California earthquake: Evidence for strike-slip motion on the Raymond fault, *Bull. Seismol. Soc. Am.*, **80**, 474-482, 1990.
- Jost, M.L., and R.B. Herrmann, A student's guide to and review of moment tensors, *Seismol. Res. Lett.*, **60**, 37-57, 1989.
- Kamb, B., L.T. Silver, M.J. Abrams, B.A. Cater, T.H. Joran, and J.B. Minster, Pattern of faulting and nature of fault movement in the San Fernando earthquake, *SGS Prof. Paper*, **733**, 41-54, 1971.

- Kanamori, H. Great earthquakes at island arcs and the lithosphere, *Tectonophysics*, **12**, 187-198, 1971.
- Kanamori, H. and D. Anderson, Theoretical basis of some empirical relations in seismology, *Bull. Seismo. Soc. Am.*, **65**, 1073-1095, 1975.
- Kanamori, H., Seismic and aseismic slip along subduction zones and their tectonic implications, in: Islands Arcs Deep Sea Trenches and Back Arc Basins, Maurice Ewing Series 1, M. Talwani and W.C. Pitmann III editors, *Am. Geophys. Union*, Washington D.C., 163-174, 1977.
- Kanamori, H., Importance of historical seismograms for geophysical research, In: Historical Seismograms and Earthquakes of the World, edited by W.H.K. Lee, H. Meyers, and K. Shimazaki, *Academic Press, Inc.*, Harcourt Brace Jovanovich, Publisher, 17-33, 1985.
- Keller, R.P., C.R. Allen, R. Gilman, N.R. Gouly, and J.A. Hileman, Monitoring slip along major faults in southern California, *Bull., Seismo. Soc. Am.*, **68**, 1187-1190, 1978.
- Keller, E.A., M.S. Bonkowski, R.J. Korsch, R.J. Salemon, Tectonic Geomorphology of the San Andreas fault zone in the southern Indio Hills, Coachella Valley, California, *Geol. Soc. Am. Bull.*, **93**, 46-56, 1982.
- Keller, B, and Prothero, W., Western Transverse Ranges crustal structure, *J. Geophys. Res.*, **92**, 7890-7906, 1987.
- King, G., D. Oppenheimer, and F. Amelung, Block verse continuum deformation in the western United States, *Earth & Plan. Sci. Lett.* **128**, 55-64, 1994.
- King, N.E., and J.C. Savage, Strain rate profile across the Elsinore, San Jacinto, and San Andreas faults near Palm Springs, California, 1973-81, *Geophys. Res. Lett.*, **10**, 55-57, 1983.
- Klein, F.W., Users' guide to HYPOINVERSE, a program for VAX and PC350 computers to solve for earthquake locations, *USGS Open File Rep.*, 85-515, 24pp.,

1985.

- Kostrov, V.V., Seismic moment and energy of earthquake, and seismic flow of rock, *Izv, Acad, Sci. USSR Phys Solid Earth*, **1**, 23-44, 1974.
- Lajoie, K.R., Kern, J.P., Wehmiller, J.F., Kennedy, G.I., Mathieson, S.A., Sarna-Wojcicki, A.M., Yerkes, R.F., and McCrory, P.F., Quaternary marine terrace shorelines and crustal deformation, San Diego to Santa Barbara, California, In: Abbott, P.L., ed., *Geologic excursions in the southern California area: San Diego, Calif., San Diego State Univ., Dep. of Geol. Sci.*, 3-15, 1979.
- Larsen, S and R. Reilinger, Global positioning system measurements of the strain accumulation across the Imperial Valley, California, 1986-1989, *J. Geophys. Res.*, **97**, 8865-8876, 1992.
- Larsen, S. C., D. C. Agnew, B. H. Hager, Strain accumulation in the Santa Barbara Channel, 1970-1988, *J. Geophys. Res.*, **98**, 2119-2133, 1993.
- Lee, W.H.K., Johnson, C.E., Henyey, T.L., and Yerkes, R.F., A preliminary study of the Santa Barbara, California, earthquake of August 13, 1978, and its major aftershocks, *USGS Circulars 797*, 11pp., 1978.
- Lettis, W.R. and Hanson, K.L., Crustal strain partitioning: Implications for seismic-hazard assessment in western California, *Geology*, **19**, 559-562, 1991.
- Lisowski, M., J.C. Savage, and W.H. Prescott, The velocity field along the San Andreas fault in central and southern California, *J. Geophys. Res.*, **96**, 8369-8389, 1991.
- Louie, J.N., C.R. Allen, D.C. Johnson, and P.C. Haase, Fault slip in southern California, *Bull. Seismol. Soc. Amer.*, **75**, 811-834, 1985.
- Li, Y-G., T. Henyey, and L.T. Silver, Aspects of the crustal structure of the western Mojave Desert, California, from seismic reflection and gravity data, *J. Geophys. Res.*, **97**, 8805-8816, 1992.
- Luyendyk, B.P., and J.S. Hornafius, Neogene crustal rotations, fault slip, and basin

- development in southern California, In: Cenozoic Basin Development of Coastal California, Rubey Volume VI, edited by R.V. Ingersoll and W.G. Ernst, *Prentice-Hall, Englewood Cliffs, N.J.*, 259-283, 1987.
- Ma, K-F, and H. Kanamori, Aftershock sequence of the 3 December 1988 Pasadena earthquake, *Bull. Seismol. Soc. Amer.*, **81**, 2310-2319, 1991.
- Magistrale, H.L., Jones, L. and Kanamori, H., The Superstition Hills, California earthquakes of 24 November, 1987, *Bull. Seismo. Soc. Am.*, **79**, 239-251, 1989.
- Magistrale, H.L., I. The Superstition Hills, California, Earthquakes of 24 November 1987. II. Three-Dimensional Velocity Structure of Southern California. *Ph.D. Thesis, California Institute of Technology*, 294pp, 1990.
- Marone, C. and C.H. Scholz, The depth of seismic faulting and the upper transition from stable to unstable slip regimes, *Geophys. Res. Lett.*, **15**, 621-624, 1988.
- Matti, J.C., Morton, D.M., and Cox, B.F., Distribution and geologic relations of fault systems in the vicinity of the Central Transverse Ranges, southern California, *USGS Open-File Report 85-365*, 23pp, 1985.
- McEvelly, T.V., Bakun, W.H., and Casaday, K.B., The Parkfield, California, earthquakes of 1966, *Bull. Seismo. Soc. Am.*, **57**, 1221-1244, 1967.
- McGill, S and K. Sieh, Holocene slip rate of the central Garlock fault in southeastern Searles Valley, California, *J. Geophys. Res.*, **98**, 14,217-14,231, 1993.
- McKenzie, D.P., The relationship between fault plane solutions for earthquakes and the directions of the principal stresses, *Bull. Seismo. Soc. Amer.*, **59**, 591-601, 1969.
- Michael, A.J., Determination of stress from slip data: Faults and folds, *J. Geophys. Res.*, **89**, 11,517-11,526, 1984.
- Michael, A.J., The use of focal mechanisms to determine stress: A control study, *J. Geophys. Res.*, **92**, 357-368, 1987.
- Millman, D.E., and T.K. Rockwell, Lateral offset of mid and late Quaternary deposits along the northern Elsinore fault, southern California, *Geol. Soc. Amer. Abstr.*

*Programs*, **17**, 370, 1985.

Minster, J.B. and T.H. Jordan, Vector constraints on Quaternary deformation of the western United States east and west of the San Andreas fault, in *Tectonics and Sedimentation along the California Margin*, edited by J.K. Crouch and S.B. Bachman, *Pac. Sect. Soc. Econ. Paleontol. Mineral.*, **38**, 1-16, 1984.

Minster, J.B., and T.H. Jordan, Vector constraints on western U.S. deformation from space geodesy, neotectonics, and plate motions: *J. Geophys. Res.*, **92**, 4798-4804, 1987.

Molnar, P, Earthquake recurrence intervals and plate tectonics, *Bull. Seism. Soc. Am.*, **69**, 115-133, 1979.

Molnar, P., and Q. Deng, Faulting associated with large earthquakes and the average rate of deformation in central and eastern Asia, *J. Geophys. Res.*, **89**., 6203-6228, 1984.

Molnar, P., Brace-Goetze strength profiles, the partitioning of strike-slip and thrust faulting at zones of oblique convergence, and stress-heat flow paradox of the San Andreas fault, in B. Evans and Teng-Fong Wong eds., *Fault Mechanics and Transport Properties of Rocks*, *Academy Press*, 435-459, 1992.

Morton, D.M., and Matti, J.C., The Cucamonga fault zone: Geologic setting and Quaternary history, In: *Recent Reverse Faulting in the Transverse Ranges, California*, *USGS Prof. Paper*, **1339**, 179-203, 1987.

Namson, J., and T.L. Davis, A structural transect of the western Transverse Ranges, California: Implications for lithospheric kinematics and seismic risk evaluation, *Geology*, **16**, 675-679, 1988.

Nicholson, C., L. Seeber, P. William, and L.P. Skyes., Seismicity and fault kinematics through the eastern Transverse Ranges, California: Block rotation, strike-slip faulting and low-angle thrust, *J. Geophys. Res.*, **91**, 4891-4908, 1986(a).

Nicholson, C., L. Seeber, P. Williams, and L. Sykes, Seismic evidence for conjugate

- slip and block rotation within the San Andreas fault system, southern California, *Tectonics*, **5**, 629-648, 1986(b).
- Nicholson, C., H. Kanamori, and C.R. Allen, Comparison of the 1948 and 1986 earthquakes along southern San Andreas fault, Coachella Valley, California, *EOS, Trans. AGU*, **68**, 1362, 1987.
- Nur, A., H. Ron, G. Beroza, and L. Alfonsi, A fault is born: the mechanical origin of the Mojave seismic line, *EOS Trans. Am. Geophys. Union*, **73**, 362, 1992.
- Pechmann, J.C., Tectonic implications of small earthquakes in the central Transverse Ranges, In: Recent Reverse Faulting in the Transverse Ranges, California, *USGS Prof. Paper*, **1336**, 97-112, 1987.
- Petersen, M.D., L. Seeber, L.R. Sykes, J.L. Nabelek, J.A. Armbruster, J. Pacheco, and K.W. Hudnut, Seismicity and fault interaction, southern San Jacinto fault zone and adjacent faults, southern California: Implications for seismic hazard, *Tectonics*, **10**, 1187-1203, 1991.
- Pinault, C.T., and T.K. Rockwell, Rates and sense of Holocene faulting on the southern Elsinore fault: Further constraints on the distribution of dextral shear between the Pacific and North American plates, *Geol. Soc. Amer. Abstr. Programs*, **16**, 624, 1984.
- Raleigh, C.B., Healy, J.H. and Bredehoeft, J.D., Faulting and crustal stress at Rangely, Colorado, In: Flow and Fracture of Rocks, *Geophys. Monogr. Ser. 6*, edited by H.C. Heard et al., 275-284, AGU, Washington, D.C., 1972.
- Ramsay, J.G., *Folding and Fracturing of Rocks*, McGraw-Hall Book Company, 568PP, 1967.
- Real, C.R., T.R. Topozada, D.L. Parke, Earthquake epicenter map of California, 1900 through 1974: *California Division of Mines and Geology Map Sheet 39*, scale **1:1,000,000**, 1978.
- Reasenberg, P. and Oppenheimer, D., FPFIT, FPLOT, and FPPAGE: FORTRAN

- computer programs for calculating and displaying earthquake fault-plane solutions, *USGS, Open File Rep.*, 85-739, 109pp., 1985.
- Richter, C.F., Allen, C.R. and Nordquist, J.M., The Desert Hot Springs earthquakes and their tectonic environment, *Bull. Seismo. Soc. Am.*, **48**, 315-337, 1958.
- Saleeby, J.B., Ocean floor accretion and volcano-plutonic arc evolution of the Mesozoic Sierra Nevada, In: *The Geotectonic Development of California*, Rubey Volume 1, edited by W.G. Ernst, *Prentice-Hall Englewood Cliffs, N.J.*, 132-181, 1981.
- Saleeby, J.B., Progress in tectonic and petrogenetic studies in an exposed cross-section of young (100 Ma) continental crust, southern Sierra Nevada, California, In: *Exposed Cross Sections of the Continental Crust*, edited by M.H. Salisbury and D.M. Fountain, *NATO ASI Series, Series C: Mathematical and Physical Series*, **317**, 137-158, Published in Cooperation with NATO Scientific Affairs Division, Netherlands, 1988.
- Sanders, C.O. and H. Kanamori, A Seismotectonic analysis of the Anza seismic gap, San Jacinto fault zone, southern California, *J. Geophys. Res.*, **89**, 5873-5890, 1984.
- Sanders, C.O., Interaction of the San Jacinto and San Andreas fault zones, southern California: Triggered earthquake migration and coupled recurrence intervals, *Science*, **260**, 973-976, 1993.
- Sauber, J.W., Thatcher, and S. Solomon, Geodetic measurement of deformation in the central Mojave Desert, California, *J. Geophys. Res.*, **91**, 12,683-12,694, 1986.
- Sauber, J., W. Thatcher, S.C. Solomon, and M. Lisowski, Geodetic slip rate for the eastern California shear zone and the recurrence time of the Mojave desert earthquakes, *Nature*, **367**, 264-266, 1994.
- Savage, J.C., W.H. Prescott, M. Lisowski, and N.E. King, Strain accumulation in southern California, 1973-1980, *J. Geophys. Res.*, **86**, 6991-7001, 1981.

- Savage, J.C., Strain accumulation in the western United States, *Ann. Rev. Earth Planet. Sci.*, **11**, 11-45, 1983.
- Savage, J.C., Prescott, W.H. and Gu, G.H., Strain accumulation in southern California, 1973-1984, *J. Geophys. Res.*, **91**, 7455-7474, 1986.
- Savage, J.C., M. Lisowski, and W.H. Prescott, An apparent shear zone trending north-northwest across the Mojave desert into Owens Valley, eastern California, *Geophys. Res. Lett.*, **17**, 2113-2116, 1990.
- Scholz, C.H. and P.A. Cowie, Determination of total strain from faulting using slip measurements, *Nature*, **346**, 837-839, 1990.
- Sharp, R.V., San Jacinto fault zone in the Peninsular Ranges of southern California, *Geol. Soc. Amer. Bull.*, **78**, 705-730, 1967.
- Sharp, R.V., Displacement on tectonic ruptures, *Calif. Div. of Mines & Geol. Bull.*, **196**, 187-194, 1975.
- Sharp, R.V., Surface faulting in Imperial Valley during the earthquake swarm of January-February, 1975, *Seismol. Soc. Amer. Bull.*, **66**, 1145-1154, 1976.
- Sharp, R.V., Variable rates of late Quaternary strike slip on the San Jacinto fault zone, southern California, *J. Geophys. Res.*, **86**, 1754-1762, 1981.
- Sharp, R.V., Comparison of the 1979 surface faulting to earlier displacements in central Imperial Valley, California, Earthquake, October 15, 1979, *U.S. Geol. Surv. Prof. Paper*, **1254**, 213-221, 1982.
- Sibson, R.H., Fault zone models, heat flow, and depth distribution of the United States, *Bull. Seismol. Soc. Amer.*, **72**, 151-163, 1982.
- Sibson, R.H., Continental fault structure and the shallow earthquake source, *J. Geol. Soc. London*, **140**, p.741-767, 1983.
- Sibson, R.H., Roughness at the base of the seismogenic zone: Contributing factors, *J. Geophys. Res.*, **89**, 5791-5799, 1984.
- Sibson, R.H., Rupture interaction with fault jogs, In: Earthquake Source Mechanics,

- edited by S. Das, J. Boatwright, and C.H. Scholz, *Geophysical Monograph* 37, Maurice Ewing Volume 6, American Geophys. Union, Washington D. C. 157-167, 1986.
- Sieh, K.E., Prehistoric large earthquakes produced by slip on the San Andreas fault at Pallett Creek, California, *J. Geophys. Res.*, **83**, 3907-3939, 1978a
- Sieh, K.E., Slip along the San Andreas fault associated with the great 1857 earthquake, *Bull. Seismol. Soc. Amer.*, **68**, 1421-1448, 1978b.
- Sieh, K.E. and R.H. Jahns, Holocene activity of the San Andreas fault at Wallace Creek, California, *J. Geophys. Res.*, **95**, 883-896, 1984.
- Silver, L.T., Are the Central Transverse Ranges undergoing active basement folding as well as faulting? *EOS, Trans.* **72**, 121, 1991.
- Smith, G.I., Large lateral displacement on the Garlock fault, California, as measured from offset dike swarm, *Bull. Amer. Assoc. Petrol. Geol.*, **46**, 85-104, 1962.
- Stein, R.S. and W. Thatcher, Seismic and aseismic deformation associated with the 1952 Kern County, California, earthquake and relationship to the Quaternary history of the White Wolf fault, *J. Geophys. Res.*, **86**, 4913-4928, 1981.
- Stierman, D. and W. Ellsworth, Aftershocks of the February 21, 1973 Point Mugu, California earthquake, *Bull. Seismo. Soc. Am.*, **66**, 1931-1952, 1976.
- Sykes, L. R. and L. Seeber, Great earthquakes and great asperities, San Andreas fault, southern California, *Geology*, **13**, 835-838, 1985.
- Sylvester, A.G., and A.C. Darrow, Structure and neotectonics of the western Santa Ynez fault system in southern California, *Tectonophysics*, **52**, 389-405, 1979.
- Thatcher, W., and T.C. Hanks, Source parameters of southern California earthquakes, *J. Geophys. Res.*, **78**, 8547-8576, 1973.
- Thatcher, W., J. A. Hileman, and T.C. Hanks, Seismic slip distribution along the San Jacinto fault zone, southern California, and its implications, *Geol. Soc. Amer. Bull.*, **86**, 1140-1146, 1975.

- Thatcher, W., Nonlinear strain buildup and the earthquake cycle on the San Andreas fault, *J. Geophys. Res.*, **88**, 5893-5902, 1983.
- Thatcher, W., Present-day crustal movements and the mechanics of cyclic deformation, in *The San Andreas Fault System, California, U.S. Geol. Survey Prof. Paper 1515*, edited by R. E. Wallace, 189-205, 1990.
- Topozada, T.R., Parke, D.L. and Higgins, C.T., Seismicity of California 1900-1931, *Calif. Div. Mines & Geol.*, Special Report **135**, 39pp., 1978.
- Wald, D.J., D.V. Helmberger, and S.H. Hartzell, Rupture process of the 1987 Superstition Hills earthquake from the inversion of strong-motion data, *Bull. Seismo. Soc. Amer.*, **80**, 1079-1098, 1990.
- Wallace, T. C., D. V. Helmberger, and J. E. Ebel, A broadband study of the 13 August 1978 Santa Barbara earthquake, *Bull. Seismo. Soc. Am.*, **71**, 1701-1718, 1981.
- Ward, S. N., Pacific-North America plate motions: New results from very long baseline interferometry, *J. Geophys. Res.*, **95**, 21,965-21,981, 1990.
- Webb, T.H. and Kanamori, H., Earthquake focal mechanisms in the eastern Transverse Ranges and San Emigdio Mountains, southern California and evidence for a regional decollement, *Bull. Seismo. Soc. Am.*, **75**, 737-757, 1985.
- Weldon, R., and K.E. Sieh, Holocene rate of slip and tentative recurrence interval for large earthquakes on the San Andreas fault, Cajon Pass, southern California, *Geol. Soc. Amer. Bull.*, **96**, 793-812, 1985.
- Weldon, R.J. and Humphreys, A kinematic model of southern California, *Tectonics*, **5**, 33-48, 1986.
- Weldon, R.J., and J.E. Springer, Active faulting near the Cajon Pass well, southern California; Implications for the stress orientation near the San Andreas fault, *Geophys. Res. Lett.*, **15**, 993-9996, 1988.
- Wernicke, B., G.J. Axen, J.K. Snow, Basin and Range extensional tectonics at the latitude of Las Vegas, Nevada, *Geol. Soc. Amer. Bull.*, **100**, 1738-1757, 1988.

- Wesnousky, S.G., Earthquakes, Quaternary faults , and seismic hazard in California, *J. Geophys. Res.*, **91**, 12,587-12,631, 1986.
- Wesnousky, S.G., C.S. Prentice, and K.E. Sieh, An offset Holocene stream channel and the rate of slip along the northern reach of the San Jacinto fault zone, San Bernardino valley, California, *Geol. Soc. Am. Bull.*, **103**, 700-709, 1991.
- Whitcomb, J.H., Allen, C.R., Garmany, J.D. and Hileman, J.A., San Fernando earthquake series, 1971: Focal mechanisms and tectonics, *Rev. Geophys.*, **11**, 693-730, 1973.
- Whitten, C.A., Crustal movements in California and Nevada, *Trans. Amer. Geophys. Union*, **37**, 393-398, 1956.
- Wright, L.A., Late Cenozoic fault patterns and stress fields in the Great Basin and westward displacement of the Sierra Nevada block, *Geology*, **4**, 489-494, 1976.
- Wright, T., Geologic summary of the Los Angeles basin, In: Petroleum Geology of Coastal Southern California, edited by T. Wright and R. Heck, *Pacific Section of American Assoc. of Petrol. Geologists*, Los Angeles Calif. 21-31, 1987.
- Wright, T. L., Structural geology and tectonic evolution of the Los Angeles basin, in: Active Margin Basins, edited by K. T. Biddle, *AAPG Mem.*, 35-134, 1991.
- Yeats, R.S., Newport-Inglewood fault, Los Angeles basin, California, *The Amer. Assoc. Petrol. Geol. Bull.*, **57**, 117-135., 1973.
- Yeats, R.S., High rates of vertical crustal movement near Ventura basin, southern California, *Science*, **196**, 295-298, 1977.
- Yeats, R.S., Stratigraphy and paleogeography of the Santa Susana fault zone, Transverse ranges, California, In: *Cenozoic Paleogeography of the Western United States, Pacific Coast Paleogeography Symposium*, edited by J.M. Armentrout, M.R. Cole, H. Ferbest, Jr., 191-204, Los Angeles, Calif., 1979.
- Yeats, R.S., Quaternary flake tectonics of the California Transverse Ranges, *Geology*, **9**, 16-20, 1981.

- Yeats, R.S., 1983, Large-scale Quaternary detachments in Ventura basin, southern California, *J. Geophys. Res.*, **88**, 569-583, 1983.
- Yeats, R.S., Faulting related to folding with examples from New Zealand, *Royal Soc. of New Zealand Bull.*, **24**, 273-292, 1986.
- Yeats, R.S., Late Quaternary slip rate on the Oak Ridge fault, Transverse Ranges, California: Implications for seismic risk, *J. Geophys. Res.*, **93**, 12,137-12,149, 1988
- Yeats, R.S. and G.J. Huftile, The Oak Ridge fault system and the 1994 North Ridge earthquake, *Nature*, **373**, 418-420, 1995.
- Yerkes, R. F., T.H. McCulloh, J.E. Schoellhamer, and J.G. Vedder, Geology of the Los Angeles basin, California - An introduction, *USGS, Prof. Paper.*, **420A**, 57PP., 1965.
- Yerkes, R.F., Geologic and seismic setting, In: Evaluating Earthquake Hazards in the Los Angeles Region: An Earth-Science Perspective, edited by J.I. Ziony, *USGS, Prof. Paper*, **1360**, 25-42, 1985.
- Yerkes, R.F., and W.H.K. Lee, Late Quaternary deformation in the western Transverse Ranges, In: Recent Reverse Faulting in the Transverse Ranges, California, *USGS, Prof. Paper*, **1339**, 71-82, 1987.
- Zhao, D and H. Kanamori, P-wave image of the crust and uppermost mantle in southern California, *Geophys. Res. Lett.*, **19**, 2329-2332, 1992
- Ziony, J.I. and R.F. Yerkes, Evaluating earthquake and surface faulting potential, In: Evaluating Earthquake Hazards in the Los Angeles Region: An Earth-Science Perspective, edited by J.I. Ziony, *USGS Prof. Paper*, **1360**, 43-91, 1985.
- Zoback, M.L. and M. Zoback, State of Stress in the conterminous United States, *J. Geophys. Res.*, **85**, 6113-6156, 1980.
- Zoback, M.D. et al., New evidence on the state of stress of the San Andreas fault system, *Science*, **238**, 1105-1111, 1987.